POLITECNICO DI TORINO

DIPARTIMENTO DI INGEGNERIA MECCANICA E AEROSPAZIALE

MSc. in Aerospace engineering

Master Degree Thesis

Blade Profile Loss Model development for Axial-Flow Fans and Compressors performance prediction using Through-Flow Simulations

Supervisors
Prof. Lorenzo Casalino
Prof. Filippo Maggi

Candidates
Raffaele Guido

Internship Tutor
Prof. Vassilios Pachidis
Director of UTC Rolls-Royce in Cranfield University
Dr. Hasani Azamar Aguirre
Research Fellow at UTC Rolls-Royce in Cranfield University

Academic Year 2017-2018

"Pensa razionalmente,
il tuo lavoro sarà perfetto.
Ma trova un pò di tempo anche
per la tua vita..."
R.A.

A mia madre, Lea, e a mio padre, Vincenzo...
...amore e ammirazione.

A mio nonno, Antonio, e a mia zia, Lucia...
...sostegno e forza.

Ai miei fratelli...
...complicità.

Summary

Aircraft gas-turbine engine design and analysis has represented a milestone discipline in the development of aviation.
Actually the continuous demand from the civil and military sector for compactness, weight and cost reduction has pushed the research in the field towards the introduction of transonic axial flow-fans and compressors: thanks to the shock induced compression, they effectively provide high stage pressure ratio meeting at the same time the requirements of compactness and lightness.
However it is necessary to satisfy the specifications in therms of efficiency and working ranges that have to be at least comparable with the previous subsonic generation.
Precisely this technological necessity has driven the researchers to explore different simulation levels to obtain high fidelity results and optimisation designs in acceptable timing and costs with industrial standards.
Even though the prediction of the flow field inside a compressor without errors and in total accordance with the experimental results still remains something unapproachable, in recent years the Reynolds-Averaged Navier-Stokes(RANS) Computational Fluid Dynamics(CFD) analysis has shown all its power in providing great predictions against experimental data of the flow field inside the aero-engines components. Its prediction capabilities have stated this technique as the most promising one in the future within the field of turbomachinery flow simulation. However nowadays CFD is still affected by two huge problems: the computational resources and the amount of time needed.
Through-flow simulation represents a valid alternative to CFD because of its capability to provide a solution of good accuracy with the need of a limited amount of computational resources and with the use of far fewer time compared to CFD, either for the simulation setting and for the running itself. In particular it should be stressed that a flexible, two-dimensional through-flow tool could potentially achieve an accurate representation of the flow field inside an engine component providing the possibility to study complex phenomena and their effect on engine performance and efficiency in a more cost and time effective manner compare to CFD.
The Stream Line Curvature(SLC) method is the most used numerical method for turbomachinery flow simulation in the field of through-flow tools. It assumes the flow to be two dimensional, compressible, inviscid and steady.
Because of these assumptions the SLC method has the necessity to take into account the viscosity effects by adding some empiricism and thanks to the incorporation of the profile and shock loss models developed through the years. Thanks to these models incorporation, a fully detailed analysis of an engine component can be achieved with an acceptable level of accuracy and with a more effective computational and time cost.
The aim of this research project is to further develop and improve the profile loss modelisation in the in-house trough-flow tool developed at Cranfield University in the UTC Rolls-Royce research centre: SOCRATES (Synthesis Of Correlations for the Robust Assessment of Turbomachinery Engine Systems). In particular a new design profile loss model based only on the use of blade profile geometrical parameters has been developed in order to substitute the previous correlation

set implemented. The latter was based on the use of design velocity ratios which, in reality, at the preliminary design analysis phase of the axial-flow compressor stage are not still known but constitute an output of the simulation, hence the importance to avoid their use in the profile loss estimation. The new model developed constitutes the core of the profile loss estimation model that has been built by defining a set of existing models and after been coupled with a shock-loss model and an off-design deviation angle model, it has been verified, validated and applied producing results in good agreement with experimental data that confirms the potentiality and reliability of through-flow performance prediction and flow field analysis in the turbomachinery preliminary design.

Acknowledgements

It is really curious how this section is put in the front but written at the last. Probably thinking about how to make an acknowledgement and to whom it should be addressed is the most difficult thing, harder then writing the whole document. Simply because using a paper and choosing the words to express gratitude is extremely difficult. Probably the entire thesis length would be nothing compared to the gratitude I would like to express to the people that I have met during this journey.

Probably it would be unconventional, but as someone says that originality is the salt of life, I decided to write this section not only in English but also in Italian, in the attempt to express as the best I can what I would like to tell to the people here mentioned.

First of all I would thank Professor Vassilios Pachidis for the opportunity to carry out my final research project in such a stimulating environment as Cranfield University and in particular the UTC Rolls Royce. He's support, expertise and help represented a fundamental part of this research and of the results achieved. Thank you.
Secondly I feel to strongly thank Dr. Hasani Azamar. Thanks to its sincere help, empathy, expertise and patience he has represented a fundamental figure in this months and his continuous insights and suggestions have represented a fundamental contribution.

I would also like to thank Professor Lorenzo Casalino for its availability and support during this months as well as Professor Filippo Maggi who accepted the role of co-supervisor for the POLIMI and ASP program.

Vorrei ringraziare mia madre, Lea, e mio padre, Vincenzo. Senza di voi nulla sarebbe stato possibile, vi devo tutto e certamente lo sapete, non serve aggiungere altro. Grazie.

Non posso non ringraziare poi i miei fratelli, Roberto e Riccardo, e i miei cari tutti, che mi sono stati vicini nei momenti difficili spronandomi e supportandomi.

Ringrazio mia zia, Lucia. Mi sarebbe piaciuto fossi presente per assistere a tutto questo, quello che sono oggi è soprattutto merito tuo. Perderti è stata un' enorme fonte di crescita, nonostante mancanza e dolore, e spero che, ovunque tu sia, io possa sempre renderti fiera di me. Mi manchi.

Vorrei chiudere questo paragrafo ringraziando chi, in questi cinque anni, c'è sempre stato, chi ormai è un pezzo di cuore e chi ha saputo comprendere i miei continui sbalzi d'umore. Grazie Roberto, Simone, Rita, Sergio e Francesco. Grazie per avermi insegnato il valore dell'amicizia. Anche se vi ho trascurato negli ultimi mesi, mi farò perdonare. Ve lo prometto.

Contents

List of Tables

List of Figures

Chapter 1

Introduction

1.1 Background

Aircraft gas-turbine engine design and analysis has represented a milestone discipline in the development of aviation.
Actually the continuous demand from the civil and military sector for compactness, weight and cost reduction has pushed the research in the field towards the introduction of transonic axial-flow fans and compressors: thanks to the shock induced compression, they effectively provide high stage pressure ratio meeting at the same time the requirements of compactness and lightness.
However it is necessary to satisfy the specifications in terms of efficiency and working ranges that have to be at least comparable with the previous generation of subsonic axial-flow compressors.
Precisely this technological necessity has driven the researchers to explore different simulation levels to obtain high fidelity results and optimisation designs in acceptable timing and costs with industrial standards. Therefore the major problem under this point of view, except from the time issue, is represented by the cost of the simulation: making a huge number of wind-tunnel hardware tests is clearly prohibit for cost's reasons. This kind of strategy has been then substituted by the wide and sometimes uncontrolled use of Computational Fluid Dynamics(CFD), making the three-dimensional(3-D) Reynolds Average Navier-Stokes(RANS) numerical simulation the most used techniques for turbomachinery flow simulation. Even though the enormous potentialities of this discipline, it requires high computational time and resources, and at the same time the user must make a careful evaluation in selecting the simulation settings and in interpreting its results: Computational Fluid Dynamics can sometimes be like a woman that we might think to understand but in reality we are very far from doing it.
Moreover the computational time is exactly the reason why a lot of effort is put in the development of 2-Dimensional (2D) through-flow methods such as Stream-Line Curvature (SLC) tools. These software try to achieve a compromise between the fidelity of the solution provided and the time required for its calculation.
Unfortunately the major difficulties in developing a SLC tool are connected to the loss modelling and to the capability of the software to capture the physics of the fluid compressibility. Overcoming this challenge can effectively give to the researchers a powerful tool capable of providing a solution of good quality with a computational time of the orders of dozen of minutes with in parallel an acceptable computational cost in terms of resources.

1.2 Axial-Flow Fans and Compressors

Almost all of passenger and military aircraft are powered by a gas-turbine engine, sometimes also called jet engine. Obviously, various types have been conceived through the years, but all of them have one component in common: the compressor.
Effectively the performance of the engine is strongly related to the compressor and fan performance. Even though the compressor can be classified in axial and centrifugal, only the first category will be here introduced and then analysed in a more detailed description in the following chapters, been it the fundamental object of this research project. Indeed axial-flow compressors are characterised by lower pressure ratio per stage at higher mass flow rates compared to centrifugal compressors; and hence these machines are preferred for civil and military aero-engines as well as for industrial gas turbines.

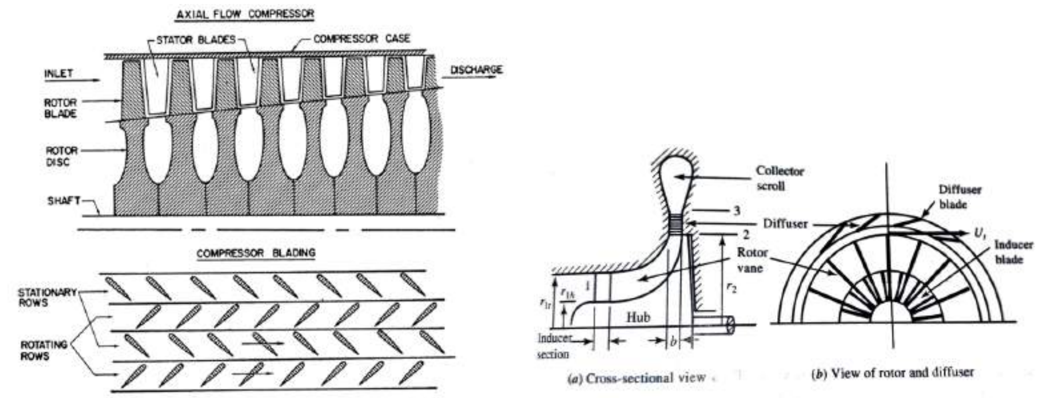

(a) *Schematic view of an axial compressor* (b) *Schematic view of a centrifugal compressor*

Figure 1.1: Compressors Schema[Pictures taken from an Internet source]

Moving therefore to consider the category of axial-flow fans and compressors, a preliminary statement about their functionality is necessary: in these turbo-machines the flow enters in the first blade row and leaves the last in the axial direction. Therefore it can be deducted that an axial compressor is typically made up of many alternating rows of rotating and stationary blades called respectively rotors and stators as shown in figure 1.7. Usually the first stationary row is called Inlet-Guide-Vane, IGV, and has the function of directing the air into the compressor at the correct angle.

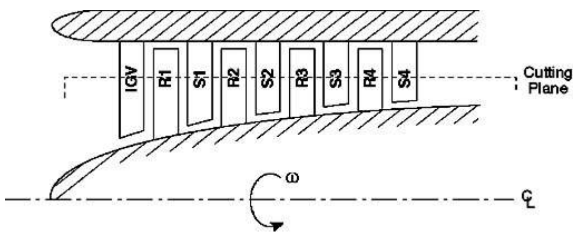

Figure 1.2: Multi-stage axial compressor schema[Picture taken from the Internet]

Moreover depending on the flow Mach number at the blade row inlet a further classification is applicable to this compressor category, it is possible to distinguish:

1. *Subsonic Axial-Compressor* which are characterized by a fully subsonic flow at the inlet blade row;

2. *Transonic Axial-Compressors* which are characterized by a relative supersonic flow at the blade tip and a subsonic flow at the hub;

3. *Supersonic Axial-Compressors* which are characterized by a fully supersonic flow along the blade height.

In particular, during the last sixty years, among the different categories cited, the one of Transonic Axial-Compressors has attracted the most attention thanks to the advantage of weight reduction and high pressure-ratios per stage capability. Actually a modern transonic fan stage is capable of producing a pressure ratio of $\simeq 1.6$, and according to what is reported by S. Farokhi[4], the Jumo004 (figure 1.3b) produces a pressure ratio of 3.14 with its eight stages, that means a pressure ratio of almost 1.15 per stage. Clearly the same performance can be achieved with two transonic stages instead of using eight stages, which results in considerable savings in terms of weight and size of the engine.

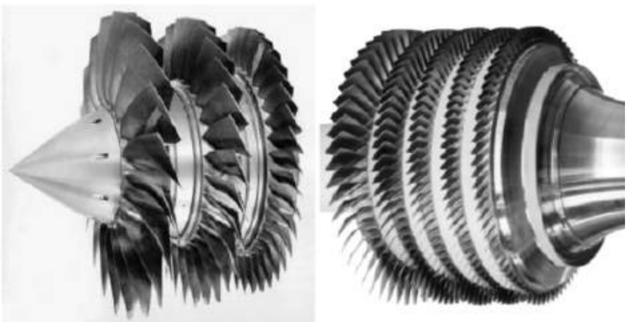

(a) *On the left LP transonic compressor and on the right HP transonic compressor of the Eurofighter*

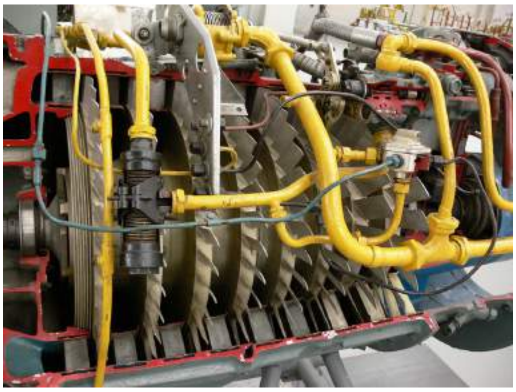

(b) *Jumo004 eight stage compressor*

Figure 1.3: Example of Modern Transonic Compressors and Subsonic Compressors[Pictures taken from the Internet]

The reduction in weight and size is also reflected on the other side in reduction of design, manufacture, operation, and maintainability costs.

This explains why important analytical and experimental researches in the field were carried out since 1960's (e.g. König et al. [8], Miller et al. [7], Chen et al. [6]). In particular the new developments in the optical experimental techniques and computational methods have represented a fundamental step in the deeper understanding of the flow characteristics in a transonic axial-flow compressor and in the related loss mechanisms[9]. In fact the flow field that develops inside these turbo-machines is extremely complex: the flow is usually discharged at subsonic velocities, hence, having mixed relative supersonic flow at the inlet and subsonic flow at the outlet in the stream-wise direction [11]. This kind of flow behaviour is clearly connected with the presence of a strong shock-wave within the blade passage, but in reality the situation is still more complex: what has been observed is the presence of a complete high-speed aerodynamic system consisting in a detached shock wave ahead of the blade leading-edge and a flow expansion at the blade entrance region. Moreover the shock-system is characterised by some degree of obliquity respect to the axial axis that lead the flow to not being circumferentially constant: the inherent 3D character of the flow reflects in a mixed supersonic and subsonic flow field along the pitch on a stream-surface of revolution.
Considering the radial direction, what is observed is an increasing of the velocity with the blade height: the velocity starts subsonic at low blade radii as the result of low blade speed and increases reaching the supersonic regime at heigh blade radii. The transition from subsonic to supersonic passes through a transonic flow region across the blade height.
As one can well imagine, the complexity of the flow field presents many challenges to compressor designers, who have to deal with several and concurring flow features such as shock waves, mixing regions, non-linearity, 3D-effects, intense secondary flows, buffeting and shock/boundary-layer interaction, corner vortex, tip-leakage vortex, corner stall separation, blockage and in many other flow phenomena that induce energy losses and efficiency reduction that have to be modelled in order to make an accurate prediction of transonic compressor performance.
In conclusion of this introduction paragraph, a final distinction should be cited according to what W.J. Calvert[10] reports in his own research paper. In general transonic compressors can be classified in:

1. *Single-stage commercial fan*;
2. *Multi-stage fan or low-pressure compressor* that are used for military applications;
3. *Multi-stage compressors* that are employed for commercial aircraft and industrial gas turbine engines.

In conclusion, the research over the years has focused on the attempt to reach high pressure-ratio per stage keeping an acceptable values of the efficiency around $85 - 90\%$[1]. This process has lead to more compact and lightweight aero-engines which are the fundamental brick of nowadays and of the future aviation world. However these necessities of compactness and lightness have lead the researchers to the continuous attempt to design high efficiency turbo-machines investigating the loss mechanisms, trying to minimizing their effects and trying to predict their impact by modelling them in the simulation software. In particular it is in this field that this research project tries to give its contribution.

[1] That means a careful and precise control over the loss-mechanisms inside the engine by achieving their maximal minimisation.

1.3 Transonic Fan Stage

The design of transonic axial compressors might be considered one of the greatest achievements in recent years within the turbomachinery field.
The use of the label *transonic* immediately highlights that the flow-field inside these turbo-machines is characterised by a part that is definitely subsonic and a part that might be supersonic.
The main difficulties in the design of Transonic Fan Stages is related with the supersonic part of the flow: effectively the shock waves presence and their interaction with the boundary layer represent the main difficulty to overcome in order to achieve a successful design. Examples of the flow field inside a transonic rotor are provided in figure 1.4, figure 1.5 and figure 1.6.

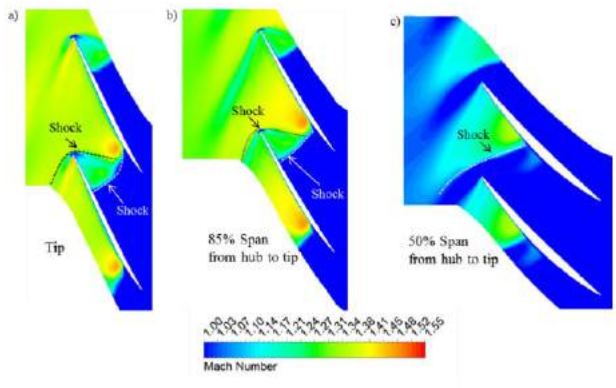

Figure 1.4: Flow field contour for the NASA Rotor 67 at 100% of design speed and near peek efficiency at tip(a), 85% span from hub to tip (b), 50% span from hub to tip (c) [11]

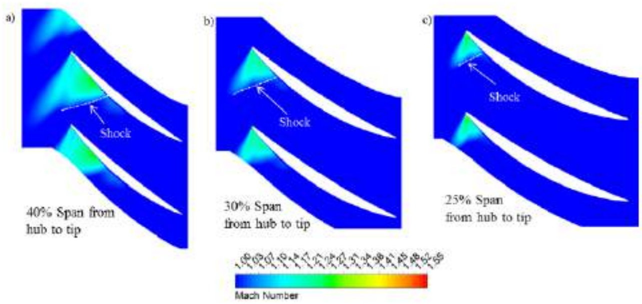

Figure 1.5: Flow field contour for the NASA Rotor 67 at 100% of design speed and near peek efficiency at 40% span from hub to tip (a), 35% span from hub to tip (b), 25% span from hub to tip (c) [11]

Therefore, the transonic flow-field within an axial-flow compressor generates a complex shock wave configuration ahead of the blade leading edge and within the blade passage region [11]. Consequently for a time it looked that the only solution applicable in order to solve the problem was to limit the Mach number of the flow approaching each blade row to a value that, after the flow acceleration over the blade surface, becomes only modestly supersonic. Clearly the limitation in the Mach number reflects in two main consequences: a limitation in the minimum diameter of the rotor needed to handle a certain mass flow rate and a limitation in the minimum stage number. In

the following part of this paragraph we will analyse these two consequences separately highlighting how the philosophy in the "shock wave management" has changed in the transonic axial-flow compressor design.
At the inlet plane of the compressor the lowest air density and the greatest required flow area are observable[2], in parallel also the air temperature is the lowest, hence, the speed of sound is on its hand the lowest. Considering at this point the rotor, the rotor speed increases linearly with the radius, thus resulting in a relative Mach number that tends to be the greatest at the blade-tip diameter. Consequently if there is the necessity to limit the blade relative Mach number approaching the blade row, this means that also the rotational speed of the rotor has to be limited.
As first consequence, the minimum diameter of the rotor is limited. Secondly, the stage pressure

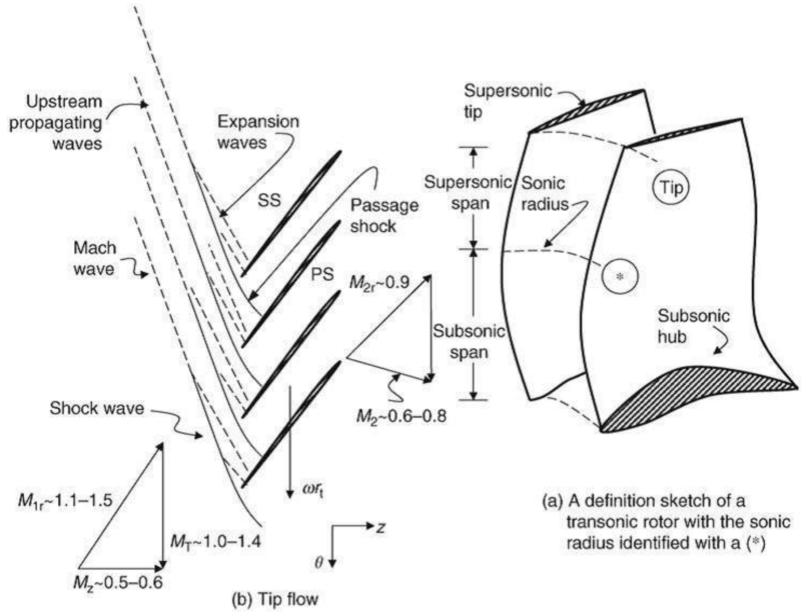

Figure 1.6: Typical flow field in a transonic rotor [4]

ratio is also affected and limited, thus resulting in an higher number of stages needed to provide a given overall pressure ratio. These two limitations explain also why a subsonic axial-flow compressor is much larger and heavier than a transonic one.
The fundamental change in the design philosophy that has lead to overcome these two limitations is the following: the design principle at the base of the conception of transonic axial-flow fans and compressors is not to avoid the shock wave presence but to take advantage of it by controlling the shock wave intensity and positioning in the blade passage area. The major attempt is to exploit the compression of the shock wave minimizing in parallel the aerodynamic losses connected with its presence.
The complexity of the shock wave configuration makes this design principle easily applicable to the first stage of the compressor where the prediction is facilitated by the more uniform flow at the inlet station and thus most likely to be predictable for design purposes. However, the need of transonic stages is not so great at the high-pressure end of the axial-flow compressors[2].
The introduction of the transonic axial-flow compressor stage alleviate the limitations previously mentioned allowing the design of smaller and lighter axial-flow compressors. Unfortunately all that glitters is not gold, in fact the transonic stage is characterised by the fact that the blade hight tends to become too small for efficient operation. Under this point of view one way to control the

blade aerodynamic load is to increase the blade solidity, that is, to place the blades relatively close together[2]: in particular the solidity tends to increase passing from a value of $\simeq 1.4$ at the rotor tip to a magnitude of $\simeq 2.45$ at the rotor root diameter. Moreover since aerodynamic and structural problems at the radius limit the fan number of blades, in order to provide an high solidity at the tip radius a blade of wide chord might be used. This creates new problems connected with the capacity of the blade to deal with vibrations, nevertheless their thinness and little camber angle. One of the solutions provided for this limitation is the introduction of snubberless that limit the lateral vibrations but on the other hand introduces also aerodynamic drag and centrifugal and bending stresses.

1.4 Turbomachinery Flow Simulation

Even though the prediction of the flow field inside a compressor without errors and in total accordance with the experimental results still remains something unapproachable. In recent years the Reynolds-Averaged Navier-Stokes(RANS) Computational Fluid Dynamics(CFD) analysis has shown all its power in providing great prediction against experimental data of the flow field inside aero-engines components. Its prediction capabilities have stated this technique as the most promising one in the future within the field of turbomachinery flow simulation. However nowadays CFD is still affected by two huge problems: the computational resources and the amount of time. Actually the computational resources needed for a 3D-CFD-RANS simulation and the time to settle up the model, all the settings, the computational time and the post-processing still constitute a huge challenge to be overcome before establishing itself has the queen of flow-filed simulation techniques for prediction and design purposes. Moreover nowadays another limitation is represented by the impossibility to perform a whole engine performance simulation [12].

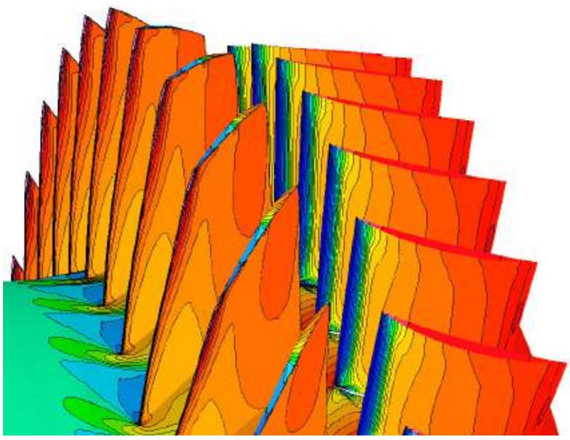

Figure 1.7: CFD Contour example in a Transonic Axial-Flow Compressor Stage(Picture taken from the Internet)

It should not also be overlooked the attention and the uncertainty that are connected with the choice of some settings like the turbulence models and the necessity of a strong critical observation and analysis of the results that came out from a 3D-CFD simulation. Finally the customizing possibilities of a CFD commercial software are really limited, there is no way for the users to incorporate different loss models or deviation angle models in order to have a result that is closer to the experimental data and usually the identification of the source of inaccuracy and the model calibration are not possible.

Whereas it follows that the lack of flexibility, the need of great computational resources, the huge amount of time are sometimes unacceptable for some industrial purposes and the needs of compressor designers: for example a real time engine prediction for diagnostic analyses.
On the other hand the through-flow simulation represents a valid alternative to CFD because of its capability to provide a solution of good accuracy with the need of a limit amount of computational resources and with the use of far fewer time compared to CFD, either for simulation setting and for the running itself. In particular it should be stressed that a flexible, 2-Dimensional through-flow tool could potentially achieve an accurate representation of the flow field inside an engine component providing the possibility to study complex phenomena and their effect on the engine performance and efficiency in a more cost and time effective manner compare to CFD [12]: in particular it is clear for the reasons mentioned before that a complete engine simulation using a CFD software has really little practical sense of existing due to cost and time reasons, while using a through-flow code could provide a complete engine simulation nevertheless the results are quite of less accuracy then the ones obtained with a 3D-CFD-RANS simulation.
However one of the feature that should not be underestimated and that represent one of the points of strength of these tools is their flexibility.
Before introducing this feature, it might be the case of briefly introducing the through-flow simulation: among the different types of through-flow codes, we will focus on the ones based on the Stream-Line Curvature(SLC) method. This because of the fact that SOCRATES, which is the tool that has been used and improved during this research project, is a SLC through-flow tool.
The SLC method is the most used numerical method for turbomachinery flow simulation in the field of through-flow software. It assumes the flow to be two dimensional, compressible, inviscid and steady. Because of these assumptions the SLC method has the necessity to take into account of the viscosity effects by adding some empiricism and thanks to the incorporation of the profile and shock loss models developed through the years[11]. Thanks to these models incorporation a fully detailed analysis of an engine component can be achieved with an acceptable level of accuracy with a little computational and time cost.
Effectively it is in these models incorporation where resides the flexibility of these tools: the possibility of incorporating different loss models gives to the designer the possibility to improve the prediction or at least to make a calibration in order to reduce the results incertitudes thanks to the incorporation of the correlation results of the high fidelity analysis into the low-fidelity engine performance simulation.
Moreover if the main purpose of the designers is the engine component optimisation, the SLC tools are the most adapted simulation software to be used due to the high time required by the CFD component optimisation. In parallel there is also the possibility of coupling the software with a low-fidelity-zero-dimensional solver for the entire engine [11].
However the through-flow simulation of transonic flow within fans and compressors still remains difficult for the intrinsic 3D nature of the flow field which is characterised also by the shock wave presence, their interaction with the boundary layer, spanwise mixing, turbulent mixing and secondary flow phenomena. Because of these characteristics the necessity to make an accurate modelisation of the profile losses in this kind of simulation is crucial to close the gap as much as possible from the experimental data in order to increase the level of accuracy of the simulation results. In particular, developing a model of profile losses at the design operating point based only on geometrical parameters represents effectively a great step further in the model generalisation, being until this point only been used models that were based on design velocity ratios deduced from the experimental reports. But in reality these data, when using the tool for analysing and designing a new compressor or fan are not known as input but constitute an output of the simulation, hence the importance to try to develop a model capable of avoiding their use. Moreover the fundamental role of the profile loss modelisation in transonic flow fans and compressors has a great importance in the off-design performance simulation and in particular at the values of the rotational speed where

the shocks are not present or where their strength is really limited: in this functionality conditions the correct profile loss estimation is a key condition for the correct and accurate performance prediction being in those cases the major loss source the one due to the blade profile characteristics.

1.5 Project Objectives and Outline

The aim of this research project is to further develop and improve the profile loss modelisation in the in-house trough-flow tool developed at Cranfield University in the UTC Rolls-Royce research centre: SOCRATES (Synthesis Of Correlations for the Robust Assessment of Turbomachinery Engine Systems). In particular a new design profile loss model based only on the use of blade geometrical parameters has been developed during this research project in order to substitute the previous correlation set implemented which was based on the use of design velocity ratios which, in reality, at the preliminary design analysis phase of the compressor stage are not still known but constitute an output of the simulation, hence the importance to avoid their use in the profile loss estimation. The new model developed constitutes the core of the profile loss estimation model that has been set by defining a set of existing models for the different quantities such as the blade design deviation angle, the blade design incidence angle , the blade stall incidence angle, the blade minimum loss incidence angle, the minimum off-design profile loss in order to finally estimate the Blade Profile Losses in the chosen off-design operating condition. Then the blade profile loss is multiplied for a new correction factor developed to take into account the difference between the reference geometry for the model construction and the under-analysis one in order to have the effective blade profile loss estimation that is then summed to the shock loss estimation to have the total loss coefficient estimation. In particular the shock loss model that has been used was the one developed By Dr. Azamar Aguirre during his PhD at Cranfield University, not being the shock model one of the object in this research perimeter it will not be described in the model definition, in fact the present research activity has focused on the blade loss estimation. However if the reader is interested, more information about it can be found in [11]. Moreover it should be explicitly mentioned also that the deviation angle model at off-design operating point is out of the perimeter of the model developed in this research project which focuses on the blade profile loss coefficient prediction, and for the estimation of this angle in the considered off-design operating condition, the methodology proposed by Johnsen and Bullock and Pollard and Gostelow, has been used.
After the model definition, it has been verified against the previous model results using the transonic fan *NASA Rotor 67* as geometry for the flow field simulation, validated using the transonic fan *NASA Rotor 37* as geometry for the flow field simulation and finally applied using as test case *the Transonic Two Stage Fan* described in the *NASA TP 1493*. The choice of those geometries for the model verification, validation and application is related to their availability in the open literature and to the possibility to publish the results obtained during the analysis.

Chapter 2

Through-Flow Simulation for Turbomachinery Preliminary Design

2.1 Introduction

In the early 50's the development of turbomachine through-flow analysis methods begun, and, over the years, the methods accuracy grew thanks to the more accurate flow-field modelisation provided: in particular more realistic models were introduced, more precise numerical algorithms were implemented and methods representing the features of the experimentally observed flow field not modelled by the equations were added.

The aim of this section is to provide the literature review concerning the turbomachinery through-flow simulation. Actually and as mentioned also before, through-flow tools represent one of the most important analysis and design instruments for the turbomachinery preliminary design and performance prediction. Effectively their characteristic of rapidity, accuracy and the high degree of flexibility in the possibility to incorporate empiricism under the form of correlations make them probably the most important tool for aerodynamic turbomachinery designers.

The through-flow method for turbomachinery performance prediction is a two-dimensional CFD method that solves azimuth-average flow in the meridional plane. Respect to the 3D-CFD simulation, the through-flow analysis can run approximately two orders-of-magnitude times faster. Consequently trough-flow methods provide a reasonable trade-off between speed and accuracy that makes them a fundamental tool for performing parametric-studies in the conceptual and preliminary design phase.

In the following sections firstly the general assumptions at the base of the turbomachinery through-flow simulation will be presented, followed by a classification of the available through-flow methods. We will focus later on the Stream-Line Curvature method which will be presented in details, being it the through-flow method on which the simulation tool SOCRATES, used and improved in this research project, is based.

Finally the in-house trough-flow tool SOCRATES (Synthesis Of Correlations for the Robust Assessment of Turbomachinery Engine Systems), developed at Cranfield University in the UTC Rolls-Royce research centre, will be presented.

2.2 General Assumptions

A through-flow calculation method is defined as *a computational technique for predicting fluid velocities and thermodynamic properties at designated locations in the internal flow path inside a turbomachine*[12].
In their simplest version a single computation location is specified and it is placed at the mean flow passage radius at the inlet and outlet of each blade row. In more sophisticated and modern methods this limitation is overcome in order to increase the simulation accuracy and consequently different computation points can be specified throughout the flow path both in the axial spaces between the rows and within the blade rows at arbitrary coordinate locations[12].
The flow field inside a turbomachine is inherently 3-Dimensional, viscous, compressible and unsteady. All these characteristics made this flow field extremely complex and several assumptions are made in the through-flow modelisation.
The following reported assumptions are made almost in any through-flow analysis.
The definition of fluid particle paths by means of the stream-lines, stream-surfaces and stream-tubes is based on the assumption of steady relative flow at the inlet and at the outlet of each blade row. As a consequence the flow field complexity is strongly simplified and its inherent 3-Dimensional character is approximated and treated as being locally 2-Dimensional.
Moreover generally control surfaces are defined[1]: they in particular subdivide the flow passage by intersecting both the hub and tip boundaries. The definition of the control surfaces is used in almost all the trough-flow methods, either if they are based on the use of differential equations, or integral equation or both. However, going deeper in details, the control surfaces might have different geometrical shape, and it is possible to distinguish:

1. Simple-plane surfaces perpendicular to the rotational axis;

2. Conical or curved surfaces that improves the conformity to the leading and trailing edge trace in the meridional plane, figure 2.2, or that allow the designer to reach some particular regions of interest in the flow path;

The concept of control surfaces, that are shown in figure 2.1, was introduced in the 1952 by Wu[35]. In particular in his paper-work, Wu introduces the concept of $S1$ and $S2$ stream-surfaces which are widely used today in the through-flow methods.

In particular the control surfaces of type $S1$ are stream-surfaces which divide the flow passage into several sections in the blade-to-blade direction. Secondly, the control surfaces of type $S2$ are through-flow surfaces which intersect both the hub and the casing.
According to Katsanis and McNally[36] and Pachidis[12], families of $S2$ control surfaces could potentially be used and identified as a third category of control surfaces in order to achieve a division of the blade-to-blade flow into hub-to-casing stream-tubes.

Another fundamental assumption made in the through-flow analysis methods is related to the flow properties: the flow is assumed of being treatable as axis-symmetric and circumferentially averaged. Considering the flow as axis-symmetric means to neglect the fluid properties variations in the circumferential direction for any given set of axial and radial flow-field coordinates. Furthermore the assumption of circumferentially averaged flow is used for the flow on some of the defined control surfaces of type $S2$. In particular considering the flow as circumferentially averaged means considering the fluid properties and velocities at all coordinate points on the $S2$ surface as the circumferential average of the values across the blade-to-blade passage at the corresponding radius

[1] sometimes also labelled as computation surfaces, calculation station or channel solution surfaces[12]

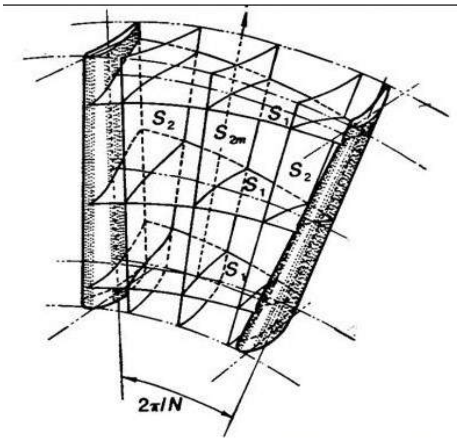

Figure 2.1: S1 and S2 control surfaces

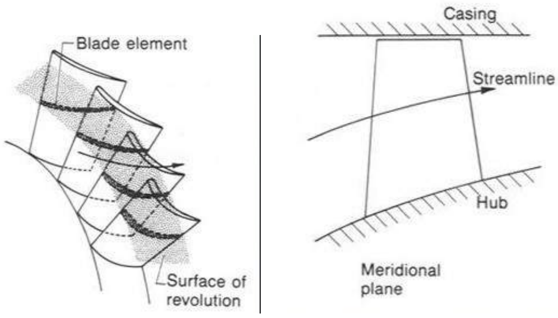

(a) (b)

Figure 2.2: Meridional Plane schema

and axial location[12].
The main consequences[37][38] of the assumptions made until this point are:

- The possibility to model the control surfaces of type $S1$ as control surfaces;
- Justification and support of the use of linear cascade data in axial-flow turbomachinery design;
- Justification and support of the flow passage circumferential measurement at constant radius;
- Justification and support of the use of stream-surface interactions with the meridional plane, figure 2.2, in order to observe the nature of the hub-to-casing flow pattern;
- The possibility to consider the hub-to-shroud surface as representative, further reducing the computational cost of the analysis.

Finally an important assumption made is that the flow is assumed to be adiabatic, which means that there is no heat transfer across stream-surfaces and between fluid elements.

2.3 Classification of the Through-Flow Methods

Before proceeding in the presentation of the Stream-Line Curvature method, on which SOCRATES is based, a presentation of the main through-flow methods with their main characteristics and a brief historical background concerning their development is provided in table 2.1.

Table 2.1: Through-Flow Methods

Through-Flow Method	Historical Background	Main Characteristics
Mean-Line Method (MLM)	The first tool based on the mean-line method is the one coded by Howell and Calvert in the 1978. Thereafter the method has been employed in the preliminary design phases with typical examples provided by the tool proposed by Casey in 1987. Arriving to recent years, to be mentioned is the mean-line flow analysis method for axial and centrifugal compressors developed by Veres in 2009 at the NASA Glenn Research Centre, in Cleveland, Ohio.	The mean-line flow modelling methodology addresses the need for a fast tool able to help the designer in the conceptualisation sizing phase of the compressor during the preliminary project of gas turbine engines. It is based on the definition of a mean-line, figure 2.3, along the flow passage on which the calculations points are specified. Once specified the coordinates of these calculation points,in correspondence of those, the fluid properties and velocities are computed using one dimensional calculations accompanied by empirical correlations obtained from statistical studies and curve fitting on experimental data. The conditions computed are supposed to be representative of the flow characteristic at the station corresponding to the calculation point on the mean-line defined. The ability to model compressor off-design performance is necessary in the system evaluation within gas turbine engines. Under this point of view the mean-line tool might be used to achieve an initial estimation of the variable geometry reset schedule of a multi-stage compressor resulting in an aerodynamically matched stages at off-design compressor speeds.

Simple Radial Equilibrium Method (SREM)	The development of this category of through-flow methods might be divided into two phases. Firstly the two-dimensional analysis tools developed were based on the use of approximate, inviscid, simple radial equilibrium equation and the blade row losses were neglected. An example is the method provided by Voit in the 1953. Secondly, and in particular starting from Hatch in the 1954, a discussion about the importance to include and evaluate the loss sources and magnitudes started. These lead to the possibility to obtain the so called non-isentropic simple radial equilibrium equation that is used in this category of through-flow methods for axial-flow fans and compressors performance prediction.	This method is based on the assumption of considering only the centripetal acceleration generated by the tangential velocity component in the radial direction, effectively this assumption is consistent with the fact that the previous mentioned term is the one having the higher magnitude for the majority of axial-flow fans and compressors in the radial equilibrium equation for momentum. Consequently in any calculation station the effects of the radial velocity component are supposed to be negligible. In particular the calculation stations defined in this method are represented by plane control surfaces perpendicular to the rotational axis: the calculation made on the control surfaces are based on the governing physics law assisted by empirical correlations to compute the distribution of fluid properties and velocities from the hub to the casing at each station considered. Finally, as reported by Pachidis[12], this method is limited to the assumption of axis-symmetric flow within axial turbo-machines.

Strea-Line Curvature Method (SLC)	This category started to be labelled with its current name only in the 1967 with the research results produced by Jansen and Moffatt. Despite this, it was in the 1949 that, Wu and Wolfenstein before, and Hamrick after, started to investigate the terms in the radial component of the equation of motion representing the stream-line slope and curvature. However only in the 1953 the effect of stream-lines shape was included in turbomachinery performance prediction thanks to the work made by Wright and Kovach, and in 1961 the first attempt to include loss distribution was made by Swan. However a fundamental step in the SLC tools development was made in 1974 when the suggestion of using correction terms to take into account the irreversibility that reflects the entropy increase generated by the fluid shearing stress along a stream-line was proposed by Bosman and Marsh. During the years an important development consisted in the introduction of calculation stations not only at the inlet and outlet of blade rows but also inbetween the blades. This improvement gave the possibility to push further the accuracy of the prediction making the analysis passing from a purely two-dimensional to a quasi-three-dimensional one.	This through-flow method is based on an iterative approach which on its hand is characterised by the determination of the stream-lines projections on the meridional flow passage within a turbomachine[12], figure 2.4.The calculation starts with the assumption of a set of stream-lines, than the iterative procedure aims at searching the degree of satisfaction imposed within the tool defining the final set of stream-lines starting from the initial one and moving it. The final stream-lines configuration is established for a given mass-flow rate, a given rotational speed and given inlet flow conditions. Finally using the governing physical law and the empirical correlations included in the tool the fluid properties and velocities are calculated at the control stations defined by the intersection of the stream-lines with the defined control surfaces. The major difficulty in this method is represented by the necessity to calculate first the stream-line pattern and then compute the curvature and slope of the stream-lines iteratively: usually a spline fit is used to obtain the shape and then differentiated one and two times to obtain respectively the slope and curvature.

Finite Difference Method (FDM)	The use of the finite difference method in through-flow analysis started in 70's with the work of Marsh first and, Devis and Millar then. In particular the interest in this category of through-flow analysis methods was subsequent to the identified necessity to perform a calculation also in correspondence of calculation stations internal to the blade row. However no development are shown in the literature concerning the flow field analysis of transonic axial-flow compressors. The most complete tool based on finite differences seems to be the one proposed in the 1974 by Bosman and Marsh where entropy distribution in the computed flow field was included thanks to correlations introduced to take into account the local viscous shear stress.	In mathematics, finite-difference methods are defined as numerical methods for solving differential equations thanks to an approximation of these equations that are written in terms of difference equations. This means that finite differences are used to approximate the derivatives, as a consequence, the finite-difference methods are considered as discretization methods. When applying these methods to a trough-flow analysis the first step consists in the definition in the domain to be studied, which in the case of turbomachinery is the flow passage, of a grid system and in particular of the definition of the position of the grid's nodes. At this point the governing physical equations and the empirical correlations for loss and deviation angle estimation are written in correspondence of each node in terms of finite differences. The resolution of the equations written in the latter form mentioned gives the fluid properties and velocities at the nodes that might be used then to construct the stream-lines pattern.

Finite Element Method (FEM)	The finite element method was originated from the need to solve complex elasticity and structural analysis in the field of aeronautical engineering. The pioneers of the method are commonly recognized as A. Hrennikoff and R. Courant which proposed the method in the early 40s. However in order to meet an application of the method in the through-flow analysis we should wait until the 70s: examples are the method published by Adler and Krimerman in the 1974 or the one published in the 1976 by Hirsch and Warzee. In particular the latter reported the finite element method three-dimensional analysis applied to the turbomachinery flow field: effectively the greatest potentiality of the FEM method is the possibility to adapt the mesh to complex turbomachinery geometries and deal with a three-dimensional flow-field.	The finite element method is based on a formulation of the problem considered that results in a system of algebraic equations. The methods yields approximates the values of the unknowns of the discrete problem formulated at each node over the domain. Its name comes from the fact that it subdivides a large and complex problem into smaller and simpler problems solved on finite elements of the domain. In particular concerning the through-flow application of this model to turbomachinery flow field simulation, the flow passage is divided in order to obtain the previous-mentioned elements. The elements are characterised by a certain number of nodes or control points that depends on the element used for the domain discretization. The governing physical equations and the empirical correlations introduced are solved iteratively and fluid properties and velocities are determined in correspondence of each node. In particular the finite element methods usually are based on the use of variational methods from the calculus of variations in order to provide an approximate solution by minimizing the associated error function. An example of finite element grid is provided in figure 2.5.

Finite Volume Method (FVM)	The introduction of finite volume methods in the through-flow simulation is dated in the 70s, like the finite difference method and the finite element method. In particular they were fist applied in the blade-to-blade flow field analysis and only the recent developments in the computational power capacity have given the possibility to apply them to the hub-to-tip flow field 3-Dimensional analysis.	The finite volume method permits the representation and evaluation of partial differential equation in the form of algebraic equations. The fundamental principle is really close to the one of the finite element method and the finite difference method. While for the two previous cited methods the values of unknowns are calculated at discrete nodes on a meshed geometry, in the finite volume method, the finite volume surrounding each node is considered. Then volume integrals in a partial differential equation, thanks to the use of the divergence theorem, are converted in surface integrals and then they are evaluated as fluxes of the unknown variable considered at the surface of each finite volume. Clearly the method is conservative, and the flux entering a given volume is equal to the flux leaving the adjacent one. In particular in the case of the application of the method to the through-flow analysis, the passage within the turbomachine is divided into small volume elements and the governing physical equations and the empirical correlations introduced are used to generate the previous mentioned integral conservation equations for each volume that, once solved iteratively, give the flow properties and velocities distribution on the finite volume surface. An example of finite volume computational grid is provided in figure 2.6.

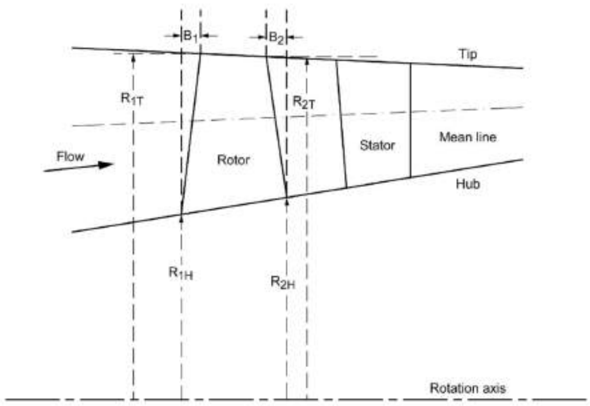

Figure 2.3: Example of Mean-line schema [39]

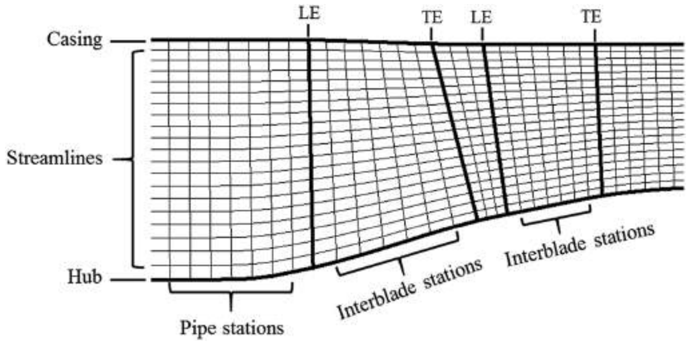

Figure 2.4: Example of Streamlines schema

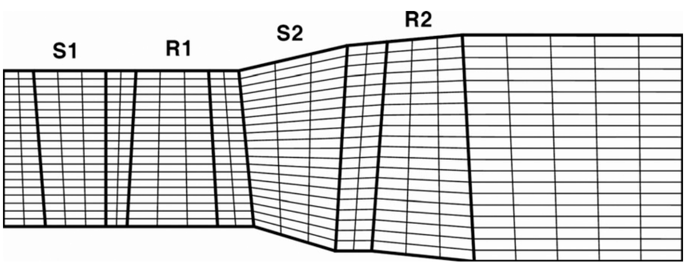

Figure 2.5: Example of Finite element grid for a two stage turbine

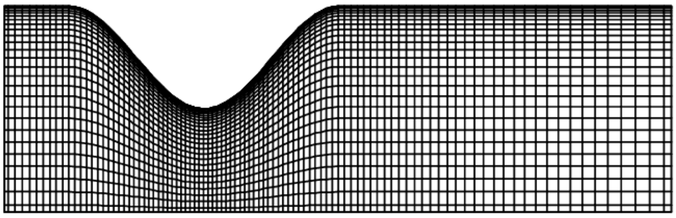

Figure 2.6: Example of Finite Volume Grid Structure of Flow Pattern

2.4 Stream-Line Curvature Method

2.4.1 Overview

This section aims at presenting more in details the theoretical background of the Stream-Line Curvature Method(SLC) and its fundamental equations in the turbomachinery flow field simulation. In fact this method is the one on which is based the simulation tool used and further developed in this research project.

Before exposing the theoretical background of the method, it should be useful to stress again the properties of the flow field inside a compressor: with its characteristics of highly 3-dimensionality, turbulence and viscosity it represents one of the more complex flow field to analyse.

The SLC method basically provides a solution of the discrete equations of continuity, motion, energy and state in a form that incorporates the full three-dimensional compressor geometry and on a computational grid which is constructed on the meridional plane[12].
As first step, there is the necessity to define the computational nodes, they are defined as the points where there is the intersection of the various stream-lines, usually chosen in odd number, and the blade edges. The second step consists in the transformation of the discrete equations, and the result is a non-linear partial differential equation solved iteratively with a finite difference approach.
At the beginning of the iterative procedure an initial guess about the stream-lines position, and consequently about the computational nodes position, is made. And while the iterations proceed, the new stream-lines position is computed at each iteration until the convergence is reached. Consequently the shape of the grid changes at each iteration and a check about the new grid generated is based comparing the new stream-lines position respect to the one that they had at the previous iteration.
Finally using the governing physical law and the empirical correlations included in the tool the fluid properties and velocities are calculated at the control stations defined.

2.4.2 Theoretical Background

As already mentioned, the Stream-Line Curvature Method follows an iterative computation procedure to compute the position, slope and curvature of the defined stream-lines with the flow assumed to be compressible, axis-symmetric, steady and inviscid. In particular the solution obtained mainly comes from the resolution of the governing equation of conservation of linear momentum, also labelled as Newton's second law.
The Newton's second law states that, considering an inertial reference frame, the rate of change of the linear momentum P of an infinitesimal continuum is connected proportionally to the resultant

of the applied forces on the infinitesimal continuum considered. Considering a control volume at a given instant of time and indicating with u_i the tensor of velocity in the direction i, we can write that

$$P = \int_{Vol} \rho u_i dVol \tag{2.1}$$

At this point supposing that the fluid is subjected to surface forces and body forces per unit volume, the resultant applied, indicating with S the surface of the volume considered with outer unit normal vector n_j, can be expressed as

$$F_i = \int_S \tau_i DS \; + \int_{Vol} f_i dVol \tag{2.2}$$

Applying the Cauchy's theorem, the surface stress might be expressed in terms of the stress field tensor obtaining $\tau_i = \sigma_{ji} n_j$, and using the Gauss theorem to transform the surface integrals into volume integrals, we obtain

$$F_i = \int_{Vol} \frac{\partial \sigma_{ji}}{\partial x_i} dVol + \int_{Vol} f_i dVol \tag{2.3}$$

At this point remembering the Newton's second law previously cited, we have that the equation of the conservation of the linear momentum is

$$\frac{DP_i}{Dt} = F_i \tag{2.4}$$

in which we might substitute the terms previously obtained. Substituting the terms indicated and expanding the substantial derivative we obtain

$$\int_{Vol} \left(\frac{\partial(\rho u_i)}{\partial t} + \frac{\partial(\rho u_i u_j)}{\partial x_j} \right) dVol = \int_{Vol} \left(\frac{\partial \sigma_{ji}}{\partial x_i} + f_i \right) dVol \tag{2.5}$$

At this point the following assumption has to be made: we can pass from an integral formulation to a differential one because the linear momentum equation must be valid for an arbitrarily domain considered. Consequently we obtain

$$\left(\frac{\partial(\rho u_i)}{\partial t} + \frac{\partial(\rho u_i u_j)}{\partial x_j} \right) = \left(\frac{\partial \sigma_{ji}}{\partial x_i} + f_i \right) \tag{2.6}$$

Arrived at this point, I would like to open a short parenthesis, and passing for a moment at considering the mass conservation law. This law states that

$$\frac{Dm}{Dt} = \frac{D}{Dt} \left(\int_{Vol} \rho dVol \right) = 0 \tag{2.7}$$

applying the same assumption to the integral formulation, we obtain the differential formulation of the mass continuity governing equation which is

$$\frac{\partial \rho}{\partial t} + \frac{\partial(\rho u_j)}{\partial x_j} = 0 \tag{2.8}$$

Substituting this equation in the equation 2.6, we obtain the Euler equation of motion of a linear continuum:

$$\rho \frac{Du_i}{Dt} = \frac{\partial \sigma_{ji}}{\partial x_i} + f_i \tag{2.9}$$

Let's now concentrate ourselves for a moment on the expression of the stress tensor, Stokes defined it as

$$\sigma_{ij} = -p\delta_{ij} + 2\mu e_{ij} - \psi e_{kk}\delta_{ij} \tag{2.10}$$

The assumption of the stream-line curvature method of inviscid flow lead to neglecting the terms related to the normal dynamic viscosity μ and to the second viscosity ψ. As a consequence the stress tensor is connected only to pressure and it results in an isentropic stress tensor. Substituting in the equation 2.9 we obtain the equation for an inviscid fluid which might be written as

$$-\frac{1}{\rho}\nabla p = \frac{Du_i}{Dt} - \frac{F_i}{m} \tag{2.11}$$

However considering the fluid flow characteristics within a turbomachine, and in particular the rotating flow characteristic, there is the necessity to add to the latter equation obtained the terms that take into account the centripetal and Coriolis acceleration, hence, we obtain

$$-\frac{1}{\rho}\nabla p = \frac{Du_i}{Dt} - \frac{F_i}{m} - (\omega_i \times \omega_i \times r_i) + (2\omega_i \times u_i) \tag{2.12}$$

Usually when analysing the flow field within an axial-flow compressor, for reason of convenience, the equation 2.12 is written using a cylindrical reference frame. Let's first analyse separately how the various terms looks like in the cylindrical reference system

$$-\frac{1}{\rho}\nabla p = -\frac{1}{\rho}\frac{\partial p}{\partial r}\vec{e_r} - \frac{1}{\rho}\frac{\partial p}{\partial \theta}\vec{e_\theta} - \frac{1}{\rho}\frac{\partial p}{\partial z}\vec{e_z} \tag{2.13}$$

$$\frac{Du_i}{Dt} = u_j\frac{\partial u_i}{\partial x_j} = u_r\frac{\partial u_i}{\partial r} + u_\theta\frac{\partial u_i}{\partial \theta} + u_z\frac{\partial u_i}{\partial z} \tag{2.14}$$

It should be stressed that the stream-line curvature method assumes th fluid to be steady, thus, the time-derivative of the velocity is null.

$$\omega_i \times \omega_i \times r_i = -(\omega^2 r)\vec{e_r} + \vec{e_\theta} + \vec{e_z} \tag{2.15}$$

In the centripetal acceleration formulation, the terms in the θ and the z directions are assumed to be negligible.

$$2\omega_i \times u_i = (-2\omega u_r)\vec{e_r} + (2\omega u_r)\vec{e_\theta} + \vec{e_z} \tag{2.16}$$

In the Coriolis acceleration formulation, the term in the z directions is assumed to be negligible.

Substituting these terms we obtain the formulation of the equation 2.12 in the cylindrical reference system

$$-\frac{1}{\rho}\frac{\partial p}{\partial r}\vec{e_r} - \frac{1}{\rho}\frac{\partial p}{\partial \theta}\vec{e_\theta} - \frac{1}{\rho}\frac{\partial p}{\partial z}\vec{e_z} = u_r\frac{\partial u_i}{\partial r} + u_\theta\frac{\partial u_i}{\partial \theta} + u_z\frac{\partial u_i}{\partial z} - (\omega^2 r)\vec{e_r} - 2\omega u_r\vec{e_r} + (2\omega u_r)\vec{e_\theta} \tag{2.17}$$

It should be noticed at this point that the pressure gradient in the radial direction has to balance the component of the flow acceleration in the radial direction. However, the radial acceleration is affected by the stream-line curvature radius r_{st}, and, indicating with m the meridional direction,

by the meridional velocity V_m which is tangent to the stream-line, and also by the meridional acceleration $\dot{V}_m$ which is tangent to the stream-line.
In particular the equation, that relates the pressure gradient in the radial direction to the component of the flow acceleration in the same direction, can be written relating the derivatives in the z direction to the geometrical shapes of the stream-lines. If the reader is interested in the whole analytical derivation of the equation it is available in [12]. The final equation obtained is

$$\frac{\partial V_m^2}{\partial s} = 2V_m^2 \cos^2\alpha \left[\frac{\cos(\phi+\lambda)}{r_{st}} - \frac{\tan\alpha \frac{\partial \alpha}{\partial s}}{\cos^2\alpha} + \sin(\phi+\lambda)\left(\frac{\tan(\phi+\lambda)}{r_{st}} - \frac{1}{\cos(\phi+\lambda)}\frac{\partial \phi}{\partial s} - \frac{\partial(ln(r\rho))}{\partial m} \right) \right] + \\ +2\cos^2\alpha \left[\frac{\partial l}{\partial s} - 2\cos(\gamma)\omega(C_\theta - U) - T\frac{\partial S}{\partial s} \right] \tag{2.18}$$

where $\vec{s}$ is the unit vector that indicates the spanwise direction, T represents the static temperature, S represent the entropy, ϕ represents the stream-line slope, λ represent the sweep angle and C and α are used to indicate the absolute velocity and the absolute flow angle. Solving this equation, labelled as full Radial Equilibrium Equation(REE), returns the meridional velocity gradient in the spanwise direction.
However the solution of the full REE just solves the gradient of the meridional velocity, hence, an additional equation to compute its magnitude is required.
This equation is the continuity confined stream-tube mass flow equation. The latter and the full REE are solved iteratively as a set on a computational mesh on the meridional plane: the mesh is built between the intersection of the stream-lines and quasi-orthogonal calculation station lines to the stream-surface[11].
Finally, it should be stressed that due to the inviscid flow assumption made in the SLC method, the compressor blading losses and deviation angles have to be considered separately but they must be added in the iterative tool loop in order to achieve an accurate and reliable performance prediction.

2.5 SOCRATES Overview

This section aims at providing to the reader a presentation of the trough-flow tool used and improved during this research project. An high level flow chart that depicts how the tool works is provided in figure 2.7.

The acronym SOCRATES states for Synthesis Of Correlations for the Robust Assessment of Turbomachinery Engine Systems. It is a 2-Dimensional SLC through-flow tool for preliminary design and flow field analysis within axial-flow fans and compressors developed at Cranfield University in the UTC Rolls-Royce research centre using Fortran 90 as programming language.

The code functioning is based on the necessity by the user to define six input files which mainly contain the axial-flow compressor model under analysis and other boundary conditions which are necessary to start the flow field simulation. In particular the input files are the following:

1. *General Settings* input file which contains the general settings about the analysis that the users has to perform, such as:
    - the number of turbo-components: it should be stressed that SOCRATES manages six different types of components which are the rotor, the stator, the swirler, the inlet guide vane, the outlet guide vane and a component called duct. The latter is not a real

physical component but it is defined in the computational domain only with the purpose of setting the initialization values of the flow field for the iterative calculation where in the flow path there is not a component in the real geometry under investigation;

- the number of stream-lines along the radius of the flow path, in particular it should be used an odd number in order to have a stream-line passing in the middle of the flow passage;
- the number of boundary points which represents the number of boundary conditions specified per turbo-component;
- the number of operating points to be computed in a single running;
- the number of geometrical reference points in the blade definition per turbo-component;
- the number of blade chord locations;
- the number of blade axial points;
- the number of flow path reference points at the tip and at the hub;
- the stream-line damping factor;
- the outlet static pressure error tolerance and the inlet mass flow error tolerance.

2. *Flow Path Data* input file which contains both the maximum length and the maximum diameter of the flow path in centimetres, and two columns hosting the axial positions of the flow path tip and hub boundaries in terms of their non-dimensional z and r coordinates. The calculation procedure of these coordinates will be presented in the verification chapter.

3. *Blade Row Data input file* input file which stores the geometrical data describing the blade row in a 2-Dimensional meridional view. Also in this case each component is referenced with non-dimensional z and r coordinates of their leading and trailing edge for every radial position. In the previous version also the velocity ratios have to be specified in order to compute the blade profile loss coefficient. Now, the use of these parameters has been avoided by the model defined in this research project and described in the chapter concerning the methodology. Consequently, the velocity ratios have not to be specified in this input file any more. Finally, for each real component, also the spacing has to be specified in this input file.

4. *Blade Profile Data* input file which contains only details about the real blade row components. In particular it stores all the data needed to generate the blade profile such as:

   - the camber line interpolation type which can be a parabolic, a circular or a multiple-circular arc;
   - the thickness distribution type which can be a double-circular, a multiple-circular or a third-degree polynomial arc;
   - the stagger angle;
   - the inlet and outlet blade angles;
   - the transition blade angle;
   - the sweep and lean blade angles;
   - the non-dimensional positions of the maximal thickness, of the transition thickness along the z axis and of the maximal thickness;
   - the non-dimensional leading and trailing edge radius.

5. *Initialisation Data* input file which contains the initialisation data for the iterative procedure that leads to the calculation of the fluid properties and velocities. In particular because of the fact that at this stage of the tool development, SOCRATES does not own a proper boundary layer model in its equations, the blockage factors defined as initialisation parameters are used to simulate the boundary layer. The blockage factors are firstly guessed in order to have a first simulation, than the flow properties at the inlet and the outlet of each turbo-component are compared with the experimental data and a new set of blockage factors is determined and used for the flow field simulation. The values contained in this input file do not affect the simulation output but are necessary to make stable the code in the first iterations.

6. *Boundary Conditions* input file which hosts the data of the different operating point to be simulated. For each operating condition the user has to insert the inlet mass flow, the rotational speed and define the boundary conditions at the inlet for the absolute temperature and pressure spanwise per turbo-component.

Once specified the input files the analysis is ready to be run. In particular the procedure is an iterative one and to start the computation a meridional velocity profile and a stream-line distribution from hub to tip are assumed.
Then during the iterative procedure, given a meridional velocity profile, velocities and flow thermodynamic properties are computed for the stream-line distribution at the present iteration. Secondly the full REE is solved numerically and the meridional velocity gradient in the spanwise direction is obtained. Integrating the meridional velocity profile the stream-tube mass flow is calculated and compared against the required mass flow set by the user to identify the operating condition to be simulated. This comparison is crucial because the difference in the two values of the mass flow is used to establish the adjustment in meridional velocity and stream-line location for the next iteration. Convergence is reached once the REE and the mass flow conservation are satisfied with the specified tolerances.
Crucial in the reliable and accurate performance prediction are the loss models incorporated in the tool. In particular the model set to predict the profile losses that has been developed during this research project is described in the chapter concerning the methodology adopted.
When the convergence is reached, the tool produces seven output files which are the following:

1. *Grid Solution* output file which stores the details of the grid used during the computation. The first grid layout defined at the beginning of the iterative procedure is built considering the number of stream-lines specified and the flow path coordinates: the stream-lines are dispatched equidistantly along the radius of each quasi-orthogonal line which links the flow path tip and hub points. The number of the quasi-orthogonal lines is calculated considering the flow path axial length and they might be defined as orthogonal interpolations obtained by comparing the orthogonal lines of the tip and hub coordinates with the derivatives that describes the shape changing in the tip and hub of the flow path.

2. *Geometry Solution* and *Blade Profile Chord* output files which respectively contain the leading and trailing edge coordinates of the constructed geometry on the base of the input entered and the three-dimensional coordinates of the camber lines, pressure and suction surfaces of two consecutive blades;

3. *Flow Solution* and *Performance Chics* output files store for every turbo-component and for every operating point simulated the results of the analysis in terms of fluid velocities and fluid thermodynamic properties. These two output files are the main output of the simulation and give the designer the data to construct the compressor performance map and the fluid properties at the inlet and outlet station of each turbo-component in order to have a complete view of the compressor performance and the flow field within the simulated turbomachine.

4. *Ansys Geometry Solution* and *Blade Geometry Solution* output files store the same informations of the *Geometry Solution* and *Blade Profile Chord* output files but in a format that could be exported in Ansys in order to perform further investigations of the flow field using a 3D-CFD simulation.

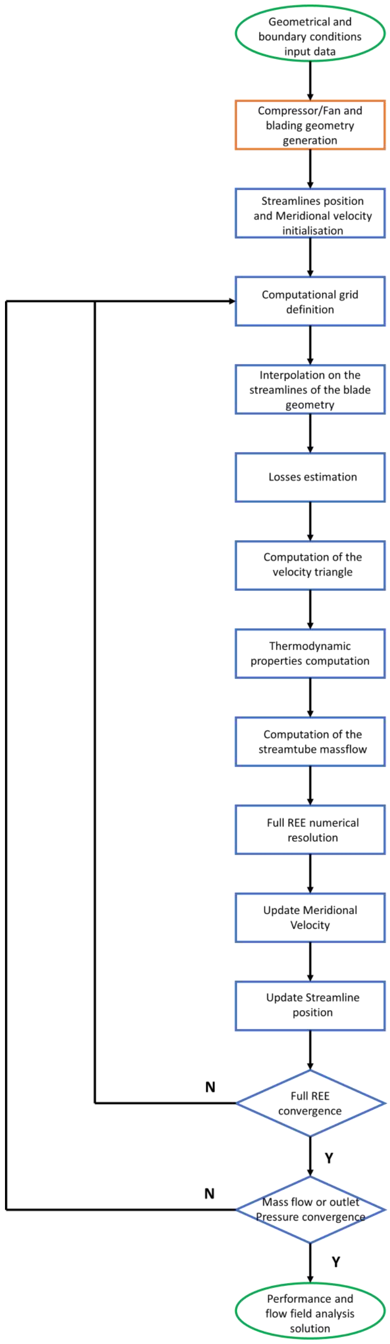

Figure 2.7: High level Flow Chart of SOCRATES

Chapter 3

Axial-Flow Fan and Compressors

3.1 Introduction

This chapter has the aim to present the literature review about some fundamental theoretical aspects concerning axial-flow fans and compressors. It will be fist presented the fundamental equations related to turbomachinery fluid-dynamics, and then follows the presentation of the velocity triangles into an axial-flow compressor, the presentation of the stage parameters, and finally it will be presented the radial equilibrium equation.
Turbomachinery is the breathing hearth of gas turbine engines and in particular, the crucial role of mechanical compression of the air in an engine is given to the compressor. Among the different compressor types, the axial-flow compressors are the most widely used into aircraft's jet engines. Into these machines the mechanical work is delivered to the fluid by a set of rotating blade rows [4]. Effectively the rotor on the one hand increases the pressure of the fluid but on the other it gives to the flow a swirl velocity. This swirl velocity component is then removed thanks to the stator blade row that is placed after the rotor. The stator blade rows are placed in between the rotor ones and they contribute to the pressurisation of the flow. The assembly of rotor and stator constitutes the compressor stage. As the main purpose of the compressor is to increase the fluid pressure, the fluid itself is subjected to an adverse pressure gradient which might cause the stall of the boundary layer, as a consequence the flow field inside the stalled compressor is completely unsteady and this flow-field condition might lead towards a compressor functional instability that is known as surge.

3.2 Angular Momentum

The angular momentum equation, usually called in the turbomachinery field also as *The Euler Turbine Equation*, is the fundamental equation in turbomachinery [4].
Let us consider a cylindrical coordinate system, in which an elementary fluid particle of mass δm is moving with a velocity composed by a radial component c_r, a tangential component c_θ and an axial component c_z as shown in figure 3.1.

The angular momentum of the particle about the z-axis can be expressed as $\delta m r c_\theta$.
Considering the coordinate system in figure 3.1 we can write the Newton's law for the particle as:

$$\vec{F} = \delta m \frac{d\vec{c}}{dt} \tag{3.1}$$

Where defining the unit vectors which identify respectively the radial, tangential and axial

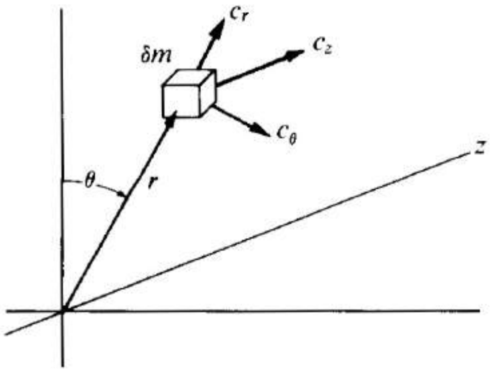

Figure 3.1: Elementary fluid particle motion into a cylindrical reference system [2]

direction as $\vec{r}$,$\vec{\theta}$,$\vec{z}$, we can express the particle velocity and the force that acts on the particle itself as:

$$\vec{F} = \vec{r}F_r + \vec{\theta}F_\theta + \vec{z}F_z$$

$$\vec{c} = \vec{r}c_r + \vec{\theta}c_\theta + \vec{z}c_z$$

Moreover the unit vectors which identify the axis directions can change their direction event though their magnitudes are constants and equal to unity:

$$\frac{d\vec{r}}{dt} = \vec{\theta}\frac{d\theta}{dt}$$

$$\frac{d\vec{\theta}}{dt} = -\vec{r}\frac{d\theta}{dt}$$

Now we have all the instruments to resolve the equation 3.1 by writing it using the components of the terms that are in the equation and we obtain:

- Equation along the radial direction

$$F_r = \delta m \left(\frac{dc_r}{dt} - c_\theta \frac{d\theta}{dt} \right) \tag{3.2}$$

- Equation along the tangential direction

$$F_\theta = \delta m \left(\frac{dc_\theta}{dt} + c_r \frac{d\theta}{dt} \right) \tag{3.3}$$

- Equation along the axial direction

$$F_\theta = \delta m \left(\frac{dc_z}{dt} \right) \tag{3.4}$$

At this point in order to obtain the expression of the torque acting on the single fluid particle considered along the z-axis, we multiply by r the equation 3.3 and considering that $c_r = \frac{dr}{dt}$ and that $c_\theta = r(\frac{d\theta}{dt})$, we obtain:

$$rF_\theta = \delta m \frac{d}{dt}(rc_\theta) \tag{3.5}$$

The equation obtained describes the time rate of change of the angular momentum of the particle which can be considered as a property of the fluid.
The equation 3.5 can be further generalised considering a control volume, using exactly an analogous procedure to the previous, the total torque acting on the control volume can be written as:

$$\sum \tau = \frac{d}{dt}\int_{cv} \rho r c_\theta dVol + \int_{cs} \rho r c_\theta (\vec{c} \cdot \vec{n}) dA \tag{3.6}$$

Where considering the right-term of the equation: the integral extended on the control volume represents the rate of change of the angular momentum stored in the control volume, while the integral extended to the control surface represents the flux of angular momentum that passes through the control volume. In particular in this integral the normal unity vector $\vec{n}$ is assumed to point outwards the control surface.
At this point, we can consider a stream-tube that enters a turbomachinery blade row [4] as shown in figure 3.2.

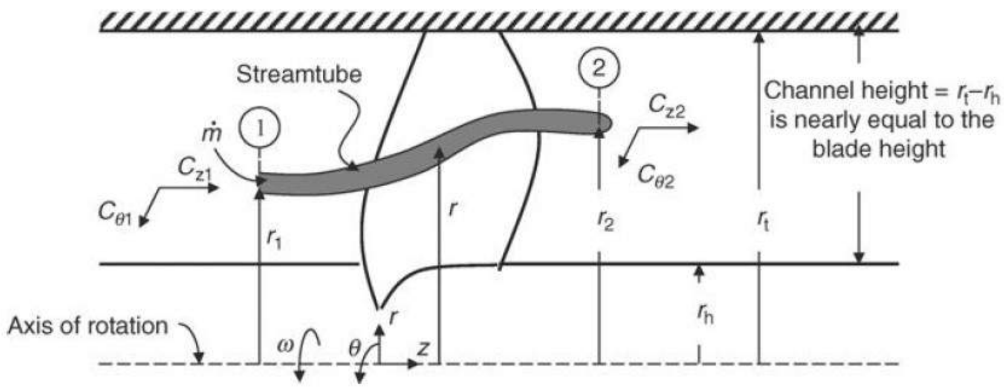

Figure 3.2: Stream-tube that enters a turbomachinery blade row [4]

Because of the blade presence and the blade row configuration, the flow within a turbomachine rotor is unsteady and asymmetric, however the unsteadiness is characterised by a periodic high frequency, hence, on average, it is possible to omit the time-dependent term of the equation 3.6 obtaining:

$$\sum \tau = \int_{cs} \rho r c_\theta (\vec{c} \cdot \vec{n}) dA \tag{3.7}$$

At this point, the following assumptions can be made [2]:

- The flow that passes through a turbomachine passage area is necessary axisymmetric, moreover the blade exerts force on the flow that produce a variation in its pressure and velocity, however upstream and downstream of the rotor, these gradients can be negligible. For this reason, because the control surface considered completely encloses the rotor, the flow at the inlet and at the outlet can be considered as axis-symmetric and steady. This assumption is reflected in the fact that both at the inlet station and at the outlet one, the velocity components are independent by r and θ;
- Because of the fact that the fluid properties can vary considerably in the radial direction, as shown in figure 3.2, we will consider the stream-tube that enters at the mean radius r_1;
- The flow will be considered as the so-called free-vortex-flow at each area that means that the product rc_θ is considered to be constant.

Making these assumptions and integrating the equation we finally obtain that the change in the fluid angular momentum between the outlet and the inlet of the stream-tube represents the torque applied on the fluid by the blade:

$$\tau_{fluid} = \dot{m}(r_2 C_{\theta 2} - r_1 C_{\theta 1}) \tag{3.8}$$

It follows:

$$\tau_{blade} = F_\theta \cdot r = -\tau_{fluid} \tag{3.9}$$

the expression is valid for the rotor as well as for the stator, however the rotor is characterized by an angular motion and the power transmitted to the fluid is:

$$P = \tau_{fluid} \cdot \omega = \dot{m}\omega(r_2 C_{\theta 2} - r_1 C_{\theta 1}) \tag{3.10}$$

Finally it should be stressed that for estimating the preliminary work, the conditions at the mean inlet and at the mean outlet radii represent suitable averages [2]. For this reason, the design procedure starts with the mean radius analysis and then the radial variation is considered to achieve refined estimations of the torque and power requirements.

3.3 Velocity Triangle

The analysis of the flow field within a turbomachine might be conducted considering two reference frames:

1. the *absolute reference frame* which is fixed and coincident with the frame of the machine;
2. the *relative reference frame* which rotates with the rotor.

In particular before proceeding it should be specified the following: the energy transfer between the blades and the fluid inside a turbomachine stage takes place in an inherently unsteady manner [4]. In particular this transmission is realised thanks to a set of rotating blades, constituting the rotor, which are three-dimensional aerodynamic surfaces that are cantilevered at the hub. The rotor is followed by the stator forming the so-called compressor stage. Also the stator blades are three-dimensional aerodynamic surfaces cantilevered from the casing. The fundamental difference is that the forces and moments experienced by the stator blades are steady and for this reason this row doesn't perform any work on the fluid.
The observer position in the previous-cited reference frames is fundamental in the description of the flow-field and of the energy exchange: the flow-field seen by a relative observer attached to

an isolated rotor in a cylinder is steady, while an absolute observer will experience an unsteady flow-field.
The use of the two reference frames is due to the related advantages in the governing equations and solution formulation. As a consequence, the relative reference frame will be employed in the flow analysis within the rotor blade row and the absolute reference frame will be employed in the flow analysis within the stator blade row. However, it should be kept in mind that in reality the flow-field in rotating turbomachinery is inherently unsteady.
The velocity components in the two reference frames are related: moreover, we observe that the tangential,or swirl, velocity is the only component that is affected by the reference frame change and consequently by the observer rotation [4].

$$Relative\,Tangential\,Velocity \;=\; Absolute\,Tangential\,Velocity \;-\Omega\cdot r$$

where the term $\Omega \cdot r$ represents the speed at which the relative observer is rotating.
Conventionally the absolute and relative velocity, that correspond respectively to the fluid velocity vectors in the two reference frames, are labelled as $\vec{C}$ and $\vec{W}$. It follows that the two vectors can be expressed in terms of their components as:

$$\vec{C} = C_r\vec{e_r} + C_\theta\vec{e_\theta} + C_z\vec{e_z}$$

$$\vec{W} = W_r\vec{e_r} + W_\theta\vec{e_\theta} + W_z\vec{e_z}$$

At this point, considering the rotor motion as a solid body rotation, we obtain that the rotor rotational velocity can be written as $\vec{U} = \omega r\vec{e_\theta}$ and the following vectorial expressions follow:

$$\vec{W} = \vec{C} - \vec{U}$$

$$\vec{C} = \vec{W} + \vec{U}$$

The vectors $\vec{W}$, $\vec{C}$ and $\vec{U}$ constitute the *velocity triangle* as shown in figure 3.3.

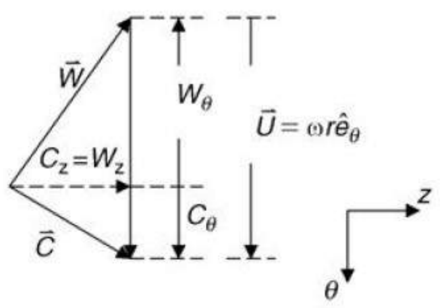

Figure 3.3: Velocity Triangle [4]

Before proceeding it should be useful to address the definition of the flow angles. In order to deal with this topic we will consider the schema reported in figure 3.4.

As observable in figure 3.4, the flow angles are defined respect to the machine axis. In particular they are indicated with α and β which respectively correspond to the absolute and relative flow velocity vectors.

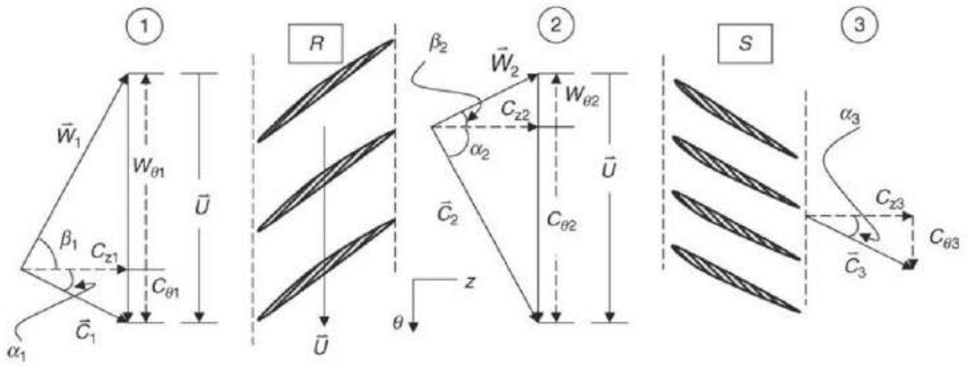

Figure 3.4: Flow Angles schema for rotor and stator at fixed radius in a compressor stage [4]

Thanks to the introduction of the flow angles, we can express the components of the absolute and relative velocity in the axial and tangential direction as follows:

$$C_{\theta 1} = C_{z1} \cdot \tan \alpha_1$$

$$W_{\theta 1} = C_{z1} \cdot \tan \beta_1$$

$$C_{\theta 2} = C_{z2} \cdot \tan \alpha_2$$

$$W_{\theta 2} = C_{z2} \cdot \tan \beta_2$$

As expectable, a turbomachinery blade row design is conducted with the attempt to maintain an attached boundary layer in normal operating conditions. Consequently, the flow angles at the exit station of the blade row are primarily related to the blade angles at the trailing edge. Hence, the exit flow angles under normal operating conditions can be considered as almost coincident with the blade trailing edge angle [4]. In parallel, the inlet flow angles change with the rotor speed.
Concerning the axial velocity components, they are related to the mass flow rate through the machine and a common design approach is to consider constant the axial velocity throughout the stages. This in reality is a simplifying assumption that loses its consistence if we take into account the wake and secondary loss effects when passing from a blade row to the other, those effects are responsible for the intrinsic 3D nature of the flow-field. Moreover this assumption might be consistent at mid-radius but the two components will not be generally equal [2] and even at mid-radius when the compressor tuns at off-design speed they may differ.
In conclusion, two of the most recurrent concepts in turbomachinery design are:

- the so-called *repeated stage* assumption: the velocity vectors at the inlet and at the exit of the stage are considered to be the same;
- the so-called *repeated row* assumption which implies that the exit relative flow angle is considered to have the same magnitude of the absolute inlet flow angle and the inlet relative flow angle is assumed to have the same magnitude of the absolute exit flow angle(assumption used in fig. 3.4).

As final remark it is important to notice that a *repeated row* assumption implies a *repeated stage* assumption but the reverse is not necessarily true.

3.4 Characteristic Performance Parameters of a Single Compressor Stage

Considering fig. 3.5 in this section we will point out the characteristic performance parameters of a single compressor stage, such as: the total temperature ratio, the total pressure ratio and the degree of reaction. Finally we will cite in this section the diffusion factor that will be addressed in more details, as also the equivalent diffusion factor, in the section concerning the compressor total pressure losses.

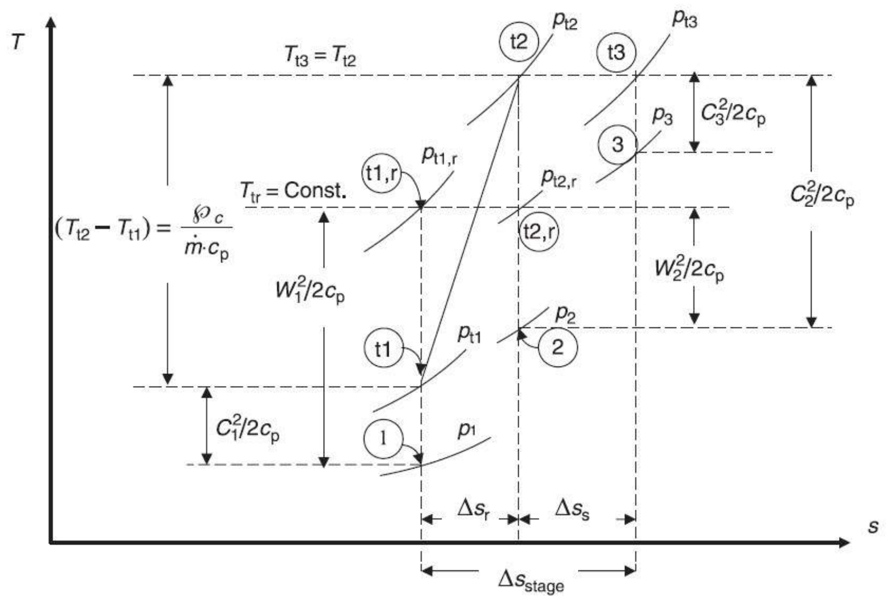

Figure 3.5: State of gas across a compressor rotor and stator [4]

Considering eq. 3.10, the ratio of the shaft power to mass flow rate is the so-called specific work of the compressor that can be expressed as:

$$w_c = \frac{P_c}{\dot{m}_c} = \Omega\Delta(rC_\theta)_c \tag{3.11}$$

The first low of thermodynamics applied to a steady and adiabatic process establishes that the change of total enthalpy of the fluid across the blade row is equal to the blade-specific work that the blade row delivers to the fluid, hence, assuming a calorically perfect gas, we obtain:

$$\frac{h_{t2}}{h_{t1}} = 1 + \frac{\Omega\Delta(rC_\theta)}{h_{t1}} = \frac{T_{t2}}{T_{t1}} \tag{3.12}$$

Note that the stator blade row doesn't make work on the fluid, in particular it works like a diffuser that reduces the velocity of the fluid, recovers the swirl velocity given to the fluid by the rotor blade row and produces a rise in the fluid pressure. As a consequence, like reported in fig. 3.5, $T_{t3} = T_{t2}$.
Replacing now the swirl or tangential velocities with the use of the relations obtained in the previous section, that involves the flow angles and the axial velocity components, we obtain:

$$\frac{T_{t2}}{T_{t1}} = 1 + \left(\frac{U^2}{c_p T_{t1}}\right)\left(\frac{C_{z1}}{U}\right)\left(\frac{C_{z2}}{C_{z1}}\tan\alpha_2 - \tan\alpha_1\right)$$

Therefore,

$$\frac{T_{t2}}{T_{t1}} = 1 + \left(\frac{U^2}{c_p T_{t1}}\right)\left[1 + \frac{C_{z2}}{U}\tan\beta_2 - \frac{C_{z1}}{U}\tan\alpha_1\right]$$

And assuming now as first design approximation a constant axial velocity design we obtain:

$$\frac{T_{t2}}{T_{t1}} = 1 + \left(\frac{U^2}{c_p T_{t1}}\right)\left[1 + \frac{C_z}{U}(\tan\beta_2 - \tan\alpha_1)\right] \tag{3.13}$$

This expression of the *total temperature ratio* can be further manipulated in order to express the ratio of total temperature as a function also of the axial Mach number M_z and the tangential Mach number M_T. For not overloading the discussion, here the author will report only the final expression, but if the reader is interested a fully detailed equation derivation is contained in [4]. In particular the final form of the equation obtained is:

$$\frac{T_{t2}}{T_{t1}} = 1 + \left[\frac{\gamma - 1}{(\frac{1}{M_T^2}) + (\frac{\gamma-1}{2\cos^2\alpha_1})(\frac{M_z}{M_T})^2}\right]\left[1 + \left(\frac{M_z}{M_T}\right)(\tan\beta_2 - \tan\alpha_1)\right] \tag{3.14}$$

Observing the equation 3.14, there are two parameters that govern the temperature ratio:

$$\tau_c = \frac{T_{t2}}{T_{t1}} = \frac{T_{t3}}{T_{t1}}$$

They are the tangential Mach number and the ratio of the axial-to-tangential Mach number. It would be useful to briefly analyse the effect of these parameters on the temperature ratio separately for given flow angles.
If the ratio of the axial-to-tangential Mach number increases, there would be a reduction in the temperature rise in the stage: the increment in the ratio of the axial-to-tangential Mach number might be due to an increase in the axial Mach number or in the mass flow rate that passes throughout the turbomachine. If the reason is the second, the augmentation in the mass flow rate keeping the blade rotational Mach number constant, there is a diminution in the blade incidence angle that lead to a drop of the total temperature ratio. The opposite effect is caused by a diminution of the mass flow rate, but in this case it should be taken into account that the diminution can not be anyone: a limitation is defined by the stall condition of the blades for a fixed shaft rotational speed. A limitation exists also in the increment of the mass flow rate and it is the so-called phenomenon of the negative stall that could manifest itself in the case of significant increasing in the inlet Mach number.
On the other hand, an increase in the tangential Mach number is followed by the stage total temperature ratio rise. The opposite is obtained in the case of a reduction of the tangential Mach number. Considering this parameter, the main limitation to its rising is constituted by the appearance of shock waves whose intensity increases with the tangential Mach number augmentation, non-linearly. The shock presence can on the one hand create an efficiency drop but on the other also can cause vibrations and centrifugal stresses in the turbomachine. In case of shock waves presence and in order to take advantage of the shock wave induced compression, proper blade design must be chosen; moreover the potential presence of bow-shocks requires much more attention from the designer.
As a consequence of the shock wave presence, wall friction, viscosity consequences (boundary layer,

wake, vortex shedding) and being the compression a real process, the entire process itself is an irreversible one. In particular the measure of the irreversibility can be quantified defining a compressor efficiency parameter. Effectively two efficiency definitions are widely used:

- *the compressor adiabatic efficiency* η_c
- *the compressor polytropic efficiency* e_c

Before defining these parameters, the stage *total pressure ratio* must be introduced. It is defined as:

$$\pi_c = \frac{p_{t3}}{p_{t1}} \tag{3.15}$$

The pressure ratio is one of the key parameters to express the performance of an axial-flow compressor or fan, being it an indicator of the effective compression work made by the turbomachine. At this point we can provide the definition of the adiabatic efficiency. In the following equations the subscript "s" will be used to indicate a quantity referred to an isentropic transformation.
In particular the adiabatic efficiency is defined as:

$$\eta_c = \frac{\Delta h_{t,isentropic}}{\Delta h_{t,actual}} = \frac{h_{t3s} - h_{t1}}{h_{t3} - h_{t2}} = \frac{\frac{T_{t3s}}{T_{t2}} - 1}{\frac{T_{t3}}{T_{t2}} - 1} \tag{3.16}$$

Considering the numerator of the equation 3.16, the temperature ratio that is present in this term can be expressed as:

$$\frac{T_{t3s}}{T_{t2}} = \left(\frac{p_{t3s}}{p_{t1}}\right)^{\frac{\gamma-1}{\gamma}} = \left(\frac{p_{t3}}{p_{t1}}\right)^{\frac{\gamma-1}{\gamma}} = \pi_c^{\frac{\gamma-1}{\gamma}}$$

Consequently, the expression of the adiabatic efficiency is:

$$\eta_c = \frac{\pi_c^{\frac{\gamma-1}{\gamma}} - 1}{\tau_c - 1} \tag{3.17}$$

The second efficiency parameter that is necessary to introduce is the polytropic efficiency e_c. This parameter is related to the adiabatic efficiency and defined as:

$$e_c = \frac{dh_{ts}}{dh_t} \tag{3.18}$$

Combining the first and second law of thermodynamics we have:

$$T_t ds = dh_t - \frac{dp_t}{\rho_t}$$

Substituting in the equation 3.18, and applying the perfect gas low we obtain:

$$\frac{dp_t}{p_t} = \frac{\gamma e_c}{\gamma - 1}\frac{dT_t}{T_t}$$

At this point integrating between the compressor inlet and outlet station, we obtain:

$$\frac{p_{t3}}{p_{t1}} = \pi_c = \left(\frac{T_{t3}}{T_{t1}}\right)^{\frac{\gamma e_c}{\gamma-1}} = \tau_c^{\frac{\gamma e_c}{\gamma-1}} \tag{3.19}$$

The latter equation obtained expresses the link between the compressor total pressure ratio and the compressor total temperature ratio:

$$\tau_c = \pi_c^{\frac{\gamma-1}{\gamma e_c}}$$

Observing the exponent of the pressure ratio in this relation it is possible to notice that the presence at the exponent's denominator of the polytropic efficiency makes the exponent itself greater than in the case of an isentropic process: this mathematical evidence has its roots in the transformation of the lost work into heat due to dissipation and irreversibility of the real process. As previously mentioned, an equation that links the two efficiency parameters defined exists and it is the following:

$$\eta_c = \frac{\pi_c^{\frac{\gamma-1}{\gamma}} - 1}{\pi_c^{\frac{\gamma-1}{\gamma e_c}} - 1} \tag{3.20}$$

Another important performance parameter for the compressor stage is the so-called *stage degree of reaction °R*. It is defined as the fraction of static enthalpy rise across the stage accomplished by the rotor [4]. However it is important to notice that although the stator does no work on the fluid, it acts like a diffuser producing a fluid deceleration, hence, causing an increment in the fluid temperature that reflects itself in an increment of the static enthalpy.
Effectively the degree of reaction measures the rotor share of the stage enthalpy rise as compared with the burden on the stator [4], and it is expressed by the following equation:

$$^\circ R = \frac{h_2 - h_1}{h_3 - h_1}$$

Usually the magnitude of this parameter is desirable to be around $0.5 \div 0.6$: this kind of split among the two stage components is based on the fact that a boundary layer on a spinning blade like the rotor one, is more stable then a corresponding boundary layer on a stationary blade like the stator. Further information and details about the equation possible further development are not reported here, where the parameter is only cited, but they can be found in [4] if the reader is interested.
Finally the last parameters that are important to mention in this paragraph but that will be presented in details in the section concerning the compressor losses are the *Diffusion Factor D* and the *Equivalent Diffusion Factor D_{eq}*. Both these parameters are important figures of merit for a blade row giving an indication on the aerodynamic loads on the blade itself. In the open literature they are expressed in function of design velocity ratios, obliging to provide a different definition for the rotor and the stator blade rows. The new model developed based only on geometrical parameters eliminates this necessity providing a unique definition for the Equivalent Diffusion Factor to be used in the blade profile loss estimation.

3.5 Radial Equilibrium

Considering that in the equations previously derived we ignored any radial variation in the flow through the compressor annulus, but the attention was restricted at the mean-radius, in order to establish a satisfactory compressor design[2], the designer has to consider the radial variations in blade speed U, axial velocity c_z, swirl or tangential velocity c_θ and static pressure.
The radial variations in the blade speed are connected to its definition $U = \Omega \cdot r$. Considering the axial velocity, at the inlet it might be considered quite uniform, but, this consideration is not applicable after the fluid has passed through two or three stages. In parallel, the tangential velocity variation is due to how the blade angles vary with the radius[2].
A little more elaborate is to express the dependency of the radial pressure gradient from the

absolute tangential velocity component. In order to derive this dependency, let us consider the schema in figure 3.6.

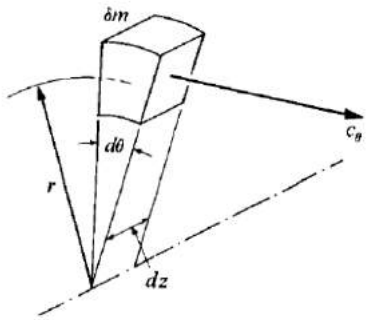

Figure 3.6: Tangential motion of an elemental fluid element [2]

Considering a fluid element, the equation that links the total radial acceleration of the fluid element and the radial pressure applied on the latter is:

$$F_r = -\delta m \left(\frac{c_\theta^2}{r} \right)$$

Being that:

$$F_r = -\frac{\partial p}{\partial r} \cdot r \cdot drd\theta dz$$

$$\delta m = \rho r \cdot drd\theta dz$$

We obtain that:

$$\frac{\partial p}{\partial r} = \rho \frac{c_\theta^2}{r} \tag{3.21}$$

The equation 3.21 is labelled as *the simple radial equilibrium equation*; and actual velocity distributions have to satisfy this relationship at the entrance and exit of each blade row[2].
Maintaining a uniform work input along the radial length of a rotor gives the possibility to achieve a reasonably uniform flow at the exit of the compressor.
Being the variation in total enthalpy along a stream-line through an axial-flow compressor stage $\Delta h_0 = U \Delta c_\theta$, the radial gradient can be expressed as:

$$\frac{\partial}{\partial r}(\Delta h_t) = \Omega \frac{\partial}{\partial r}(r \Delta c_\theta) \tag{3.22}$$

That highlights the fact that the product $r\Delta c_\theta$ must be constant with the radius in order to keep constant the fluid total enthalpy.
Various configurations that satisfy this requirement have been proposed in [5]. Regarding the radial angular momentum distribution as a design choice, that will affect the velocity triangles configuration directly, it is possible to choose among:

- *Free Vortex* design configuration

$$rc_\theta = a$$

- *Forced Vortex* design configuration
$$rc_\theta = ar^2$$
- *Exponential* design configuration
$$rc_\theta = ar + b$$
- *Constant reaction* design configuration
$$rc_\theta = ar^2 + b$$

The coefficients a and b in these equations are constants. More precisely, a is a positive constant while the constant b could be either positive or negative.
Expressed the different design configuration available, finally, it is necessary to express the radial equilibrium requirement in terms of velocity. Starting from the state equation:

$$T\frac{ds}{dr} = \frac{dh}{dr} - \frac{1}{\rho}\frac{dp}{dr} \tag{3.23}$$

And considering that:

1. the total enthalpy can be written as $h_t = h + \frac{c_\theta^2 + c_z^2}{2}$ with $c_r^2 << c_z^2$;
2. we can assume that the radial gradients of entropy and total enthalpy are zero;

We obtain that:

$$\frac{d}{dr}(c_z^2) = -\frac{1}{dr}(rc_\theta)^2 \tag{3.24}$$

That relates the radial gradient of the angular momentum with the axial velocity component.

Chapter 4

Cascade Aerodynamics

4.1 Cascade Aerodynamics

Aim of this section is to present the literature review about the fundamental aspects of one of the more complex topics in turbomachinery: *The Cascade Aerodynamics.* Clearly this argument is a very widespread one, consequently, the aspects that will be reported in this section are the ones functional to the whole discussion. However if the reader is interested, further informations and a more complete treatment of the topic can be found in [1],[4] and [2].
In general, a cascade is defined as a stationary array of blades constructed for blading performance measurement in order to simulate the blade rows used in axial-flow compressors.

In particular as shown in figure 4.1, the cascade is characterised by the presence of the end-walls, however, they are usually porous and suction is applied in order to reduce the wall boundary layer thickness in the attempt to obtain a flow between the blades as much as possible nearly the two-dimensional [2]. Consequently it is important to notice that the study of the flow over the blades is conducted in controlled conditions that exclude the effects of the end-wall boundary layer and the radial velocity variations, that instead are present in an axial-flow compressor blade row and should be carefully taken into account for an accurate loss-mechanisms modelisation and performance prediction. Nevertheless, the measurement conducted in the cascade are aimed at relating the fluid turning angles to the blade geometry characteristics and at measuring the losses in total pressure due to friction and blade characteristics and interactions between the various flow field phenomena. The experiments conducted during the years using this methodology have clarified the effects of the boundary layer separation[1] and the blade performance sensitivity to Reynolds and Mach number.
Before going deeper in the topic presentation, it would be important to briefly analyse the principal cascade parameters, reported also in 4.1c. The first parameter to mention is the *cascade solidity* σ defined as the ratio of chord-to-blade spacing:

$$\sigma = \frac{c}{s}$$

Having a look at this parameter it might be noticed that an high solidity blading is characterised by an higher net turning angle than a low solidity one, hence, an high solidity cascade is less susceptible to stall[4].

[1]That becomes evident when the fluid exit angle is markedly different from the blade exit metal angle and the stagnation pressure is substantially greater than its minimum value[2].

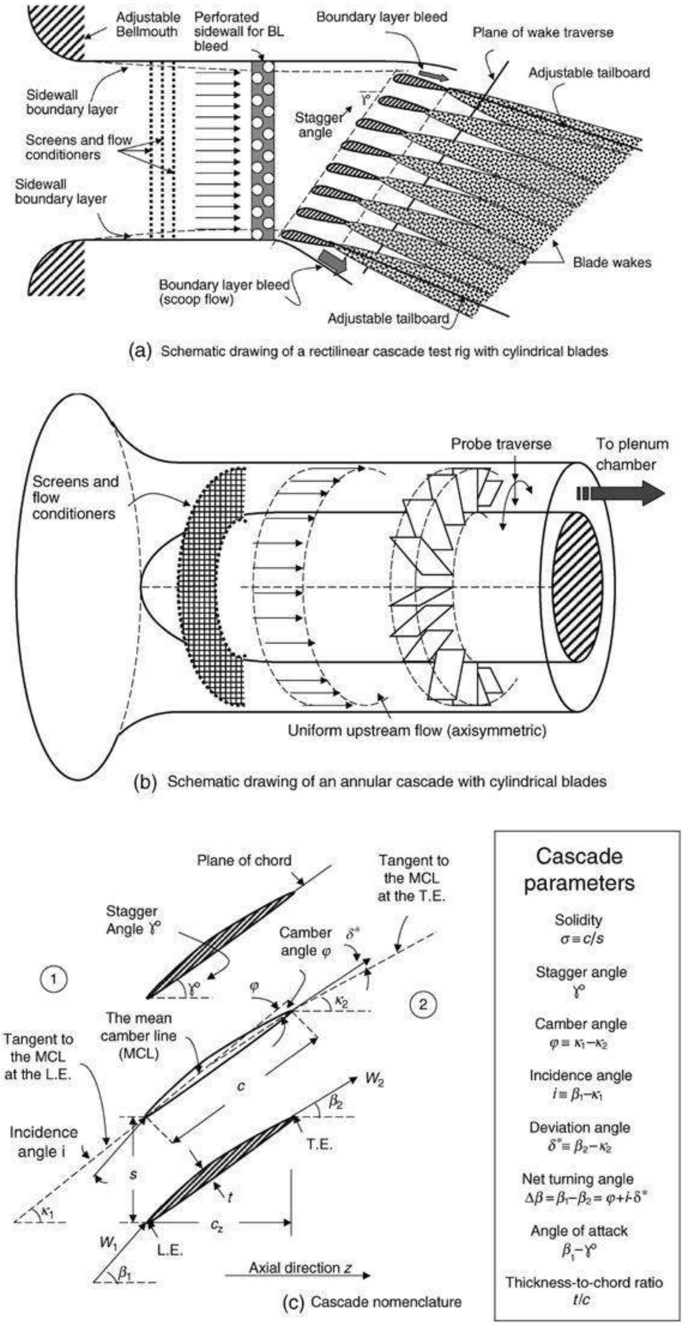

Figure 4.1: Cascade schema and parameters [4]

The second parameter to consider is *the mean camber line angle* that is used at the leading and trailing edge as a reference parameter in order to measure respectively *the inlet flow incidence angle* i and *the outlet flow deviation angle* δ^*. The first of the latter two parameters is defined as the flow angle between the tangent direction to the mean camber line and the relative velocity vector at the blade row inlet. In particular it is possible to define an *optimum inlet flow incidence angle*

as the value for the incidence angle that produces the minimum losses in terms of total pressure across the blade row.
Another parameter to be introduced for the cascade is the so-called *camber angle* ϕ, defined as the angle formed at the intersection of the two tangent to the mean camber line at the leading and trailing edge[4]. It might be interesting to notice that a cascade with an high camber angle could be affected by a large flow turning that might result into an higher sensitivity of the cascade to flow separation. This tendency is increased by the adverse pressure gradient that the flow observes while passing through the compressor blade rows. Consequently, a compressor blade is characterised by a lower value of the chamber angle if compared with a turbine where it is possible to have an higher magnitude for this angle also because of the favourable pressure gradient experienced by the fluid. The blade chord angle with respect to the axial direction is labelled with the symbol γ and referred to with the name of *stagger angle* or sometimes also with the name of *blade-setting angle.* Because of the fact that the blade rotational speed increases linearly with the radius, the blade stagger angle increases with the radius. Moreover it should be mentioned that the difference between the relative inlet flow angle and the stagger angle is defined as the *angle of attack.* And finally, as last parameter to be introduced, *the net turning angle* is defined as the difference between the inlet and exit flow angles.

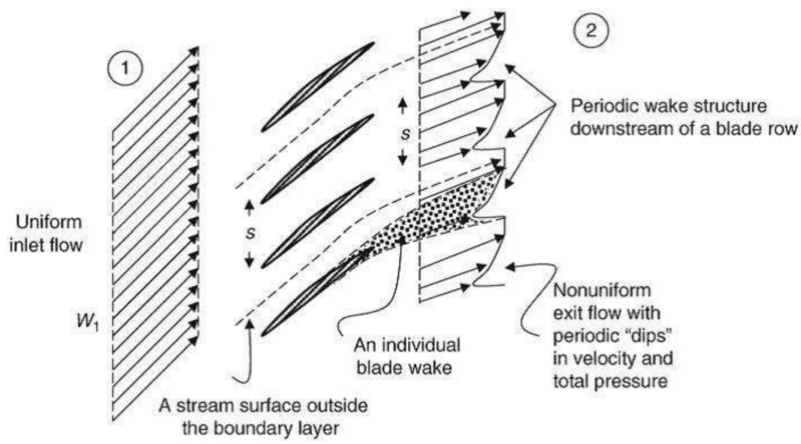

Figure 4.2: Wake-velocity profile [4]

The cascade flow field is characterised by the presence of the boundary layer, the wake, the wakes' interaction, tip vortex, trailing edge vortex, possible presence of shock waves and a wide range of other phenomena responsible for the production of the total pressure loss ω that, making reference for the subscripts stations to the figure 4.2, can be defined as follows:

$$\omega = \frac{p_{t1} - p_{t2}}{\frac{\rho_1 W_1^2}{2}} \tag{4.1}$$

The typical shape of the total pressure losses is shown in figure 4.3.

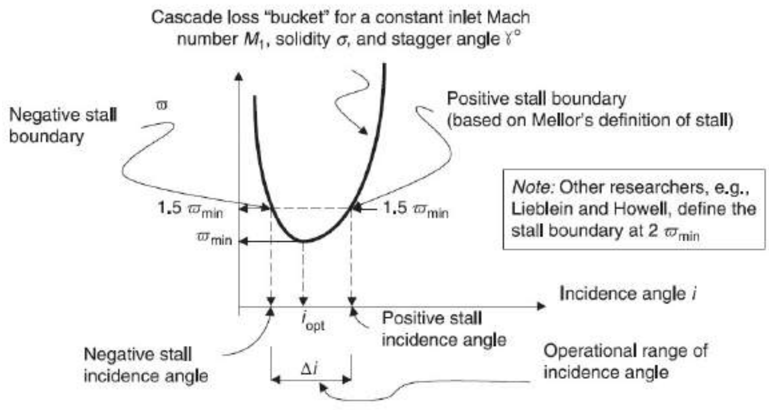

Figure 4.3: Typical Compressor Loss Shape [4]

The mechanisms and phenomena that are responsible for these losses in total pressure will be analysed in details in a separate section, in particular the last of this chapter, where also the literature review about their modelisation will be provided. In the present section the discussion about the cascade aerodynamics will remain at a more general level to present the fundamental aspects related to the topic.
Interesting to notice in the aerodynamic analysis of a cascade is that the range of "possible" flow angles, which may be exploited, is limited by the stall[2].
The *stall* might be defined as the result of boundary layer separation on the blade surface. Effectively the separation of the boundary layer is responsible for the production of a thicker wake. Being on its hand the wake a region characterised by a deficit in total pressure representative of the dissipation occurred, it appears clear that the stall creates a rapid increasing in the pressure loss across the blade row. Consequently the designer should carefully examine the wake profile downstream the blade row to quantify the total pressure loss related to it, nevertheless the wake represents one of the most challenging flow field to be modelled due to its inherent 3D nature and presence of streamwise vortices and turbulent mixing regions. This phenomena can be observed either in case of excessive increasing of the inlet flow angle and in this case it is labelled as *Positive Stall*, and in case of excessive decreasing of the inlet flow angle and in this case it is observed the so-called *Negative Stall*. Respectively the boundary layer separation takes place on the pressure or on the suction side of the blade. However it is important to stress the fact that in a compressor blade row, the blade profile drag is only one of the sources of total pressure loss, other sources such as the end-wall boundary layer and the so-called secondary flows must be taken into account and a detailed description of these loss mechanisms will be provided in the following section.
Moreover the effect of Reynolds and Mach number should be considered in order to have an accurate model of the cascade flow field. In particular defined the cascade Reynolds number as:

$$Re = \frac{\rho_1 W_1 c}{\mu_1}$$

In case of Re of magnitude of 10^6 or greater the loss coefficient changes very little with change in Reynolds number[2]; but if a critical value is reached the loss coefficient starts to rise, perhaps sharply, as the Re decreases: it should be put in evidence that the magnitude of the previous mentioned critical value is strongly related to the free-stream turbulence. In particular the loss rise with lower Reynolds number in the cascade is related to the property of the boundary layer that at low Re values is more likely to be laminar and consequently more susceptible to separation.

Considering at this point the effects of Mach number, when the flow moves-around the convex surface of the blade, it is subjected to an expansion process. The flow accelerates and if the magnitude of the acceleration is enough it can reach a transonic or supersonic regime. This means that a shock wave may appear: it has been demonstrated with experimental studies that the shock wave appears at values of the upstream Mach number of 0.75, and even at lower values if the inlet relative flow angle increases[2]. The appearance of the shock wave introduces another total pressure loss source category: besides the losses introduced by the shock wave itself, now it is also necessary to consider the shock-boundary layer interaction, the possible presence of a detached shock if the Mach reaches higher values, the possible interaction of shock waves and other secondary flow phenomena induced by the shock wave presence that contributes to the rise of the total pressure loss across the cascade.
Finally as a conclusion for this section, being previously said that the blade passage of the compressor blade row acts "like" a diffuser, it would be extremely important to state the main differences between these two flow fields, mainly because of the fact that the nature of the compressor end wall boundary layer and its stalling characteristics are more complex than a simple diffuser. The main differences between the two flow-fields are the followings:

1. Compared to the diffuser case, for a compressor, the presence of large streamwise and radial pressure gradients leads towards a higher 3-Dimensional flow separation;
2. In a diffuser the relative motion between adjacent blade rows is absent, as a consequence the inherent unsteadiness connected with this relative motion is absent;
3. In a diffuser the absence of the blade rows is clearly related to the absence of the blades wake presence and interaction;
4. The formation of end wall regions secondary vortex and scraping vortex structures is absent in a diffuser.

4.2 Loss Mechanisms

The flow field inside a turbomachine is one of the most complex being it compressible, viscous, 3-Dimensional and unsteady. Due to its characteristics, several loss mechanisms appear and render the flow process in a turbomachinery stage irreversible. In particular before describing them, it would be useful to consider the following classification[4]:

- End wall losses
    1. Secondary flow losses
    2. Tip clearance losses
    3. Labyrinth seal and leakage flow losses
- Shock losses
    1. Total pressure losses
    2. Shock-boundary layer interaction
- Blade wake losses
    1. Viscous profile drag
    2. Induced drag losses

3. Radial flow losses

- Unsteady flow losses
   1. Upstream wake interaction
   2. Vortex shedding in the wake
- Turbulent mixing

The complexity of the situation described by this list is raised up by the 3-Dimensional interactions between the various flow phenomena.
Going deeper in the details, the no-slip condition imposed by the wall to the fluid is responsible for the presence of velocity gradients that activates the viscosity effects resulting in the presence of a flow field known as boundary layer. The flow within the boundary layer is subjected to a velocity gradient and as a result the flow viscosity retards the flow within the boundary layer through a friction-induced shear stress that on its hand produces an entropy rise that reflects in a loss production. Moreover the flow field inside an axial-flow compressor is subjected to an adverse pressure gradient. Under this condition the boundary layer tends to grow faster until it separates. This tendency is accentuated because of the fact that in a compressor the chord-wise flow-diffusion slows down the velocity distribution normal to the blade surfaces, hence, increasing the boundary layer thickness and thus, raising the friction-force-induced losses[11]. In this scenario there is an element that has still to be considered: the rotation of the rotor blades is responsible for the introduction of unsteadiness[13] in the flow field producing an intermittent air flow resulting in a cyclic wake appearance and in a non-constant but periodic back pressure. Consequently the blade operates in an unsteady pressure field that results in what is often labelled as *unsteady potential interaction*. Being the blade an elastic structure the vibrations in bending, twist and torsion are inevitable. These vibrations create a spanwise variation of the incidence angle, hence, they produces an unsteady lift with a subsequent vortex shedding in the wake[4], figure 4.4. These losses, as mentioned also in the previous paragraph, are strongly influenced by the Reynolds number: in particular the loss rise with lower Reynolds numbers in the cascade is related to the property of the boundary layer that at low *Re* values is more likely to be laminar and consequently more susceptible to separation.

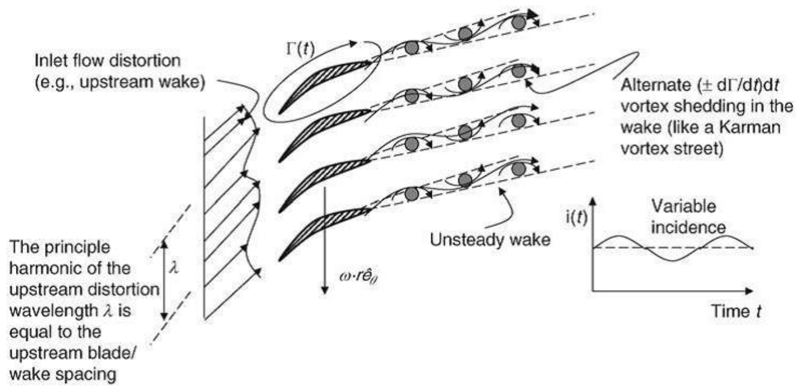

Figure 4.4: Periodic vortex shedding in the wake [4]

Considering at this point the category of the *end wall losses*, it includes the losses connected with the annulus boundary layer, corner vortex, tip clearance flow(figure 4.5) and the seal leakage flow. These loss mechanisms together with the spanwise mixing are often labelled also as *Secondary losses*.

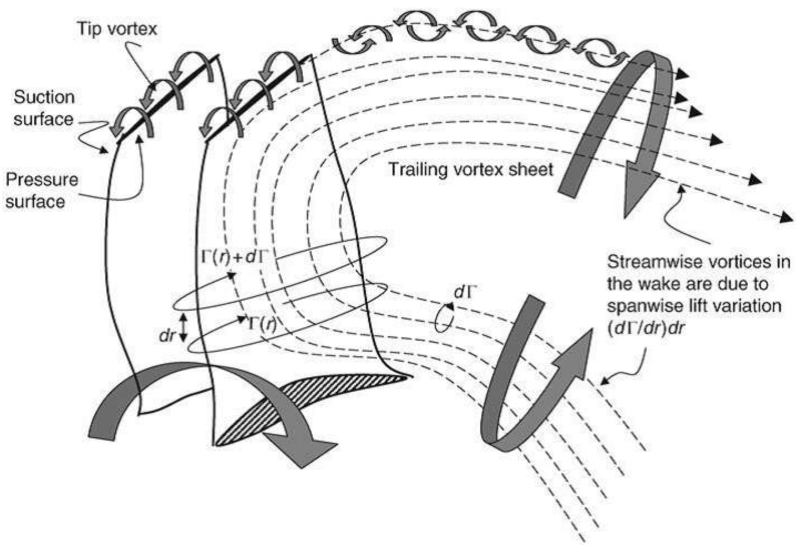

Figure 4.5: Tip clearance flow schema [4]

Observing more in details the end-wall losses category, we can notice that the tip clearance flow is a pressure-driven phenomenon that relieves the fluid on the pressure side towards the suction surface. Secondly, the boundary layer formation on the annulus, as observed also for the blade boundary layer, is expected to grow with the distance and under the effect of the adverse pressure gradient. Howell[14] demonstrates the growth of the boundary layer with the number of stages due also to the continuous deformation of the axial velocity distribution. Moreover the end-wall interactions between the annulus wall boundary layer and the blade rows lead to tip clearance flow and corner separation[11].
Moreover the corner separation at the shroud and at the hub might produce corner vortices at the latter.
The effect of the secondary flows might be increased in case of further disturbance from other flow phenomena such as unsteady inlet conditions, inlet end-wall boundary layer thickness and flow skew.
The losses addressed up to this point represent the main total pressure loss mechanisms in a subsonic axial-flow compressor, but, in the case of a transonic one, additional losses are observable. The shock waves presence and their interactions with the flow itself, between them and with the boundary layer, represent additional loss mechanisms to be taken into account in this kind of turbo-machines. Starting from the shock wave itself, it can be defined as *"a sharp change of pressure in a narrow region travelling through a medium, especially air, caused by explosion or by a body moving faster than sound"*. The disruptive change in pressure, temperature and density of the flow is the result of this irreversible phenomenon, thus, responsible for an entropy rise and, hence, for a loss production. In fact by definition, a shock wave is a dissipative phenomenon observable under particular conditions in a flow field. In a transonic axial-flow compressor or fan, depending on the inlet Mach number of the blade row considered, two type of shock waves are observable: a detached bow shock wave and a passage shock wave.
The presence of a bow shock wave is observable for really high inlet Mach numbers, and, produces an extremely strong compression making the flow passing from the supersonic to the subsonic regime. The bow shock waves might interact producing regions whit an extremely complex shock wave configuration that produces an output flow characterised by different directions according to

the point in which it has intercepted and interacted with the shock wave. The subsequent acceleration on the blade surface could lead the flow again to be supersonic and creating the conditions for the manifestation of the so-called passage shock wave.
However, as mentioned before, the blade surface is characterised by the presence of the boundary layer and consequently the interaction between the latter and the passage shock wave is inevitable. The presence of the shock wave magnifies the adverse pressure gradient magnitude, consequently the boundary layer thickness increases faster and this can eventually result in reverse flow, generating a separation bubble and contributing to the aerodynamic losses. Moreover the interaction could result also in the buffeting phenomenon, which represents a shock wave instability due to the interaction of the latter with the boundary layer: it results in a periodic oscillation of the shock wave position that has two main consequences. On the one hand it introduces unsteadiness in the growth of the boundary layer augmenting the probability of separation and reverse flow creation, however, on the other hand it is responsible also for the creation of aeroelastic loads on the blade and vibrations stresses.
After the interaction with the shock wave, the boundary layer could reattach or not before the trailing edge: in the case of no reattachment the wakes dimension increases downstream of the trailing edge and losses are raised.
To be taken into account is also the spanwise flow migration that occurs at the blade suction side downstream the passage shock wave. Radial flow motion forms a low-momentum region at the blade trailing edge contributing to the thickening of the boundary layer and hence, building up for wake development, leading to an unfavourable stability by shortening the engine working range[11].
Finally it should be necessary to consider the interaction between the secondary flows and the shock wave because of its high influence on the entropy production. According to Biollo and Benini[15], the pressure gradient between the suction and pressure side pulls up the flow towards the tip surface, consequently a jet is generated throughout the main flow and the result of the interaction is the production of a vortex labelled as tip-clearance or tip-leakage vortex. This phenomenon is responsible in particular for a decrement in rotor performances. This is the result of its development in the passage area after the manifestation at the leading edge: within the passage area it interacts with the passage shock wave and with the casing boundary layer creating a loss rise. Moreover, if the compressor operating point moves towards the surge condition, the unsteadiness connected with this condition increases the blade loading and inducts a tip-clearance vortex breakdown, defined as a sudden change in the vortex core structure[16]. As a consequence a blockage near the blade tip and oscillations occur leading to rotor functioning instability due to the production of shock-induced separation that varies in time.

The pressure losses due to entropy generation inside a transonic axial-flow compressor can be quantified as the pressure difference between the ideal outlet total pressure and the actual outlet total pressure, and reported to the inlet pressure conditions as:

$$\omega = \frac{p_{t2\,ideal} - p_{t2}}{p_{t1} - p_1} \tag{4.2}$$

By definition, the ideal outlet total-pressure is equal to the inlet uniform total pressure because of the fact that the ideal situation is characterised by the absence of total pressure losses, hence, we obtain:

$$\omega = \frac{p_{t1} - p_{t2}}{p_{t1} - p_1} \tag{4.3}$$

Using at this point the isentropic relation between the total and static conditions, and considering the relative frame of reference for the rotor case, the total-loss coefficient or factor transforms in:

$$\omega = \frac{1-\pi_c}{1-\left(1+\frac{\gamma-1}{2}M_1'^2\right)^{\frac{\gamma}{1-\gamma}}}$$

Where π_c represents the total-pressure ratio between the inlet and the outlet.
As a result of the analysis of the present section on the loss mechanisms, the total loss coefficient can be expressed as the summation of the different source-loss coefficients:

$$\omega = \omega_{profile} + \omega_{shock} + \omega_{secondary\ sources} \tag{4.4}$$

Finally, it should be stressed that suddenly in the literature this coefficient is redefined according to the model proposed by the author. Under this point of view, while the coefficients representing the blade profile and shock wave losses are usually provided with the same definition, the coefficient of the secondary sources is more widely subject to changes according in particular to the secondary loss mechanisms considered in the model.

4.3 Blade Profile Loss Models in the open Literature

This paragraph has the aim of providing the literature review of the correlations available in the open literature concerning the blade profile loss modelling. The shock and secondary losses will not be considered being them out of the perimeter of this research project. Nevertheless, as underlined before in the introduction, the shock losses will be taken into account for compressor performance prediction thanks to the use of the model developed in [11] and already implemented in SOCRATES. The secondary losses will not be taken into account in this research project whilst their consideration would be necessary for a more accurate performance prediction, in particular under the efficiency point of view. This consideration would be clarified later and its consequences observable in the model application to the NASA two stage transonic axial-flow compressor.

Through-flow calculation codes represent the most important tool of the compressor aerodynamic designer. Their main objective is to provide a spanwise prediction of thermodynamic and other flow properties so that suitable blade profiles can be selected [17]. They could be either of analysis or design type. In the former case, which is the more extensively used, the blade geometry is specified and solutions are sought for the resulting flow pattern. To determine realistic solutions with both techniques, the reasonable prediction of entropy gradient resulting from viscous effects is crucial. Moreover the solution obtained from an analysis program is very dependent upon the predicted values of blade exit flow angles[17]. Hence, loss and deviation models are crucial to perform a prediction of the overall turbomachine performance. Effectively, the very complex flow field has made almost impossible to resolve the loss and deviation angle theoretically, thus, it follows the necessity to introduce empirical correlation and prediction methods determined from statistics-based two-dimensional cascade ring-test data to be used for the total-pressure loss estimation.

The first study to mention, is the one made by Howell[14]. He tried in 1945 to estimate the loss in terms of the familiar drag and lift coefficients used for aircraft analysis. He defines the drag coefficient for the determination of the efficiency as:

$$C_D = C_{D\ p} + C_{D\ a} + C_{D\ s}$$

Where $C_{D\ p}$ is the profile drag coefficient obtained from cascade tunnels, $C_{D\ a}$ is the annulus drag coefficient corresponding to friction on the walls of the annulus, and $C_{D\ s}$ covers all the secondary losses contribution. The drag coefficient was then related to the pressure loss coefficient. The technique proposed by Howell was then substituted by the work made by Lieblein.

The studies of S. Lieblein[18][19] have represented a milestone in the development of empirical correlation models for blade profile loss prediction and modelling. In particular Lieblein introduced two indicators of the blade loading to be used in the loss estimation. Respectively in 1953[19] he introduced the definition of the diffusion factor D and in 1959[18] he introduced the definition of the equivalent diffusion factor D_{eq}. Both these factors are a function of the maximum relative flow velocity in the blade passage, and also function of the relative inlet and the relative exit flow velocities. In particular Lieblein defined them as[2]:

$$D = \left(1 - \frac{V_2}{V_1}\right) + \frac{\Delta V_\theta}{2\sigma V_1}$$

$$D_{eq} = \left(\frac{V_{max}}{V_1}\right) \frac{V_1}{V_2}$$

The definition reported in Lieblein paper-works considers the velocity to be taken relative to the blade. Those definitions in this form are clearly applicable to a rotor blade row, and in order to be used also for a stator one, the relative velocity ratios have to be substituted by the corresponding absolute velocity ratios.
The diffusion factor and the equivalent diffusion factor were used by Lieblein to estimate the boundary layer momentum thickness, on its hand used then for the blade profile loss coefficient estimation. The fundamental state of Lieblein contribution was that he showed that the losses around a blade profile are connected to the boundary layer momentum thickness, and as the aerodynamic loading on a compressor blade increases, the diffusion on the suction surface increases while the diffusion on the pressure side stays approximately constant. The correlations and equations developed by Lieblein were obtained from studies done on purely 2-Dimensional, low speed cascades with $NACA\ 65 - (A_{10})$ and British $C4$ circular arc blade profiles.

The methodology developed by Lieblein was then used also by Koch and Smith[20] in 1976. Nevertheless they performed operations similar to the one performed by Lieblein, the model presented was the most comprehensive proposed until that time. Effectively they took into account for compressibility, Reynolds number and stream-tube contraction effects found in real axial-flow compressors. In devising the model, they identified four primary sources of losses: blade profile losses due to surface diffusion and trailing edge thickness, losses due to end-wall boundary layers and clearances, shock losses ad losses due to part-span shrouds[20].

Subsequently in the 1980 Starke[25] produced an adaptation of the purely two-dimensional correlations developed by Lieblein in order to take into account also the characteristics of the quasi-two-dimensional flow to increase the accuracy of the prediction of the flow field observable across axial-flow compressor blade sections.

After a couple of years, in the 1993, Denton[21] proposes a model based on the assumption that conceptually the loss could be considered equivalent to entropy production. Effectively Denton emphasized the fundamental necessity to understand the physical origin of loss rather than to rely on conventional empirical correlations. As a result, the two-dimensional estimation of the loss coefficient is in function of the total entropy produced in the boundary layer by the mass flow rate

[2]The symbols used are the same of the ones used in his previous cited paper-works.

and a reference dynamic head[21].

Considering the field of transonic axial-flow fans and compressors, correlations were developed respectively by Swan[22], Cetin et al.[17], König et al.[23] and Roy and Kumar[24]. Their studies were based on the same methodology used by Lieblein. In the 1989, Cetin et al.[17] evaluated a wide range of empirical correlations available until that time defining a complete set for the axial-flow compressor performance prediction capable of producing accurate and reliable results. They based their work on the one of Koch and Smith[20], Carter[27][28] and Creveling[26], proposing a new empirical correlation for the off-design loss prediction and for the minimum loss incidence angle.
In particular König et al.[23] proposed a blade profile loss model both for the subsonic flow and for the supersonic flow field. Stated that new blading concepts, as used in modern transonic axial-flow compressors, require improved loss and deviation angle correlations. They proposed a model that treats the blade-row flow fields having subsonic and supersonic inlet conditions separately. Respectively starting from the previous results of Cetin et al.[17], they first extended the profile loss correlations for subsonic flow field to quasi-two-dimensional conditions and to custom-tailored blade designs[23] improving the prediction accuracy. Secondly they focused on the extension of the correlation developed by Gustafson[29] for cascade losses with supersonic inlet flow fields originally developed for DCA blades and adapted to blade rows having low-cambered, arbitrarily designed blades including pre-compression blades.

Thereafter in the 1997 Schobeiri[30][31] presented a new loss model for reliable efficiency calculation of high-subsonic and transonic compressor stages. The model pays special attention to shock and profile losses, since they contribute significantly to the total pressure loss balance, specifically for transonic compressor stages[30]. Nevertheless for the conditions considered by Schobeiri his correlations seem accurate, but some corrections are needed in case of considering different inlet flow conditions limiting the generality of the model proposed.

In recent years, new CFD-based correlations have been developed, examples are the ones proposed by Kim et al.[32] and by Xiaoxiong et al.[33]. These models provide accurate results if compared to the CFD data on which they have been calibrated, as obvious. However, the CFD results are on their hand affected by the turbulence model chosen and by the settings defined by the designer. As a consequence the generality and accuracy of these models appears to be limited and their use could be considered only in conditions that reflects the same boundary conditions set for the CFD simulation. If this doesn't happen, the results and predicted performance from those models have to be evaluated carefully before attesting their accuracy and reliability.

Of interest is also the model proposed by Liu et al.[34]. Their paper presents a model for predicting the reference minimum-loss incidence and deviation angles of a blade arrangement with splitter vanes, which is probably a solution for future ultra-highly loaded axial-flow compressor designs[34]. In particular they firstly propose basic correlations for the model considering the blade loading, camber angle and solidity. Then, geometric and aerodynamic corrections are introduced and three-dimensional effects are empirically incorporated. According to what reported in the paper-work[34], the model is able to provide accurate and reliable predictions for the minimum-loss incidence and deviation angle.

Clearly, this sections reports only the most important correlations found during the literature review phase for the present research project and has not the purpose to provide a complete and detailed catalogue of all the correlations available in the open literature.

Chapter 5

Methodology: Profile Loss Model Definition

5.1 Introduction

This chapter focuses on the presentation of the profile loss model defined to have the blade profile loss coefficient estimation to be used in the performance prediction of axial-flow fans and compressors.
As the reader can notice the set defined to achieve the estimation of the blade profile loss coefficient is composed by several models chosen from the open literature with which the new models developed during this research project have been coupled.
The set defined has been used in the through-flow SLC tool SOCRATES. After a calibration procedure applied to the model, it has been verified against the previous set defined in the tool, validated and then applied to a two-stage transonic axial-flow compressor. The latter three steps are described in the following chapter sections.
It should be highlighted that the model defined and improved in this research project focuses on the estimation of the blade profile losses for axial-flow fans and compressors. These are then summed with the shock losses to have the estimation of the total loss coefficient. All the losses coming from the secondary flow effects were not added separately using other models available in the open literature. Clearly, an important step to push further the tool development should be to incorporate a modelisation of those effects maybe defining new models or incorporating models taken from the open literature. This would probably lead to an increasing in the level of accuracy for the compressor performance prediction in the case of multi-stage configurations with more then three stages.

5.2 Design Incidence Angle

The model used for the estimation of the design incidence angle is the one reported by Aungier[1] and developed by Lieblien.
Considering the figure 5.1, it might be noticed that the flow enters the cascade with a relative velocity W_1 and with a flow angle β_1 respect to the axial direction. Indicating with κ_1 the blade inlet angle respect to the axial direction, the incidence angle is defined as:

$$i = \beta_1 - \kappa_1 \tag{5.1}$$

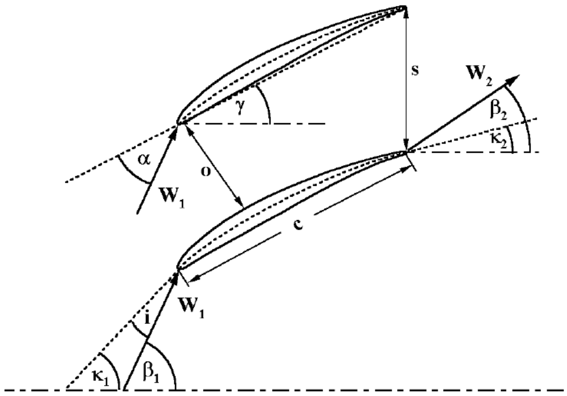

Figure 5.1: Cascade Nomenclature [1]

As reported by Aungier, in the 1960 Lieblein developed a correlation to estimate the design incidence angle which is defined to be the minimum loss incidence angle using the following equation:

$$i^* = K_{sh} K_{t,i} (i_0^*)_{10} + n\theta \tag{5.2}$$

Where

- θ is the blade profile camber angle;
- n is the slope of the variation in incidence with camber computed as:

$$n = 0.025\sigma - 0.06 - \frac{\left(\frac{\beta_1}{90}\right)^{(1+1.2\sigma)}}{1.5 + 0.43\sigma}$$

- the term K_{sh} takes into account the thickness distribution around the leading edge, in particular its magnitude is 1 for NACA-65 aerofoils, 1.1 for the C4 aerofoils and 0.7 for DCA blade profiles;
- the term $K_{t,i}$ is introduced in order to take into account the different impact on the design incidence angle of the different maximum thickness to chord ratio and is computed as:

$$K_{t,i} = \left(10\frac{t_b}{c}\right)^{\frac{0.28}{\left[0.1+\left(\frac{t_b}{c}\right)^{0.3}\right]}}$$

- the term $(i_0^*)_{10}$ represents the minimum-loss incidence for a reference NACA-65 cascade of zero camber and 10% of thickness to chord ratio, and it is computed as reported by Aungier as:

$$(i_0^*)_{10} = \frac{\beta_1^{0.914+\frac{\sigma^3}{160}}}{5 + 46e^{-2.3}} - 0.1\sigma^3 e^{\left(\frac{\beta_1 - 70}{4}\right)}$$

Finally in the relative frame of reference the air minimum loss inlet angle can be computed as:

$$\beta_1^* = \kappa_1 - i^* \tag{5.3}$$

As the reader might imagine, the air inlet angle β_1 in the design condition coincides with the air minimum loss inlet angle, consequently, being β_1 in the equation for the computation of n and $(i_0^*)_{10}$ it is required to adopt an iterative calculation procedure.

5.3 Design Deviation Angle

The model used for the design deviation angle estimation is the one developed by Lieblein in the 1960 and reported by Aungier[1].
Lieblein proposed a correlation for the calculation of the design deviation angle δ^* which represents the flow deviation angle corresponding to operations at the design incidence angle. The equation proposed is the following:

$$\delta^* = K_{sh} K_{t,\delta} (\delta_0^*)_{10} + m\theta \tag{5.4}$$

Where

- the term K_{sh} takes into account the thickness distribution around the leading edge, in particular its magnitude is 1 for NACA-65 aerofoils, 1.1 for the C4 aerofoils and 0.7 for DCA blade profiles;

- the term $(\delta_0^*)_{10}$ represents the zero-camber deviation angle for a reference NACA-65 cascade of zero camber and 10% of thickness to chord ratio, and it is computed as reported by Aungier as:

$$(\delta_0^*)_{10} = 0.01\sigma\beta_1^* + [0.74\sigma^{1.9} + 3\sigma]\left(\frac{\beta_1^*}{90}\right)^{(1.67+1.09\sigma)}$$

- the parameter m represents the slope of the variation in the deviation angle with camber and is computed as:

$$m = \frac{m_{\sigma=1}}{\sigma^b}$$

  with:

  1. in the case of NACA 65-series camber-line:

$$m_{\sigma=1} = 0.17 - 0.0333\frac{\beta_1^*}{100} + 0.333\left(\frac{\beta_1^*}{100}\right)^2$$

  2. in the case of circular-arc camber-lines:

$$m_{\sigma=1} = 0.249 + 0.074\frac{\beta_1^*}{100} - 0.132\left(\frac{\beta_1^*}{100}\right)^2 + 0.316\left(\frac{\beta_1^*}{100}\right)^3$$

  and with:

$$b = 0.9625 - 0.17\frac{\beta_1^*}{100} - 0.85\left(\frac{\beta_1^*}{100}\right)^3$$

- the term $K_{t,\delta}$ is introduced in order to take into account the different impact on the design deviation angle of the different maximum thickness to chord ratio and is computed as:

$$K_{t,\delta} = 6.25\left(\frac{t_b}{c}\right) + 37.5\left(\frac{t_b}{c}\right)^2$$

Finally in the relative frame of reference the air minimum loss outlet angle can be calculated as:

$$\beta_2^* = \kappa_2 + \delta^* \tag{5.5}$$

5.4 Design Profile Loss

This section constitutes the core of the set defined for the blade profile loss coefficient calculation and presents the procedure for the design profile loss coefficient evaluation. The model that will be presented here has been entirely developed during this research project and is not taken from the open literature that however has provided a fundamental support for its definition.
It is based only on the use of blade profile geometrical parameters and on the results obtained from the two previous sections that on their hand are based only on blade profile geometrical parameters as well. As the reader might notice, the previous sentence is characterised by the repetition of the expression *"based only on blade profile geometrical parameters"*. This is not an accident. Effectively the objective is to stress the concept that the great contribution and potential of the model developed is in the use of only this characteristics of the blade in order to compute the design blade profile loss coefficient. The models available in the open literature and used until this time were based on the use of design velocity ratios that in reality had to be an output of the simulation. The lack of a correct value for those ratios reflects into an impossibility to run the flow field analysis or in the production of completely non-sense results. Thus the software applicability was limited to the compressors whose experimental data about those design velocity ratios were available. Actually this limitation has been overcome and the accuracy of the prediction improved.
In the following paragraphs the model will be presented. Firstly the equivalent diffusion factor is calculated, secondly this parameter is used to compute the design profile loss coefficient using as starting point a correlation proposed by Aungier but modified to improve its accuracy through an optimisation driven approach. The last paragraph provides the details about the calibration of the model and how it has been performed in order to incorporate the largest possible number of flow phenomena responsible for the total pressure loss production.
The model derivation will be presented here considering a generic blade profile just for reason of generality. Effectively being the final equations obtained only based on the blade profile geometrical parameters, the same equations will be used in the case of a turbo-component like a stator, an IGV or an OGV or in the case of a turbo-component like a rotor. Nevertheless during the calibration procedure, the different types of turbo-components have been analysed separately in order to define a set of constants for the rotor and a set of constants for the stator,IGV and OGV.

5.4.1 Equivalent Diffusion Factor

As underlined in chapter 2, the equivalent diffusion factor represents an estimation of the blade profile loading.

Considering the figure 5.2, the model assumes as a starting point the definition of the equivalent diffusion factor provided by Wright and Miller[41] which is the following:

$$D_{eq} = \left[1 - \frac{V_2}{V_1} + \left[0.1 + \frac{t}{c}\left(10.116 - 34.15\frac{t}{c}\right)\right]\frac{s}{c}\left(\frac{V_{w1} - V_{w2}}{V_1}\right)\right]\frac{V_1}{V_2} + 1 \tag{5.6}$$

Where t represents the blade maximum thickness, c represents the blade chord and s represents the blade circumferential spacing. In order to achieve a formulation of the equivalent diffusion factor as function only of the geometrical shape of the blade profile, the following hypothesis have been made:

1. Considering the on-design condition, the axial velocity is supposed to remain constant in its magnitude across the blade row as a preliminary design approximation. Later in the paragraph the correction introduced to take into account the axial velocity variation within the turbomachine, when passing throughout the various blade rows, will be presented.

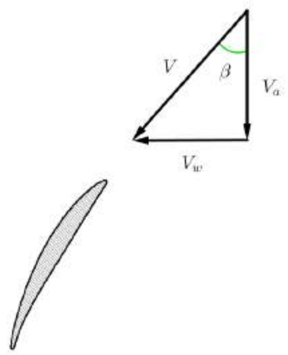

Figure 5.2: Blade Schema for D_{eq} equation derivation

2. Considering the on-design condition, and considering that this operating point is the one for which the turbomachine design is conceived, the blade metal angles are supposed to be equal to the flow angles

$$\kappa_1 = \beta_1 \; and \; \kappa_2 = \beta_2$$

in the rest of the paragraph the notation with the flow angles will be used, however the reader has to keep in mind this hypothesis that is crucial in the model for the design profile loss coefficient calculation.

As a result of these two hypothesis the velocity ratios in the equation 5.6 can be expressed as function of the flow angles, hence, being them supposed equal to the blade angles for the second hypothesis, the velocity ratios can be expressed as function of the geometrical blade profile metal angles.
Calculating the velocity ratios with simple trigonometric relations, and applying the hypothesis mentioned, the final equation for the equivalent diffusion factor obtained is:

$$D^*_{eq} = \left[1 - \frac{\cos\beta_1}{\cos\beta_2} + \left[0.1 + \frac{t}{c}\left(10.116 - 34.15\frac{t}{c}\right)\right]\frac{s}{c}(\sin\beta_1 - \tan\beta_2\cos\beta_1)\right]\frac{cos\beta_2}{\cos\beta_1} + 1 \quad (5.7)$$

That, making show up explicitly the blade metal angles, remembering the second hypothesis, assumes the following form:

$$D^*_{eq} = \left[1 - \frac{\cos\kappa_1}{\cos\kappa_2} + \left[0.1 + \frac{t}{c}\left(10.116 - 34.15\frac{t}{c}\right)\right]\frac{s}{c}(\sin\kappa_1 - \tan\kappa_2\cos\kappa_1)\right]\frac{cos\kappa_2}{\cos\kappa_1} + 1 \quad (5.8)$$

Being the objective of this model the performance prediction of the design profile losses of multi-stage axial-flow compressors, the first of the hypothesis made lead to the necessity to introduce a way to take into account the change in the axial velocity that characterizes the multi-stage configuration. Hence, a correction in order to improve the accuracy of the method has been introduced. The correction is applied to all the turbo-components following the first.
A crucial step in the correction formulation has been the analysis of the work made by Jansen and Moffatt[40] who proposed the introduction of the equivalent flow angles in order to take into account the axial velocity variation within a multi-stage compressor. In the correction introduction to improve the performance prediction of multi-stage axial-flow compressors, it has been assumed that

the axial velocity at the mid-span of the blade remains constant, in this way the correction proposed by Jansen and Moffatt can be expressed only using geometrical parameters, hence, respecting the constraints imposed for the model and improving its accuracy when multi-stage geometries are considered. The basic assumption made by Jansen and Moffatt for the equivalent flow angles formulation is that the circulation about the cascade remains unchanged with changes in axial velocity along the blade span. Adding to this assumption, the previous cited about the conservation of the axial velocity only at the mid-span station, the equivalent angles formulation is:

$$\tan\beta_{e1} = \frac{2\tan\beta_1}{1 + \frac{\cos\beta_{mid1}}{\cos\beta_{mid2}}}$$

$$\tan\beta_{e2} = \frac{\tan\beta_2}{\frac{1}{2}\left(\frac{\cos\beta_{mid2}}{\cos\beta_{mid1}} + 1\right)}$$

The hypothesis concerning the equality of blade metal angles and flow angles at the on-design operating condition is still considered to be valid, consequently:

$$\tan\beta_{e1} = \frac{2\tan\kappa_1}{1 + \frac{\cos\kappa_{mid1}}{\cos\kappa_{mid2}}}$$

$$\tan\beta_{e2} = \frac{\tan\kappa_2}{\frac{1}{2}\left(\frac{\cos\kappa_{mid2}}{\cos\kappa_{mid1}} + 1\right)}$$

The equivalent angles are computed for all the turbo-components following the first and then they are used in the equivalent diffusion factor computation at the place of the blade angles.

5.4.2 Design Profile Loss Coefficient

Once calculated the equivalent diffusion factor, the next step in the model is the design profile loss coefficient calculation. The equation used for this purpose is based on the formulation provided by Aungier[1], but it has been generalized and modified in order to increase the performance prediction accuracy and the spectrum of applicability. Moreover, being the operating point considered the on-design one, operation at the minimum loss flow angles is assumed.
The original equation provided by Aungier is the following:

$$\frac{\omega^* \cos\beta_2^*}{2\sigma}\left(\frac{V_1^*}{V_2^*}\right)^2 = K_1[K_2 + 3.1(D_{eq}^* - 1)^2 + 0.4(D_{eq}^* - 1)^8]$$

Considering this equation, two have been the main modifications done:

- Aungier defined the velocity ratio on the left side of the equation as the one that is connected with the design operating point at the on-design incidence angle, hence, the operating condition characterised by the minimum profile loss across the blade row. This definition allows to express this radio considering the axial velocity almost constant across the blade row and the relative flow angles to be respectively the inlet and outlet minimum loss fluid angles, as a result, and being these hypothesis consistent with the initial definition, the following expression for this ratio has been obtained:

$$\frac{V_1^*}{V_2^*} = \frac{\cos\beta_2^*}{\cos\beta_1^*}$$

- The constants defined by Aungier have been substituted, and in particular a set of four constants has been defined, only the definition of the constant K_2 as calculated from geometrical parameters has been maintained. The procedure employed for the constants definition is reported later, in the paragraph concerning the model calibration. Effectively the constants definition represents a crucial step in the model formulation and it is mainly connected and determined by the range of flow field phenomena that the developer would like to capture and include in the model. Clearly the more effects are captured the more the performance prediction would be accurate.

As a result, the final equation that has been used for the design profile loss coefficient calculation is:

$$\frac{\omega^* \cos\beta_2^*}{2\sigma}\left(\frac{\cos\beta_2^*}{\cos\beta_1^*}\right)^2 = K_1[K_2 + A_1(D_{eq}^* - 1)^2 + A_2(D_{eq}^* - 1)^8] \tag{5.9}$$

5.4.3 Calibration

The calibration procedure is a crucial step in the model definition. Effectively the constants defined during this phase are strongly linked to the different flow field phenomena that the designer tries to include and capture in the model. As obvious, the higher is the number of flow phenomena correctly accounted for, the more accurate is the performance prediction obtained.
However the major difficulty in this step is represented by the necessity to maintain an high level of generalisation that makes the model applicable with good results to the largest number of axial-flow fans and multi-stage compressors[1]. Under this point of view, the easiest choice, but at the same time the least reasonable, is represented by a continuous calibration on the considered compressor geometry: effectively this choice might produce really accurate results, but produces also the destruction of the definition of the model itself. Applying this kind of calibration would mean to change continuously the model adapting it to the case considered with a consequent total absence of generality and range of applicability.
Consequently the choice for this research project has been the definition of a unique set of constants to be incorporated in the model, one for the rotor, and one for the stator. Clearly the accuracy of the constants defined might be increased by applying a further statistical study but this will be discussed at the end of this thesis in the section concerning the possible future improvements.
In the following part of the paragraph the calibration procedure will be presented and the set of constants defined will be provided.

The previous equations for the estimation of the design profile losses derives from two-dimensional cascade tests, as a consequence the necessity in the performance prediction to account for flow phenomena not specifically modelled in those equations such as the wake effects, the thickening of the boundary layer and the secondary flow phenomena, lead to the necessity to define a set of constants where those effects has to be preliminarily incorporated to achieve an accurate and reliable performance prediction for preliminary design purposes.
In particular the constants K_1,K_2,A_1 and A_2 are empirical constants or functions to be determined by comparing the model prediction with the available experimental results. Their precise form strongly depends on how the performance analysis is formulated and on which loss sources are lumped into them.
In particular the constant K_2 has been implemented using the following empirical formulation[1]

[1]The reader must be aware of the fact that the definition of a model universally applicable is something impossible due to the complexity and to the peculiarity of the flow field within different type of compressors.

that takes into account the skin friction and end-wall loss in a cascade:

$$K_2 = 1 + \frac{s}{h} \cos \beta_2^* \tag{5.10}$$

Where s represents the blade pitch and h represents the blade height.
Several authors states that a good level of accuracy might be reached simply defining a single value for each of the constants considered, however, this kind of approach makes impossible to account for the blade loading variation along the spanwise direction. Consequently the first decision towards the constants definition made has been to define them along the spanwise direction at the stations disposed every 10% of the span and then, during the calculation into SOCRATES, to apply an interpolation on the base of the values defined in order to extrapolate the value of the constants for each stream-line position. This has permitted to take into account the difference in the various blade profiles along the spanwise direction in terms of loading and contribution to the loss production. While the constant K_2, according to the equation provided, was directly computed in the tool, the other constants have been determined with an optimisation study conducted using the data coming from a selected compressor geometry.

Once established the spanwise definition of the constants and the formula of K_2, there was the necessity to decide which compressor and which stage of that compressor has to be considered for the calibration of K_1,A_1 and A_2. In particular in order to try to define a set of constants capable of making the model applicable with good results to a wider range of axial-flow multi-stage compressors, it has been decided to consider a compressor whose first stage was characterised by a transonic rotor, in particular under this point of view, due to the accessibility of data the NASA two stage fan with transonic rotor 67 as first component has been chosen. Clearly the calibration of the constants of the design profile loss model has to be made considering one rotor and one stator of that compressor. On the base that the model should be applicable not only to axial-flow fans but also to multi-stage axial-flow compressors, where the wake and the thickening of the boundary layer are two of the major sources of losses. And in order to take into account for them, the second stage rotor and the second stage stator data have been considered.

Using the data contained in the NASA report, an optimisation study has been made. In particular the objective function selected has been the minimisation of the square sum of the residuals along the spanwise direction between the losses predicted from the NASA tools and the one predicted by the model here developed. Thanks to this procedure two set of constants have been found, one for the rotor, table 5.1, and one for the stator, table 5.2.

Table 5.1: Rotor Constants

Percent Span	K_1	A_1	A_2
100	0.0102	3.7513	12.0001
90	0.0194	2.9369	11.0002
80	0.0241	2.3130	8.0002
70	0.0185	1.0053	7.7002
60	0.0157	0.9866	7.7002
50	0.0133	0.9741	7.7003
40	0.0096	0.9473	7.7004
30	0.0158	1.0498	7.7023
20	0.0226	2.5462	8.0081
10	0.0204	2.5439	11.0066
0	0.0117	2.5636	11.9689

Table 5.2: Stator Constants

Percent Span	K_1	A_1	A_2
100	0.0310	0.5097	5.0011
90	0.0254	0.5158	4.5008
80	0.0190	0.5106	3.0001
70	0.0142	0.5052	3.0000
60	0.0131	0.5039	3.0000
50	0.0113	0.5011	3.0000
40	0.0105	0.4994	2.9999
30	0.0107	0.4990	2.9999
20	0.0148	0.5043	3.0006
10	0.0424	0.5916	4.5620
0	0.0530	0.5789	5.1593

These sets of constants have been implemented in the model for the present research study. However, a new input file has been created in order to take into account further and future developments aimed at defining new sets of constants in order to increase the prediction accuracy and the model flexibility for future studies.

5.5 Blade Stall Incidence Angle

The model used for the positive and negative stall incidence angle computation is the one reported by Aungier[1].

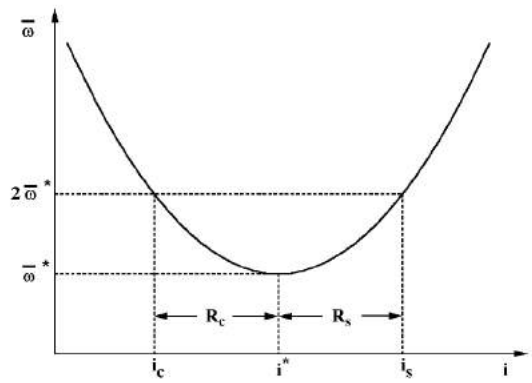

Figure 5.3: Off-Design blade profile loss coefficient[1]

Observing the figure 5.3, it is important to notice that for a range of incidence around the design incidence angle, the loss coefficient is almost constant but by moving away considerably from the design incidence angle, the loss rapidly increases.
Consequently it is necessary to define the values of the negative and positive incidence angle in correspondence of which a great increment in the loss coefficient is observed. According to the convention adopted by Aungier, the limits of low-loss operation are defined by the positive and negative stall incidence angles, respectively i_s and i_c, where the loss coefficient becomes twice the minimum loss coefficient.
The base of the model reported by Aungier is the empirical correlations developed by Herrig[42]

in the 1957 for the computation of the positive and negative stall angles of attack, which are the following:

$$\alpha_c - \alpha^* = -9 + \left[1 - \left(\frac{30}{\beta_{1c}}\right)^{0.48}\right] \frac{\theta}{4.176} \tag{5.11}$$

$$\alpha_s - \alpha^* = 10.3 + \left[2.92 - \frac{\beta_{1s}}{15.6}\right] \frac{\theta}{8.2} \tag{5.12}$$

Those equations, where all the angles are expressed in degrees, were derived using experimental data of the NACA 65-series blades, but, as reported by Aungier, it has been proven that they are effective also when used for performance analysis of double circular-arc blades. Consequently they are applicable also to the C4 circular arc blades and modern compressor MCA blades.
An important remark should be made, since α_c and α_s are functions respectively of β_{1c} and β_{1s} being in general terms:

$$\beta_1 = \alpha + \gamma$$

It is clear that these equations are not directly applicable in a performance analysis but an iterative solution procedure has to be used.
Since $\alpha - \alpha^*$ is simply the incidence angle range to stall, the low-loss working ranges are defined as:

$$R_c = \alpha^* - \alpha_c = i^* - i_c \tag{5.13}$$

$$R_s = \alpha^* - \alpha_s = i^* - i_s \tag{5.14}$$

As result of the work of Johnsen and Bullock[43], it has been noticed that as the Mach number increases, $i^* - i_c$ and $i_s - i^*$ are reduced approximately of the same amount in case of moderate Mach numbers. However for high Mach number $i^* - i_c$ is reduced much faster than $i_s - i^*$ as Mach number increases. Aungier proposed two correlations for the compute of the negative and positive stall incidence angles which are the following:

$$i_c = i^* - \frac{R_c}{1 + 0.5M_1'^3} \tag{5.15}$$

$$i_s = i^* + \frac{R_s}{1 + 0.5K_{sh}M_1'^3} \tag{5.16}$$

Where M_1' represents the relative inlet Mach number in the considered off-design operating point and K_{sh} is the shape correction factor that takes into account the thickness distribution around the leading edge. For the latter Aungier introduced the limitation $K_{sh} \leq 1$ and consequently he states the factor to be equal to 1 for NACA-65 series and C4 blades, and 0.7 for DCA blades.
Finally the model imposed a lower limit for the negative stall incidence angle. Under this point of view first the sonic flow gas density ρ_{sonic} and velocity W_{sonic} are calculated for the local inlet relative total thermodynamic conditions. Assuming the stream sheet thickness to be constant between the inlet and the throat of the blade passage, and applying the conservation of the mass, Aungier obtained a formula for computing the inlet flow angle corresponding to choke:

$$\rho_1 W_1 \cos\beta_{1\ choke} = o\rho_{sonic}W_{sonic} \tag{5.17}$$

Where o represents the throat opening. And this imposes a lower limit on the negative stall incidence angle which is the following:

$$i_c \geq \beta_{1\ choke} - \kappa_1 + 1^\circ \tag{5.18}$$

As a result, when the computed i_c is lower than the limit imposed by the model, the minimum value is then imposed in the computation. In reality the loss should become infinite when the blade passage is choked. However the milder choke condition used in Aungier's model seems to be more appropriate for an axial-flow compressor performance analysis: effectively the blade passage choke is often a local condition along the blade and produces a redistribution of the mass flow towards the un-choked sections of the blade. Moreover considering the numerical computational aspects, a too severe loss increase near choke might represent a frequent cause for calculus divergence. This final aspect has to be overcome before a precise implementation of a choke incidence lower limit computation. The model proposed by Aungier is however an acceptable compromise between accuracy and stability.

5.6 Blade Minimum Loss Incidence Angle

Changes in the magnitude of the inlet relative Mach number produces changes in the loss coefficient as showed in figure 5.4. Consequently it may also be necessary to re-adjust the minimum loss incidence angle and the minimum loss coefficient for the considered operating Mach number. In particular this section presents the model provided by Aungier[1] and used in order to compute the blade minimum loss incidence angle.

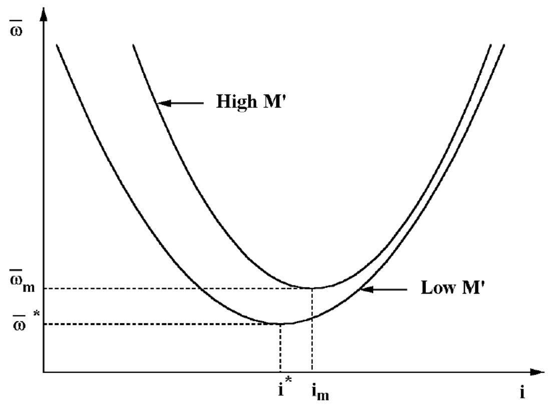

Figure 5.4: Mach Effect on Off-Design blade profile loss coefficient[1]

The minimum loss incidence angle is defined by:

$$i_m = i_c + \frac{R_c}{R_c + R_s}(i_s - i_c) \tag{5.19}$$

It is important to notice that for moderate values of Mach number and blade profiles far from the choked flow limit, it might be consistent to assume that $i_m = i^*$. However for high values of the Mach number or in case of being close to the choke limit, it is observable that $i_m > i^*$ resulting in a major magnitude of losses also at the minimum loss incidence compared with the design operating condition.

5.7 Blade Minimum Loss Profile Loss

Once calculated the minimum loss incidence angle, using the model proposed by Aungier[1] and making reference to the figure 5.4, the minimum profile loss, corresponding to an operating Mach

number different form the one of the on-design operating condition, is computed.
In particular the minimum loss profile loss are calculated using the following equation:

$$\omega_m = \omega^* \left[1 + \frac{(i_m - i^*)^2}{R_s^2}\right] \tag{5.20}$$

However loss coefficients at the minimum loss incidence angle show little variation with Mach number until the fluid velocities on the blade surface become supersonic[1]. Effectively if the flow reaches the supersonic regime on the blade surface, shock-waves can occur interacting with the boundary layer and eventually causing its separation which is followed by a significantly increase in the minimum loss coefficient. Consequently a correction to the previous equation has to be introduced when the critical relative Mach number is reached. The first step is to calculate the maximum velocity reached on the blade surface, and, for this purpose, Aungier proposes the following formulation:

- Case of the Rotor:

$$W_{max} = W_1 \left[1.12 + 0.61 \frac{\cos^2 \beta_1}{\sigma} \frac{r_1 W_{\theta 1} - r_2 W_{\theta 2}}{r_1 W_{m1}} + \alpha (i - i^*)^{1.43}\right]$$

  where W_m represents the relative meridional velocity.

- Case of the Stator:

$$C_{max} = C_1 \left[1.12 + 0.61 \frac{\cos^2 \beta_1}{\sigma} \frac{r_1 C_{\theta 1} - r_2 C_{\theta 2}}{r_1 C_{m1}} + \alpha (i - i^*)^{1.43}\right]$$

  where C_m represents the absolute meridional velocity.

Then the critical Mach number is computed. For reason of simplicity the procedure from this point to the end of the paragraph will be conducted for the Rotor, however, the procedure is completely analogous for the stator.
The critical Mach number is calculated as:

$$M_c' = M_1' \frac{W_{sonic}}{W_{max}}$$

And then if the inlet Mach number exceeds the critical value, the minimum loss coefficient is calculated as:

$$\omega_m = \omega^* \left[1 + \frac{(i_m - i^*)^2}{R_s^2}\right] + K_{sh} \left[\frac{M_1'}{M_c' - 1} \frac{W_{sonic}}{W_1}\right]^2 \tag{5.21}$$

Clearly this correction is able to give the possibility to evaluate the losses produced by the boundary layer after the interaction with a shock wave. As already anticipated, the shock losses produced by the shock wave itself are evaluated thanks to the model proposed by Dr. Azamar Aguirre[11].

5.8 Blade Profile Loss and Total Loss Coefficient Estimation

Once calculated the minimum loss corresponding to the off-design operating condition, the blade profile loss are then computed according to the methodology proposed by Aungier.
The first step in this final part of the procedure towards the total loss coefficient estimation is based on the definition of a normalized incidence angle parameter as:

1. if $i \geq i_m$

$$\xi = \frac{i - i_m}{i_s - i_m}$$

2. if $i < i_m$

$$\xi = \frac{i - i_m}{i_m - i_c}$$

Then the blade profile loss coefficient is computed thanks to the following empirical correlations reported by Aungier himself:

1. if $-2 \leq \xi \leq 1$

$$\omega_{prof} = \omega_m(1 + \xi^2)$$

2. if $\xi < -2$

$$\omega_{prof} = \omega_m(5 - 4(\xi + 2))$$

3. if $\xi > 1$

$$\omega_{prof} = \omega_m(2 + 2(\xi - 1))$$

Once computed the blade profile loss coefficient, also the shock loss coefficient ω_s is calculated. In particular for the calculation of the latter the model used, as also anticipated previously, it the one developed during his PhD. at Cranfield University by Dr. Aguirre. Being this model out of the perimeter of this research project, it will not be described but, if the reader is interested, further details about it can be found in the PhD. Thesis[11].
Hence, the total loss coefficient is calculated as:

$$\omega = k_{SF} \cdot \omega_{prof} + \omega_{sw} = \omega_{prof\ effective} + \omega_{sw} \tag{5.22}$$

The shape factor k_{SF} takes into account the different impact of the blade geometry on the loss production. Its description and development is reported in details in the following subsection.

5.8.1 Shape Factor Definition

Arrived at this point, the reader has noticed that the entire profile loss prediction is based only on geometrical parameters and minimum loss flow angles[2] and in particular a crucial role is the one of the constants incorporated in the design profile loss model.
The constants have been calibrated on a precise geometry and clearly their definition in order to achieve the maximum accuracy should change every time and an ad-hoc calibration on the compressor geometry considered would be necessary. However this kind of approach would kill the model generality and consequently it is not applicable.
As a result of the above consideration it has been considered the necessity to introduce a correction factor able to take into account the effect of considering different geometries from the one chosen for the calibration on the overall profile loss coefficient, hence, giving the possibility to improve Aungier's correlation and computing the effective profile loss coefficient for the considered axial-flow compressor geometry and the considered operating condition.
In the definition of this factor it has been looked for the operating condition and the turbo-component which gave the possibility to have the best quantitative measurement of the impact of the blade profile geometry shape on the profile loss production.
Consequently the following assumptions have been made:

[2] Also this angles, used in the design profile loss computation, are on their hand calculated using only geometrical blade profile characteristics.

- The first turbo-component, the rotor 67, of the compressor used for the calibration has been considered. The reason for this choice is that its profile losses are mainly due to the geometrical characteristics of the blade profile and the incidence of wake and secondary flow effects is limited being it the first component of the turbomachine. Moreover the wake and secondary effects incidence on the minimum loss flow angles used in the design profile loss computation for this turbo-component is the minimum for the above reasons.

- The design operating condition and the mid-span blade location have been considered. This choice is justified by the fact that the design profile losses at the blade mid span for the first turbo-component are representative of the condition and of the span-wise location where the incidence of the secondary flow effects, of the boundary layer thickening and of the wake is the most limited one.

Moreover it should also be stressed that, in order to assure the consistency of the methodology, the rotor used for the calibration for the rotating blade rows was characterised at mid-span by the same blade profile type as the one used for the NASA Rotor 67: the MCA type. Consequently to this fact and to the previous assumptions, the reference geometry chosen for the correction factor has been the *NASA Rotor 67*.
The scope of the previous assumptions was the attempt to develop a profile loss correction factor for the geometry mostly based on the taking into account just the blade profile shape impact on the loss production. The introduction of this factor takes into account the difference into the constants defined when the blade profile geometry is changed providing a correction and increasing the accuracy of the prediction without compromising the generality of the model defined.
As a result of the previous considerations and assumptions, the factor definition is:

$$k_{SF} = \frac{\omega^*_{prof\ mid-span\ case\ study}}{\omega^*_{prof\ mid-span\ Rotor\ 67}} \tag{5.23}$$

Where both the design profile loss coefficient in the equation are calculated using the previously described design profile loss model based only on the use of geometrical parameters.
Finally the reader would probably at this point be wondering why the correction has not been applied directly to design profile loss coefficient. Effectively the model set presented, that has its climax in the profile loss coefficient calculation, uses a set of empirical constants not only in the design profile loss coefficient computation. For this reason the choice to apply the correction at the final stage of the process is explained by the attempt to take into account how effectively the geometrical blade profile shape influence the blade profile total losses that reflects how all these constants in a certain sense should be modified in order to take into account the shape changes in the blade profile respect to the geometry used for the definition of the various models, whose functionality for the MCA blade type has been stated and verified by Aungier himself.
Under the definition point of view, the simulation of the isolated rotor for the model verification has been crucial.
Clearly the choice made is not compulsory but it is a consequence of the calibration strategy adopted. A certain degree of flexibility is available and the user can define a new reference geometry in the case he/she decides to change the constants sets used applying a different calibration strategy. For this purpose a new input file has been introduced in the tool.
Moreover a possible improvement that will be discussed in the final chapter would probably be the introduction of different reference geometries, one for the rotor and one for the stator. The first necessity would be to simulate the two reference geometries as isolated components and then the unique difficulty would be to incorporate the references chosen in the tool. Probably this would increase the accuracy in the simulation of the multi-stage configuration, in particular when more than two stages are considered. However in the present research study, a single reference

geometry has been considered for the reasons mentioned above. Moreover in reality, this choice is also consistent with the major criticality of the correct performance prediction of the rotating blade rows respect to the stationary ones. Effectively this author is convinced that the introduction of a reference geometry also for the stator would be carefully evaluated and requires in particular the comparison of the results of the isolated blade row analysis with the experimental simulation of the stator alone, which is something not reported in the NASA reports. Consequently an experimental investigation is also strongly recommended before attesting the reliability and accuracy of the introduction of a different reference geometry for the stator. In addiction, probably the introduction of this second reference geometry would only slightly improve the results obtained which are already in good agreement with the experimental data as a result of the major impact of the reliable and accurate rotor performance prediction in the correct simulation of the whole axial-flow compressor flow field.

Chapter 6

Results and Discussion

6.1 Introduction

This section aims at presenting the results obtained within the model application to two different transonic fan and a transonic two stage axial-flow compressor and the related comments. As the reader might imagine the results have been obtained thanks to through-flow simulations using the model in the tool SOCRATES developed in the UTC Rolls Royce at Cranfield University. An accurate loss model employment is crucial in achieving reliable performance prediction in through-flow tools due to the inviscid flow assumption made in those methods.
In particular the procedure adopted for the results production consists in three steps. Firstly the model has been verified using as test geometry the *NASA Rotor 67*. The verification procedure, as the expression might suggest, consists in the first application of the model with the aim of verifying on a test geometry the results produced respect to the previous set employed in the tool. The objective is to observe the model behaviour and the results that it produces in terms of performance prediction and fluid properties comparing them with the previous tool version in order to verify if the model contributes to an improvement in the prediction accuracy or, at least, in the production of results of a comparable level of precision respect to the previous model employed.
Once completed the verification, the model has been validated using as test geometry the *NASA Rotor 37*. The validation phase consists in the first application of the model to a fan or compressor geometry not previously analysed using SOCRATES in order to attest the model functionalities and the steps further made in the tool development. In particular an historical reason was at the base of the choice of this transonic fan for the model validation. Effectively the previous profile loss model implemented in SOCRATES, even though the geometry was produced and the simulation was running, was unable to produce consistent results in terms of performance prediction of this transonic rotor. Consequently applying the model to the NASA Rotor 37 in order to achieve the validation was a milestone in this research project, and it has confirmed the further steps made in the tool development and accuracy improvement.
Finally the model has been applied to a transonic two stage axial-flow compressor geometry. As the reader might notice going from the verification to the application phase the difficulty and complexity of the geometry tested and of the simulations have been increased. The application to the NASA transonic two stage fan has showed the potentiality of the model that is able to produce a good level of accuracy also in the performance prediction of multi-stage configurations. Clearly the model might be further improved, further flow field phenomena could be captured and multi-stage configurations with more than two stages could be considered in the future development in order to final achieve an high level of accuracy also for this axial-flow compressor configurations. However in the following sections the results obtained and the related discussion will be presented,

and the reader, at the end of this chapter, would probably be aware of the potentialities of the model in terms of axial-flow fans and compressors performance prediction.

6.2 Model Verification

6.2.1 Rotor 67

As previously mentioned the transonic fan chosen for the model verification is the *NASA Rotor 67*, shown in figure 6.1.

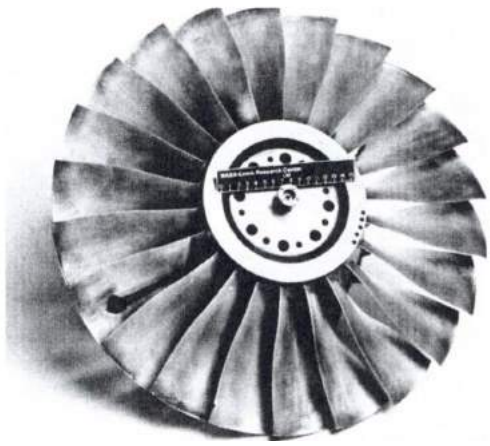

Figure 6.1: Nasa Rotor 67 Geometry [44]

The *NASA Rotor 67* is an undampered low-aspect ratio design rotor characterised by the use of MCA blade profiles. Historically it has been used since the late 80s in order to verify and validate aerodynamic computational algorithms, and in particular those which deal with viscosity terms and aerodynamic loss modelisation.
The design point parameters for the considered rotor are shown in the table 6.1.

Table 6.1: Rotor 67 Design Point Specifications

Parameter	Magnitude
Number of Rotor Blades	22
Rotational Speed [rpm]	16043
Pressure Ratio	1.63
Mass flow [kg/s]	33.25
Rotor tip speed [m/s]	429
Inlet Tip Relative Mach Number	1.38

The fundamental interest in this rotor through the years is connected to its transonic behaviour in a single rotor blades as underlined also by the tip inlet Mach number of 1.38 reached at the on-design operating condition. In addiction to the design parameters reported in the table 6.1, it is necessary to specify that the aspect ratio of the rotor based on average span/root axial chord is 1.56. Moreover the inlet and outlet tip diameters are respectively 51.4 *cm* and 48.5 *cm*. In parallel, the inlet and outlet hub to tip radius ratios are respectively 0.375 and 0.478.
The flow path coordinates in the meridional plane for the tip and the hub were provided by the

NASA technical report 2879[45] and before inserting them into the SOCRATES input file, they were de-dimensioned using the following equations:

$$\%\ max\ length = \frac{z}{z_{max}}$$

$$\%\ max\ diameter = \frac{r}{r_{max}}$$

The main characteristics of the flow path for the considered rotor are reported in the table 6.2.

Table 6.2: Rotor 67 Flow Path Characteristics

Parameter	Magnitude
Length [cm]	53.5022
Radius Length [cm]	16.8364
z_{min} [cm]	-18.0598
z_{max} [cm]	35.4423
r_{min} [cm]	8.8618
r_{max} [cm]	25.6982

It is important to notice that the sign minus at the z_{min} magnitude is due to the fact that the origin of the z-axis corresponds with the rotor location.
Moreover also the blade profile data[46] have to be elaborated using the following equations before inserting them into the SOCRATES input files:

- Blade profile r coordinates

$$\%r_{le} = \frac{r_{le} - r_{le\ Hub}}{r_{le\ Tip} - r_{le\ Hub}}$$

$$\%r_{te} = \frac{r_{te} - r_{te\ Hub}}{r_{te\ Tip} - r_{te\ Hub}}$$

- Blade profile z coordinates

$$\%z_{le} = \frac{z_{le} - z_{le\ Hub}}{r_{le\ Tip} - r_{le\ Hub}}$$

$$\%z_{le} = \frac{z_{te} - z_{le\ Hub}}{r_{le\ Tip} - r_{le\ Hub}}$$

- Blade profile characteristics

$$\%\ max\ thickness\ z\ position = \frac{z_{mc} - z_{ic}}{z_{oc} - z_{ic}}$$

$$\%\ max\ thickness = \frac{t_m}{z_{oc} - z_{ic}}$$

$$\%\ transition\ thickness\ z\ position = \frac{z_{tc} - z_{ic}}{z_{oc} - z_{ic}}$$

$$\%\ leading\ edge\ radius = \frac{t_{le} \cdot 0.5}{z_{oc} - z_{ic}}$$

$$\%\ trailing\ edge\ radius = \frac{t_{te} \cdot 0.5}{z_{oc} - z_{ic}}$$

The blade profile angles are entered as reported in the NASA Technical papers.
For reason of completeness the author reported here also the spacing equation to be used in case of more than one turbo-component which is the following:

$$\%spacing = \frac{z_{le\ Hub\ 2} - z_{le\ Hub\ 1}}{\frac{(r_{le\ Tip\ 1} - r_{le\ Hub\ 1}) + (r_{te\ Tip\ 1}) - r_{te\ Hip\ 1}}{2}}$$

Once entered the fan model into SOCRATES, the boundary conditions and the operating points to be simulated it has been possible to calculate the performance map of the rotor and the flow properties and velocities[1] reported with the related comments in the following sections.

6.2.2 Performance Map

In the axial-flow fan and compressors performance prediction a crucial role is the one of the loss models incorporated into the through-flow tools. Effectively the inviscid flow assumption of those methods lead towards the introduction of empirical correlation which are included in order to take into account the viscosity, deviation and losses. Without those models an effective and accurate performance prediction would be impossible.
In the figures 6.2 and 6.3 the rotor total pressure ratio and the rotor adiabatic efficiency as functions of the corrected mass flow are reported. The experimental data provided in the NASA technical report and the results both for the previous model used in SOCRATES and for the new one are presented in those performance maps.

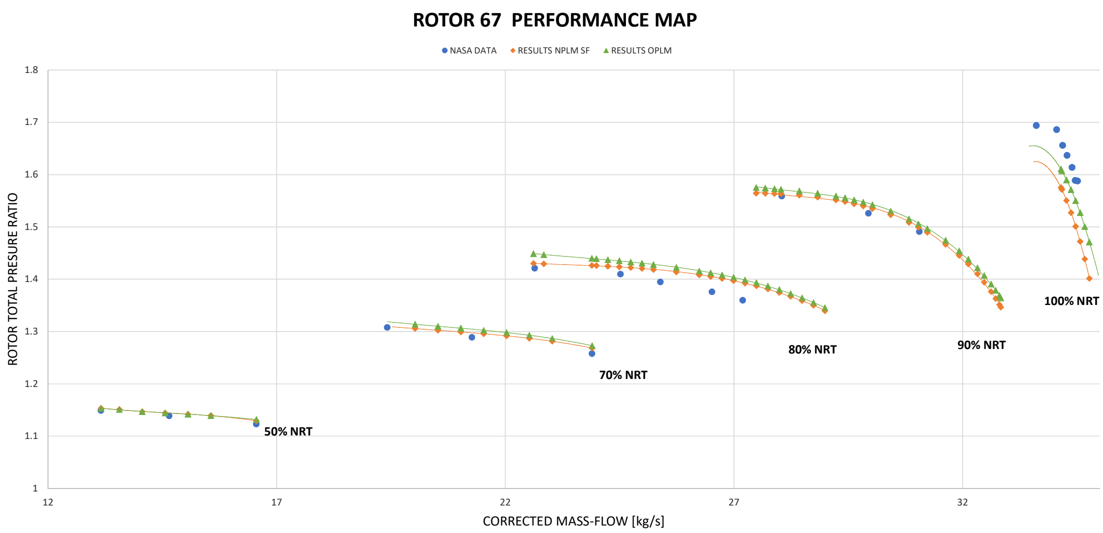

Figure 6.2: Nasa Rotor 67 Performance Map - Total Pressure Ratio

As previously underlined the scope of the analysis conducted on the NASA Rotor 67 was the model verification against the previous results obtained with SOCRATES. As general comment, before going deeper in the analysis details, the reader might notice that the prediction accuracy,

[1]It has been chosen to insert in the thesis the flow properties and velocities for the near-peak efficiency operating point for every speed-line, for reasons of length and to nor bore the reader.

both in terms of total pressure ratio and in terms of adiabatic efficiency, has been improved at the speed-lines from 50% to 90% of the design speed: it is important to notice that at those percentage of design speed the losses are mostly due to the blade profile. Consequently the accuracy reached states the functionality of the profile loss model.
At the same time the performance prediction at 100% of design speed produces results comparable with those obtained using the previous profile loss model but in both the cases the error is larger then for the other speed-lines. Under this point of view the reader must be aware of the fact that at 100% of design speed, the rotor considered shows its transonic nature, and as it will be underlined later, when the analysis on the flow properties and velocities will be conducted, the flow field along the span-wise direction is in the transonic regime and reaches a slightly supersonic regime at the blade tip. As a consequence the losses at this value of the design speed are not only due to the blade profile losses but an important contribution is also produced by the shock-waves that characterize the operating conditions at 100% of design speed.

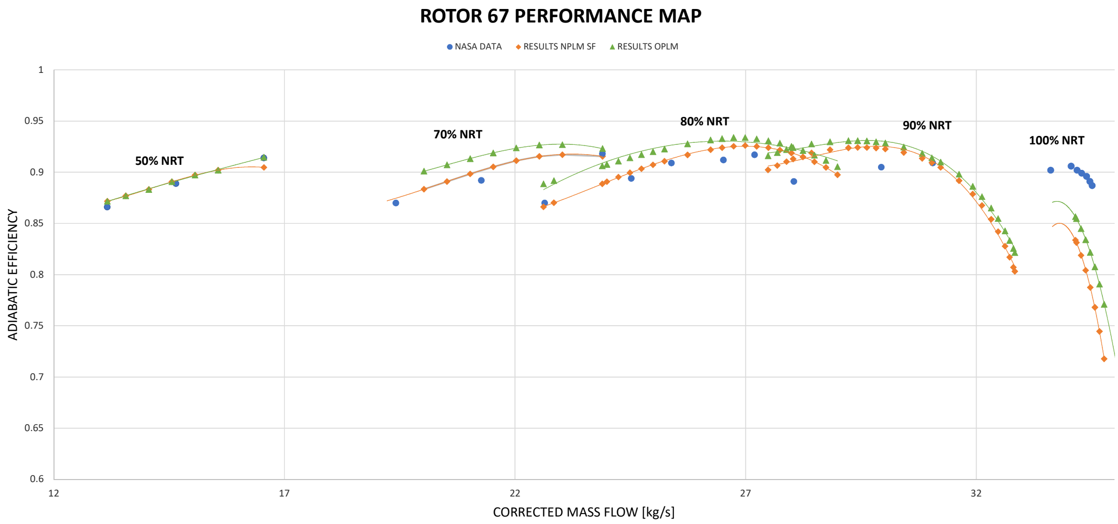

Figure 6.3: Nasa Rotor 67 Performance Map - Adiabatic Efficiency

Consequently the losses predicted at those operating conditions are the sum of the profile losses predicted with the model previously presented[2] and the shock loss model previously cited which is the one reported in the PhD. Thesis[11]. Comparing the prediction of the tool with the previous model and with the new one, it might be stated that the error committed in the performance prediction is mainly due to the shock model employed in the tool. Therefore capturing the flow field characteristics in the transonic regime using a through-flow simulation represent something really challenging and difficult to achieve due to the inherent 3-Dimensional nature of the flow-field and the loss mechanisms.

[2]The Shape Factor in this case is equal to unity as a consequence of its definition.

Table 6.3: Rotor 67 Performance Prediction Maximum Errors

% of Design Speed	Maximum Error on the TPR [%]		Maximum Error on the AE [%]	
	Previous Model	Current Model	Previous Model	Current Model
50	0.712	0.53	0.5	1.09
70	0.69	0.22	3.45	1.14
80	2.94	2.21	1.63	0.87
90	1.37	0.85	1.64	1.24
100	2.96	4.14	5.09	7.54

Nevertheless those difficulties, the results produced by the tool with both the profile loss models are of an acceptable level of accuracy for preliminary design purposes.
In particular in the table 6.3 the maximum errors per speed-line are reported both for the total pressure ratio prediction and for the adiabatic efficiency prediction.
Observing those errors the previous statement about the model accuracy is confirmed. The maximum errors reached within the performance prediction underlines the potentialities of the through-flow tools if a corrected modelisation of the loss mechanisms is provided. Even though a maximum error of 4.14% percent reached at 100% of Design Speed represent an acceptable error considering all the assumption and approximations made during the model development and considering the empirical correlations used.
Moreover it should be noticed that the maximum error in the performance prediction is usually greater in the case of the adiabatic efficiency then in the case of the total pressure ratio. Effectively, the adiabatic efficiency prediction accuracy depends both on the prediction accuracy of the total pressure ratio and of the total temperature ratio. The modelisation of the secondary flow losses under this point of view and their impact on the entropy production are crucial but as the maximum errors analysis confirms, the level of accuracy reached is already acceptable. Finally considering the maximum error in the adiabatic efficiency prediction at 100% of Design Speed, it should be highlighted that in this case the difficulty in the flow field modelisation is increased by the presence of the shock-waves and by the higher magnitude of the previous cited secondary flow phenomena. In this condition another phenomenon, that occurs, is the interaction of the shock-waves with the boundary layer, the modelisation of this phenomenon could definitely increase the accuracy of the prediction but, the through-flow tools don't deal with the boundary layer equations resolution and consequently the modelisation of such a complex phenomenon using only empirical correlations is clearly of a tremendous level of difficulty. Also and in particular for the problematic aspects connected with the experimental measurements of the boundary layer properties within a turbomachine, especially in the rotating components.

6.2.3 Flow Properties and Velocities

As the title of the section might suggest, in the following paragraphs the flow properties and velocities trend along the spanwise direction obtained within the model verification simulations will be presented.
For reason of length, in the following paragraphs the operating condition for each speed-line considered will be the near peak efficiency operating point.
For each percentage of the design speed the following properties at the inlet and at the outlet of the transonic axial-flow fan considered will be provided:

1. total pressure;

2. total temperature;

3. meridional velocity;

4. meridional Mach number;

5. relative velocity;

6. relative Mach number.

Effectively the necessity to analyse also the trend of the previous cited properties is necessary considering the fact that the through-flow tools aim at providing a complete analysis of the flow field within the turbomachine in the meridional plane. The analysis is not limited to the performance prediction but also at considering the evolution of the fluid characteristics along the spanwise direction of the blade for each blade row. Those information are fundamental in the preliminary design phase in order to understand if the blade row designed effectively satisfies the requirements both in terms of pure performance and in terms of flow field characteristics.
As the reader have noticed already with the performance maps presented and as he will observe in the paragraphs related to the flow properties, the current model gives results at least of a comparable level of accuracy respect to the previous model employed. Consequently the current model could be considered as verified.

50% of Design Speed

In the figures 6.4, 6.5 and 6.6 the meridional velocity, the meridional Mach number, the relative velocity, the relative Mach number, the total pressure and total temperature at 50% of the design speed for the near peak efficiency operating point are reported respectively.
The operating point considered is characterised by a rotating speed of 8017.2 rpm and a corrected mass flow of $\dot{m}_{corr} = 16.55\ kg/s$.

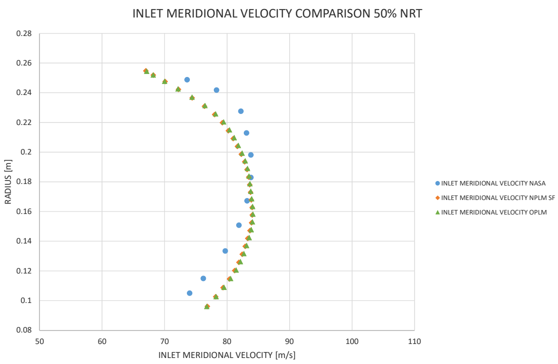

(a) *Inlet Meridional Velocity*

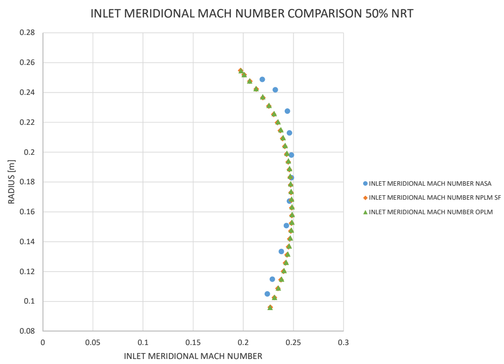

(b) *Inlet Meridional Mach number*

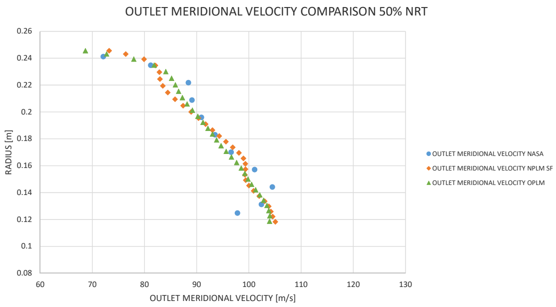

(c) *Outlet Meridional Velocity*

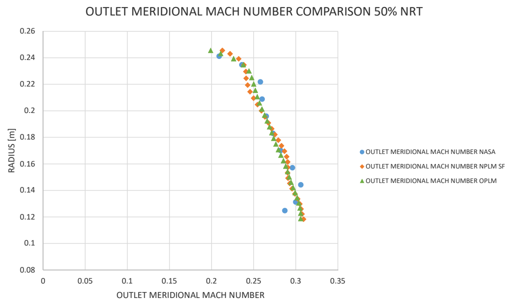

(d) *Outlet Meridional Mach number*

Figure 6.4: Rotor 67 Meridional Velocity and Meridional Mach Number at 50% of Design Speed and $\dot{m}_{corr} = 16.55\ kg/s$

Observing those figures the first general consideration that might be done is that the model is able to reproduce with accuracy both the shape and magnitude of the flow properties considered along the spanwise direction at this percentage of the design speed. Effectively this should be expected considering the accuracy provided for this speed-line concerning the performance prediction.

In the following part of the paragraph we will go deeper in the analysis details analysing each of the properties reported.

Firstly let us considering the figure 6.4 and consequently the meridional velocity and meridional Mach number prediction against the data provided in the NASA Technical Report.

The shape detected at the blade row inlet for those quantities is consistent with the presence of the casing and the annulus boundary layer. This is valid also for the higher rotating speeds and for the other two geometries analysed and consequently this statement will not be repeated in order to not bore the reader.

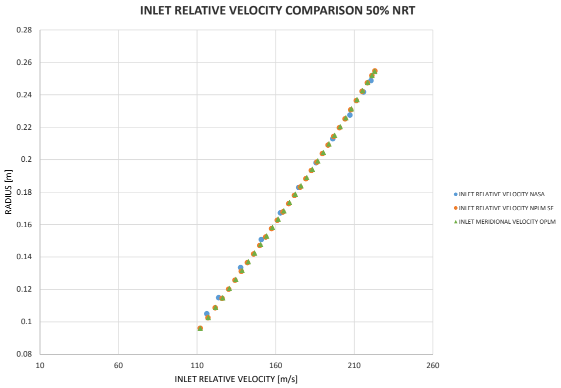

(a) *Inlet Relative Velocity*

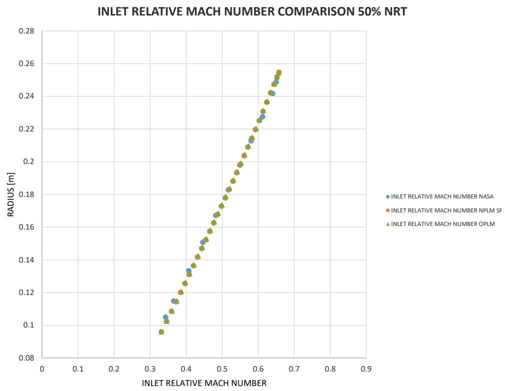

(b) *Inlet Relative Mach number*

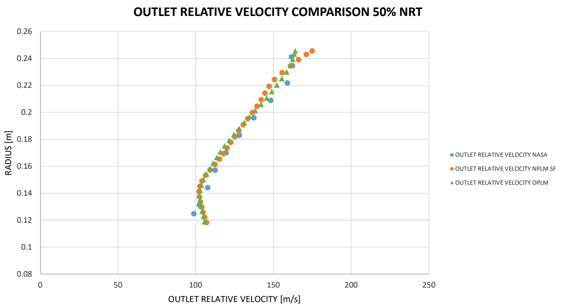

(c) *Outlet Relative Velocity*

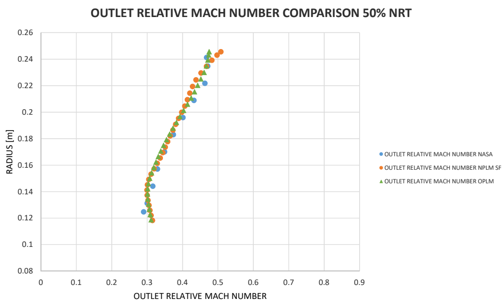

(d) *Outlet Relative Mach number*

Figure 6.5: Rotor 67 Relative Velocity and Relative Mach Number at 50% of Design Speed and $\dot{m}_{corr} = 16.55\ kg/s$

At the row inlet station the shape and magnitude of the meridional velocity and meridional Mach number are correctly captured with a good level of accuracy. However considering the outlet station, it must be noticed that the accuracy in the prediction reached at the tip of the blade is greater then the accuracy at the hub. Effectively at this value of the rotating speed, the secondary flow phenomena and vortices at the tip region have a really low intensity whilst the source of inaccuracy in correspondence of the hub could be identified in the boundary layer modelisation. The reader must be aware that one of the limitations of the through-flow tools in general is highlighted by the error made in the prediction in the hub region. Effectively the through-flow tools don't deal with the resolution of the boundary layer equations and this lead to a greater inaccuracy at the hub respect to the tip of the blade. Nevertheless the error is greater, as observable considering the table 6.4, the maximum error committed in the meridional velocity and Mach number prediction is still lower than 10%.
Considering the figure 6.5, the prediction of the relative velocity and of the relative Mach number reaches an extremely high level of accuracy at the inlet station. In parallel considering the outlet station of the blade row the evolution of the relative velocity and relative Mach number along the blade radius is correctly captured by the model. Again the major errors are observable in the hub region. Nevertheless their small magnitude, their presence is mainly related to the approximations made in the tool in dealing with the boundary layer region.

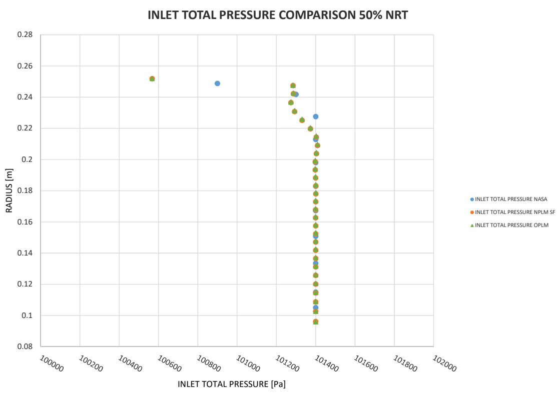

(a) *Inlet total pressure*

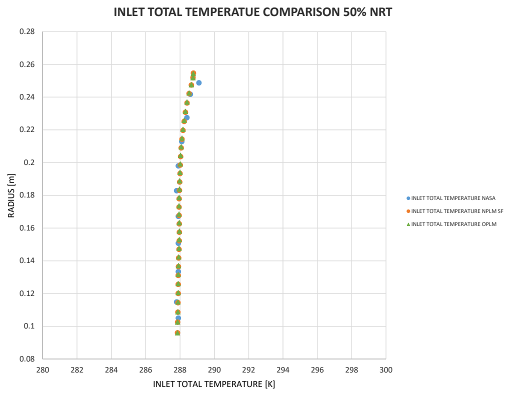

(b) *Inlet total temperature*

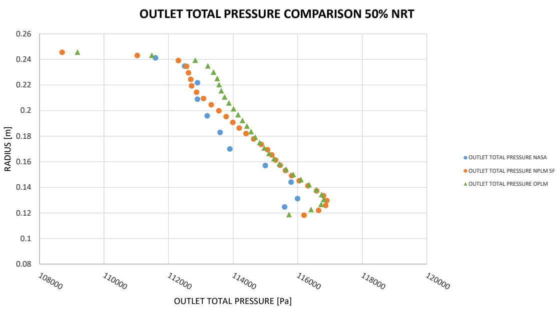

(c) *Outlet total pressure*

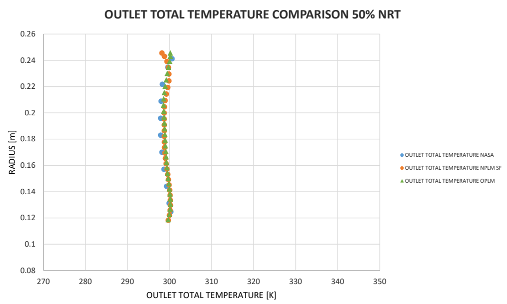

(d) *Outlet total temperature*

Figure 6.6: Rotor 67 Total Pressure and Total Temperature at 50% of Design Speed and $\dot{m}_{corr} = 16.55\ kg/s$

Finally considering the figure 6.6, it could be noticed that at the blade row inlet the total pressure and total temperature are calculated with a maximum error which is less than 1%. Moreover considering the blade row outlet and in particular the tip region, it should be highlighted that the current model is able to better capture the total pressure shape consistently with the better level of accuracy showed in the pressure ratio performance map for this speed-line respect to the previous model employed[3]. The same consideration might be done considering the outlet total temperature. The correct capturing of those flow properties is consistent also with the accurate prediction of the rotor adiabatic efficiency as showed also in the previous paragraph by the correspondent performance map.

[3] Already characterised by an high level of accuracy.

Table 6.4: Rotor 67 Near Peak Efficiency Flow Properties Prediction at 50% of Design Speed and $\dot{m}_{corr} = 16.55\ kg/s$

Fluid Property	Previous Model Maximum Error [%]	Current Model Maximum Error [%]
$V_{in\ Merid}$	5.68	5.40
$M_{in\ Merid}$	5.93	5.93
$V_{out\ Merid}$	8.37	9.05
$M_{out\ Merid}$	5.93	5.93
$V_{in\ Rel}$	0.77	0.60
$M_{in\ Rel}$	0.87	0.58
$V_{out\ Rel}$	6.27	6.98
$M_{out\ Rel}$	6.21	6.89
$p_{in\ tot}$	0.33	0.33
$T_{in\ tot}$	0.049	0.048
$p_{out\ tot}$	0.697	0.78
$T_{out\ tot}$	0.20	0.40

70% of Design Speed

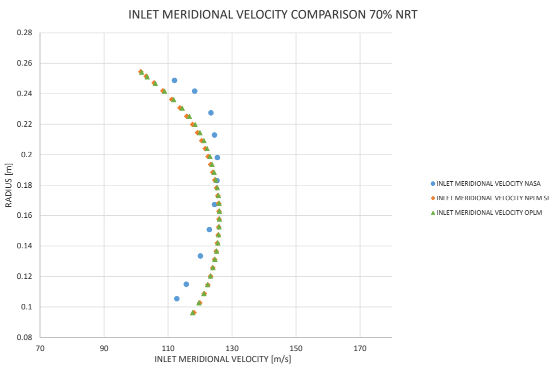

(a) *Inlet Meridional Velocity*

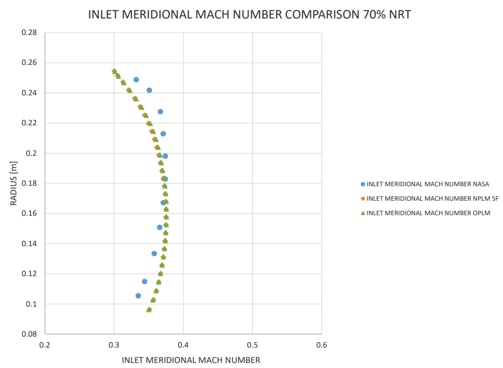

(b) *Inlet Meridional Mach number*

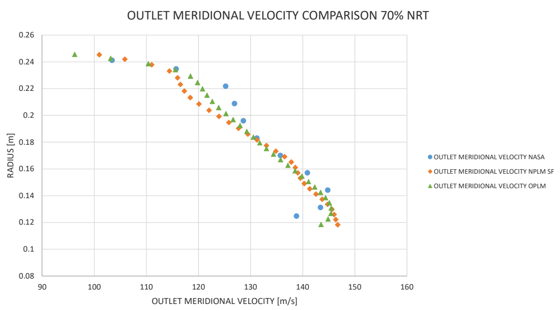

(c) *Outlet Meridional Velocity*

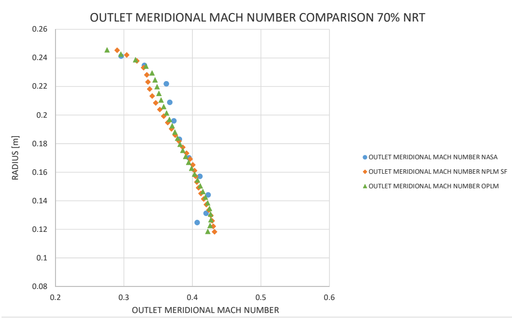

(d) *Outlet Meridional Mach number*

Figure 6.7: Rotor 67 Meridional Velocity and Meridional Mach Number at 70% of Design Speed and $\dot{m}_{corr} = 23.89\ kg/s$

In the figures 6.7, 6.8 and 6.9 the meridional velocity, the meridional Mach number, the relative velocity, the relative Mach number, the total pressure and total temperature at 70% of the design speed for the near peak efficiency operating point are reported respectively. The operating point considered is characterised by a rotating speed of 11230.1 rpm and a corrected mass flow of $\dot{m}_{corr} = 23.89\ kg/s$.

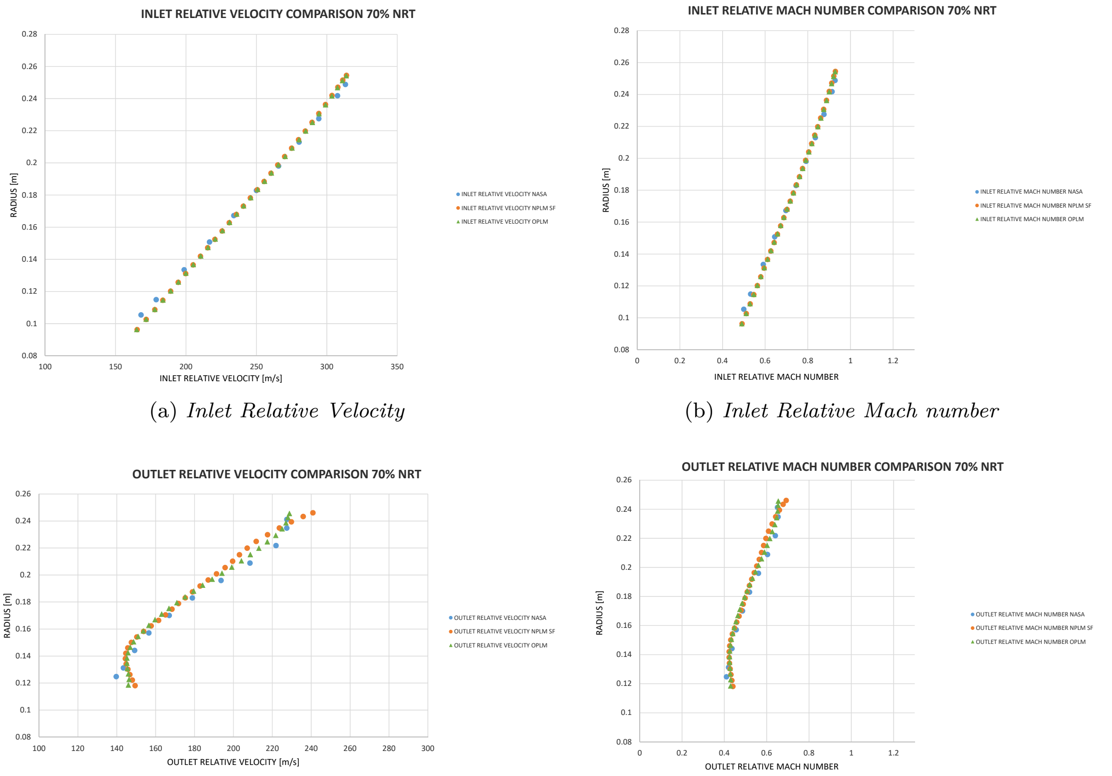

(a) *Inlet Relative Velocity* (b) *Inlet Relative Mach number*

(c) *Outlet Relative Velocity* (d) *Outlet Relative Mach number*

Figure 6.8: Rotor 67 Relative Velocity and Relative Mach Number at 70% of Design Speed and $\dot{m}_{corr} = 23.89\ kg/s$

Considering the figure 6.7, at the inlet blade row station, the shape, that describes the evolution of the inlet meridional velocity and of the inlet meridional Mach number, is correctly captured by the model. Again a slightly over-estimation in the hub region is observable. Probably the prediction in this region could be further improved introducing the numerical resolution of the boundary layer equations in the tool, but this would be against the general philosophy of the through-flow tools. Passing to the blade row outlet station similar considerations to the ones made for the case at 50% of design speed could be made.

Making reference to the figure 6.8, similar considerations to the ones already formulated for the case at 50% of design speed could be formulated. However in this case it is interesting to notice that in the relative frame of reference, and in particular in the tip region, the flow has reached the transonic regime. Nevertheless the inherent non-linearity connected with this fluid regime of motion, as stated by the figure 6.9, the total pressure and total temperature evolution along the blade radius are captured with a good level of accuracy both at the tip and at the hub region. Particularly the current model increases the accuracy at the blade tip both for the total pressure magnitude and total temperature magnitude prediction providing more accurate results in terms of total pressure ratio and adiabatic efficiency prediction.

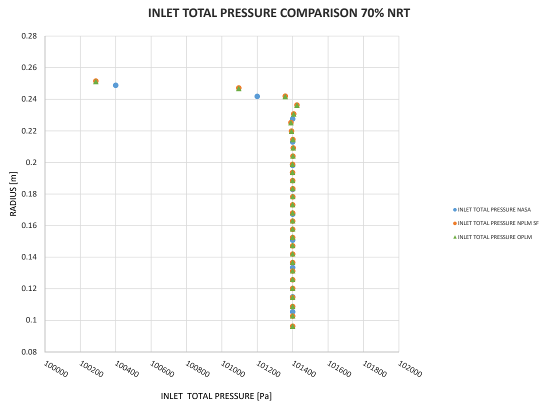

(a) *Inlet total pressure*

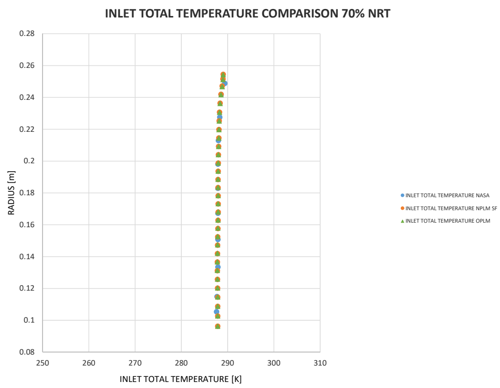

(b) *Inlet total temperature*

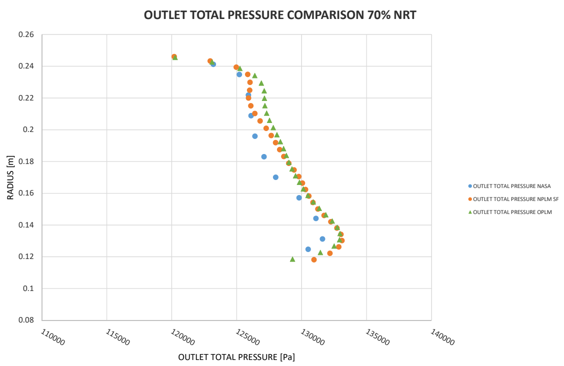

(c) *Outlet total pressure*

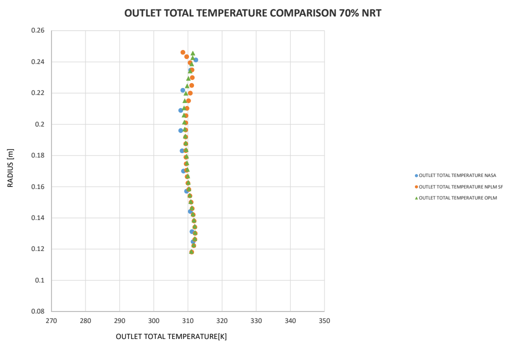

(d) *Outlet total temperature*

Figure 6.9: Rotor 67 Total Pressure and Total Temperature at 70% of Design Speed and $\dot{m}_{corr} = 23.89\ kg/s$

Finally it should be noticed that, as also observable at 50% of the design speed, the hub region is characterised by an higher outlet total pressure magnitude respect to the blade tip. The reasons for this are in particular connected with the fact that the pressure losses at the tip region produced by the presence of clearance vortices, of the casing boundary layer and of the secondary flow phenomena are responsible for an higher total pressure loss respect to the loss sources at the blade hub such as the annulus boundary layer.

Table 6.5: Rotor 67 Near Peak Efficiency Flow Properties Prediction at 70% of Design Speed and $\dot{m}_{corr} = 23.89\ kg/s$

Fluid Property	Previous Model Maximum Error [%]	Current Model Maximum Error [%]
$V_{in\ Merid}$	6.12	6.39
$M_{in\ Merid}$	6.27	6.51
$V_{out\ Merid}$	2.86	3.79
$M_{out\ Merid}$	4.67	5.65
$V_{in\ Rel}$	2.12	2.19
$M_{in\ Rel}$	2.16	2.2
$V_{out\ Rel}$	4.51	5.02
$M_{out\ Rel}$	4.54	5.09
$p_{in\ tot}$	0.11	0.11
$T_{in\ tot}$	0.07	0.07
$p_{out\ tot}$	1.02	1.14
$T_{out\ tot}$	0.42	0.86

80% of Design Speed

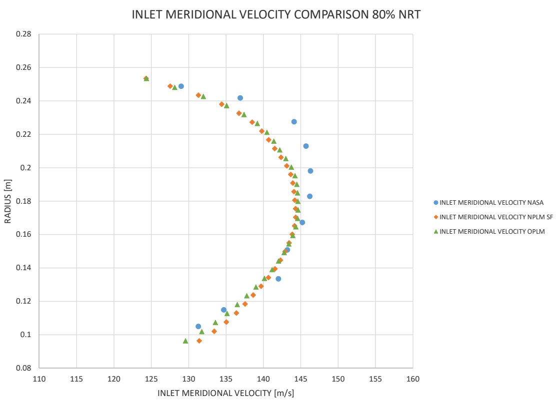

(a) *Inlet Meridional Velocity*

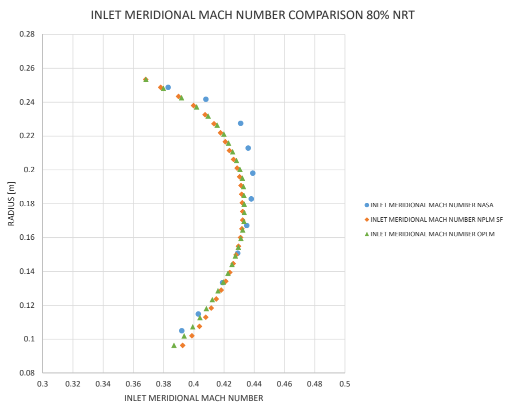

(b) *Inlet Meridional Mach number*

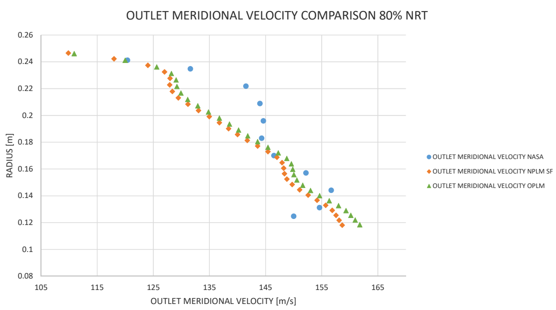

(c) *Outlet Meridional Velocity*

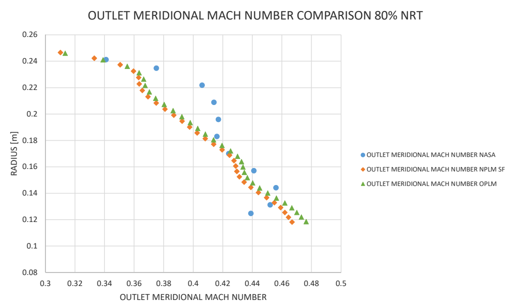

(d) *Outlet Meridional Mach number*

Figure 6.10: Rotor 67 Meridional Velocity and Meridional Mach Number at 80% of Design Speed and $\dot{m}_{corr} = 27.25\ kg/s$

In the figures 6.10, 6.11 and 6.12 the meridional velocity, the meridional Mach number, the relative velocity, the relative Mach number, the total pressure and total temperature at 80% of the design speed for the near peak efficiency operating point are reported respectively.
The operating point considered is characterised by a rotating speed of 12834.8 rpm and a corrected mass flow of $\dot{m}_{corr} = 27.25\ kg/s$.
Considering those figures it appears immediately clear how the flow properties are accurately captured at the blade row inlet station. Passing at considering the blade row outlet the following consideration could be made. For what concerns the outlet meridional velocity and the outlet meridional Mach number, respect to the NASA data, both the models underestimate this properties in proximity of the blade tip and this reflects also in an overestimation of the outlet total pressure that is consistent with the previously underlined error in the pressure ratio and in the adiabatic efficiency prediction at this percentage of the design speed. The maximum error is reached in the hub region, and its magnitude is higher than in the two previous cases as expectable: effectively the thickening of the boundary layer together with the increasing of the design speed produces an higher level of total pressure losses. Capturing this loss mechanism without effectively providing an approximate solution of the boundary layer equations is quite challenging also because of the difficulties of realising experimental measurement in the boundary layer in order to built an empirical correlation capable of modelling the impact of this phenomena on the turbomachine performance.

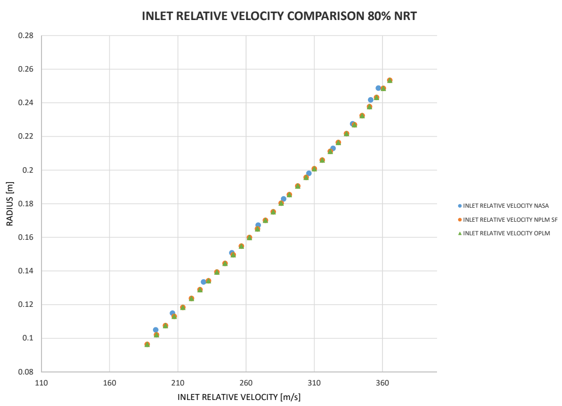

(a) *Inlet Relative Velocity*

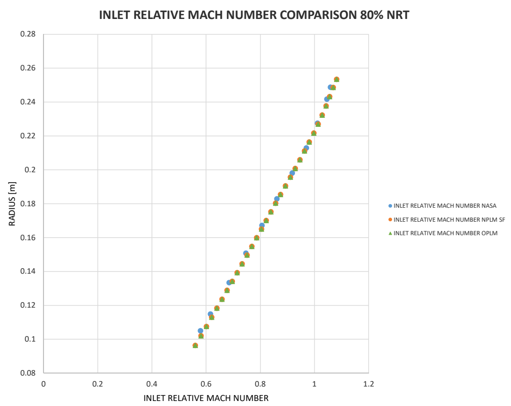

(b) *Inlet Relative Mach number*

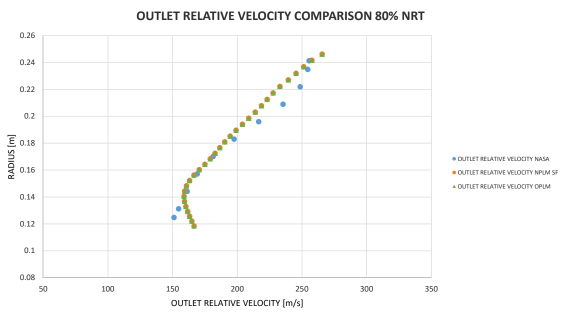

(c) *Outlet Relative Velocity*

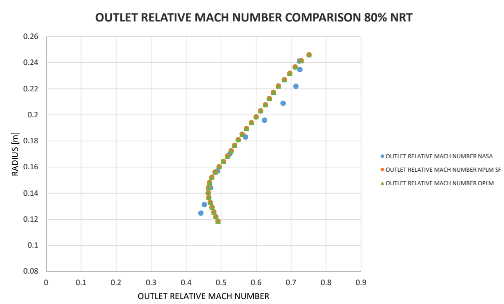

(d) *Outlet Relative Mach number*

Figure 6.11: Rotor 67 Relative Velocity and Relative Mach Number at 80% of Design Speed and $\dot{m}_{corr} = 27.25\ kg/s$

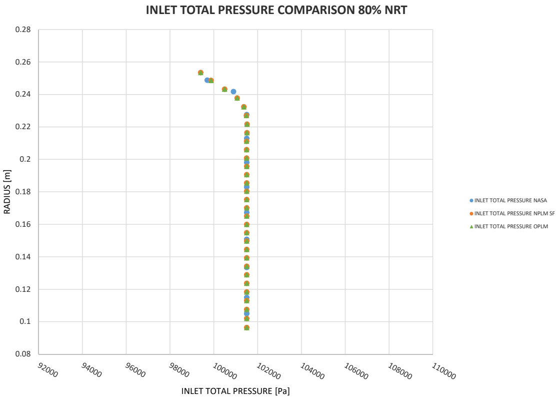

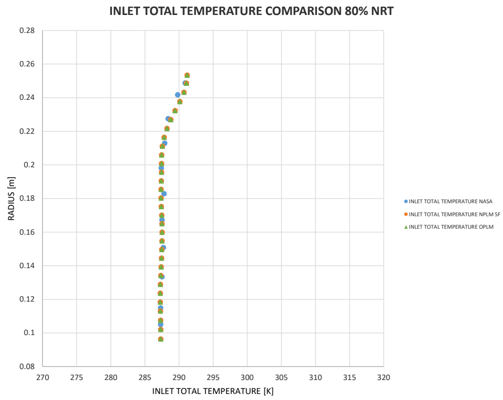

(a) *Inlet total pressure* (b) *Inlet total temperature*

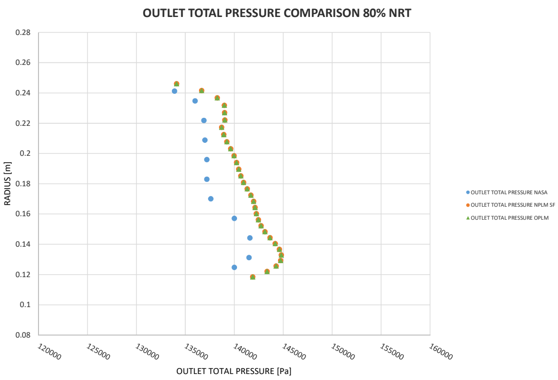

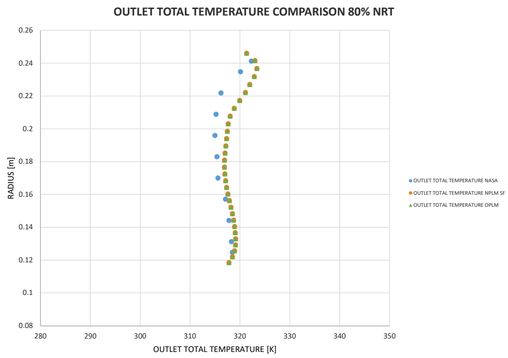

(c) *Outlet total pressure* (d) *Outlet total temperature*

Figure 6.12: Rotor 67 Total Pressure and Total Temperature at 80% of Design Speed and $\dot{m}_{corr} = 27.25\ kg/s$

Table 6.6: Rotor 67 Near Peak Efficiency Flow Properties Prediction at 80% of Design Speed and $\dot{m}_{corr} = 27.25\ kg/s$

Fluid Property	Previous Model Maximum Error [%]	Current Model Maximum Error [%]
$V_{in\ Merid}$	3.41	3.89
$M_{in\ Merid}$	3.71	4.17
$V_{out\ Merid}$	8.94	10.07
$M_{out\ Merid}$	8.21	9.42
$V_{in\ Rel}$	0.29	0.29
$M_{in\ Rel}$	0.35	0.34
$V_{out\ Rel}$	8.05	8.04
$M_{out\ Rel}$	6.34	6.33
$p_{in\ tot}$	0.18	0.17
$T_{in\ tot}$	0.94	0.94
$p_{out\ tot}$	2.30	2.28
$T_{out\ tot}$	1.52	1.51

90% of Design Speed

In the figures 6.13, 6.14 and 6.15 the meridional velocity, the meridional Mach number, the relative velocity, the relative Mach number, the total pressure and total temperature at 90% of the design speed for the near peak efficiency operating point are reported respectively.
The operating point considered is characterised by a rotating speed of 14505 rpm and a corrected mass flow of $\dot{m}_{corr} = 31.05\ kg/s$.

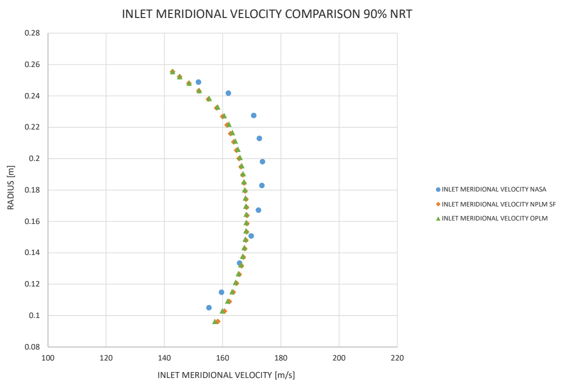

(a) *Inlet Meridional Velocity*

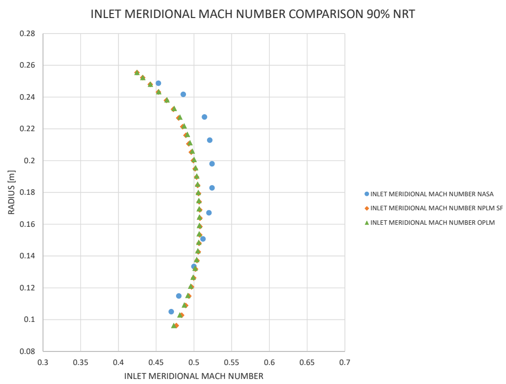

(b) *Inlet Meridional Mach number*

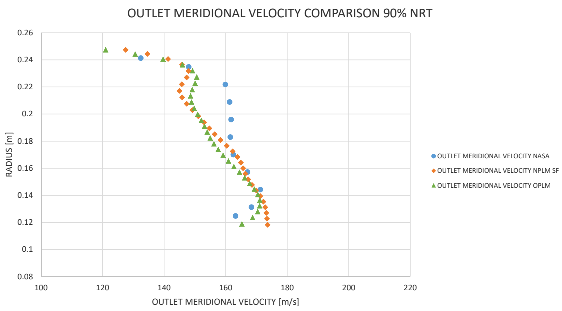

(c) *Outlet Meridional Velocity*

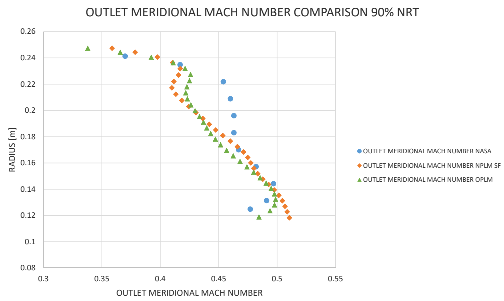

(d) *Outlet Meridional Mach number*

Figure 6.13: Rotor 67 Meridional Velocity and Meridional Mach Number at 90% of Design Speed and $\dot{m}_{corr} = 31.05\ kg/s$

As obtained for the operating points considered at 50%,70% and 80% of design speed, also in this case at the blade row inlet station the fluid properties are captured with an high level of accuracy.
Passing at considering the blade row outlet station and the figures related to the meridional velocity and meridional Mach number, it could be observed that the current model improves the prediction in the region across the blade radius of 0.18 m whilst it loses in accuracy in the hub region respect to the previous model. At this point in the analysis of the results, once having observed the model behaviour in the hub region, nevertheless the error respect to the flow properties prediction committed in this region has an acceptable magnitude for preliminary design purposes, it puts in evidence a limitation of the model in dealing with the hub boundary layer. Despite this, the prediction in terms of total pressure and total temperature results more accurate and consequently also the performance prediction in terms of pressure ratio and adiabatic efficiency

has been improved in terms of accuracy respect to the previous model.
In particular it should be put in evidence that half of the blade is characterised by a relative Mach number equal or greater than one. Consequently the presence of a shock wave along the blade might be expected. Under this point of view, considering the figure related to the outlet total pressure, it could be observed how the gradient of the total pressure shape changes in the region of the radius 0.18 m.
The change in the total pressure gradient together with the fact that around this value of the blade radius the flow is characterized by a relative Mach number greater than one that confirms the hypothesis of the presence of a shock-wave in this region within the blade passage area at this percentage of the design speed and for the value of the corrected mass flow considered.
Considerations on the strength of the shock-wave could be made observing the inlet and outlet relative Mach number. Whilst as mentioned before at the inlet half of the blade experiences transonic flow, at the outlet station the flow is in the subsonic regime and reaches the transonic condition only in correspondence of the blade tip. The magnitude of the meridional Mach number at the inlet and its value at the outlet of the blade row suggests the presence in the region across the radius 0.18 m of an oblique shock-wave.
Consequently this operating condition is not only characterised by blade profile losses and secondary flow losses, but also by the total pressure losses produced by the shock-wave itself.

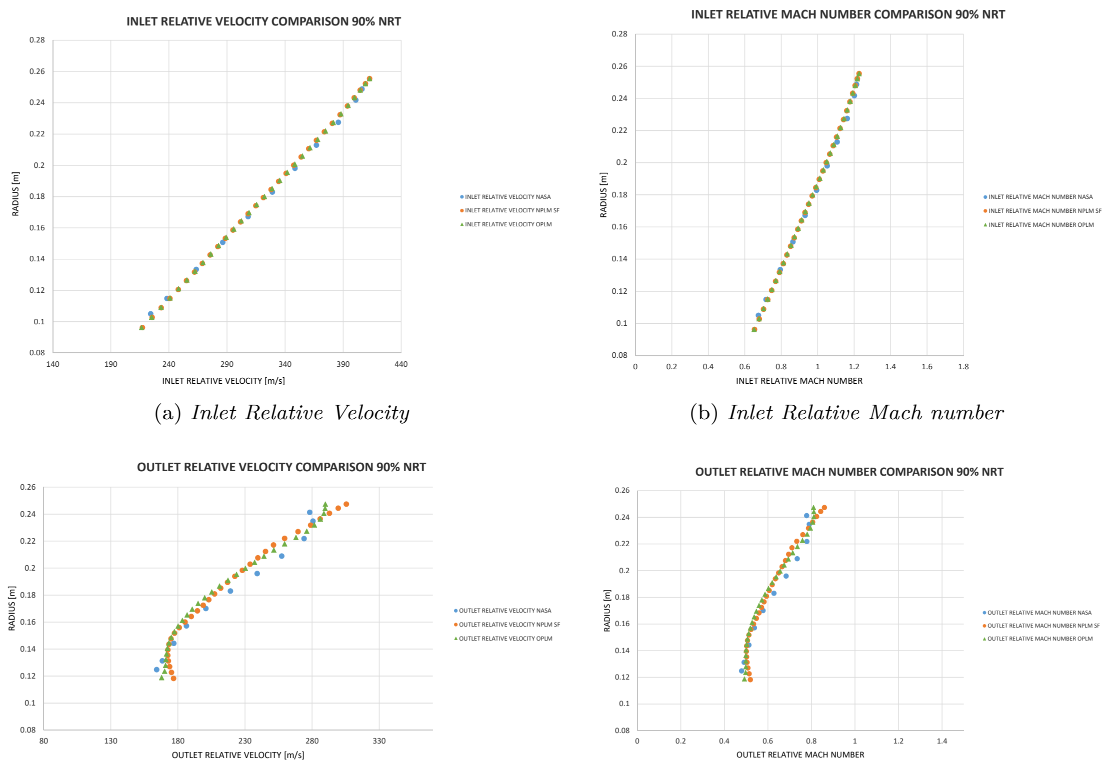

(a) *Inlet Relative Velocity*

(b) *Inlet Relative Mach number*

(c) *Outlet Relative Velocity*

(d) *Outlet Relative Mach number*

Figure 6.14: Rotor 67 Relative Velocity and Relative Mach Number at 90% of Design Speed and $\dot{m}_{corr} = 31.05\ kg/s$

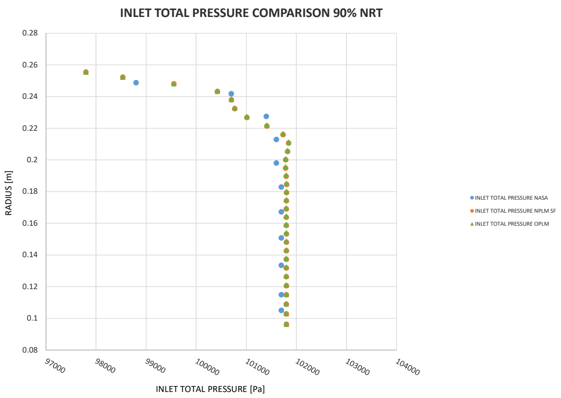

(a) *Inlet total pressure*

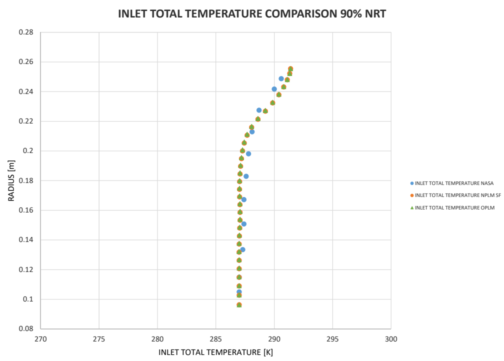

(b) *Inlet total temperature*

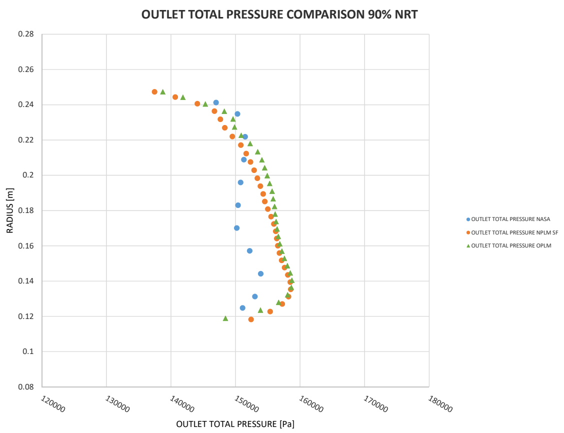

(c) *Outlet total pressure*

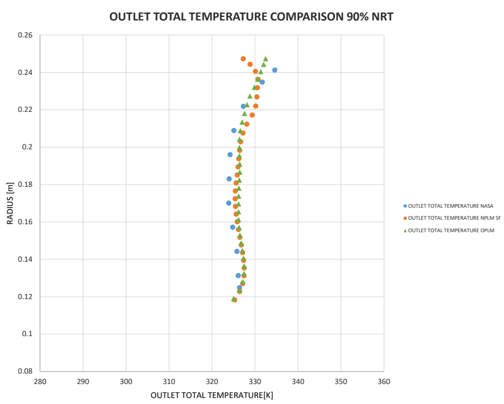

(d) *Outlet total temperature*

Figure 6.15: Rotor 67 Total Pressure and Total Temperature at 90% of Design Speed and $\dot{m}_{corr} = 31.05\ kg/s$

Table 6.7: Rotor 67 Near Peak Efficiency Flow Properties Prediction at 90% of Design Speed and $\dot{m}_{corr} = 31.05\ kg/s$

Fluid Property	Previous Model Maximum Error [%]	Current Model Maximum Error [%]
$V_{in\ Merid}$	5.01	5.37
$M_{in\ Merid}$	5.25	5.64
$V_{out\ Merid}$	7.14	7.51
$M_{out\ Merid}$	6.74	7.39
$V_{in\ Rel}$	0.45	0.53
$M_{in\ Rel}$	0.44	0.59
$V_{out\ Rel}$	6.73	6.94
$M_{out\ Rel}$	4.25	4.97
$p_{in\ tot}$	0.27	0.26
$T_{in\ tot}$	0.17	0.17
$p_{out\ tot}$	4.05	3.82
$T_{out\ tot}$	1.07	1.16

100% of Design Speed

In the figures 6.16, 6.17 and 6.18 the meridional velocity, the meridional Mach number, the relative velocity, the relative Mach number, the total pressure and total temperature at 100% of the design speed for the near peak efficiency operating point are reported respectively.
The operating point considered is characterised by a rotating speed of 16043 rpm and a corrected mass flow of $\dot{m}_{corr} = 34.18\ kg/s$.
The performance and fluid properties prediction at this percentage of the design speed are made more difficult by the transonic flow experienced by the blade across its entire height.
After having observed the performance prediction in terms of pressure ratio and adiabatic efficiency, what was expected in this paragraph was to compare the fluid properties calculated with the models respect to the NASA results. This would help in order to understand the models limitations in the attempt to improve their accuracy in the future. The reader, however, must be aware that the obtained performance prediction for a transonic rotor has already a good level of accuracy considering that it has been obtained using through-flow simulations and the related assumptions and empiricism in the various models incorporated in the tool.

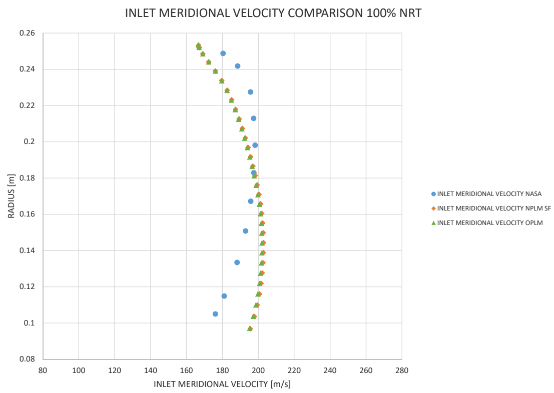

(a) *Inlet Meridional Velocity*

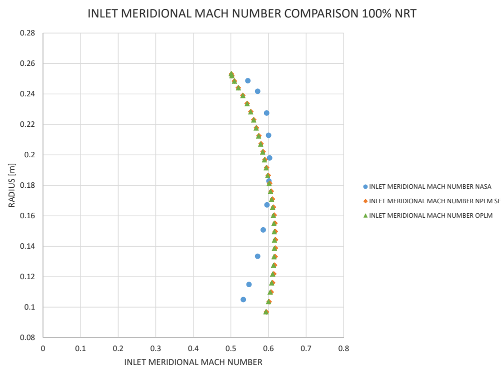

(b) *Inlet Meridional Mach Number*

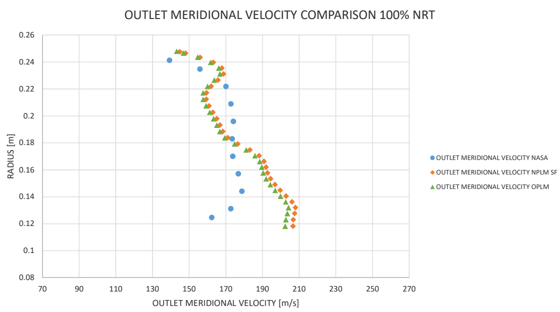

(c) *Outlet Meridional Velocity*

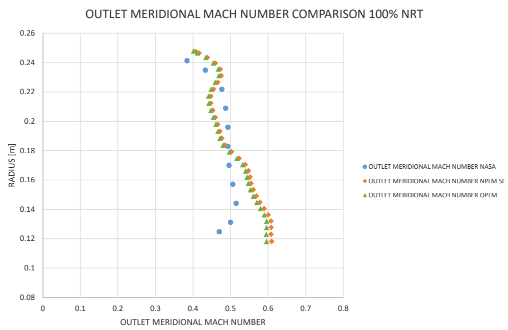

(d) *Outlet Meridional Mach Number*

Figure 6.16: Rotor 67 Meridional Velocity and Meridional Mach Number at 100% of Design Speed and $\dot{m}_{corr} = 34.18\ kg/s$

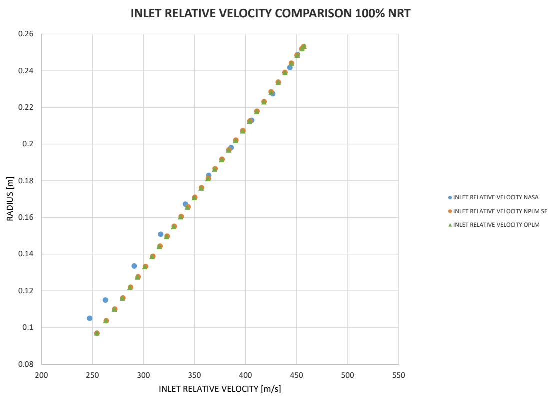

(a) *Inlet Relative Velocity*

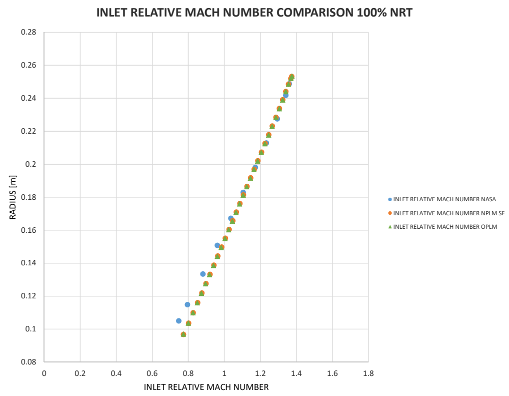

(b) *Inlet Relative Mach number*

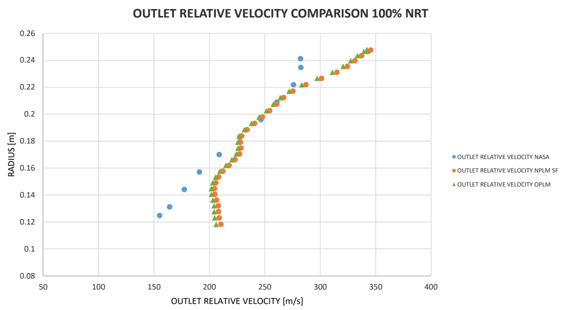

(c) *Outlet Relative Velocity*

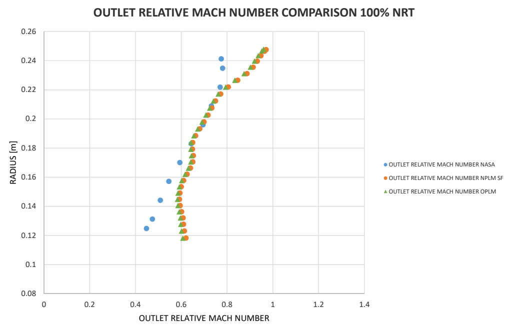

(d) *Outlet Relative Mach number*

Figure 6.17: Rotor 67 Relative Velocity and Relative Mach Number at 100% of Design Speed and $\dot{m}_{corr} = 34.18\ kg/s$

Respect to the results obtained at the lower values of the rotating speed, now an increasing error in the fluid properties prediction is observable at the blade row inlet station. The incidence of the error characterises in particular the hub region: it should be stressed how the extension of this area grows passing from 50% to 100% of the design speed as expectable because of the increasing in the rate of thickening of the boundary layer.
Observing the inlet relative Mach number it might be noticed that the whole blade experiences at this value of the design speed a transonic flow whilst the tip region is also characterised by a slightly supersonic regime.
The gradient change in the outlet pressure plot suggests the presence of an oblique shock-wave across the region correspondent to the blade radius 0.16 m.
The increased magnitude of the loss mechanisms and the inherent complexity of the flow field at this design speed are not captured accurately by both the models which provides an underestimation of the total pressure and total temperature at the blade row outlet that is consistent with the previous error put in evidence in the obtained performance maps presentation.
Interesting to notice is the high accuracy reached in the outlet relative velocity prediction in the zone between the radius 0.18 m and 0.22 m. The errors increase in the zone across the shock-wave position becoming greater in correspondence of the tip and the hub as result for the not accurate capturing of the annulus and casing boundary layer, of the tip vortices and for the turbulent mixing whose magnitude is increased by the shock-wave presence and intensity.

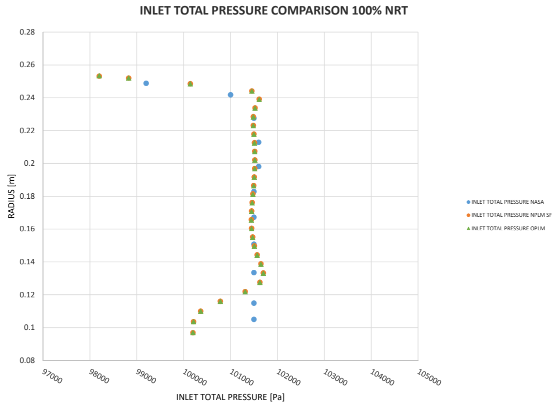

(a) *Inlet total pressure*

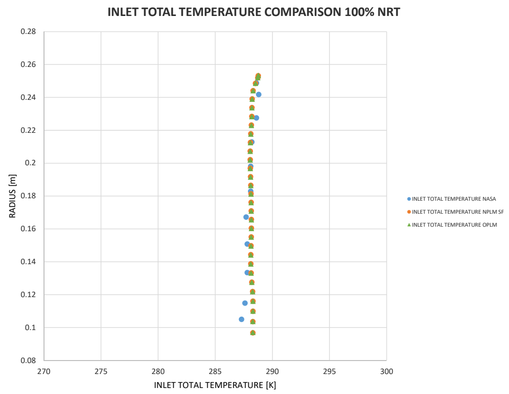

(b) *Inlet total temperature*

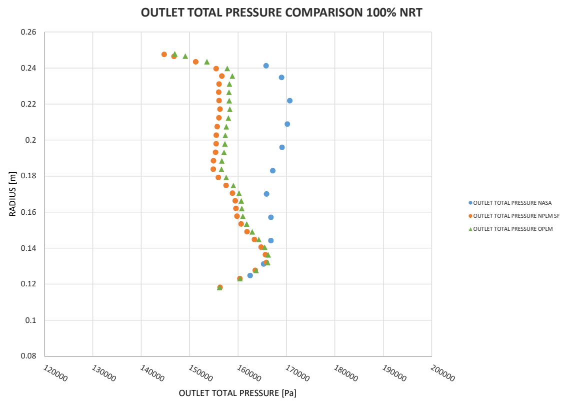

(c) *Outlet total pressure*

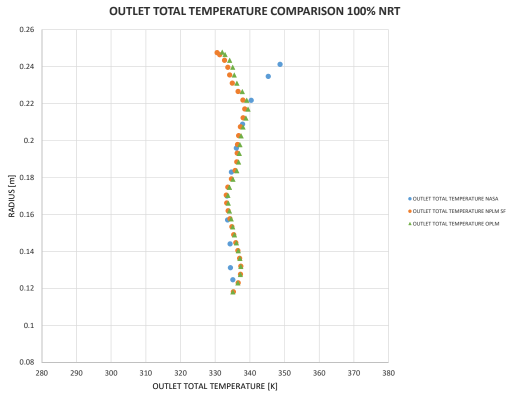

(d) *Outlet total temperature*

Figure 6.18: Rotor 67 Total Pressure and Total Temperature at 100% of Design Speed and $\dot{m}_{corr} = 34.18\ kg/s$

Table 6.8: Rotor 67 Near Peak Efficiency Flow Properties Prediction at 50% of Design Speed and $\dot{m}_{corr} = 34.18\ kg/s$

Fluid Property	Previous Model Maximum Error [%]	Current Model Maximum Error [%]
$V_{in\ Merid}$	11.98	12.15
$M_{in\ Merid}$	12.38	12.57
$V_{out\ Merid}$	20.23	20.57
$M_{out\ Merid}$	20.53	20.72
$V_{in\ Rel}$	6.42	6.55
$M_{in\ Rel}$	7.09	7.23
$V_{out\ Rel}$	23.12	23.22
$M_{out\ Rel}$	19.95	20.00
$p_{in\ tot}$	1.27	1.27
$T_{in\ tot}$	0.34	0.34
$p_{out\ tot}$	7.33	8.59
$T_{out\ tot}$	3.78	4.22

Nevertheless, the capturing of the properties evolution along the blade radius underlines the possibility to further improve the prediction by introducing in the tool empirical correlation models to take into account the loss mechanisms induced by the shock presence in transonic rotors and not only the pressure losses connected with the shock-wave itself. However, taking always in consideration that the tool used was a 2-Dimensional SLC simulator, the assumptions made and the modelisation of the viscosity effects with empirical models, an acceptable agreement has been reached between the calculated results and the measured data nevertheless the inherent 3-Dimensional and viscous character of the flow field within a transonic rotor.

6.3 Model Validation

6.3.1 Rotor 37

After having verified the model, the second phase consists in validating it. The transonic fan chosen for the validation as test geometry has been the *NASA Transonic Rotor 37*, shown in figure 6.19.
The chosen transonic fan has been selected due to an historical reason concerning the tool development. Effectively, historically, the NASA Transonic Rotor 37 has represented one of the most problematic transonic fan geometries that SOCRATES has to deal with during its development. Although on the one hand the tool was able to start iterating and the convergence was reached, on the other the flow solution and the performance prediction provided was completely inconsistent and the results obtained did not respect the physics of the compression within this type of turbomachine.
Consequently the choice to perform the validation over such geometry has represented an important testing bench for the model that once completed as attested its robustness and potential because of the providing of accurate results concerning both the performance and the flow properties prediction.

Figure 6.19: Nasa Rotor 37 Geometry [NASA website]

The *NASA Rotor 37*[47] is a transonic rotor with aspect ratio of 1.19. It is part of a transonic stage, labelled as stage 37, which is characterised by the rotor 37 coupled with the stator 37, characterised by aspect ratio of 1.26. The whole single-stage axial-flow transonic compressor has got a design pressure ratio of 2.05. This single stage compressor is one of a series of single stages

that were designed and tested to investigate the performance characteristics of low-aspect-ratio blading for the inlet stages of an advanced-core compressor[47].
The stage was designed for a total-pressure ratio of 2.05, an airflow of 20.2 kg/s and a rotor tip speed of 454 m/s.

Table 6.9: Rotor 37 Design Point Specifications

Parameter	Magnitude
Number of Rotor Blades	36
Rotational Speed [rpm]	17188.7
Pressure Ratio	2.106
Mass flow [kg/s]	20.188
Rotor tip speed [m/s]	454.136
Inlet Tip Relative Mach Number	1.493

The rotor inlet Mach number has a magnitude of 1.493 at the tip and decreases going towards the hub reaching the value of 1.125. Both rotor and stator have multiple circular arc MCA blade shapes, and in particular, the rotor has a tip solidity of 1.3 and an aspect ratio of 1.9.
The flow path data were reported in the NASA Technical Report[47] and the main characteristics of the flow path for the considered rotor are reported in the table 6.10.

Table 6.10: Rotor 37 Flow Path Characteristics

Parameter	Magnitude
Length [cm]	41.054
Radius Length [cm]	12.8270
z_{min} [cm]	-22.860
z_{max} [cm]	15.4000
r_{min} [cm]	17.526
r_{max} [cm]	25.654

It is important to remark that the sign minus at the z_{min} magnitude is due to the fact that the origin of the z axis corresponds with the rotor location.
As done during the verification phase, also for the validation, once entered the fan model into SOCRATES, the boundary conditions and the operating points to be simulated, it has been possible to calculate the performance map of the rotor and the flow properties and velocities[4] reported with the related comments in the following sections.
However, just a final consideration before proceeding: respect to the *NASA Rotor 67*, for the *NASA Rotor 37* the data provided in the NASA Technical Report were only about 70%, 90% and 100% of the design speed. Consequently the error evaluation in the performance prediction in the following sections will be conducted only for those percentage of the design speed.

[4]It has been chosen to insert in the thesis the flow properties and velocities for the near-peak efficiency operating point for every speed-line as done during the verification phase.

6.3.2 Performance Map

In the figures 6.20 and 6.21 the rotor total pressure ratio and the rotor adiabatic efficiency plotted respect to the corrected mass flow are reported. As general comment before going deeper in the analysis details, it should be put in evidence how the model has overcome the limitation of the previous one giving the possibility not only to simulate the *NASA Rotor 37*, but also to obtain a good level of accuracy in its performance prediction. The final statement is in particular confirmed by the maximum error analysis on the performance prediction against the data provided in the NASA Technical Report and reported in the table 6.11.
Before proceeding it is important to mention that the calculated shape factor according to the model definition for the transonic fan geometry selected for the validation is

$$k_{SF} = 0.5581$$

.

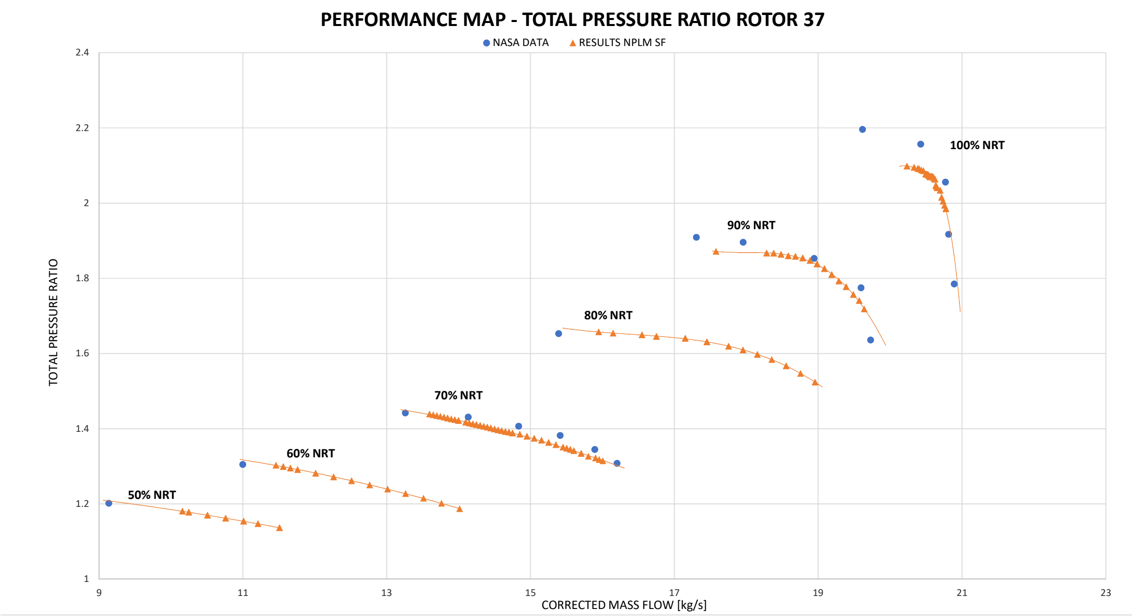

Figure 6.20: Nasa Rotor 67 Performance Map - Total Pressure Ratio

Considering the total pressure ratio performance map, figure 6.20, it is observable the great accuracy in the performance prediction achieved not only at the lower values of the rotating speed but also at the 100% of the design speed. Respect to the case of Rotor 67, where the complex λ shock-wave structure was difficult to be captured accurately. Now, the oblique shock-wave structure that characterises the operating points of the NASA Rotor 37 at 100% of the design speed and the connected shock induced losses are correctly modelled. Another reason for this is the slight supersonic regime experienced at 100% of design speed by the rotor blades, easier to be captured than the transonic character of the flow within the verification geometry, in particular because of the inherent non-linearity that characterize the transonic flow. Consequently the accuracy of the prediction is improved and has reached a good level of agreement against the data provided in the NASA Technical Report.
In particular the chocking region at the higher speed-lines is characterised by a higher level of accuracy in the performance prediction respect to the near-surge region, where in particular at 90%

and 100% of design speed the maximum errors in the total pressure ratio are reached. Effectively the near-surge region represents an inherent non-linear behaviour zone for the fluid, and this characteristic is accentuated by the increasing in rotating speed. However, the reader should be aware, as stressed already a lot of times, that the agreement level reached is already acceptable and of a good level for preliminary design purposes. Clearly a more accurate modelisation could be reached using 3D CFD, but this would increase of at least two orders of magnitude the computational time and resources needed.
Interesting is to observe also the value of the total pressure ratio provided by a single transonic rotor that confirms what already stressed in the introduction chapter.
As final consideration on the total pressure ratio performance map, it should be stressed that the lack of experimental data for the speed-lines at 50%,60% and 80% of the design speed makes impossible the evaluation of the accuracy of the prediction, however the shape of those curves appears consistent with the physics of the phenomena and the prediction in the near-surge region seems to be of a sufficient level of accuracy if compared with the single point available for those values of the rotating speed.

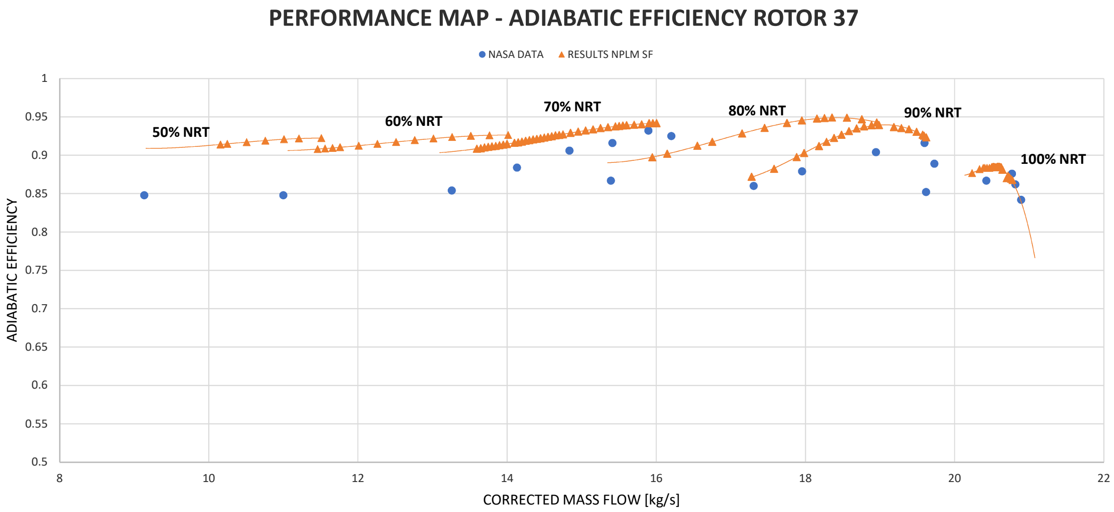

Figure 6.21: Nasa Rotor 67 Performance Map - Adiabatic Efficiency

For what concerns the adiabatic efficiency prediction, figure 6.21,the evolution of this property as a function of the corrected mass flow is well captured. However, going deeper in details, in particular for the lower speed-lines, from 50% to 70%, the error increases when moving towards lower values of the corrected mass flow. This means that the model shows a limitation in capturing the adiabatic efficiency of the turbo-component in the near-surge region. Clearly the agreement level is sufficient considering the 2-Dimensional tool, the assumptions made and the empirical correlation used. Actually capturing the efficiency level in this operating region results difficult also employing 3D-CFD-RANS simulations. As stated also in the previous paragraph, but important to be stressed, the errors made in the adiabatic efficiency prediction are in particular due to a not completely correct modelisation of the entropy production mechanisms and in particular of the secondary flow phenomena. As its definition underlines, both the total pressure gradient and the total temperature gradient has been correctly captured not only in shape but also in magnitude. The difficulties to capture the secondary flow phenomena lead to the discrepancy underlined. Consequently it derives, as it will be discussed in the future improvements, a correct modelisation of those phenomena will be crucial for the application of the tool to axial-flow multi-stage compressors. Obviously all depends on the level of accuracy that it would like to be achieved and on the domain of application of the tool. If it will be limited to the domain of turbomachinery preliminary design, the level of accuracy reached would be extremely high, but improvements are also welcome and would help in reducing the time spent in the preliminary design phase optimising the whole design process.

Table 6.11: Rotor 37 Performance Prediction Maximum Errors

% of Design Speed	Maximum Error on the TPR [%]	Maximum Error on the AE [%]
70	1.35	3.61
90	1.93	3.87
100	4.37	3.97

6.3.3 Flow Properties and Velocities

As the title of the section might suggest, in the following paragraphs the flow properties and velocities trend along the spanwise direction obtained within the model validation simulations will be presented.
For reason of length, in the following paragraphs the operating condition for each speed-line considered will be the near peak efficiency operating point.
For each percentage of the design speed the following properties at the inlet and the outlet station of the transonic fan considered will be provided:

1. total pressure;
2. total temperature;
3. meridional velocity;
4. meridional Mach number;
5. relative velocity;
6. relative Mach number.

The fluid properties calculated and their evolution along the blade radius will be compared against the data provided in the NASA Technical Report. Due to the availability of data only for the speed-lines at 70%, 90% and 100% of the design speed, the comparison would be performed only for the previous cited operating condition at those values of the turbomachine rotating speed.

70% of Design Speed

In the figures 6.22, 6.23 and 6.24 the meridional velocity, the meridional Mach number, the relative velocity, the relative Mach number, the total pressure and total temperature at 70% of the design speed for the near peak efficiency operating point are reported respectively.
The operating point considered is characterised by a rotating speed of 12038.9 rpm and a corrected mass flow of $\dot{m}_{corr} = 15.9\ kg/s$.
The maximum errors committed in the fluid properties and velocities predictions are reported in the table 6.12.
Considering firstly the meridional velocity and the meridional Mach number, the shape and magnitude of those quantities are correctly captured by the model both at the blade inlet row station and at the outlet station.

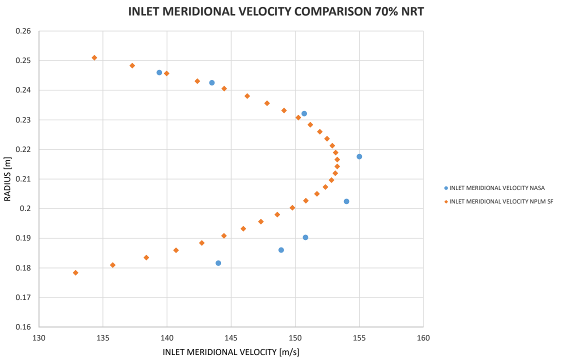

(a) *Inlet Meridional Velocity*

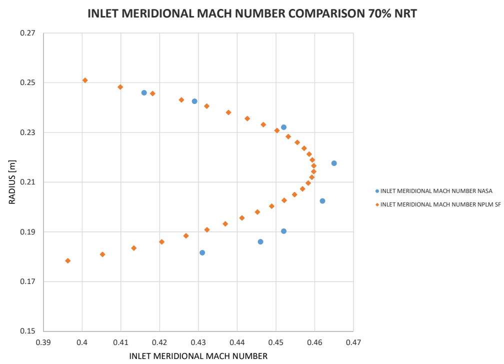

(b) *Inlet Meridional Mach number*

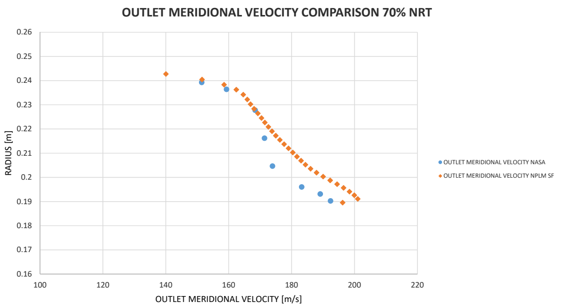

(c) *Outlet Meridional Velocity*

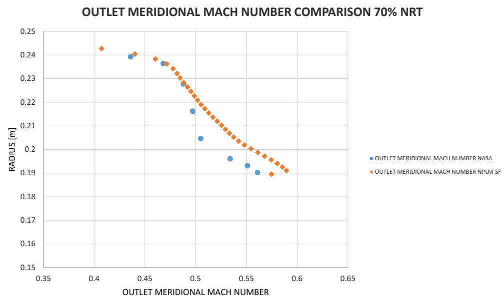

(d) *Outlet Meridional Mach number*

Figure 6.22: Rotor 37 Meridional Velocity and Meridional Mach Number at 70% of Design Speed and $\dot{m}_{corr} = 15.9\ kg/s$

The same statement is applicable also to the relative velocity and Mach number. In particular observing the magnitude of the latter at the blade row inlet, it is possible to notice that the blade tip region is characterised by transonic flow. Moreover considering the relative velocity and Mach number at the blade row outlet, it might be remarked how the evolution of those quantities along the blade radius is well captured except in the tip region where the error increases due to the difficulties to capture the transonic flow field properties also for the possible presence of clearance tip vortices and for the inherent non-linearity of this motion regime. However the grade of agreement still remains of an acceptable level as stated by the maximum errors analysis.
Moreover the overestimation of both the meridional and relative velocity at the blade row outlet underlines also in this case the already mentioned difficulties in dealing with the annulus boundary layer. At this percentage of the design speed in particular, the error in this region is not characterised by a significant magnitude but, as it will be possible to observe in the following sections, it will increase with the increasing in the rotating speed. This is an expected behaviour because of the fact that the augmentation in the rotating speed will produce an higher rate of thickening of the boundary layer, and at the same time will boost the dissipative phenomena intensity and, in particular the intensity of the mixing at the boundary layer frontier as well as the magnitude of the secondary flows.

Finally considering the figure 6.24, it is possible to notice that the total pressure and temperature plots show a good level of agreement against the data provided in the NASA Technical Report both for the blade row inlet and outlet station.

Observing more in details the shape of the outlet total pressure along the blade radius, it might be noticed a change in the curve gradient in correspondence of the region where the relative flow reaches a Mach number equal to unity. These two conditions coupled together suggest the presence of a weak oblique-shock wave in this region.

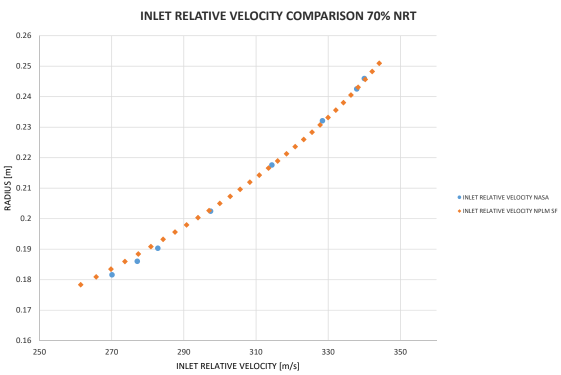

(a) *Inlet Relative Velocity*

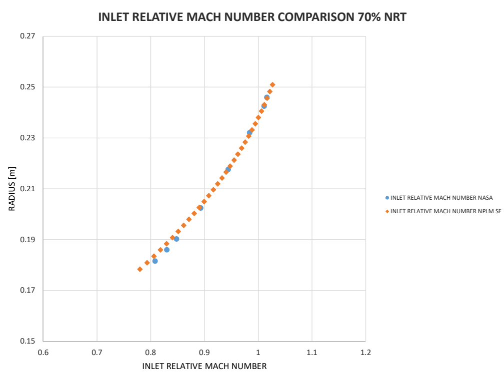

(b) *Inlet Relative Mach number*

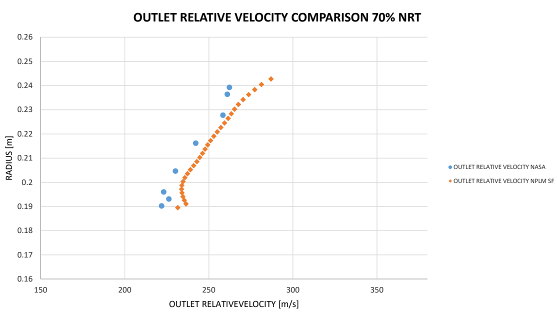

(c) *Outlet Relative Velocity*

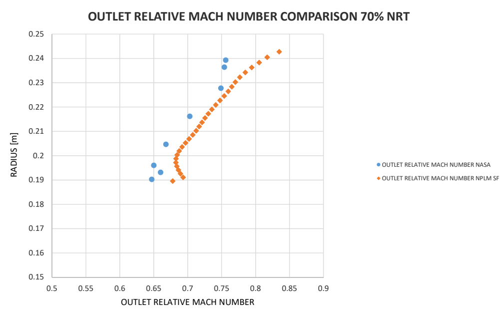

(d) *Outlet Relative Mach number*

Figure 6.23: Rotor 37 Relative Velocity and Relative Mach Number at 70% of Design Speed and $\dot{m}_{corr} = 15.9\ kg/s$

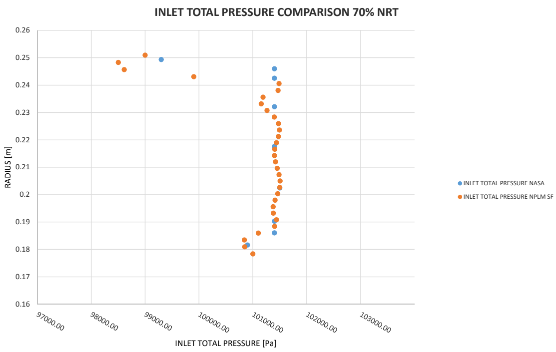

(a) *Inlet total pressure*

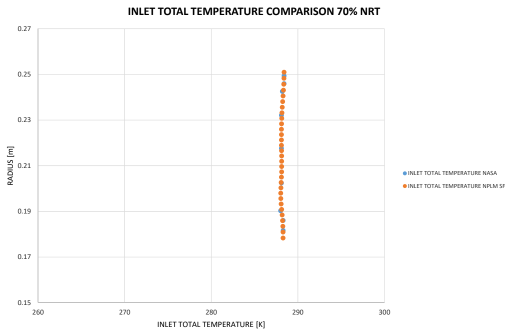

(b) *Inlet total temperature*

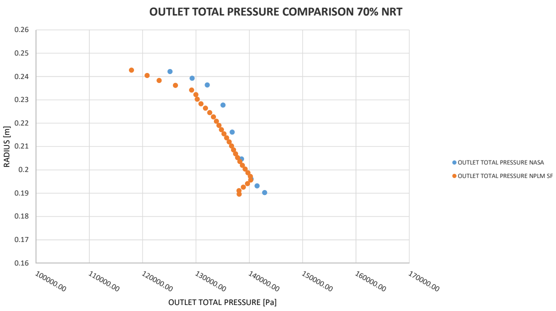

(c) *Outlet total pressure*

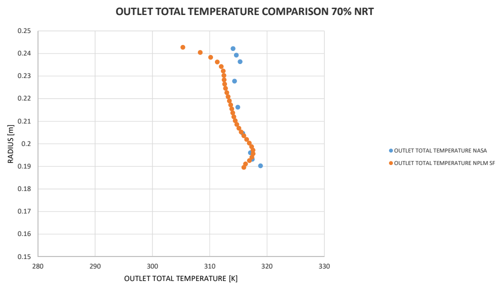

(d) *Outlet total temperature*

Figure 6.24: Rotor 37 Total Pressure and Total Temperature at 70% of Design Speed and $\dot{m}_{corr} = 15.9\ kg/s$

Table 6.12: Rotor 37 Near Peak Efficiency Flow Properties Prediction at 70% of Design Speed and $\dot{m}_{corr} = 15.9\ kg/s$

Fluid Property	Current Model Maximum Error [%]
$V_{in\ Merid}$	2.23
$M_{in\ Merid}$	2.44
$V_{out\ Merid}$	6.98
$M_{out\ Merid}$	6.93
$V_{in\ Rel}$	1.62
$M_{in\ Rel}$	1.86
$V_{out\ Rel}$	4.08
$M_{out\ Rel}$	4.39
$p_{in\ tot}$	2.75
$T_{in\ tot}$	0.007
$p_{out\ tot}$	3.36
$T_{out\ tot}$	1.42

90% of Design Speed

In the figures 6.25, 6.26 and 6.27 the meridional velocity, the meridional Mach number, the relative velocity, the relative Mach number, the total pressure and total temperature at 90% of the design speed for the near peak efficiency operating point are reported respectively.
The operating point considered is characterised by a rotating speed of 15469.6 rpm and a corrected mass flow of $\dot{m}_{corr} = 19.6\ kg/s$.
The maximum errors committed in the fluid properties and velocities predictions are reported in the table 6.13.

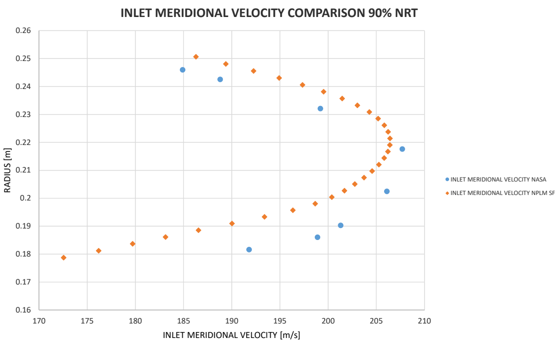

(a) *Inlet Meridional Velocity*

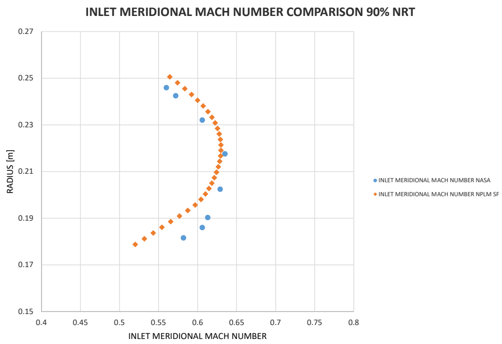

(b) *Inlet Meridional Mach number*

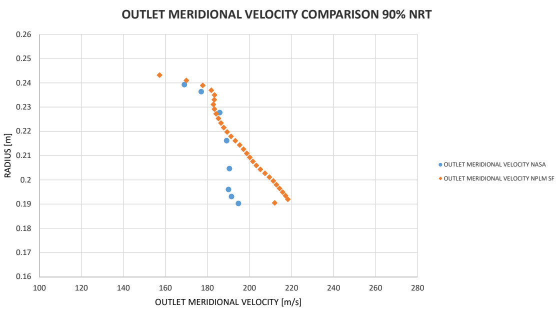

(c) *Outlet Meridional Velocity*

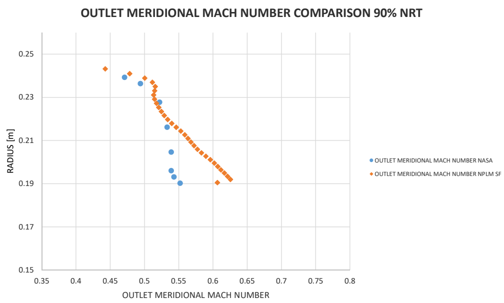

(d) *Outlet Meridional Mach number*

Figure 6.25: Rotor 37 Meridional Velocity and Meridional Mach Number at 90% of Design Speed and $\dot{m}_{corr} = 19.6\ kg/s$

For all of the fluid properties and velocities plotted, their shape and magnitude is correctly captured at the blade row inlet station.
Observing in particular the magnitude of the relative inlet Mach number, it should be noticed that the entire blade experiences a transonic flow and, in particular, the tip region, on its hand, is characterised by a slightly supersonic flow.
Passing at considering the blade row outlet station and the meridional velocity, the accuracy reached in the shape and magnitude prediction of this quantity in the tip region clashes with the lower accuracy at the blade hub. The thickening of the boundary layer, whose equations are not solved into the through-flow tools, with the increasing in the rotating speed makes greater the region characterised by a lower accuracy in the meridional velocity magnitude detected with the tool. However the maximum error committed, considering all the assumptions made and the

empirical correlations used, makes still acceptable the result nevertheless the meridional velocity overestimation at the blade hub.

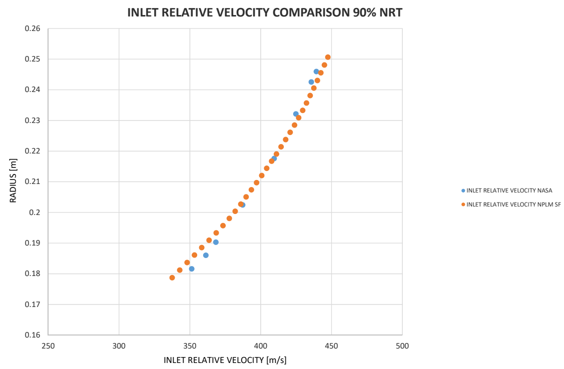

(a) *Inlet Relative Velocity*

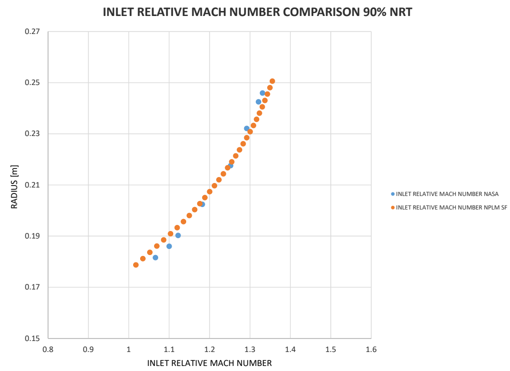

(b) *Inlet Relative Mach number*

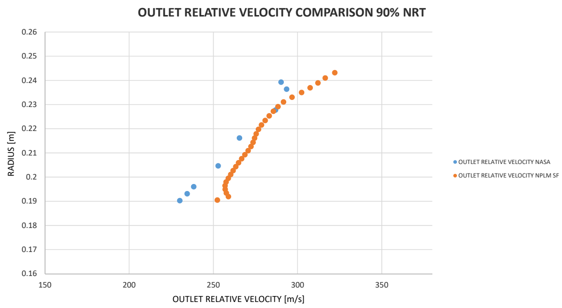

(c) *Outlet Relative Velocity*

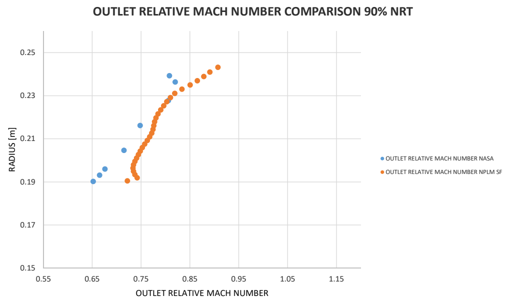

(d) *Outlet Relative Mach number*

Figure 6.26: Rotor 37 Relative Velocity and Relative Mach Number at 90% of Design Speed and $\dot{m}_{corr} = 19.6\ kg/s$

Observing the outlet total pressure evolution along the blade radius and in particular the region across the blade radius value of 0.23 m, it might be noticed a change in the total pressure gradient that, considering the relative Mach number experienced by the blade across this value of the radius, suggests the presence of an oblique shock-wave in this region within the blade passage.
The presence of the shock wave is responsible for the increasing in the flow rotational character, for the increasing in intensity of the mixing region and for its interaction with the boundary layer determining an higher level of total pressure losses.
These phenomena are not completely detected by the tool as underlined by the outlet relative velocity shape in the tip region and by the overestimation of its magnitude. Under this point of view the introduction of a spanwise mixing model and of a model capable of detecting the effects of the interaction between the boundary layer and the shock-wave would definitely improve the results produced. Clearly an analytical approach to those phenomena modelisation is not suitable, also considering the related implications in terms of computational time and cost. Probably it would be preferable to adopt a numerical approach driven by experimental results with all the difficulties connected with the application of the latter.
Interesting to notice is also the higher level of total pressure losses in the tip and hub region respect to the middle of the blade: the dissipative secondary flow phenomena effectively characterise those zones and their effect compared to the mixing, usually observable at the blade mid-radius, is higher

under the loss production point of view.

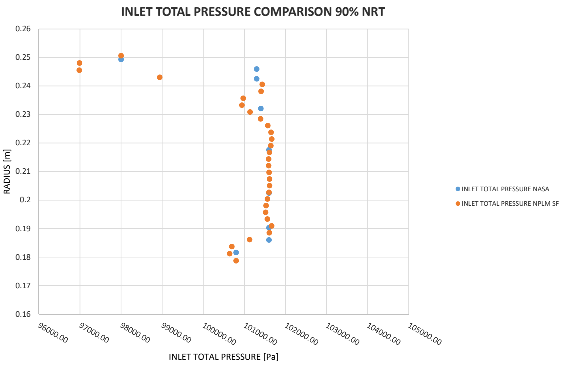

(a) *Inlet total pressure*

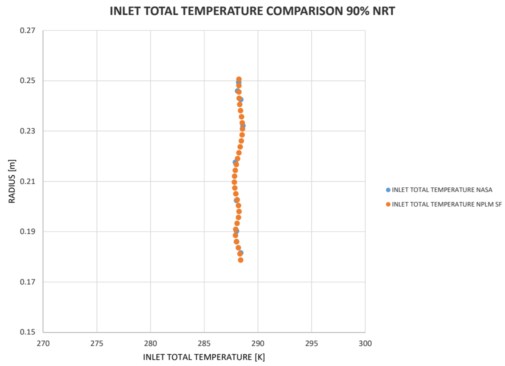

(b) *Inlet total temperature*

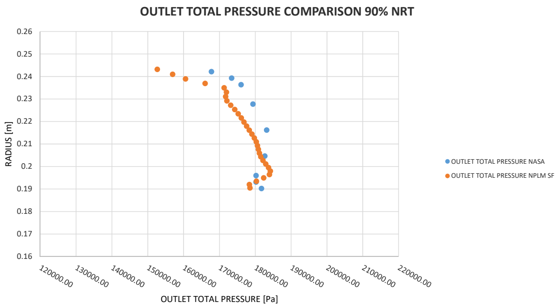

(c) *Outlet total pressure*

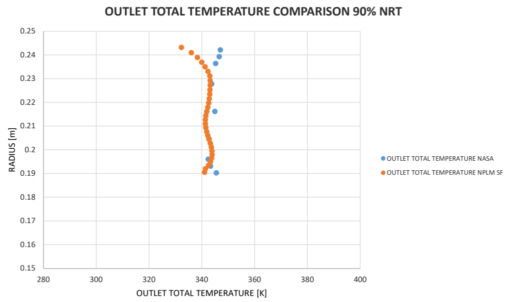

(d) *Outlet total temperature*

Figure 6.27: Rotor 37 Total Pressure and Total Temperature at 90% of Design Speed and $\dot{m}_{corr} = 19.6\ kg/s$

Table 6.13: Rotor 37 Near Peak Efficiency Flow Properties Prediction at 90% of Design Speed and $\dot{m}_{corr} = 19.6\ kg/s$

Fluid Property	Current Model Maximum Error [%]
$V_{in\ Merid}$	6.20
$M_{in\ Merid}$	6.70
$V_{out\ Merid}$	13.43
$M_{out\ Merid}$	14.36
$V_{in\ Rel}$	2.41
$M_{in\ Rel}$	2.91
$V_{out\ Rel}$	9.94
$M_{out\ Rel}$	10.83
$p_{in\ tot}$	2.32
$T_{in\ tot}$	0.005
$p_{out\ tot}$	3.47
$T_{out\ tot}$	4.24

100% of Design Speed

In the figures 6.28, 6.29 and 6.30 the meridional velocity, the meridional Mach number, the relative velocity, the relative Mach number, the total pressure and total temperature at 100% of the design speed for the near peak efficiency operating condition are reported respectively.
The operating point considered is characterised by a rotating speed of 17188.7 rpm and a corrected mass flow of $\dot{m}_{corr} = 20.6\ kg/s$.
The maximum errors committed in the fluid properties and velocities predictions are reported in the table 6.14.

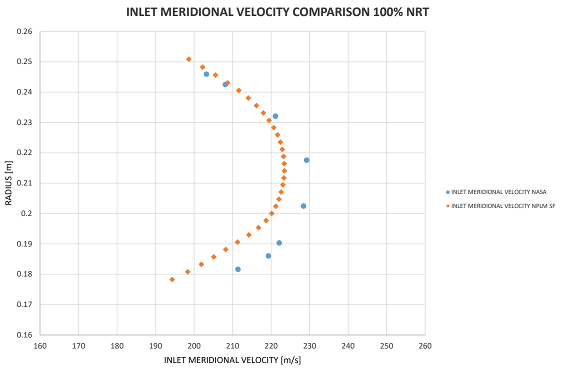

(a) *Inlet Meridional Velocity*

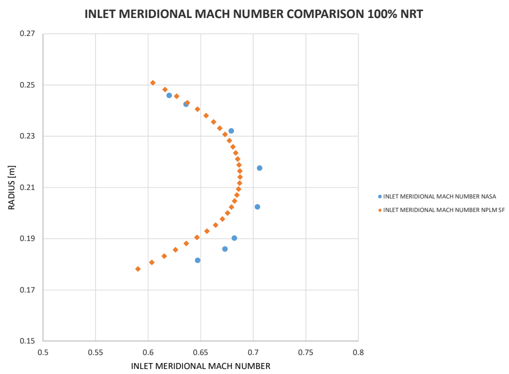

(b) *Inlet Meridional Mach number*

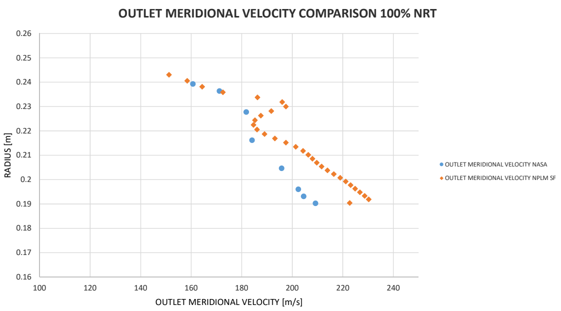

(c) *Outlet Meridional Velocity*

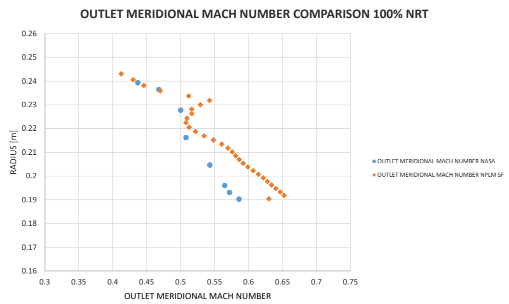

(d) *Outlet Meridional Mach number*

Figure 6.28: Rotor 37 Meridional Velocity and Meridional Mach Number at 100% of Design Speed and $\dot{m}_{corr} = 20.8\ kg/s$

The flow properties and velocities detected at the blade row inlet show a good level of agreement against the data provided in the NASA Technical Report, as confirmed by the maximum error analysis.
In addiction to the usual discrepancy caused by the boundary layer modelisation in the hub region at which the reader should have used to, interesting to notice in the shape of the meridional and relative outlet velocity along the blade radius is the presence of a cusp. The same trend as expectable is observed for the related Mach numbers.

Observing more in details those diagrams, the location of the cusp is at $r_{blade} = 0.23\ m$. Keeping in mind this positions and considering the diagrams related to the outlet total pressure and total temperature, these two properties in correspondence of the previous mentioned value of the blade radius present a strong change in the gradient imputable to the presence of an oblique shock wave. The presence of the shock wave is confirmed by the fact that the blade experiences in the hub region a slightly supersonic flow whilst the rest of the blade is characterised by a definitely supersonic region, and in correspondence of the detected radius the relative flow at the blade row inlet is supersonic. Moreover the hypothesis on the oblique character of the shock is confirmed comparing the inlet and outlet relative Mach number, the Mach number at the blade row outlet at this value of the blade radius is still transonic and consequently the shock wave type is with all probability an attached oblique shock wave.

Nevertheless the shock wave presence, the different and lower complexity of the shock wave configuration has permitted to reach an high level of accuracy also at 100% of design speed respect to the lower level of precision reached in the Rotor 67 fluid properties and velocities prediction as showed previously.

Finally, it is also interesting to focus the attention on the blade tip region and in particular on the outlet total pressure diagram. Observing this graph for the different percentage of the design speed considered, it is possible to notice that the rate of reduction in the outlet total pressure magnitude in the tip region raises with the increasing in the rotational speed. This underlines the increasing magnitude of the tip clearance vortices and secondary effects mainly responsible for the total pressure loss production in this region.

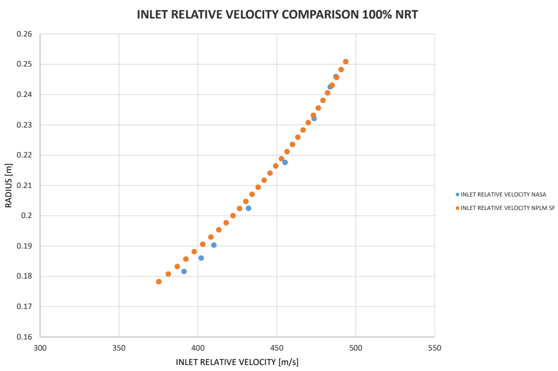

(a) *Inlet Relative Velocity*

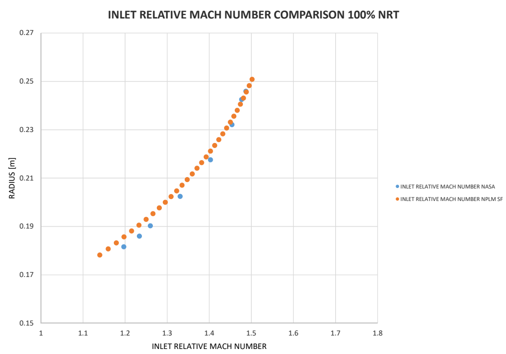

(b) *Inlet Relative Mach number*

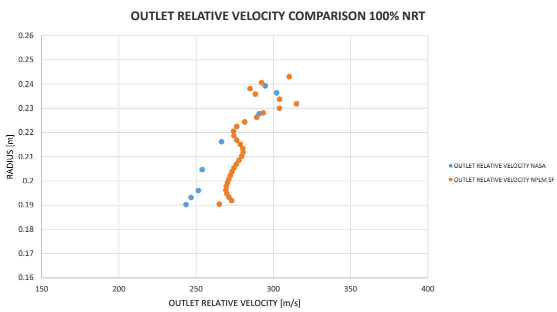

(c) *Outlet Relative Velocity*

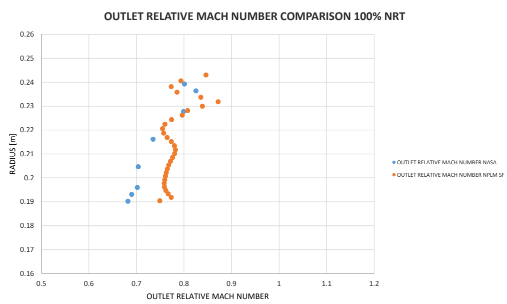

(d) *Outlet Relative Mach number*

Figure 6.29: Rotor 37 Relative Velocity and Relative Mach Number at 100% of Design Speed and $\dot{m}_{corr} = 20.8\ kg/s$

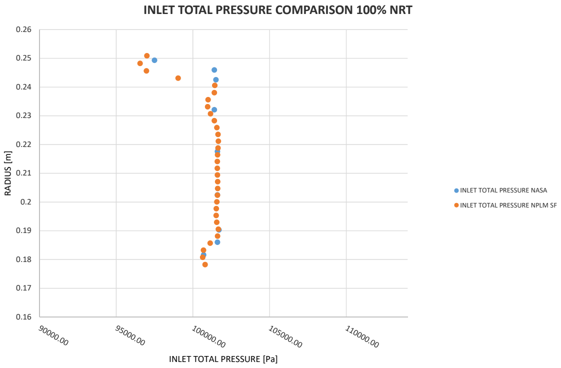

(a) *Inlet total pressure*

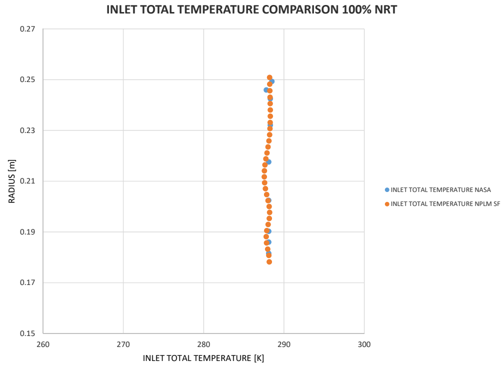

(b) *Inlet total temperature*

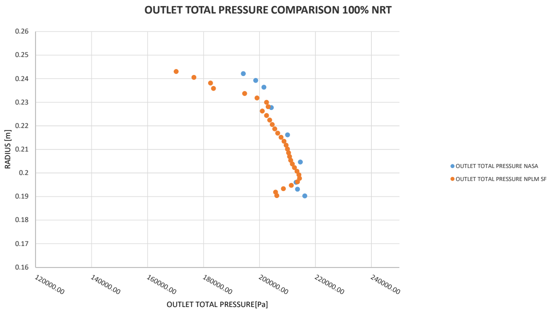

(c) *Outlet total pressure*

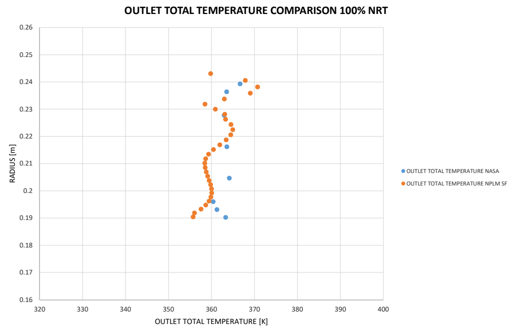

(d) *Outlet total temperature*

Figure 6.30: Rotor 37 Total Pressure and Total Temperature at 100% of Design Speed and $\dot{m}_{corr} = 20.8\ kg/s$

Table 6.14: Rotor 37 Near Peak Efficiency Flow Properties Prediction at 100% of Design Speed and $\dot{m}_{corr} = 20.8\ kg/s$

Fluid Property	Current Model Maximum Error [%]
$V_{in\ Merid}$	4.50
$M_{in\ Merid}$	4.95
$V_{out\ Merid}$	11.78
$M_{out\ Merid}$	12.94
$V_{in\ Rel}$	2.56
$M_{in\ Rel}$	3.17
$V_{out\ Rel}$	9.91
$M_{out\ Rel}$	10.14
$p_{in\ tot}$	2.43
$T_{in\ tot}$	0.15
$p_{out\ tot}$	5.48
$T_{out\ tot}$	2.081

6.4 Model Application

6.4.1 NASA Two Stage Fan

Once completed the verification and validation of the model, the final step has consisted in the application to an example of multi-stage transonic compressor. Due to the availability of the experimental data and the necessity to chose data available in the open literature, the choice is spill-over the *NASA Two Stage Fan*[46], shown in figure 6.31.

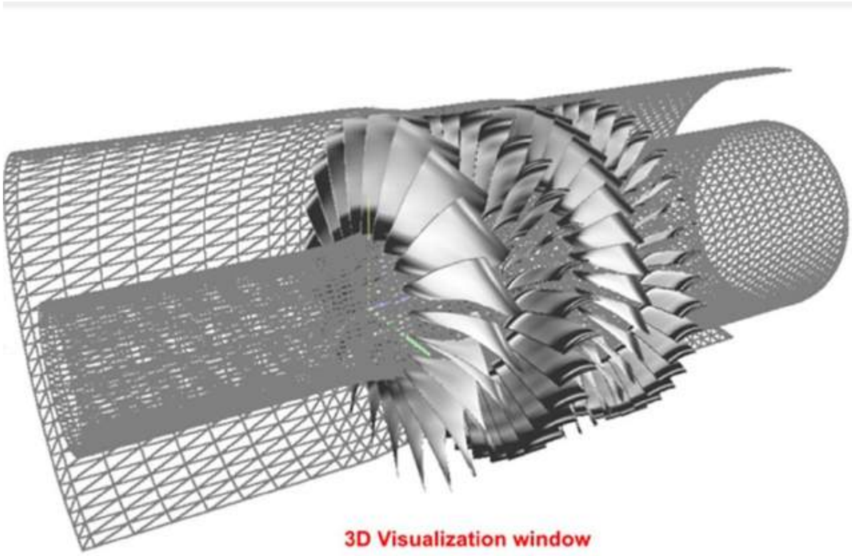

Figure 6.31: Nasa Two Stage Fan - Compressor 3D Render - SOCRATES GUI

This two stages transonic axial-flow compressor has been designed for a mass flow of 33.248 kg/s, an overall pressure ratio of 2.4, an adiabatic efficiency of 0.846 and a rotative speed of 16042.8 rpm. Before proceeding it should be stressed that, as reported in the NASA Technical report, the velocity diagrams and the flow conditions data provided by the NASA researchers were calculated by using a stream-line analysis computational procedure, which provided an axisymmetric, compressible-flow solution to the continuity, energy, and radial equilibrium equations.
The first stage rotor of this compressor is the NASA transonic Rotor 67, whose characteristics were presented in details in the section concerning the model verification and consequently they will not be reported again in this section. The second stage rotor is characterised by a blading that is of the MCA-type from the tip to 44% of the span and DCA-type over the remainder span. For what concerns the two stators, both have DCA-type blading over their entire span. The design point specifications for the *NASA Two Stage Fan* are shown in the table 6.15.
Interesting to remark is that the blade thickness distribution of the two stators varied linearly from the blade hub to tip whilst the blade thickness distribution of the second-stage rotor follows a cubic relation. These design choice are in particular driven by the necessity to provide an acceptable frequency margin between the first bending mode and the two-per-revolution excitation at 110% of the design speed[48].
Moreover the first stage stator, the second stage rotor and the second stage stator are respectively characterised by an aspect ratio of 1.98, 1.89 and 1.85.

Table 6.15: NASA Two Stage Fan Design Point Specifications

Parameter	Magnitude
Number of 1st Stage Rotor Blades	22
Number of 1st Stage Stator Blades	34
Number of 2nd Stage Rotor Blades	38
Number of 2nd Stage Stator Blades	42
Rotational Speed [rpm]	16042.8
Pressure Ratio	2.4
Adiabatic Efficiency	0.846
Mass flow [kg/s]	33.248
1st Rotor tip speed [m/s]	426.72
2nd Rotor tip speed [m/s]	405.341

Originally, the first rotor of the two stages fan was not the NASA Rotor 67 but a rotor constituted by 43 blades and an aspect ratio of 2.9. In particular its blades were characterised by a linear thickness distribution and were of the MCA-type. This rotor was also equipped with part-span dampers aimed at reducing the blade vibratory stresses and located at the 42% of the blade span from the outlet rotor tip. The reasons for the substitution of this rotor with the Rotor 67 were basically the following:

- low-aspect-ratio turbomachinery blading offers the relevant advantage of fewer blades and lower fabrication cost;
- more rugged blading thanks to the longer cord and consequent elimination of dampers and their aerodynamic induced losses;
- higher efficiency;
- reduction of the radial pressure gradients induced by the dampers, resulting in an increase in the efficiency and performance of both the first stage stator and the second stage.

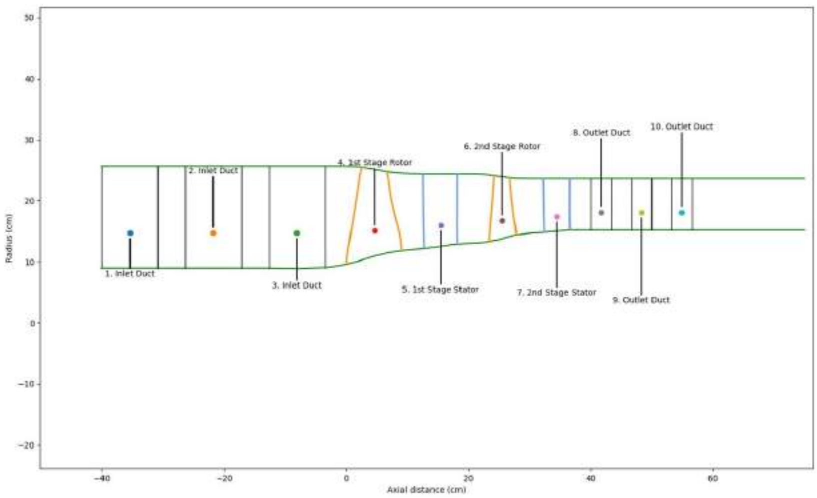

Figure 6.32: Nasa Two Stage Fan - Flow Path Render - SOCRATES GUI

The flow path coordinates in the meridional plane for the blade tip and hub were provided by the NASA technical report 1493[46], the flow path sketch is showed in figure 6.32 and its main characteristics are reported in the table 6.16.

Table 6.16: NASA Two Stage Fan Flow Path Characteristics

Parameter	Magnitude
Length [cm]	100.00
Radius Length [cm]	16.8364
1st Rotor Spacing [%]	21.068
1st Stator Spacing [%]	25.4341
2nd Rotor Spacing [%]	43.2168
2nd Stator Spacing [%]	44.6871

Respect to the coordinates reported in the NASA Technical Report, some "ducts" components have been added as observable by the sketch reported. The ducts are not real physical components but are defined in the computational domain only with the purpose of setting the initialization values of the flow for the iterative calculation.
As done during the previous phases, once entered the fan model into SOCRATES, the boundary conditions and the operating point to be simulated, it has been possible to calculate the performance map of the compressor and the flow properties and velocities[5] reported with the related comments in the following sections.

6.4.2 Performance Map

In the figures 6.33 and 6.34 the rotor total pressure ratio and the rotor adiabatic efficiency respected to the corrected mass flow are reported.
Before proceeding, it is important to provide to the reader the calculated shape factor per turbo-component according to the model definition for the geometry selected for the model application which are:

1. 1st Stage Rotor $k_{SF} = 1$;
2. 1st Stage Stator $k_{SF} = 0.5541$;
3. 2nd Stage Rotor $k_{SF} = 0.8955$;
4. 2nd Stage Stator $k_{SF} = 0.5331$.

Moreover in addiction to the performance maps for the entire two stage axial-flow compressor, in the figures 6.35 and 6.36 the total pressure ratio map and the adiabatic efficiency map for the first stage are shown whilst in the figures 6.37 and 6.38 the total pressure ratio map and the adiabatic efficiency map for the second stage are shown. Important to remark is the fact that the corrected mass flow in the single stage maps is related to the inlet conditions of the stage considered.

[5] It has been chosen to insert in the thesis the flow properties and velocities for the near-peak efficiency operating point for every speed-line as done during the verification and validation phase.

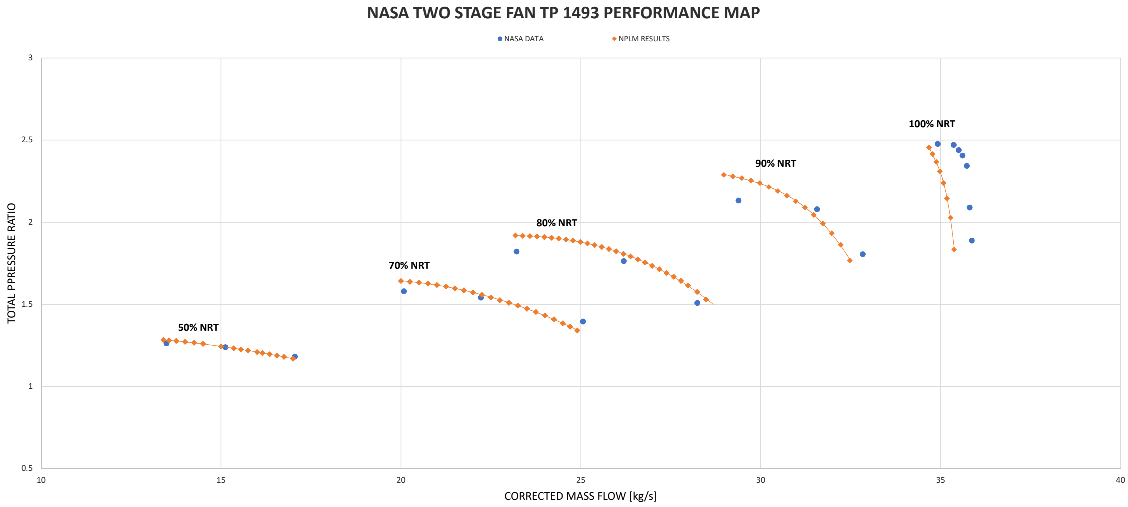

Figure 6.33: Nasa Two Stage Fan Performance Map - Total Pressure Ratio

Table 6.17: NASA Two Stage Fan Performance Prediction Maximum Errors - Current Model

% of Design Speed	Maximum Error on the TPR [%]	Maximum Error on the AE [%]
50	1.66	6.62
70	3.93	12.06
80	4.88	11.94
90	6.89	12.91
100	15.10	13.34

Considering the performance maps obtained for the considered two stage compressor a general comment might be made. The results obtained show a general good level of agreement against the data provided in the NASA Technical Report.
Considering the total pressure ratio map, a general rise of the error in the performance prediction is observable with the increasing in the compressor rotating speed. In particular at 100% of the design speed, the error committed seems to be due to the chocking model employed in the tool and developed with the shock loss model. The compressor on this speed-line effectively seems to chock at a value of the corrected mass-flow which is lower than the one predicted by the NASA data.
Generally the performance prediction accuracy level is acceptable for the preliminary design phase. However further improvements should be considered. The flow field losses within a multi-stage axial-flow compressor are strongly related to the wake and the boundary layer thickening. In particular the wake produced by each blade and its interaction both with the following turbo-component and with the wake of the adjacent blades are among the major total pressure loss sources. At this stage of its development, the tool is not equipped with a reliable wake loss model and the only way the wake has been taken into account in the profile loss model has been through the calibration procedure. This kind of modelisation produces good results but it is based on a preliminary modelisation. Going deeper into the analysis and equipping SOCRATES with a reliable model capable of predicting the wake effects and interactions would definitely improve the performance prediction accuracy, in particular at the higher values of the rotating speed when the magnitude of the wake and secondary flow phenomena increases in terms of total pressure loss

production.

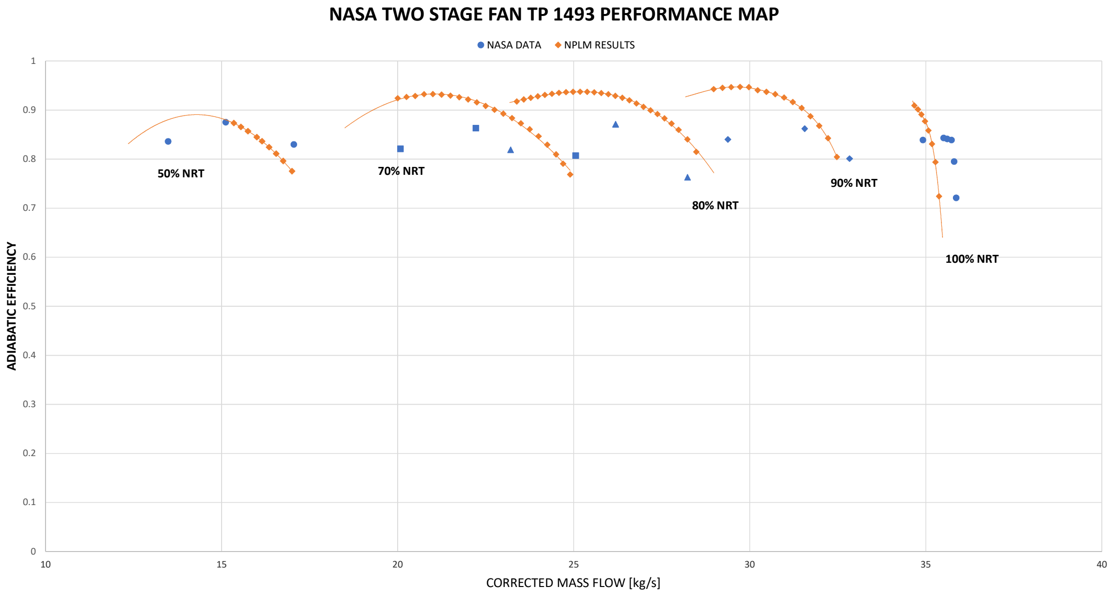

Figure 6.34: Nasa Two Stage Fan Performance Map - Adiabatic Efficiency

The necessity to improve the wake and secondary flow phenomena effects and their interactions is highlighted also by the results shown in the adiabatic efficiency map. In particular the results obtained are coherent with the evolution of the adiabatic efficiency as a function of the corrected mass-flow for each percentage of the design speed. The error committed in the magnitude prediction, although the accuracy of the results is good, might be reduced thanks to a better capture of the effect of the previous mentioned flow phenomena under the entropy production point of view. Also in this case it is possible to remark the increasing maximum error committed with the increasing in the rotating speed, as expectable due to the rise in magnitude of the previous mentioned wake and secondary flows effects.

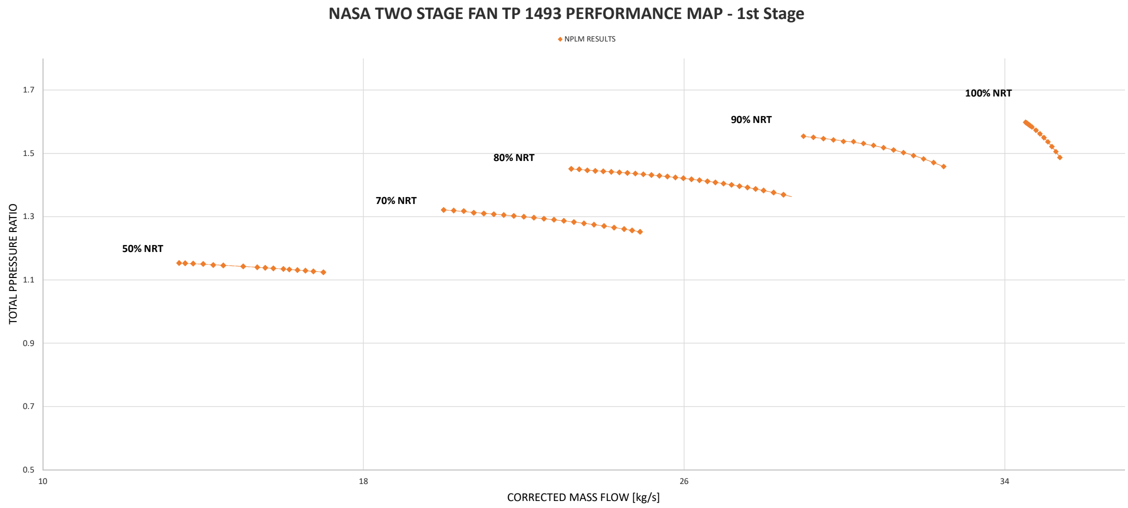

Figure 6.35: Nasa Two Stage Fan Performance Map - 1st Stage - Total Pressure Ratio

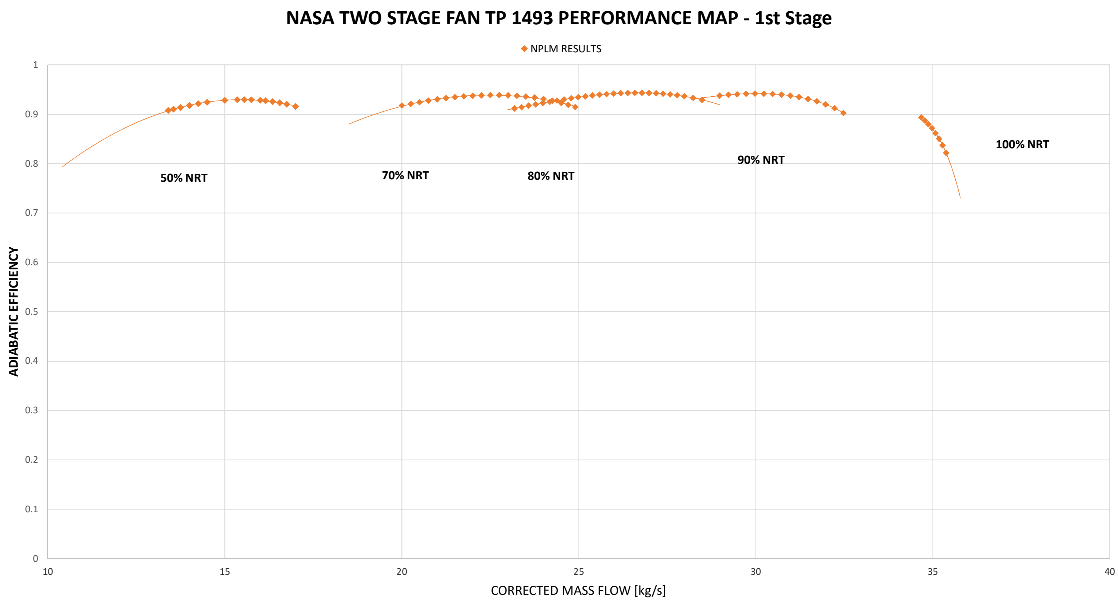

Figure 6.36: Nasa Two Stage Fan Performance Map - 1st Stage - Adiabatic Efficiency

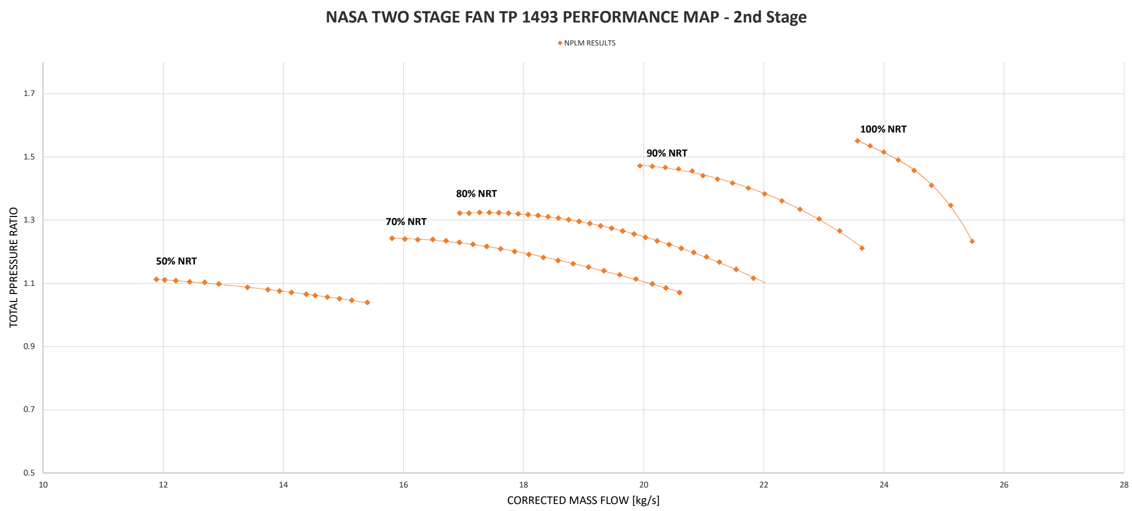

Figure 6.37: Nasa Two Stage Fan Performance Map - 2nd Stage - Total Pressure Ratio

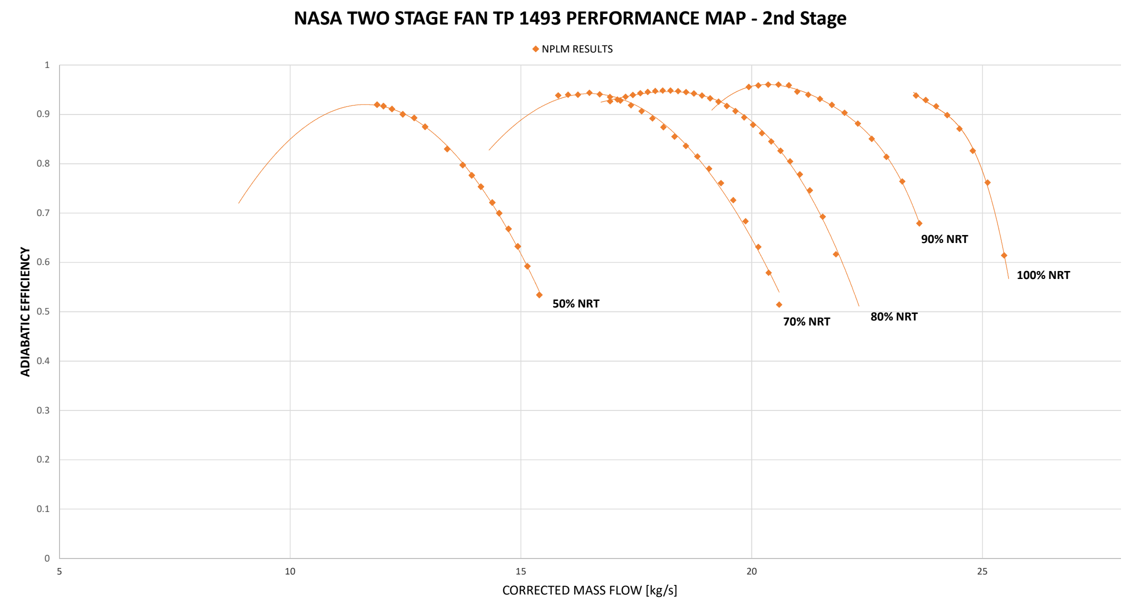

Figure 6.38: Nasa Two Stage Fan Performance Map - 2nd Stage - Adiabatic Efficiency

6.4.3 Flow Properties and Velocities

As the title of the section might suggest, in the following paragraphs the flow properties and velocities trend along the spanwise direction obtained within the model application simulations will be presented.
For reason of length, in the following paragraphs the operating condition for each speed-line considered will be the near peak efficiency operating point.
For each percentage of the design speed the following properties at the inlet and the outlet of each

compressor turbo-component will be presented:

1. total pressure;
2. total temperature;
3. meridional velocity;
4. meridional Mach number;
5. relative velocity;
6. relative Mach number.

For reasons of compactness the diagrams of those properties in the following sections will be organized per-stage. As for the sections concerning the flow properties and velocities for the model verification and validation, also in this case the considered operating condition would be the near-peak-efficiency operating point for each speed-line.

50% of Design Speed

The figures 6.39, 6.40, 6.41, 6.42, 6.43 and 6.44 show the flow properties and velocities evolution along the blade radius at 50% of the design rotational speed and a corrected mass flow of 15.12 kg/s for the two stages of the considered transonic axial-flow compressor.
In particular at this percentage of the design speed, as observable considering the figures previously mentioned, the flow properties and velocities at the inlet and at the outlet of each turbo-component are captured both in shape and magnitude with an high level of accuracy.
The lower incidence of the secondary flows and wake effects at this value of the rotating speed is strongly related with the accuracy level reached.

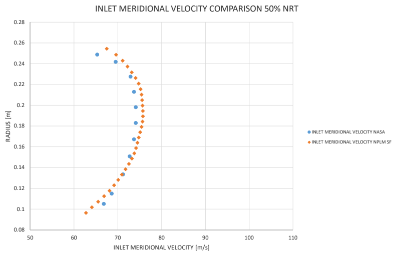

(a) *Inlet Meridional Velocity - 1st Rotor*

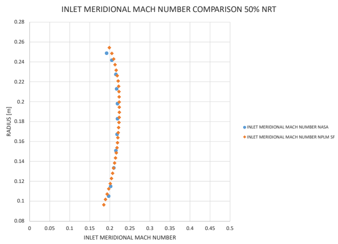

(b) *Inlet Meridional Mach number - 1st Rotor*

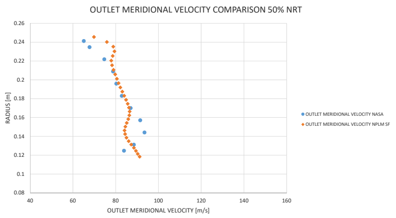

(c) *Outlet Meridional Velocity - 1st Rotor*

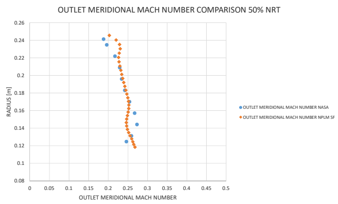

(d) *Outlet Meridional Mach number - 1st Rotor*

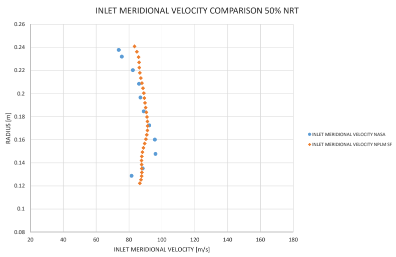

(e) *Inlet Meridional Velocity - 1st Stator*

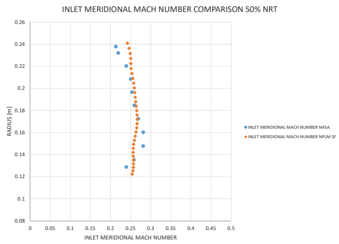

(f) *Inlet Meridional Mach number - 1st Stator*

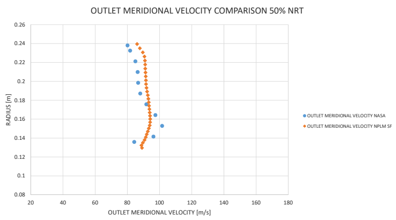

(g) *Outlet Meridional Velocity - 1st Stator*

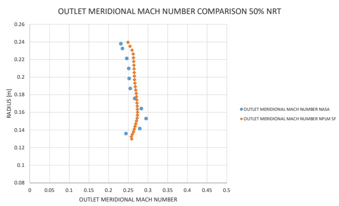

(h) *Outlet Meridional Mach number - 1st Stator*

Figure 6.39: Two Stage Fan - 1st Stage - Meridional Velocity and Meridional Mach Number at 50% of Design Speed and $\dot{m}_{corr} = 15.12\ kg/s$

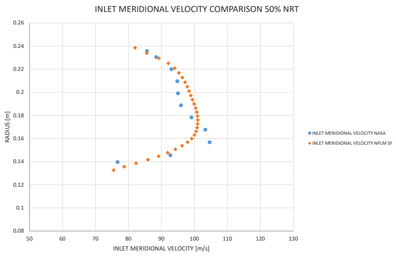

(a) *Inlet Meridional Velocity - 2nd Rotor*

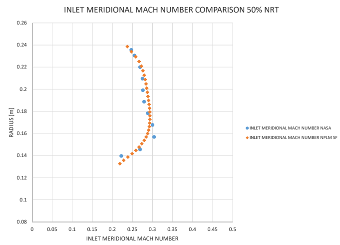

(b) *Inlet Meridional Mach number - 2nd Rotor*

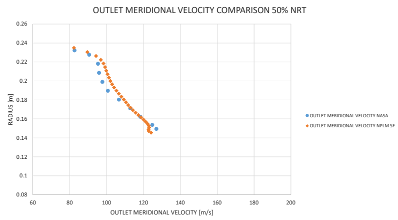

(c) *Outlet Meridional Velocity - 2nd Rotor*

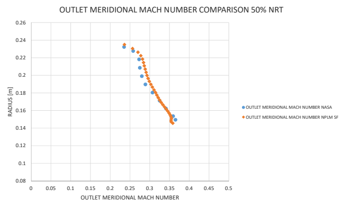

(d) *Outlet Meridional Mach number - 2nd Rotor*

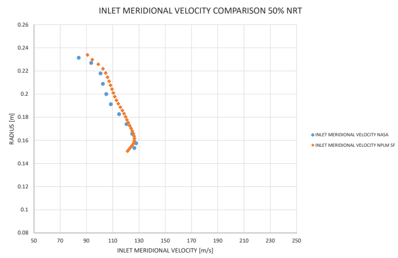

(e) *Inlet Meridional Velocity - 2nd Stator*

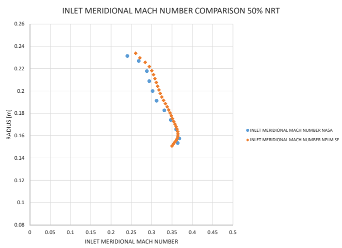

(f) *Inlet Meridional Mach number - 2nd Stator*

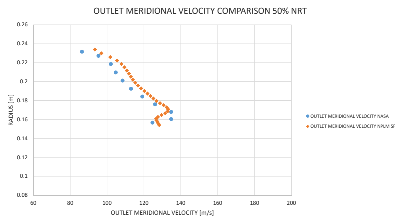

(g) *Outlet Meridional Velocity - 2nd Stator*

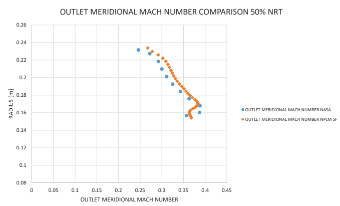

(h) *Outlet Meridional Mach number - 2nd Stator*

Figure 6.40: Two Stage Fan - 1st Stage - Meridional Velocity and Meridional Mach Number at 50% of Design Speed and $\dot{m}_{corr} = 15.12\ kg/s$

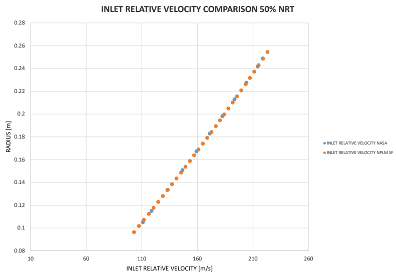

(a) *Inlet Relative Velocity - 1st Rotor*

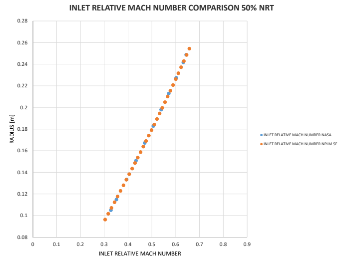

(b) *Inlet Relative Mach number - 1st Rotor*

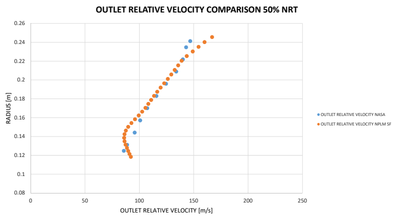

(c) *Outlet Relative Velocity - 1st Rotor*

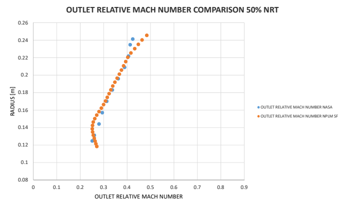

(d) *Outlet Relative Mach number - 1st Rotor*

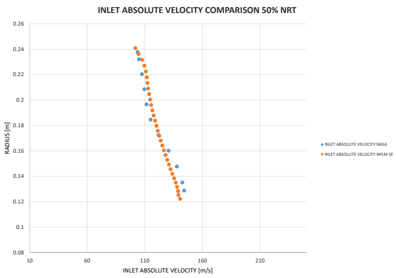

(e) *Inlet Absolute Velocity - 1st Stator*

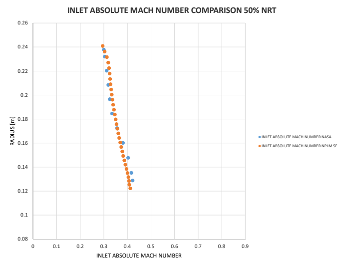

(f) *Inlet Absolute Mach number - 1st Stator*

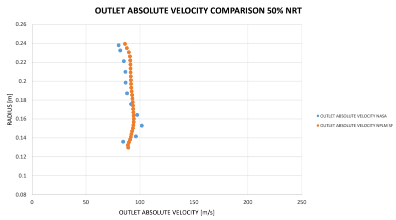

(g) *Outlet Absolute Velocity - 1st Stator*

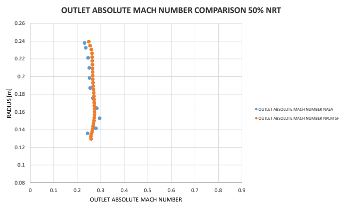

(h) *Outlet Absolute Mach number - 1st Stator*

Figure 6.41: Two Stage Fan - 1st Stage - Rotor Relative Velocity and Relative Mach Number and Stator Absolute Velocity and Absolute Mach Number at 50% of Design Speed and $\dot{m}_{corr} = 15.12\ kg/s$

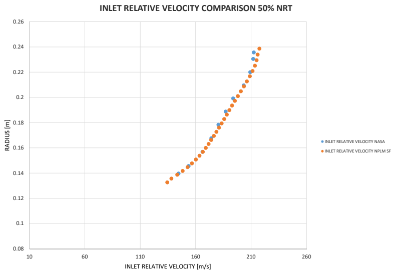

(a) *Inlet Relative Velocity - 2nd Rotor*

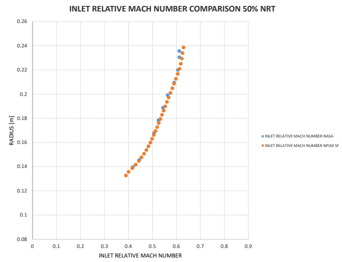

(b) *Inlet Relative Mach number - 2nd Rotor*

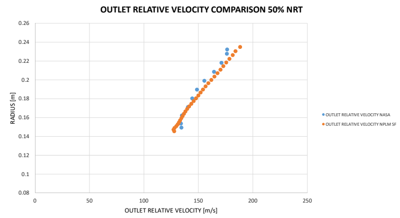

(c) *Outlet Relative Velocity - 2nd Rotor*

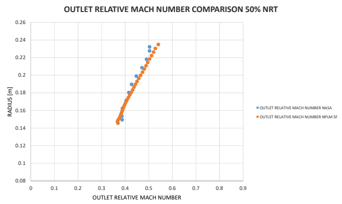

(d) *Outlet Relative Mach number - 2nd Rotor*

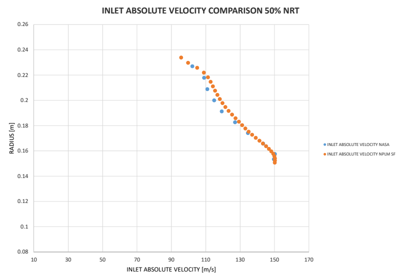

(e) *Inlet Absolute Velocity - 2nd Stator*

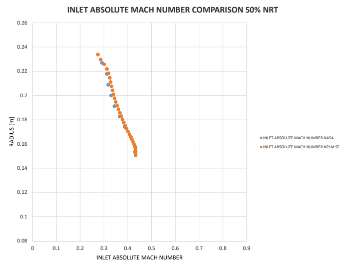

(f) *Inlet Absolute Mach number - 2nd Stator*

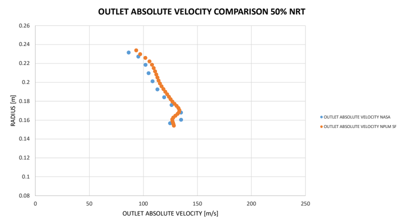

(g) *Outlet Absolute Velocity - 2nd Stator*

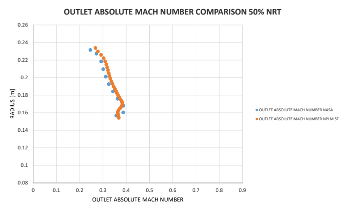

(h) *Outlet Absolute Mach number - 2nd Stator*

Figure 6.42: Two Stage Fan - 2nd Stage - Rotor Relative Velocity and Relative Mach Number and Stator Absolute Velocity and Absolute Mach Number at 50% of Design Speed and $\dot{m}_{corr} = 15.12\ kg/s$

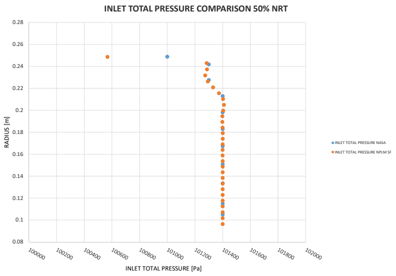

(a) *Inlet Total Pressure - 1st Rotor*

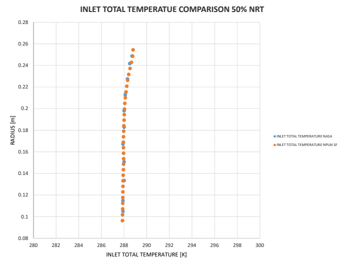

(b) *Inlet Total Temperature - 1st Rotor*

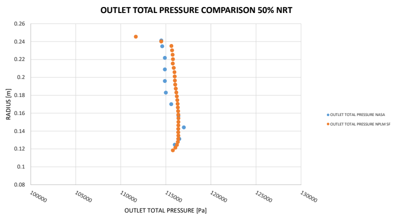

(c) *Outlet Total Pressure - 1st Rotor*

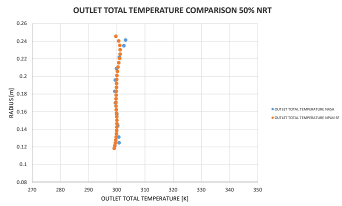

(d) *Outlet Total Temperature - 1st Rotor*

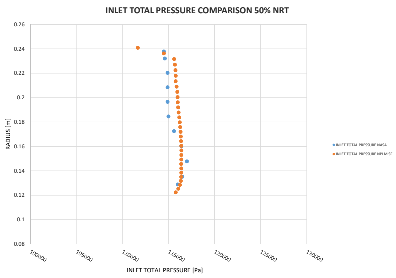

(e) *Inlet Total Pressure - 1st Stator*

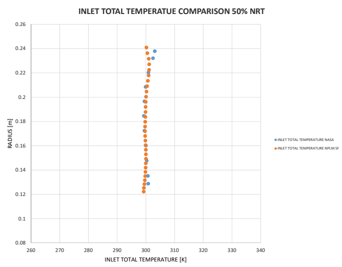

(f) *Inlet Total Temperature - 1st Stator*

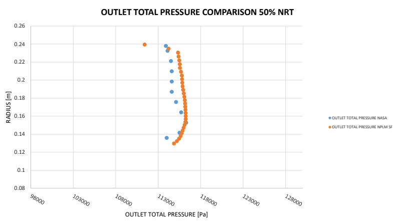

(g) *Outlet Total Pressure - 1st Stator*

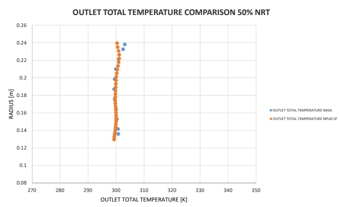

(h) *Outlet Total Temperature - 1st Stator*

Figure 6.43: Two Stage Fan - 1st Stage - Total Pressure and Total Temperature at 50% of Design Speed and $\dot{m}_{corr} = 15.12\ kg/s$

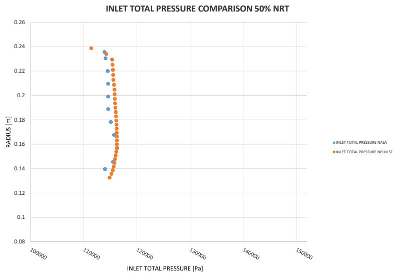

(a) *Inlet Total Pressure - 2nd Rotor*

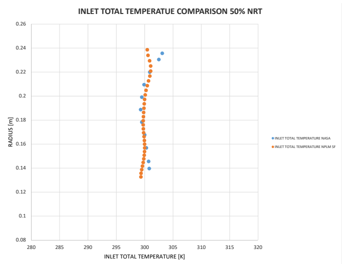

(b) *Inlet Total Temperature - 2nd Rotor*

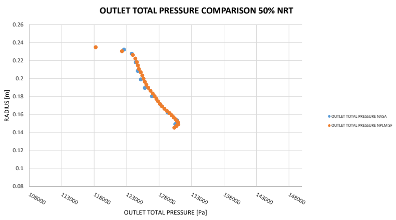

(c) *Outlet Total Pressure - 2nd Rotor*

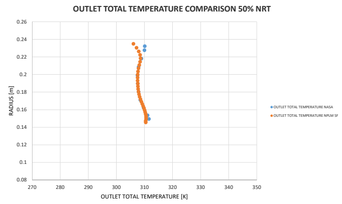

(d) *Outlet Total Temperature - 2nd Rotor*

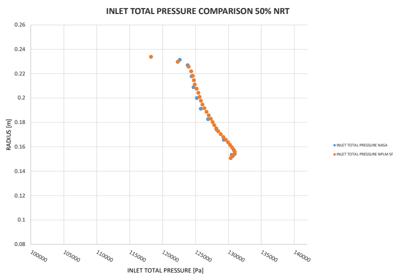

(e) *Inlet Total Pressure - 2nd Stator*

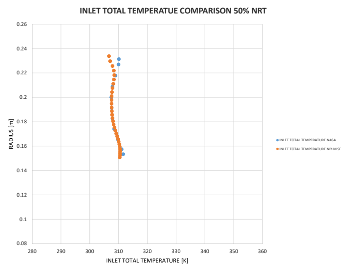

(f) *Inlet Total Temperature - 2nd Stator*

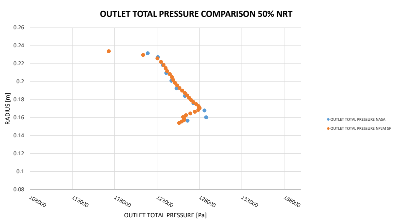

(g) *Outlet Total Pressure - 2nd Stator*

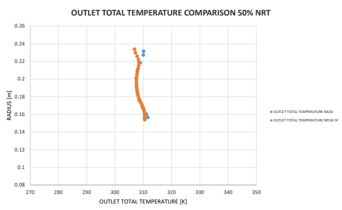

(h) *Outlet Total Temperature - 2nd Stator*

Figure 6.44: Two Stage Fan - 2nd Stage - Total Pressure and Total Temperature at 50% of Design Speed and $\dot{m}_{corr} = 15.12\ kg/s$

In particular the accuracy in the total pressure and total temperature prediction is extremely high consistently with the performance maps results for this operating condition.

70% of Design Speed

The figures 6.45, 6.46, 6.47, 6.48, 6.49 and 6.50 show the flow properties and velocities evolution along the blade radius for 70% of the design rotational speed and a corrected mass flow of 22.22 kg/s for the two stages of the considered transonic axial-flow compressor.

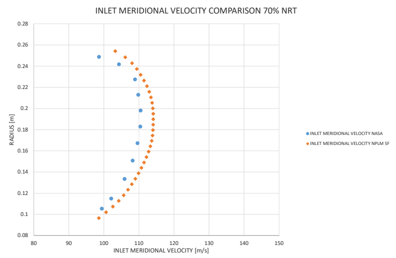

(a) *Inlet Meridional Velocity - 1st Rotor*

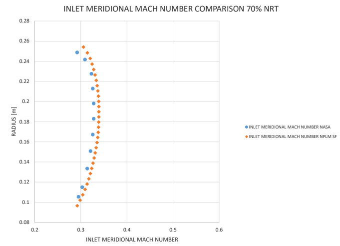

(b) *Inlet Meridional Mach number - 1st Rotor*

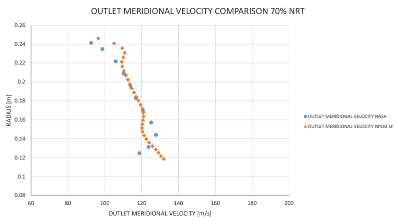

(c) *Outlet Meridional Velocity - 1st Rotor*

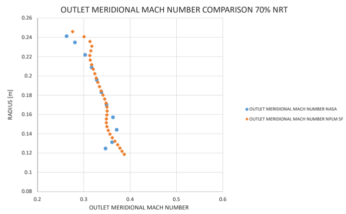

(d) *Outlet Meridional Mach number - 1st Rotor*

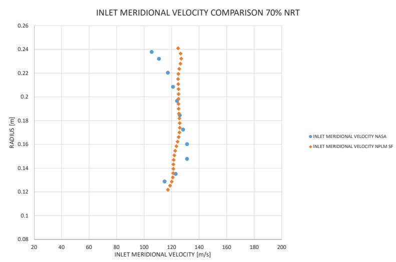

(e) *Inlet Meridional Velocity - 1st Stator*

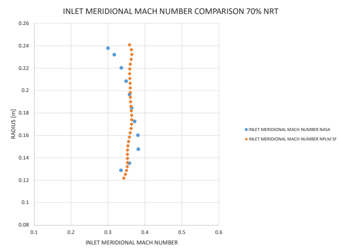

(f) *Inlet Meridional Mach number - 1st Stator*

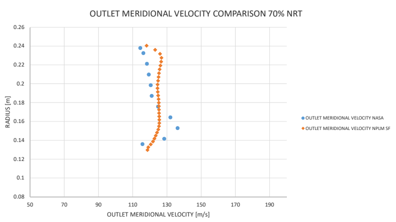

(g) *Outlet Meridional Velocity - 1st Stator*

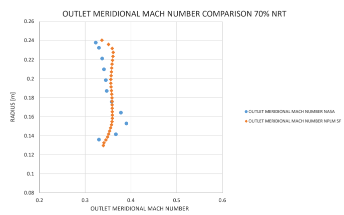

(h) *Outlet Meridional Mach number - 1st Stator*

Figure 6.45: Two Stage Fan - 1st Stage - Meridional Velocity and Meridional Mach Number at 70% of Design Speed and $\dot{m}_{corr} = 22.22\ kg/s$

Also at this percentage of the design speed, the figures underlines a good level of agreement both in shape and magnitude of the predicted fluid properties and velocities against the data provided by the NASA Technical Report.

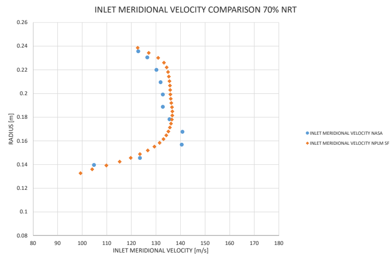

(a) *Inlet Meridional Velocity - 2nd Rotor*

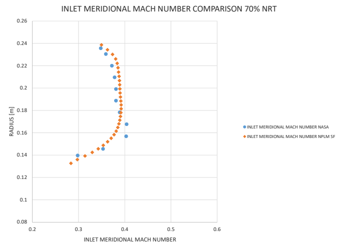

(b) *Inlet Meridional Mach number - 2nd Rotor*

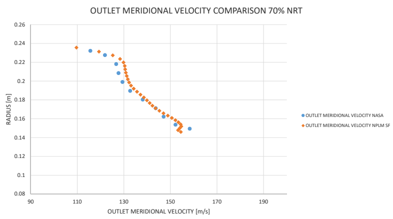

(c) *Outlet Meridional Velocity - 2nd Rotor*

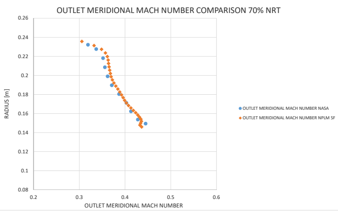

(d) *Outlet Meridional Mach number - 2nd Rotor*

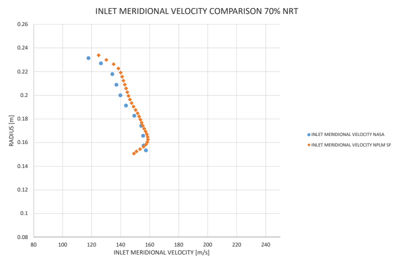

(e) *Inlet Meridional Velocity - 2nd Stator*

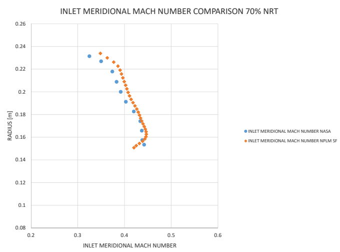

(f) *Inlet Meridional Mach number - 2nd Stator*

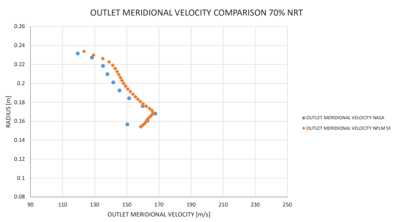

(g) *Outlet Meridional Velocity - 2nd Stator*

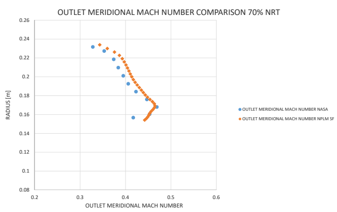

(h) *Outlet Meridional Mach number - 2nd Stator*

Figure 6.46: Two Stage Fan - 1st Stage - Meridional Velocity and Meridional Mach Number at 70% of Design Speed and $\dot{m}_{corr} = 22.22\ kg/s$

Remarkable, considering the first rotor and the meridional velocity, is the difficulty in dealing with the annulus boundary layer in the hub region for the through-flow tools due to the already underlined reasons concerning its modelisation in those software.

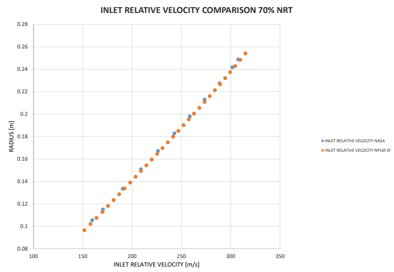

(a) *Inlet Relative Velocity - 1st Rotor*

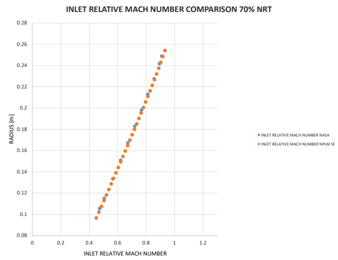

(b) *Inlet Relative Mach number - 1st Rotor*

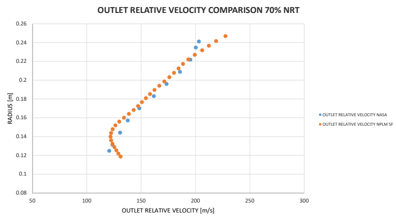

(c) *Outlet Relative Velocity - 1st Rotor*

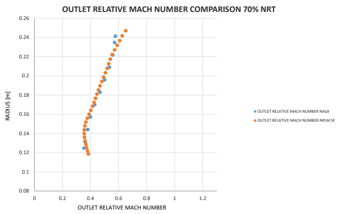

(d) *Outlet Relative Mach number - 1st Rotor*

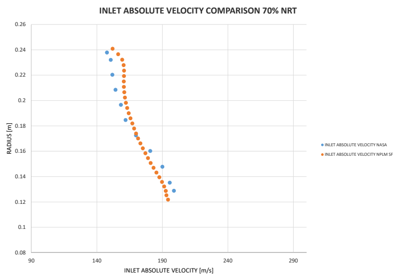

(e) *Inlet Absolute Velocity - 1st Stator*

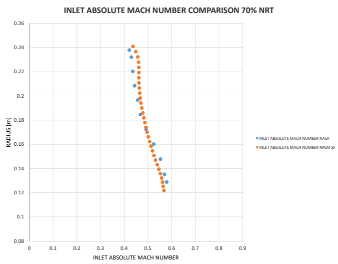

(f) *Inlet Absolute Mach number - 1st Stator*

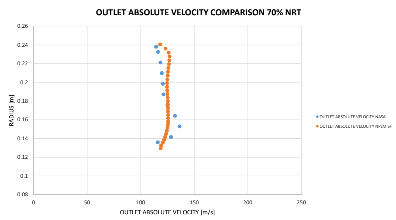

(g) *Outlet Absolute Velocity - 1st Stator*

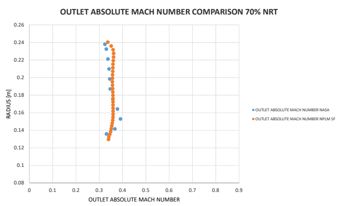

(h) *Outlet Absolute Mach number - 1st Stator*

Figure 6.47: Two Stage Fan - 1st Stage - Rotor Relative Velocity and Relative Mach Number and Stator Absolute Velocity and Absolute Mach Number at 70% of Design Speed and $\dot{m}_{corr} = 22.22\ kg/s$

The first rotor blades experiences a transonic flow regime across the tip region whilst the second rotor is characterized by such flow regime only in correspondence of the blade tip as expectable for the relative velocity reduction within the compressor as result of the compression mechanism.

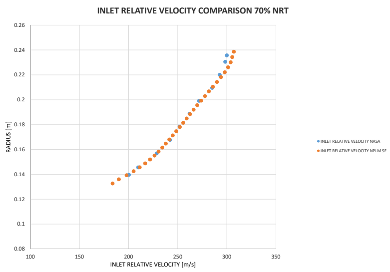

(a) *Inlet Relative Velocity - 2nd Rotor*

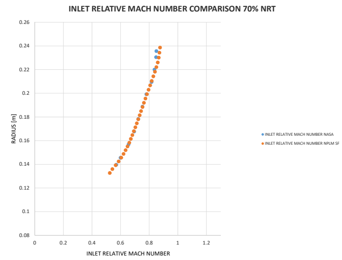

(b) *Inlet Relative Mach number - 2nd Rotor*

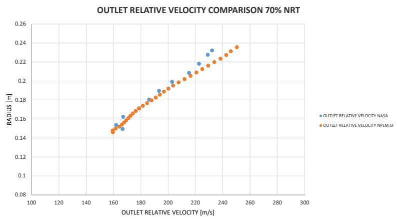

(c) *Outlet Relative Velocity - 2nd Rotor*

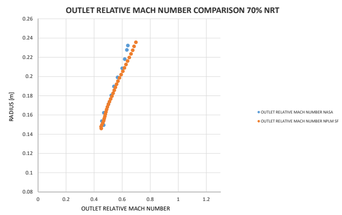

(d) *Outlet Relative Mach number - 2nd Rotor*

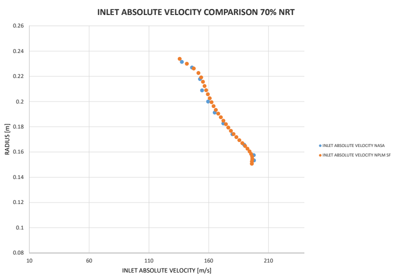

(e) *Inlet Absolute Velocity - 2nd Stator*

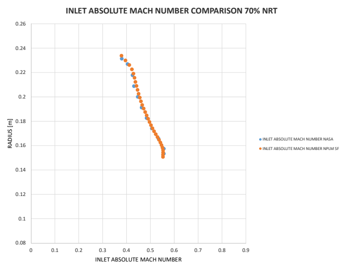

(f) *Inlet Absolute Mach number - 2nd Stator*

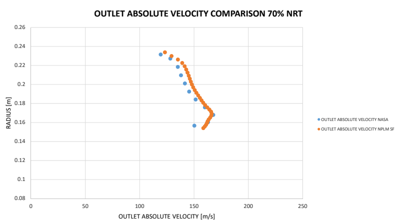

(g) *Outlet Absolute Velocity - 2nd Stator*

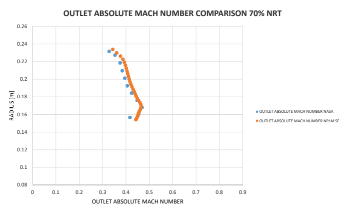

(h) *Outlet Absolute Mach number - 2nd Stator*

Figure 6.48: Two Stage Fan - 2nd Stage - Rotor Relative Velocity and Relative Mach Number and Stator Absolute Velocity and Absolute Mach Number at 70% of Design Speed and $\dot{m}_{corr} = 22.22\ kg/s$

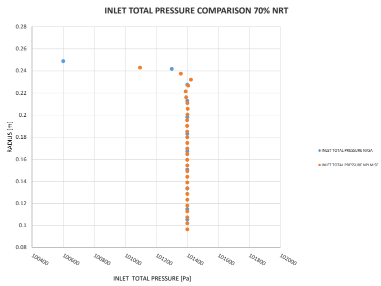

(a) *Inlet Total Pressure - 1st Rotor*

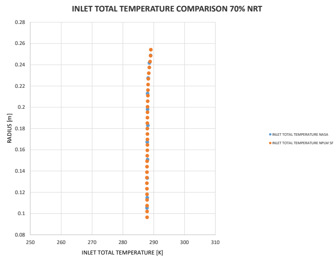

(b) *Inlet Total Temperature - 1st Rotor*

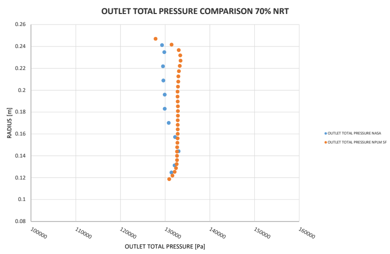

(c) *Outlet Total Pressure - 1st Rotor*

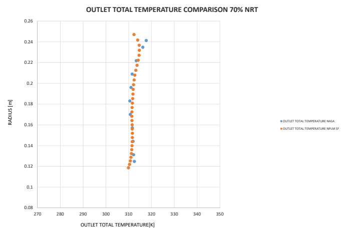

(d) *Outlet Total Temperature - 1st Rotor*

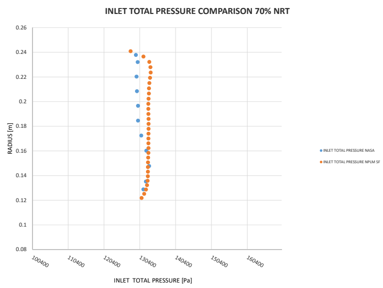

(e) *Inlet Total Pressure - 1st Stator*

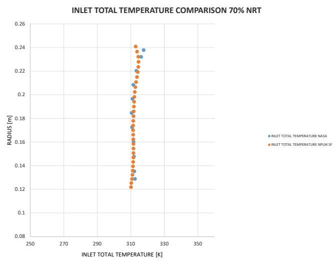

(f) *Inlet Total Temperature - 1st Stator*

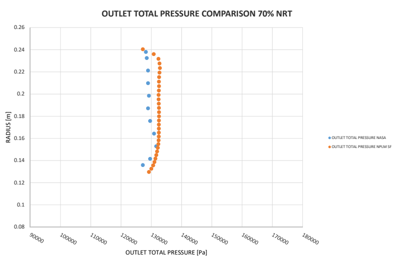

(g) *Outlet Total Pressure - 1st Stator*

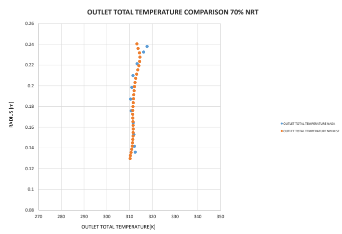

(h) *Outlet Total Temperature - 1st Stator*

Figure 6.49: Two Stage Fan - 1st Stage - Total Pressure and Total Temperature at 70% of Design Speed and $\dot{m}_{corr} = 22.22\ kg/s$

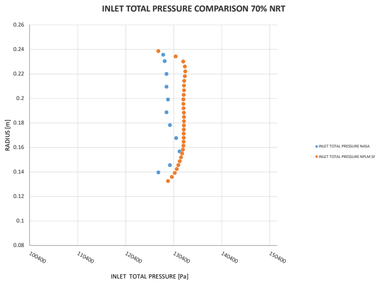

(a) *Inlet Total Pressure - 2nd Rotor*

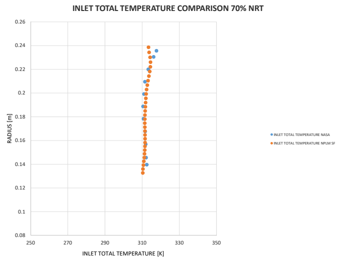

(b) *Inlet Total Temperature - 2nd Rotor*

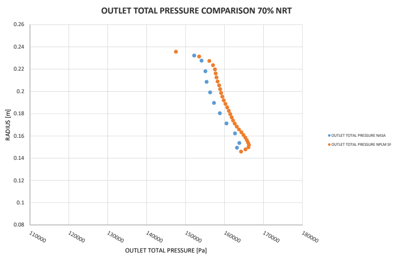

(c) *Outlet Total Pressure - 2nd Rotor*

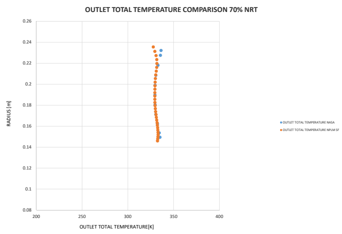

(d) *Outlet Total Temperature - 2nd Rotor*

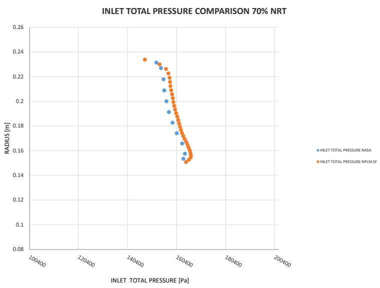

(e) *Inlet Total Pressure - 2nd Stator*

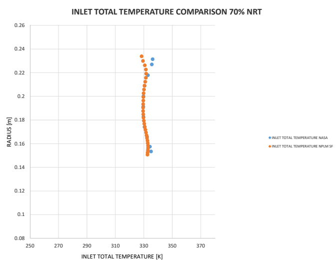

(f) *Inlet Total Temperature - 2nd Stator*

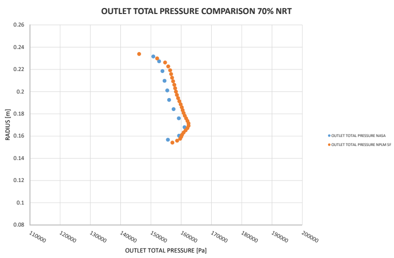

(g) *Outlet Total Pressure - 2nd Stator*

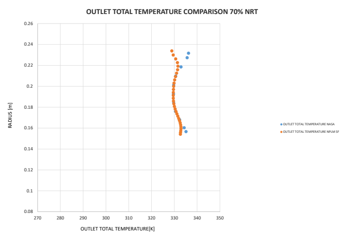

(h) *Outlet Total Temperature - 2nd Stator*

Figure 6.50: Two Stage Fan - 2nd Stage - Total Pressure and Total Temperature at 70% of Design Speed and $\dot{m}_{corr} = 22.22\ kg/s$

Extremely accurate is the prediction for the stator blade rows where the absence of the rotation makes lower the complexity of the flow field. Effectively the rotation enhances the inherent 3-Dimensional character of the boundary layer within a turbomachine determining also an increasing level in its instability due to the rise of the adverse pressure gradient imposed to the flow.

80% of Design Speed

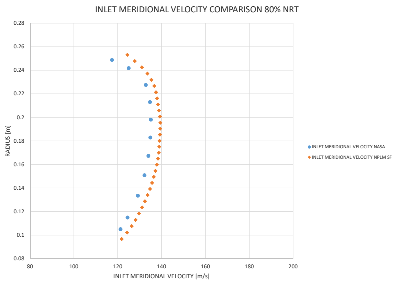

(a) *Inlet Meridional Velocity - 1st Rotor*

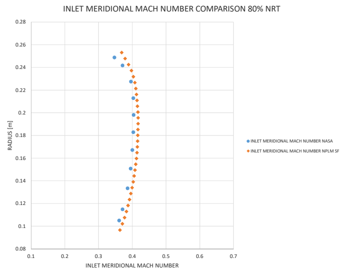

(b) *Inlet Meridional Mach number - 1st Rotor*

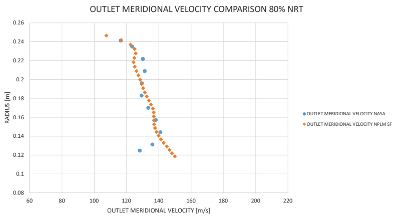

(c) *Outlet Meridional Velocity - 1st Rotor*

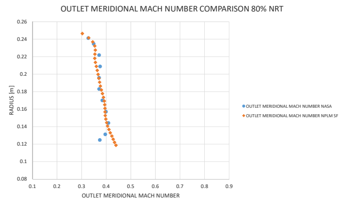

(d) *Outlet Meridional Mach number - 1st Rotor*

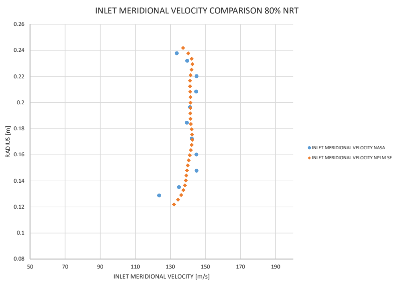

(e) *Inlet Meridional Velocity - 1st Stator*

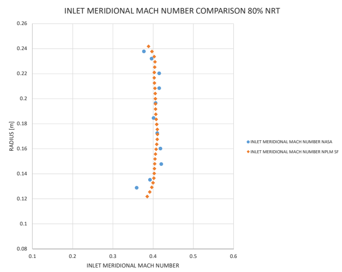

(f) *Inlet Meridional Mach number - 1st Stator*

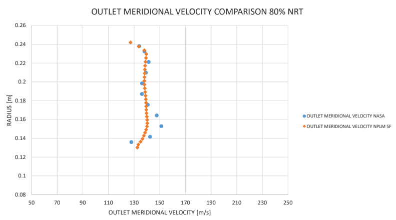

(g) *Outlet Meridional Velocity - 1st Stator*

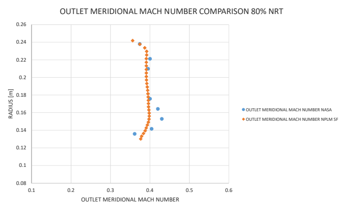

(h) *Outlet Meridional Mach number - 1st Stator*

Figure 6.51: Two Stage Fan - 1st Stage - Meridional Velocity and Meridional Mach Number at 80% of Design Speed and $\dot{m}_{corr} = 26.19\ kg/s$

The figures 6.51, 6.52, 6.53, 6.54, 6.55 and 6.56 show the flow properties and velocities evolution along the blade radius for 80% of the design rotational speed and a corrected mass flow of 26.19 kg/s for the two stages of the considered transonic axial-flow compressor.

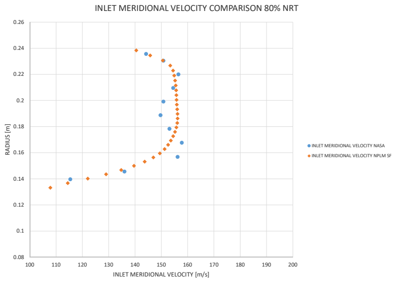

(a) *Inlet Meridional Velocity - 2nd Rotor*

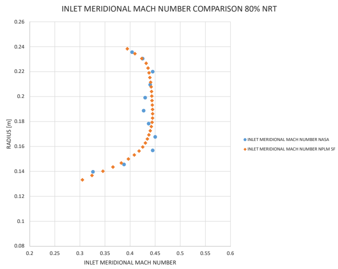

(b) *Inlet Meridional Mach number - 2nd Rotor*

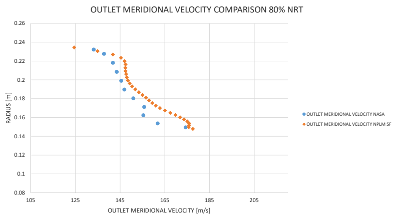

(c) *Outlet Meridional Velocity - 2nd Rotor*

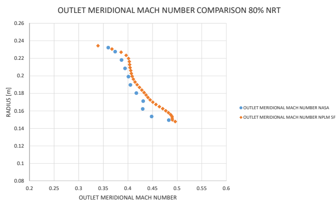

(d) *Outlet Meridional Mach number - 2nd Rotor*

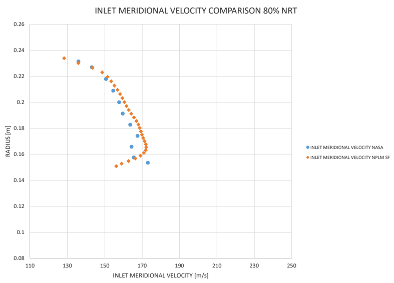

(e) *Inlet Meridional Velocity - 2nd Stator*

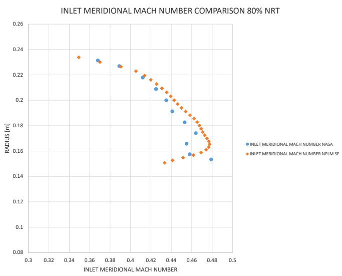

(f) *Inlet Meridional Mach number - 2nd Stator*

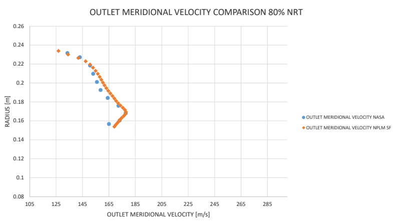

(g) *Outlet Meridional Velocity - 2nd Stator*

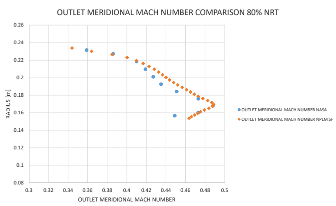

(h) *Outlet Meridional Mach number - 2nd Stator*

Figure 6.52: Two Stage Fan - 1st Stage - Meridional Velocity and Meridional Mach Number at 80% of Design Speed and $\dot{m}_{corr} = 26.19\ kg/s$

The upper half of the first rotor blades experiences a transonic flow in the relative frame of reference which reached also a slightly supersonic regime at the blade tip. At the value of the radius where the sonic condition is reached, the changing in the total pressure and total temperature gradients suggest the presence of a weak oblique shock wave within the blade passage area.
Considering the second rotor the blade observes the passage of transonic flow in the relative frame of reference in the tip region with a value of the Mach number equal to unity that is reached in correspondence of the blade tip.

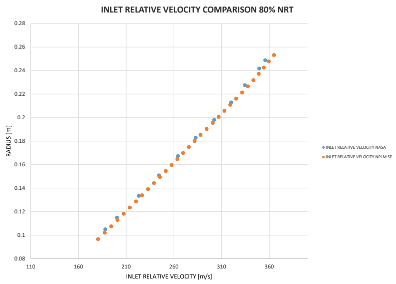

(a) *Inlet Relative Velocity - 1st Rotor*

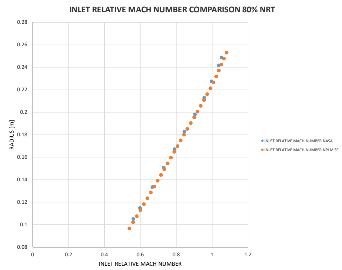

(b) *Inlet Relative Mach number - 1st Rotor*

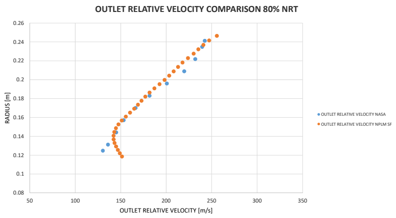

(c) *Outlet Relative Velocity - 1st Rotor*

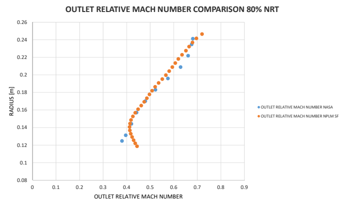

(d) *Outlet Relative Mach number - 1st Rotor*

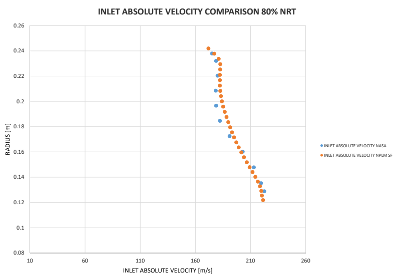

(e) *Inlet Absolute Velocity - 1st Stator*

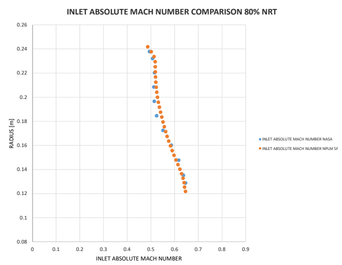

(f) *Inlet Absolute Mach number - 1st Stator*

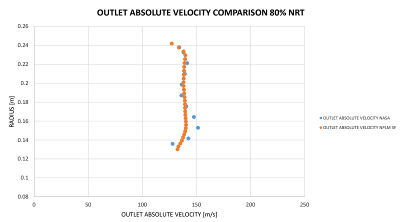

(g) *Outlet Absolute Velocity - 1st Stator*

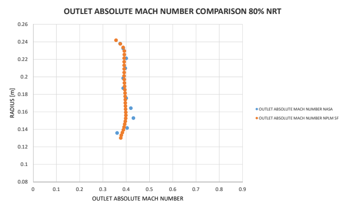

(h) *Outlet Absolute Mach number - 1st Stator*

Figure 6.53: Two Stage Fan - 1st Stage - Rotor Relative Velocity and Relative Mach Number and Stator Absolute Velocity and Absolute Mach Number at 80% of Design Speed and $\dot{m}_{corr} = 26.19\ kg/s$

Both the stators experience fully subsonic flow.
Considering the second stage inlet total pressure, it might be observed an inlet total pressure higher respect to the NASA data. This stresses the not completely accurate modelisation of the first stage

wake dissipative effect. The under-estimation of the dissipation due to wake and secondary flow-phenomena is consistent with the slightly over-estimation of the compressor performance at this value of the design rotating speed as stated by the performance maps in the previous section.

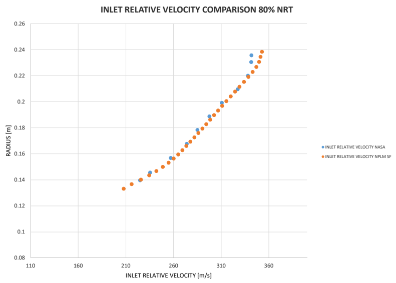

(a) *Inlet Relative Velocity - 2nd Rotor*

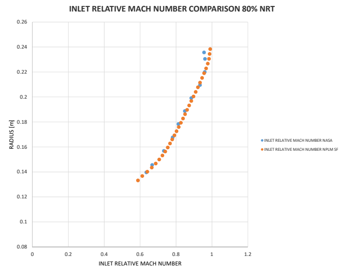

(b) *Inlet Relative Mach number - 2nd Rotor*

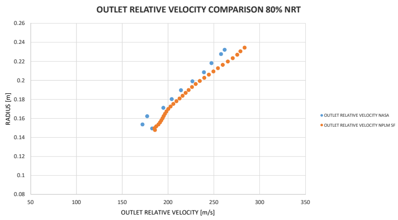

(c) *Outlet Relative Velocity - 2nd Rotor*

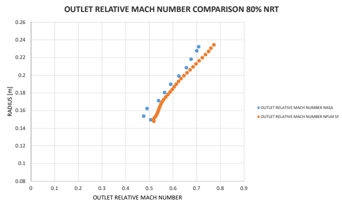

(d) *Outlet Relative Mach number - 2nd Rotor*

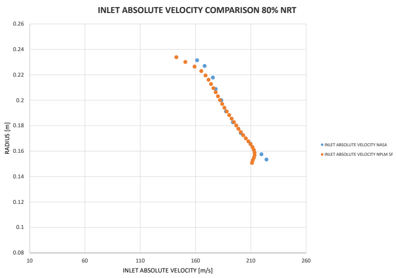

(e) *Inlet Absolute Velocity - 2nd Stator*

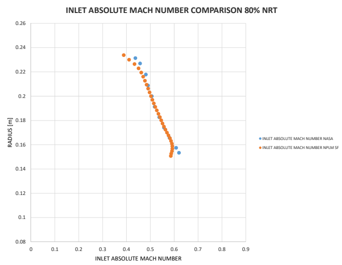

(f) *Inlet Absolute Mach number - 2nd Stator*

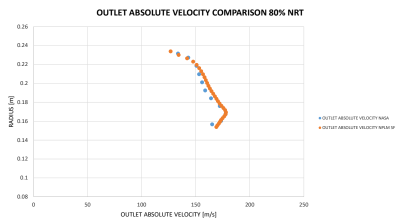

(g) *Outlet Absolute Velocity - 2nd Stator*

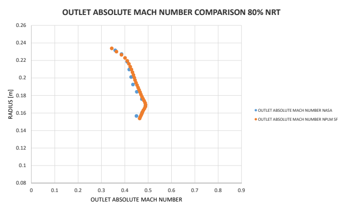

(h) *Outlet Absolute Mach number - 2nd Stator*

Figure 6.54: Two Stage Fan - 2nd Stage - Rotor Relative Velocity and Relative Mach Number and Stator Absolute Velocity and Absolute Mach Number at 80% of Design Speed and $\dot{m}_{corr}$ = 26.19 kg/s

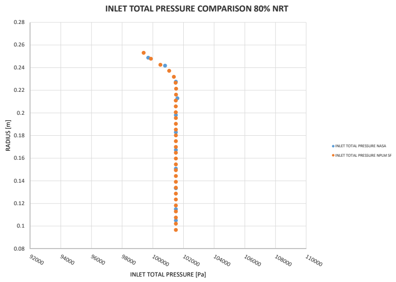

(a) *Inlet Total Pressure - 1st Rotor*

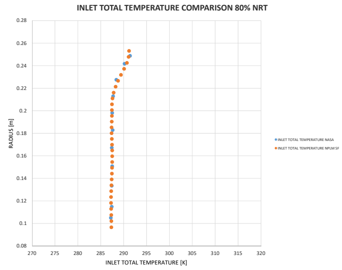

(b) *Inlet Total Temperature - 1st Rotor*

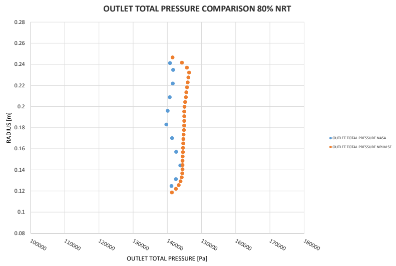

(c) *Outlet Total Pressure - 1st Rotor*

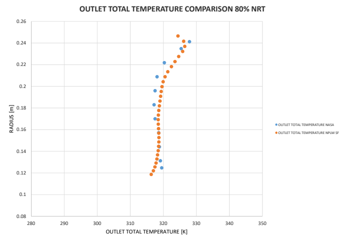

(d) *Outlet Total Temperature - 1st Rotor*

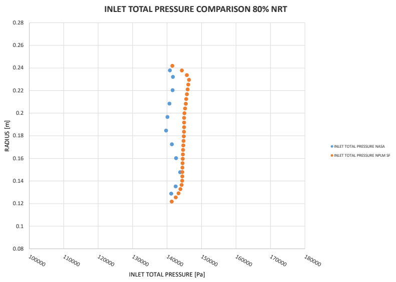

(e) *Inlet Total Pressure - 1st Stator*

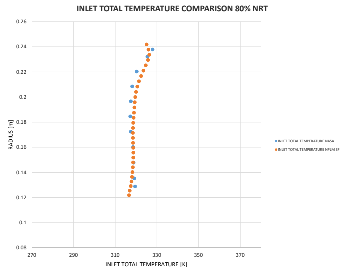

(f) *Inlet Total Temperature - 1st Stator*

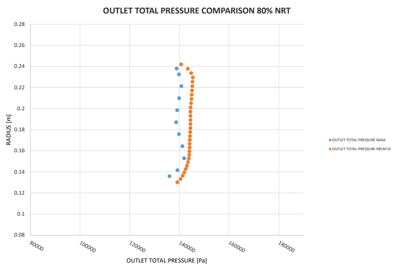

(g) *Outlet Total Pressure - 1st Stator*

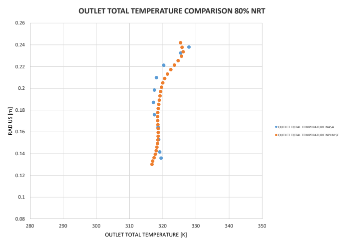

(h) *Outlet Total Temperature - 1st Stator*

Figure 6.55: Two Stage Fan - 1st Stage - Total Pressure and Total Temperature at 80% of Design Speed and $\dot{m}_{corr} = 26.19\ kg/s$

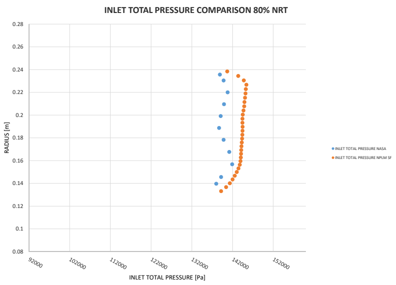

(a) *Inlet Total Pressure - 2nd Rotor*

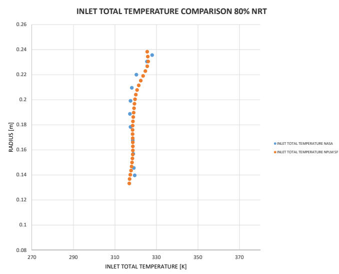

(b) *Inlet Total Temperature - 2nd Rotor*

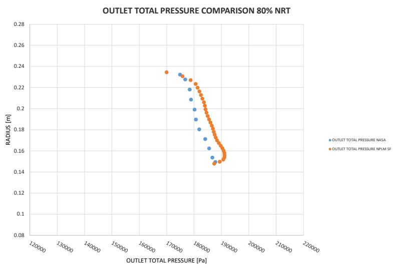

(c) *Outlet Total Pressure - 2nd Rotor*

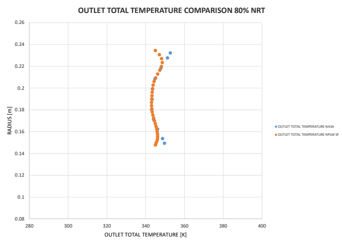

(d) *Outlet Total Temperature - 2nd Rotor*

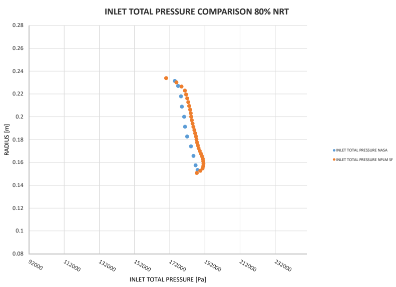

(e) *Inlet Total Pressure - 2nd Stator*

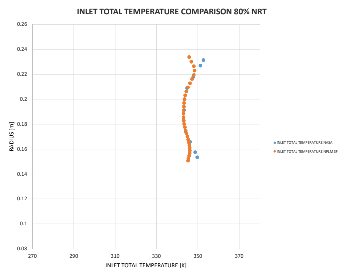

(f) *Inlet Total Temperature - 2nd Stator*

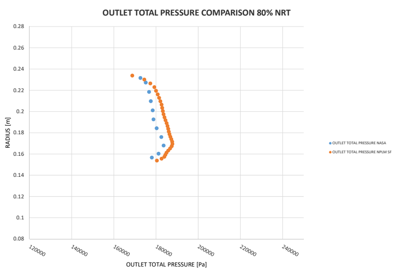

(g) *Outlet Total Pressure - 2nd Stator*

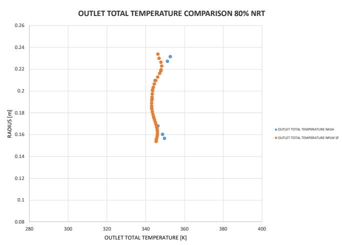

(h) *Outlet Total Temperature - 2nd Stator*

Figure 6.56: Two Stage Fan - 2nd Stage - Total Pressure and Total Temperature at 80% of Design Speed and $\dot{m}_{corr} = 26.19\ kg/s$

Also the typical meridional velocity profile due to the wake effects at the second stage rotor inlet at the blade mid-radius is not completely captured by the model as expectable due to the absence of a complete wake modelisation in the tool. However the accuracy at this rotating speed is still high due also to the not excessive magnitude of the wake, but as observable in the next sections, a wake modelisation would be fundamental to increase the accuracy at the higher values of the rotating speed. Even if the fundamental purpose of the tool is the preliminary design and the accuracy reached is already acceptable at this stage of the design process.

90% of Design Speed

The figures 6.57, 6.58, 6.59, 6.60, 6.61 and 6.62 show the flow properties and velocities evolution along the blade radius for 90% of the design rotational speed and a corrected mass flow of 31.56 kg/s for the two stages of the considered transonic axial-flow compressor.
At this percentage of the rotating speed the effects of the wake and of the thickening of the boundary layer start to put in evidence the limitations connected with the use of empirical correlations in the compressor performance prediction. This becomes evident in particular considering the compressor second stage.
Nevertheless the level of agreement in terms of shape and magnitude of the fluid properties and velocities is still good, observing more in details the blade tip and hub region of each turbo-component, they put in evidence a slightly decreasing accuracy due to the thickening of the boundary layer with the increasing in the rotating speed. Moreover as observed in the previous case, the dissipative effect of the wake and the meridional velocity profile that it determines at the second-stage inlet is not completely captured due to the absence of the wake complete modelisation. Under this point of view the reader should be aware of the fact that an analytical approach in the wake modelisation is inapplicable due to time and computational cost. An experimental driven approach might be considered, but, the possibility to elaborate an empirical correlation to model the wake effects might produce accurate results only for the testing geometry used to elaborate it due to the inherent strong relation between the blade profile characteristics and the wake shape. Moreover the strong dependency of the wake field characteristics on the incidence and the flow Reynolds number provides further complications to the elaboration of an empirical correlation applicable on a sufficient large scale of axial-flow compressors.
Considering the related frame of reference it is possible to observe that the first stage rotor blade row experiences a transonic flow already in the hub region, the sonic condition is reached at $r = 0.18\ m$ and the tip of the blade is characterised by a slightly supersonic flow. For what concerns the second stage rotor the whole blade is characterised by transonic flow.
As for the previous percentage of the rotating speed the two stators are fully subsonic.
However observing the over-estimation of the absolute velocity in the second stage stator outlet in the hub region, it underlines the under-estimation of the boundary layer effects as confirmed also by the slight over-estimation of the outlet total pressure in the same region.

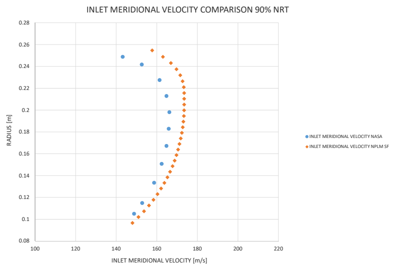

(a) *Inlet Meridional Velocity - 1st Rotor*

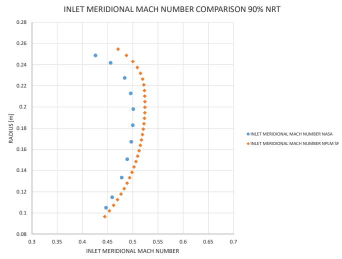

(b) *Inlet Meridional Mach number - 1st Rotor*

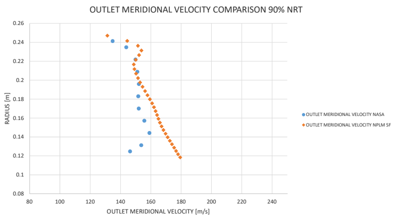

(c) *Outlet Meridional Velocity - 1st Rotor*

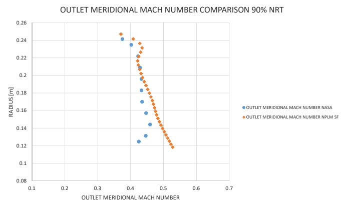

(d) *Outlet Meridional Mach number - 1st Rotor*

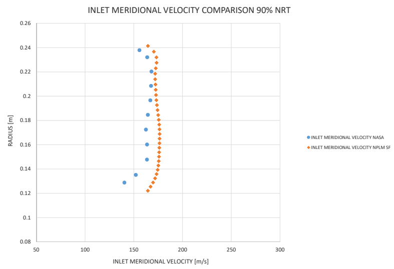

(e) *Inlet Meridional Velocity - 1st Stator*

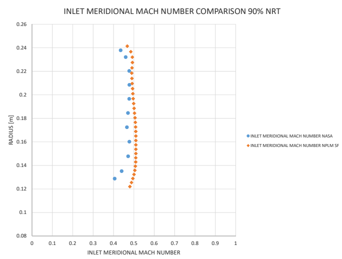

(f) *Inlet Meridional Mach number - 1st Stator*

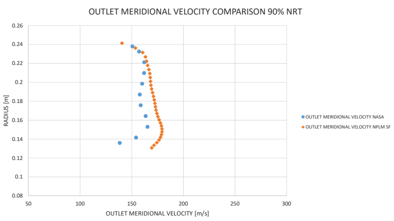

(g) *Outlet Meridional Velocity - 1st Stator*

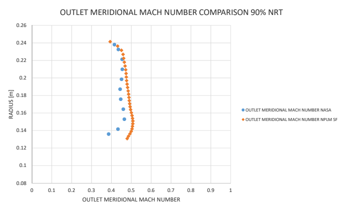

(h) *Outlet Meridional Mach number - 1st Stator*

Figure 6.57: Two Stage Fan - 1st Stage - Meridional Velocity and Meridional Mach Number at 90% of Design Speed and $\dot{m}_{corr} = 31.56\ kg/s$

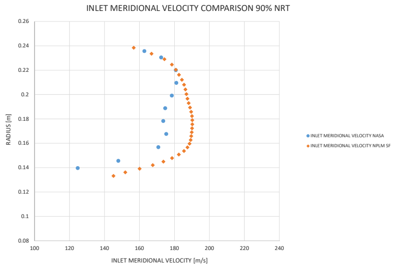

(a) *Inlet Meridional Velocity - 2nd Rotor*

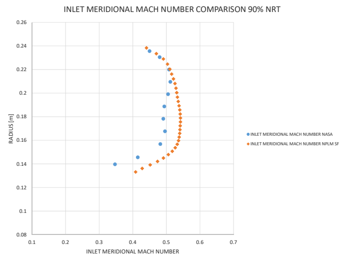

(b) *Inlet Meridional Mach number - 2nd Rotor*

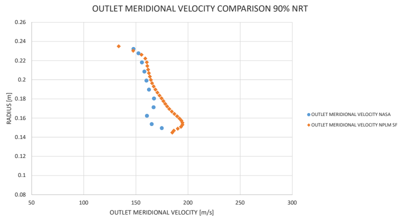

(c) *Outlet Meridional Velocity - 2nd Rotor*

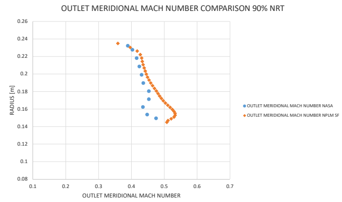

(d) *Outlet Meridional Mach number - 2nd Rotor*

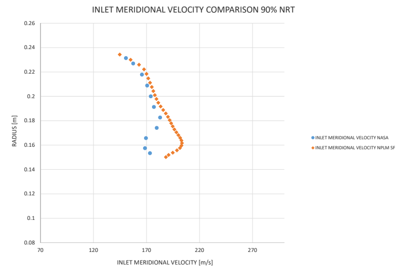

(e) *Inlet Meridional Velocity - 2nd Stator*

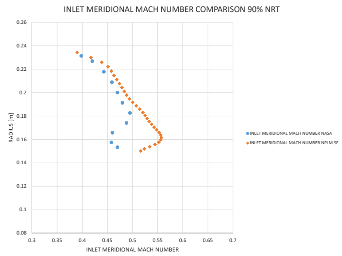

(f) *Inlet Meridional Mach number - 2nd Stator*

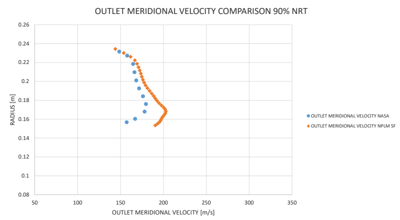

(g) *Outlet Meridional Velocity - 2nd Stator*

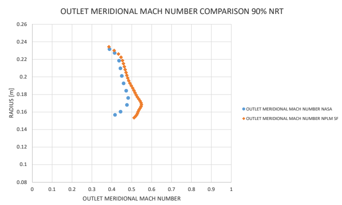

(h) *Outlet Meridional Mach number - 2nd Stator*

Figure 6.58: Two Stage Fan - 1st Stage - Meridional Velocity and Meridional Mach Number at 90% of Design Speed and $\dot{m}_{corr} = 31.56\ kg/s$

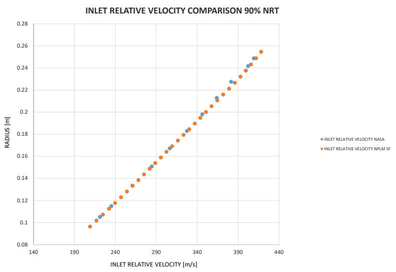

(a) *Inlet Relative Velocity - 1st Rotor*

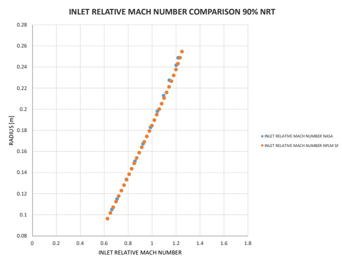

(b) *Inlet Relative Mach number - 1st Rotor*

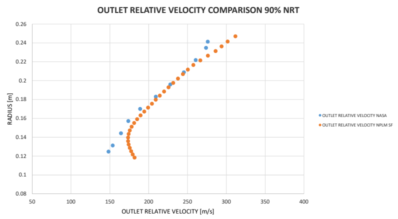

(c) *Outlet Relative Velocity - 1st Rotor*

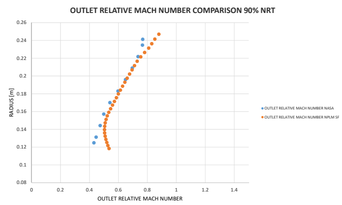

(d) *Outlet Relative Mach number - 1st Rotor*

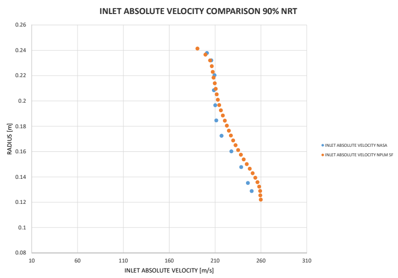

(e) *Inlet Absolute Velocity - 1st Stator*

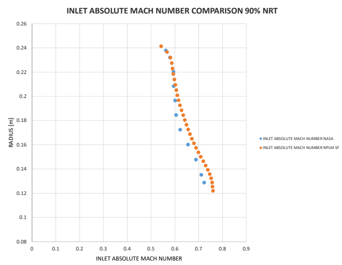

(f) *Inlet Absolute Mach number - 1st Stator*

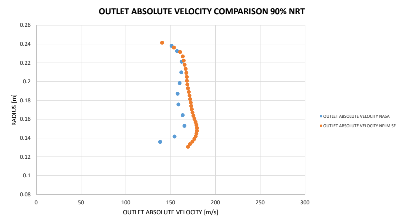

(g) *Outlet Absolute Velocity - 1st Stator*

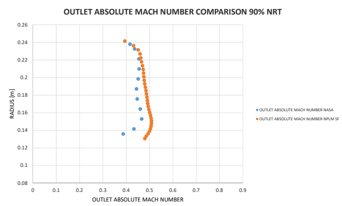

(h) *Outlet Absolute Mach number - 1st Stator*

Figure 6.59: Two Stage Fan - 1st Stage - Rotor Relative Velocity and Relative Mach Number and Stator Absolute Velocity and Absolute Mach Number at 90% of Design Speed and $\dot{m}_{corr} = 31.56\ kg/s$

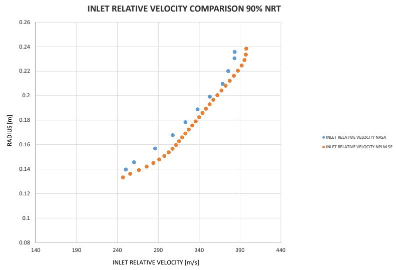

(a) *Inlet Relative Velocity - 2nd Rotor*

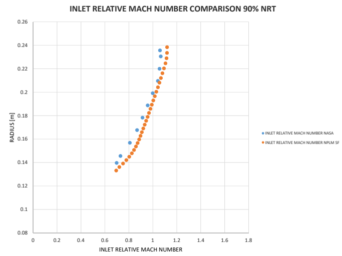

(b) *Inlet Relative Mach number - 2nd Rotor*

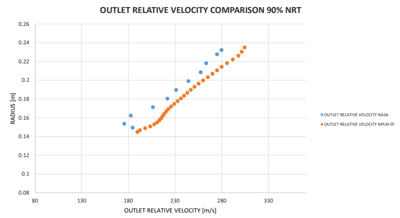

(c) *Outlet Relative Velocity - 2nd Rotor*

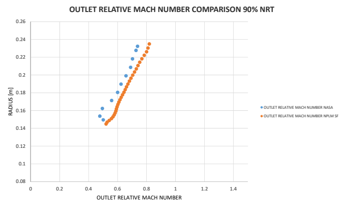

(d) *Outlet Relative Mach number - 2nd Rotor*

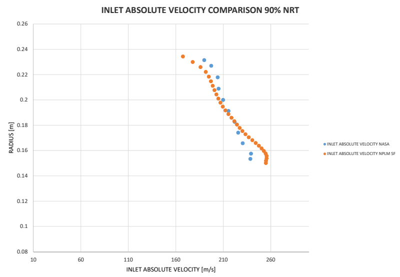

(e) *Inlet Absolute Velocity - 2nd Stator*

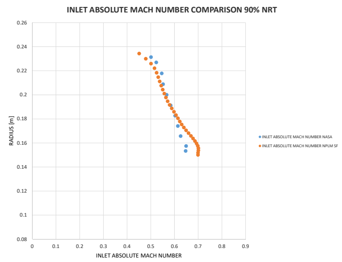

(f) *Inlet Absolute Mach number - 2nd Stator*

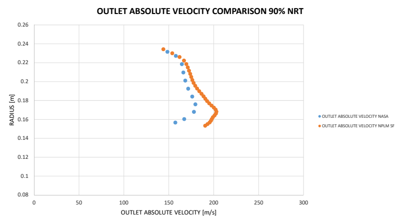

(g) *Outlet Absolute Velocity - 2nd Stator*

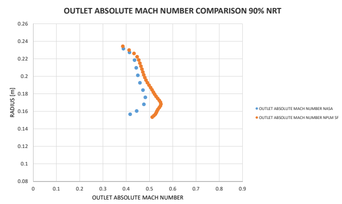

(h) *Outlet Absolute Mach number - 2nd Stator*

Figure 6.60: Two Stage Fan - 2nd Stage - Rotor Relative Velocity and Relative Mach Number and Stator Absolute Velocity and Absolute Mach Number at 90% of Design Speed and $\dot{m}_{corr} = 31.56\ kg/s$

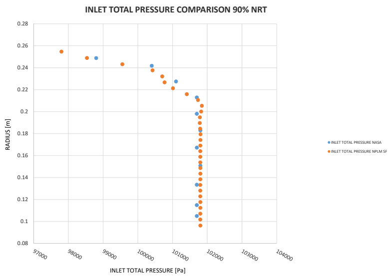

(a) *Inlet Total Pressure - 1st Rotor*

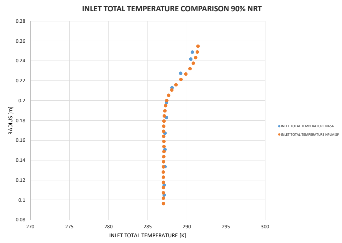

(b) *Inlet Total Temperature - 1st Rotor*

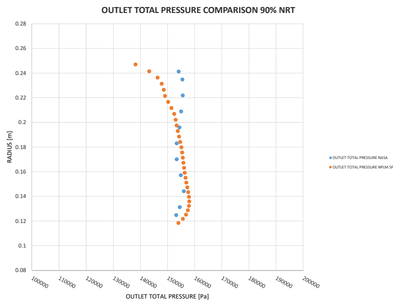

(c) *Outlet Total Pressure - 1st Rotor*

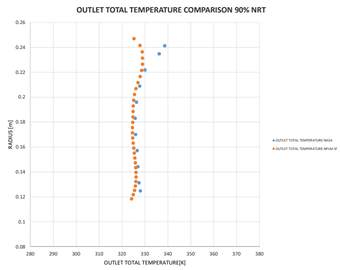

(d) *Outlet Total Temperature - 1st Rotor*

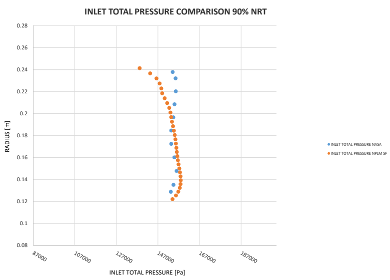

(e) *Inlet Total Pressure - 1st Stator*

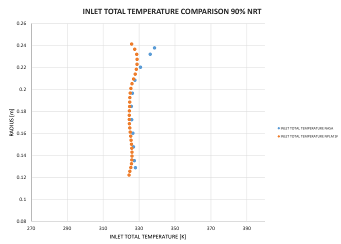

(f) *Inlet Total Temperature - 1st Stator*

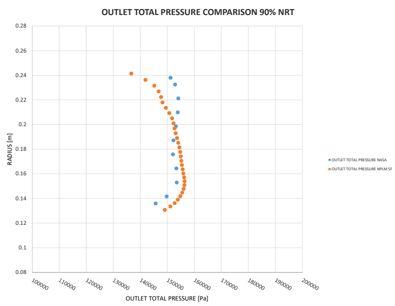

(g) *Outlet Total Pressure - 1st Stator*

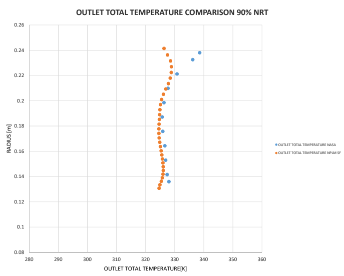

(h) *Outlet Total Temperature - 1st Stator*

Figure 6.61: Two Stage Fan - 1st Stage - Total Pressure and Total Temperature at 90% of Design Speed and $\dot{m}_{corr} = 31.56\ kg/s$

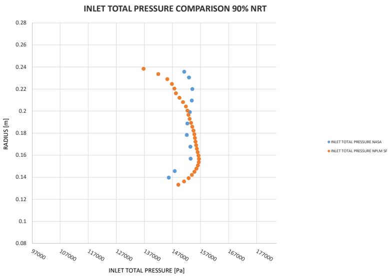

(a) *Inlet Total Pressure - 2nd Rotor*

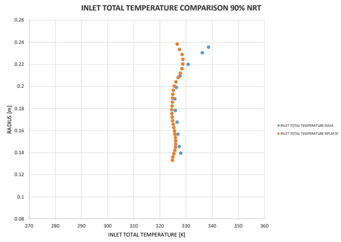

(b) *Inlet Total Temperature - 2nd Rotor*

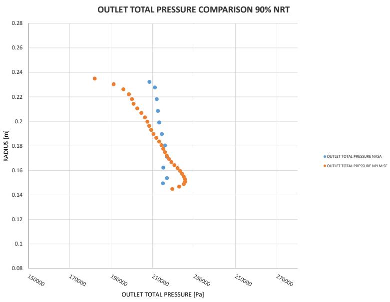

(c) *Outlet Total Pressure - 2nd Rotor*

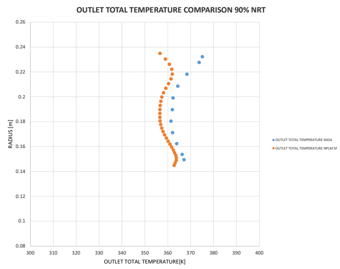

(d) *Outlet Total Temperature - 2nd Rotor*

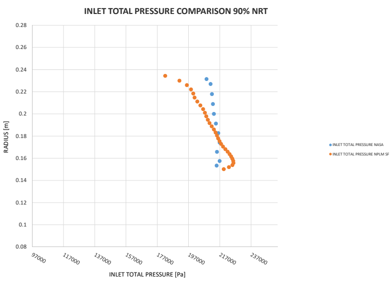

(e) *Inlet Total Pressure - 2nd Stator*

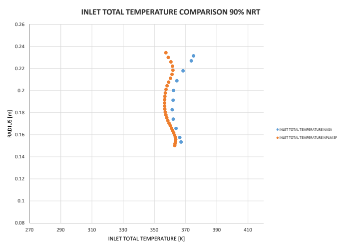

(f) *Inlet Total Temperature - 2nd Stator*

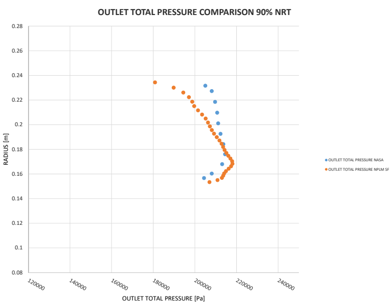

(g) *Outlet Total Pressure - 2nd Stator*

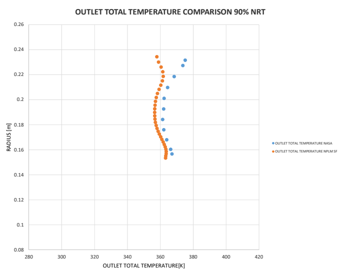

(h) *Outlet Total Temperature - 2nd Stator*

Figure 6.62: Two Stage Fan - 2nd Stage - Total Pressure and Total Temperature at 90% of Design Speed and $\dot{m}_{corr} = 31.56\ kg/s$

100% of Design Speed

The figures 6.63, 6.64, 6.65, 6.66, 6.67 and 6.68 show the flow properties and velocities evolution along the blade radius for 100% of the design rotational speed and a corrected mass flow of 35.36 kg/s for the two stages of the considered transonic axial-flow compressor.

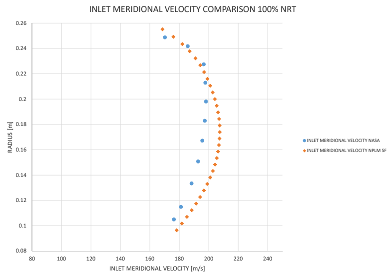

(a) *Inlet Meridional Velocity - 1st Rotor*

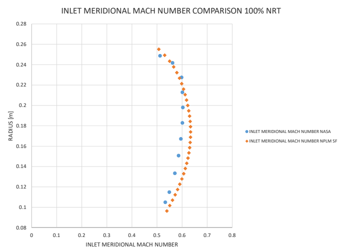

(b) *Inlet Meridional Mach number - 1st Rotor*

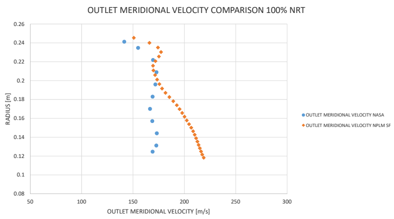

(c) *Outlet Meridional Velocity - 1st Rotor*

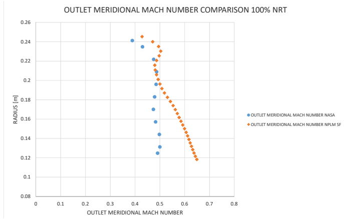

(d) *Outlet Meridional Mach number - 1st Rotor*

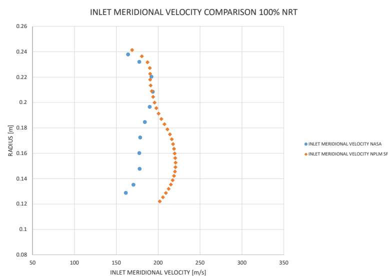

(e) *Inlet Meridional Velocity - 1st Stator*

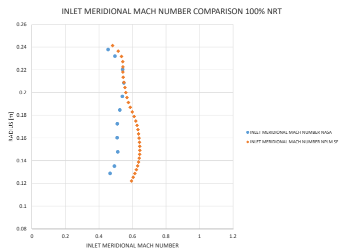

(f) *Inlet Meridional Mach number - 1st Stator*

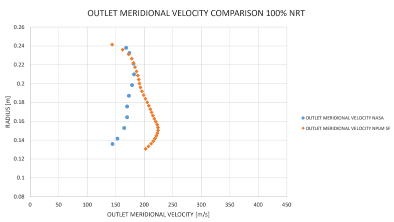

(g) *Outlet Meridional Velocity - 1st Stator*

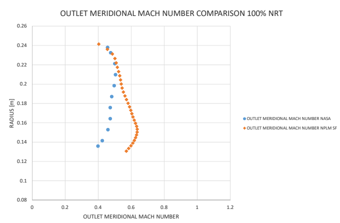

(h) *Outlet Meridional Mach number - 1st Stator*

Figure 6.63: Two Stage Fan - 1st Stage - Meridional Velocity and Meridional Mach Number at 100% of Design Speed and $\dot{m}_{corr} = 35.36\ kg/s$

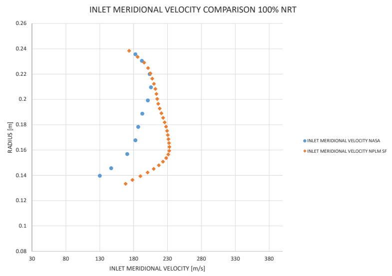

(a) *Inlet Meridional Velocity - 2nd Rotor*

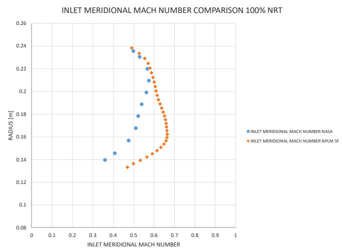

(b) *Inlet Meridional Mach number - 2nd Rotor*

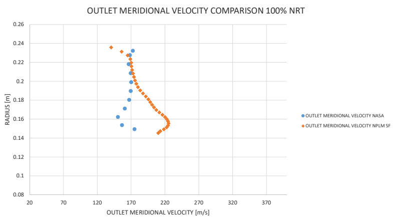

(c) *Outlet Meridional Velocity - 2nd Rotor*

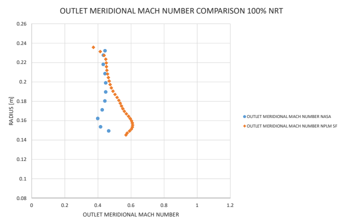

(d) *Outlet Meridional Mach number - 2nd Rotor*

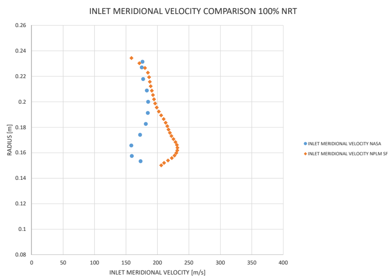

(e) *Inlet Meridional Velocity - 2nd Stator*

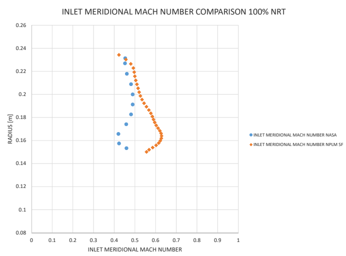

(f) *Inlet Meridional Mach number - 2nd Stator*

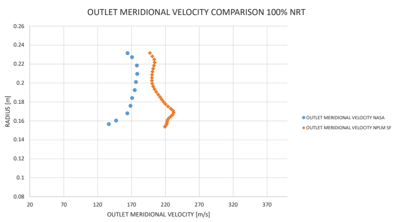

(g) *Outlet Meridional Velocity - 2nd Stator*

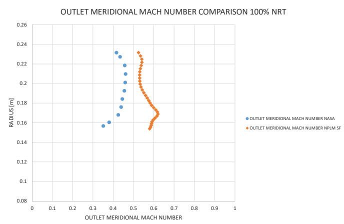

(h) *Outlet Meridional Mach number - 2nd Stator*

Figure 6.64: Two Stage Fan - 1st Stage - Meridional Velocity and Meridional Mach Number at 100% of Design Speed and $\dot{m}_{corr} = 35.36\ kg/s$

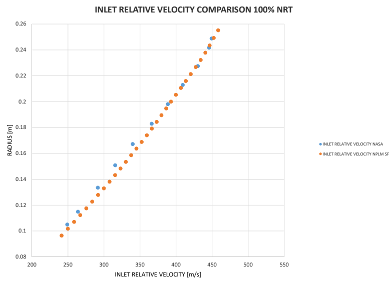

(a) *Inlet Relative Velocity - 1st Rotor*

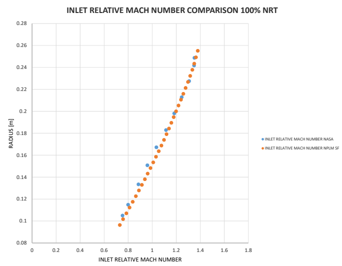

(b) *Inlet Relative Mach number - 1st Rotor*

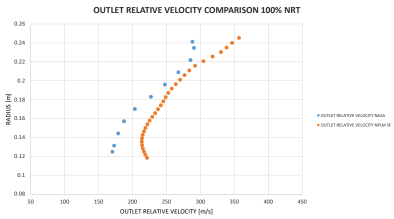

(c) *Outlet Relative Velocity - 1st Rotor*

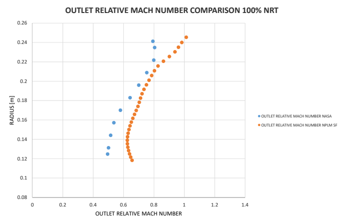

(d) *Outlet Relative Mach number - 1st Rotor*

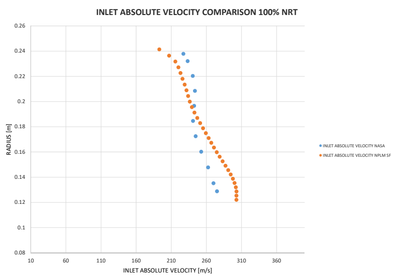

(e) *Inlet Absolute Velocity - 1st Stator*

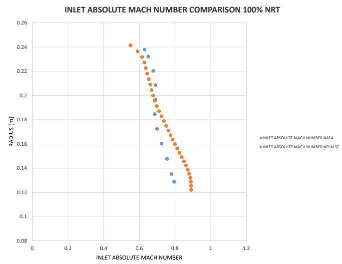

(f) *Inlet Absolute Mach number - 1st Stator*

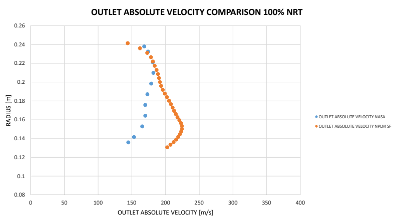

(g) *Outlet Absolute Velocity - 1st Stator*

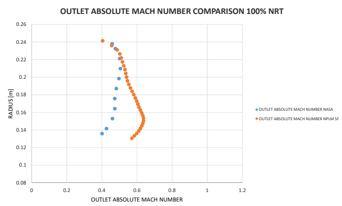

(h) *Outlet Absolute Mach number - 1st Stator*

Figure 6.65: Two Stage Fan - 1st Stage - Rotor Relative Velocity and Relative Mach Number and Stator Absolute Velocity and Absolute Mach Number at 100% of Design Speed and $\dot{m}_{corr} = 35.36\ kg/s$

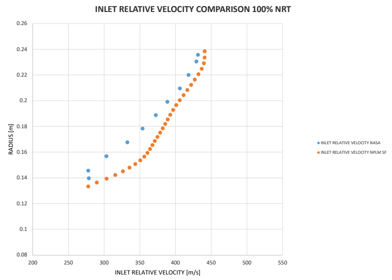

(a) *Inlet Relative Velocity - 2nd Rotor*

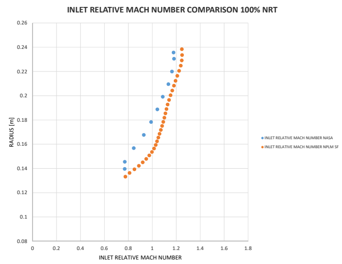

(b) *Inlet Relative Mach number - 2nd Rotor*

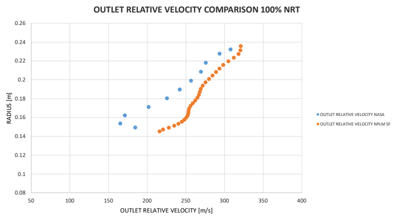

(c) *Outlet Relative Velocity - 2nd Rotor*

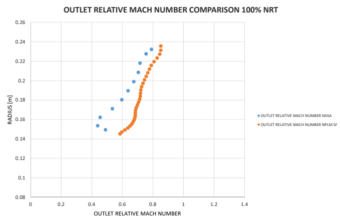

(d) *Outlet Relative Mach number - 2nd Rotor*

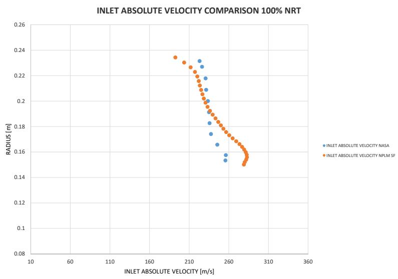

(e) *Inlet Absolute Velocity - 2nd Stator*

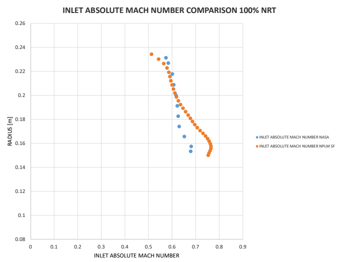

(f) *Inlet Absolute Mach number - 2nd Stator*

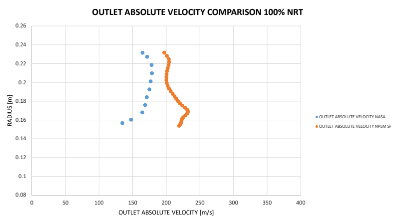

(g) *Outlet Absolute Velocity - 2nd Stator*

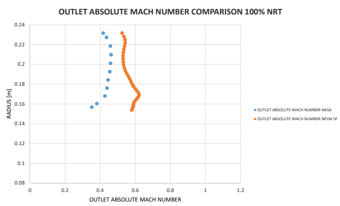

(h) *Outlet Absolute Mach number - 2nd Stator*

Figure 6.66: Two Stage Fan - 2nd Stage - Rotor Relative Velocity and Relative Mach Number and Stator Absolute Velocity and Absolute Mach Number at 100% of Design Speed and $\dot{m}_{corr} = 35.36\ kg/s$

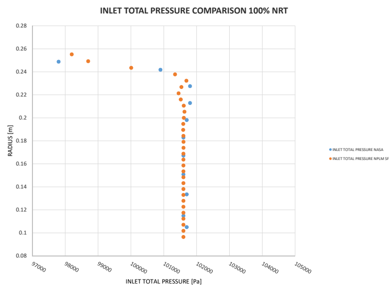

(a) *Inlet Total Pressure - 1st Rotor*

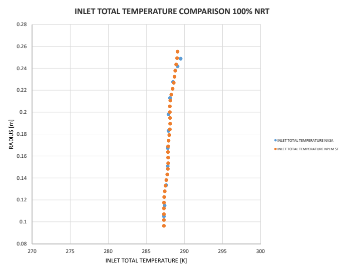

(b) *Inlet Total Temperature - 1st Rotor*

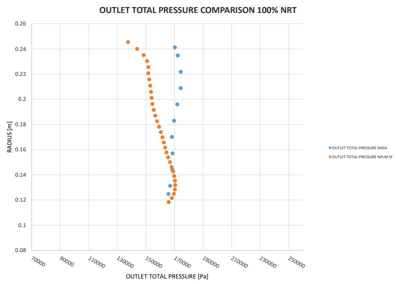

(c) *Outlet Total Pressure - 1st Rotor*

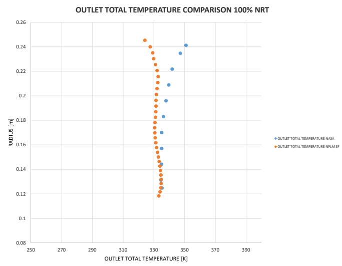

(d) *Outlet Total Temperature - 1st Rotor*

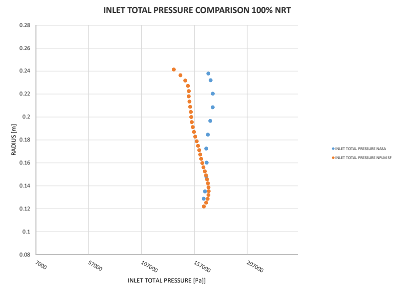

(e) *Inlet Total Pressure - 1st Stator*

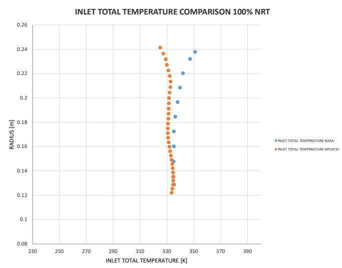

(f) *Inlet Total Temperature - 1st Stator*

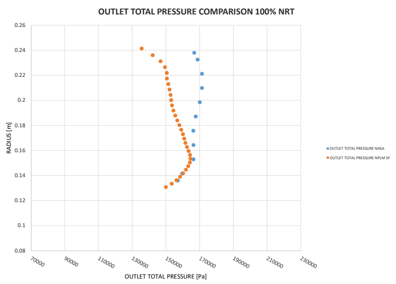

(g) *Outlet Total Pressure - 1st Stator*

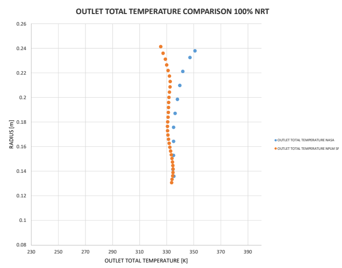

(h) *Outlet Total Temperature - 1st Stator*

Figure 6.67: Two Stage Fan - 1st Stage - Total Pressure and Total Temperature at 100% of Design Speed and $\dot{m}_{corr} = 35.36\ kg/s$

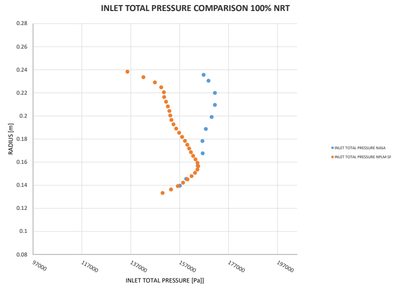

(a) *Inlet Total Pressure - 2nd Rotor*

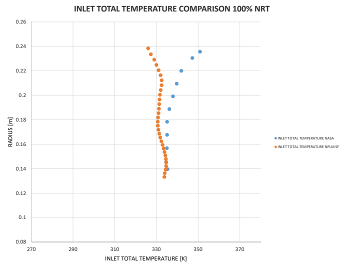

(b) *Inlet Total Temperature - 2nd Rotor*

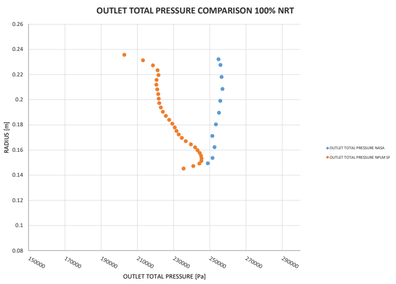

(c) *Outlet Total Pressure - 2nd Rotor*

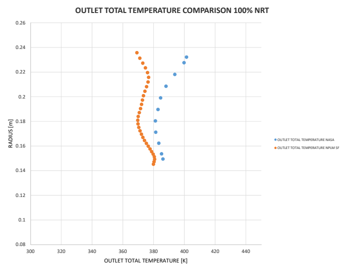

(d) *Outlet Total Temperature - 2nd Rotor*

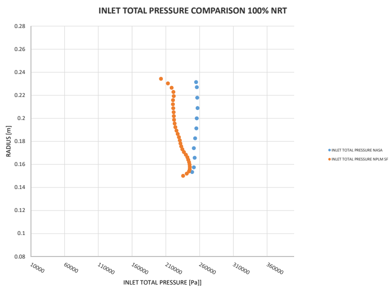

(e) *Inlet Total Pressure - 2nd Stator*

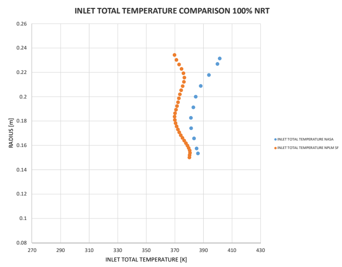

(f) *Inlet Total Temperature - 2nd Stator*

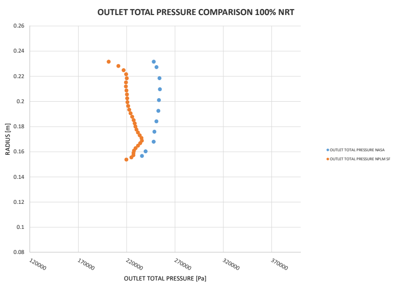

(g) *Outlet Total Pressure - 2nd Stator*

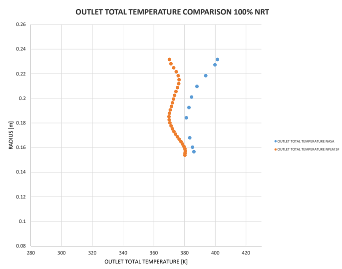

(h) *Outlet Total Temperature - 2nd Stator*

Figure 6.68: Two Stage Fan - 2nd Stage - Total Pressure and Total Temperature at 100% of Design Speed and $\dot{m}_{corr} = 35.36\ kg/s$

The wake, secondary flows and boundary layer effects intensity reaches their maximum intensity at 100% of the design speed. Moreover the transonic character of the compressor considered increases the flow field complexity due to the shock-wave presence.
All this phenomena which characterise the flow field within the compressor contribute to increase the difficulty to achieve an accurate, fast and computational-cost-effective prediction of the flow properties and velocities. Under this point of view a trade-off between accuracy and computational cost has to be accepted.
The meridional velocity overestimation is connected with the wake and boundary layer effects underestimation. However, even if preliminary, the modelisation provided in the tool provides consistent results and an acceptable level of accuracy in terms of predicted shape and magnitude. Their improvement is clearly possible but the general philosophy of the through-flow tools must be respected.
Analogous considerations to the ones made at 90% of the design speed might be done in the relative frame of reference for the two rotors.
The underestimation of both the outlet total pressure and outlet total temperature at the blade tip for the two compressor rotors, where the flow experienced by the blades is in the slight supersonic condition, suggests an higher pressure loss calculation which, considering the region where the under-estimation occurs, might be due to an overestimation of the shock-wave induced losses.
Considering on the other hand the stator blades, the underestimation of the total pressure in correspondence of the blade tip region might be due to an overestimation of the losses induced by the interaction of the rotor wake with the following stator which is imputable to the calibration procedure chosen and to the absence of a complete and reliable wake modelisation in the tool.
Clearly the accuracy of the results obtained is acceptable for preliminary design purposes and considering the computational cost and time needed to produce those results once built the compressor model and defined the boundary conditions.
As everything also these results can be improved as will be discussed in the section concerning the future works. However the application of the model has comprehensively produced results in good agreement with the NASA data stating the functionality status of the model and its applicability to multi-stage transonic axial-flow fans and compressors, demonstrating its potential and flexibility thanks to the possibility to improve the performance prediction simply applying a different calibration strategy, or incorporating more accurate empirical correlations and correction factors, thus, to achieve a growing precision in the flow field modelisation.

Chapter 7

Conclusion

7.1 Project findings

The research project described in this M.Sc. Thesis started with the aim of developing a profile loss model based only on the use of empirical correlations and geometrical parameters to be used in through-flow simulations in order to provide reliable and accurate performance prediction of transonic axial-flow fans and compressors.
The major difficulties were represented by the necessity to respect the general philosophy of the through-flow tools and simultaneously incorporate in the model the major number of dissipative flow phenomena effects with the highest precision level possible in compatibility with the time and computational cost restrictions.
Those general complications were augmented by the absence in the open literature of design profile loss models respecting the previous mentioned constraints. In particular the major problem was represented by the diffusion or equivalent diffusion factor definition employed in the models available in the open literature. The previous proposed models had the great limitation of using the design velocity ratios spanwise distribution as an input to compute the profile losses, whilst they had to be an output of the simulation. This lead to the impossibility to apply the model to compressor geometries without any trousseau of experimental data or in the necessity to perform an initial guess with the probability to obtain an unacceptable flow solution with an high rise in the time needed to set-up the entire simulation. This means a rise in the time dedicated to the preliminary design phase which reflects into a rising in the duration of the entire process. The necessity to overcome this limitation was evident and the scope of the thesis was to develop a model capable of going beyond it and providing reliable and accurate results once coupled with a shock loss and an off-design deviation angle loss model.
The design profile loss model developed coupled with the models taken from the open literature and reported in Aungier's book[1] has meet the requirement of being based only on geometrical parameters and empirical correlations. The calibration strategy chosen has permitted a preliminary consideration of the wake and boundary layer thickening effects giving the model the capacity of reaching an accurate performance prediction also when applied to multi-stage axial-flow compressors. Crucial under this point of view is the shape factor defined, capable of taking into account how the profile shape affects the profile losses.
The potentiality of the model has been investigated and stated thanks to the verification, validation and application conducted over three different transonic axial-flow fans and compressors. The definition of a new input file in the analysis tool has also increased its flexibility: the user has the possibility to investigate and apply different calibration strategies, respecting the general consistency between the constant calibration and the correction factor definition. This flexibility

represent the key for further development and improvements in the performance predictions model. Clearly the definition of a model generally applicable to a wide range of compressor geometries is something that clashes with the use of empirical correlations. The results obtained however are of an accuracy level comparable with 3D CFD when the tool is applied to simple compressor geometries but the time needed for the results computation is of orders of magnitude lower. Accepting a slightly lower accuracy when real multi-stage geometries with more than 3 stages are investigated is something suitable in the preliminary design phase for selecting the candidates on which further and deeper investigations would be made with the use of 3D CFD RANS or LES simulations. This approach would definitely reduce the process time, giving to the compressor designers a powerful, fast and reliable tool which will be crucial in the research of optimised compressor geometries to power the future of aviation.

7.2 Future Works

As emphasized several times in the section concerning the results and discussion, some future activities are recommended in order to improve the model accuracy and reliability in terms of performance prediction. This section aims at summarizing the previous discussed improvements during the results presentation, evidencing how those activities could effectively push the trough-flow methods towards a level of accuracy extraordinary high if compared with the time and computational cost needed to provide the solution.
Firstly a statistical driven approach might be considered to improve the model calibration without changing the strategy used. Considering various transonic axial-flow compressors, calibrating the constants of the model on each of them and then apply a statistical treatment to the various set obtained by weighting each of them also considering the stages number of each compressor would probably lead to a model with an higher spectrum of applicability. However, increasing the spectrum of applicability of the model is often followed by a reduction in terms of accuracy and reliability of the results.
In addiction to this approach it might be the case to consider a different reference geometry for the shape factor that follows automatically if the calibration strategy applied changes. Probably choosing for each compressor considered the first turbo-component as reference geometry if the statistical driven constant definition is applied would give the user the possibility to increase the spectrum of applicability of the model with the possibility to improve the prediction accuracy in terms of both compressor performance and flow properties.
Finally an application to a multi-stage compressor with more than two stages must be considered. The author suggests the application at least to a three stage axial-flow compressor with IGV. This kind of analysis would definitely clarify the necessity already mentioned to introduce in the tool a concrete modelisation of the blade rows wake and of the annulus and casing boundary layer. Into a multi-stage axial-flow compressor, those flow phenomena are two of the major sources of pressure losses. Modelling the blade wake, its interaction with the wake produced by the adjacent blades, with the casing and the annulus boundary layer would definitely represent an incredible step further in the through-flow tool accuracy improvement. Adding also a reliable boundary layer modelisation will give to this simulation and analysis tools the possibility to provide comparable results with the 3D-CFD-RANS simulations when multi-stage configuration are considered. Therefore the latter improvements mentioned, as everything, are easy to say but really challenging to do in particular if the general philosophy of the through-flow simulation has to be respected. Providing an empirical correlation applicable to a wide range of compressor for those flow phenomena is extremely difficult both for the connected difficulties in realising experimental measurement in such complex flow field and for their strong connection to the Reynolds number and the blade profile shape and incidence with which the simulation is conducted. The accuracy level is already

in an extremely good agreement with experimental data, but this author is convinced that a gain in precision terms of 5% at the higher rotating speed is still achievable if an approximate modelisation of those phenomena would be introduced.
As final statement of the whole thesis, I would like to thank the reader for having spent time on this work and I would like to evidence that the model developed would be further investigated by the author in the next months and presented as a paper, already accepted, in the next ISABE international conference in Marc 2019.

Bibliography

[1] H. Aungier, *Axial-Flow Compressors: A Strategy for Aerodynamic Design and Analysis*, ASME PRESS New York, 2003.

[2] P.G. Hill and C.R. Peterson, *Mechanics and Thermodynamics of Propulsion*, PEARSON Second edition, 2010.

[3] A.B. McKenzie, *Axial Flow Fans and Compressors: Aerodynamic Design and Performance*, Cranfield Series on Turbomachinery ASHGATE, 1997.

[4] S. Farokhi, *Aircraft Propulsion*, Jhon Wiley & Sons, 2008.

[5] J.H. Horlock, *Axial Flow Compressors*, Jhon Wiley & Sons, 2008.

[6] N. Chen et al., *Similarity Analysis of Compressor Tip Clearence Flow Structure*, ASME Journal of Turbomachinery Vol. 113 No. 2, April 1991.

[7] G.R. Miller et al., *Shock Losses in Transonic Compressor Blade Rows*, ASME Journal of Engineering for Power Vol. 83 No. 3, July 1961.

[8] W.M. Konig et al., *Improved Blade Profile Loss and Deviation Angle Models for Advanced Transonic Compressor Bladings - Part II - A Model for Supersonic Flow*, ASME Journal of Turbomachinery Vol. 118 No. 1, January 1996.

[9] R. Biollo et al., *State-of-Art of Transonic Axial Compressors, Advances in Gas Turbine Technology*,InTech, 2011.

[10] W.J. Calvert et al., *Transonic fan and compressor design*,Proceedings IMechE Part C: Journal of Mechanical Engineering Science p.419-436, 1999.

[11] H. Azamar Aguirre, *Analytical Transonic Flow Simulation in Streamline Curvature Methods for Axial-flow Compressor Design*,PhD Thesis - School of Aerospace, Transport and Manufacturing - Cranfield University, March 2018.

[12] V.A. Pachidis, *Gas Turbine Advanced Performance Simulation*,PhD Thesis - School of Aerospace, Transport and Manufacturing - Cranfield University, January 2006.

[13] J.L. Kerrebrock and A.A. Mikolajczak, *Intra-Stator Transport of Rotor Wakes and Its Effects on Compressor Performance*,ASME Journal of Engineering for Power, October 1970, p.359.

[14] A.R. Howell, *Design of Axial Compressors*, Proceedings of Institution of Mechanical Engineers, London, Vol. 153, 1945.

[15] R. Biollo and E. Benini, *Recent Advances in Transonic Axial Compressor*, Progress in Aerospace Sciences, Vol. 56 p.1-18, 2013.

[16] C. Han and H.W. Shin, *Study of Near-Stall Flow Behaviour in a Modern Transonic Fan with Compound Sweep*,ASME Journal of Fluids Engineering, Vol. 134 p.1-7, 2012.

[17] M. Cetin et al., *Application of modified loss and deviation correlations to transonic axial compressors*, AGARD Report, No. 745, November 1987.

[18] S. Lieblein, *Loss and stall analysis of compressor cascades*, Transactions of the ASME, Journal of Basic Engineering, p. 387-400, September 1959.

[19] S. Lieblein et al., *Diffusion factor for estimating losses and limiting blade loadings in axial-flow compressor blade elements*, NAXA Research Memorandum Lewis Flight Propulsion Laboratory, Cleveland, Ohio, pp.1-34, 1953.

[20] C.C. Koch and L.H. Smith Jr., *Loss Sources and Magnitudes in Axial-Flow Compressor*, Transactions of ASME, Journal of Engineering for Power, p. 411-424, July 1976.

[21] J.D. Denton, Loss mechanisms in turbomachines, Transactions of the ASME, Journal of Turbomachinery, Vol. 115, p.621-656, October 1993.

[22] W.C. Swan, *A practical method of predicting transonic compressor performance*, Transaction of ASME, Journal of Engineering for Power, p. 332-330, July 1961.

[23] W.M. König, D.K. Hennecke and D.K. Fottner, *Improved blade loss and deviation models for advanced transonic bladings*, Transaction of ASME, Journal of Turbomachinery, Vol. 117, p. 81-87, January 1996.

[24] B. Roy and S. Kumar, *Reduced order loss modelling with tip clearance, aspect ratio and blockage effects for axial flow compressor*, International Society for Air Breathing Engines and American Institute of Aeronautics & Astronautics, ISABE 99-7190, September 1999.

[25] J. Starke, *The effect of axial velocity density ratio on the aerodynamic coefficients of compressor cascades*, Transaction of ASME, Presented at the Gas Turbine Conference & Products show, New Orleans 1980.

[26] H.F. Creveling, *Axial-Flow Compressor Computer Program for Calculating Off-Design Performance*, NASA CR 72472, 1968.

[27] A.D.S. Carter and H.P. Hughes, *A Theoretical Investigation into the Effect of Profile Shape on the Performance of Aerofoils in Cascade*, ARC Rep. and Memo. 2384, 1950.

[28] A.D.S. Carter, *The Low Speed Performance of Related Aerofoils in Cascades*, ARC CP 29, 1950.

[29] B.A. Gustafson, *A Simple Method for Supersonic Compressor Cascade Performance Prediction*, ASME Paper No.76-GT-64, 1975.

[30] M.T. Schobeiri, *Advanced Compressor Loss Correlations, Part I: Theoretical Aspects*, OPA, International Journal of Rotating Machinery, Vol.3, No. 3, p. 163-177, 1997.

[31] M.T. Schobeiri, *Advanced Compressor Loss Correlations, Part II: Experimental Verifications*, OPA, International Journal of Rotating Machinery, Vol.3, No. 3, p. 179-187, 1997.

[32] S. Kim et al., New Profile Loss Model for improved prediction of transonic axial flow compressor performance in chocking region, Proceedings of ASME TurboExpo 2015: Turbine Technical Conference and Exposition, Montréal, Canada, June 2015.

[33] W. Xiaoxiong et al., Development of an improved streamline curvature approach for transonic axial compressor, Proceedings of ASME TurboExpo 2016: Turbomachinery Technical Conference and Exposition, Seoul, South Korea, June 2016.

[34] B. Liu et al., *Development of a Preliminary Design Method for Subsonic Splittered Blades in Blades in Highly Loaded Axial-Flow Compressors*, MDPI, Journal of Applied Sciences, March 2017.

[35] C.H. Wu, *A General Theory of Three-Dimensional Flow in Subsonic and Supersonic Turbomachines of Axial,Radial and Mixed-Flow Types*, NACA Technical Note 2604, Lewis Flight Propulsion Laboratory, p. 1-93, 1952.

[36] T. Katsanis and W. McNally, *Revised FORTRAN program for calculating velocities and streamlines on the hub-shroud mid-channel stream surface of an axial,radial, or mixed flow turbomachine or annular duct*, NASA TN D-8430, 1977.

[37] L.H. Smith, *The radial-equilibrium equation of turbomachinery*, Transaction of ASME, Journal of Engineering for Power, Vol. 116, p. 1-12, 1966.

[38] J.H. Horlock and H. Marsh, *Flow models for turbomachiney*, Journal of Mechanical Engineering Science, Vol. 13, p. 358-368, 1971.

[39] J.P. Veres, *Axial and Centrifugal Compressor Mean Line Flow Analysis Method*, NASA/TM - 215585, Glenn Research Center, Cleveland, Ohio, 2009.

[40] W. Jansen and W.C. Moffatt *The Off-Design Analysis of Axial-Flow Compressors*, ASME, Journal of Engineering for Power, October 1967.

[41] P.I. Wright and D.C. Miller, *An improved compressor performance prediction model*, Proceedings of the Institution of Mechanical Engineers, Turbomachinery: Latest Developments in a Changing Scene, 1991.

[42] L.J. Herrig et al., *Systematic Two-Dimensional Cascade Tests of NACA 65-Series Compressor Blades at Low Speeds*, NACA TN 3916, NACA, Washington, DC, 1957.

[43] I.A. Johnsen et R.O. Bullock, *Aerodynamic Design of Axial Flow Compressors*, NASA SP-36, NASA, Washington, DC, 1965.

[44] M.S. Liou et W. Yao, *Flutter Analysis for Turbomachinery using Volterra Series*, Proceedings of ASME Turbo Expo, GT2014-25474, Dusseldorf, Germany, June 16-20, 2014.

[45] A.J. Strazisar et al., *Laser Anemometer Measurements in a Transonic Axial-Flow Fan Rotor*, NASA technical Paper 2879, November 1989.

[46] D.C. Urasek et al., *Performance of Two-Stage Fan Having Low-Aspect-Ratio, First-Stage Rotor Blading*, NASA technical Paper 1493, August 1979.

[47] R.D. Moore and L. Reid, *Performance of Single-Stage Axial-Flow Transonic Compressor with Rotor and Stator Aspect Ratios of 1.19 and 1.26, respectively, and with Design Pressure Ratio of 2.05*, NASA technical Paper 1659, April 1980.

[48] W.S. Cunnan et al., *Design and Performance of a 427-Meter-Per-Second-Tip-Speed Two-Stage Fan having a 2.40 Pressure Ratio*, NASA technical Paper 1314, October 1978.